2012

Incorporating Remotely Sensed Data into Coastal Hydrodynamic Models: Parameterization of Surface Roughness and Spatio-Temporal Validation of Inundation Area

Stephen Conroy Medeiros
University of Central Florida

INCORPORATING REMOTELY SENSED DATA INTO COASTAL HYDRODYNAMIC MODELS: PARAMETERIZATION OF SURFACE ROUGHNESS AND SPATIO-TEMPORAL VALIDATION OF INUNDATED AREA

by

STEPHEN CONROY MEDEIROS
B.S. Florida Institute of Technology, 1999
M.S. Florida Institute of Technology, 2001

A thesis submitted in partial fulfillment of the requirements
for the degree of Doctor of Philosophy
in the Department of Civil, Environmental, and Construction Engineering
in the College of Engineering and Computer Science
at the University of Central Florida
Orlando, Florida

Spring Term
2012

Major Professors: Scott C. Hagen and John F. Weishampel

ABSTRACT

This dissertation investigates the use of remotely sensed data in coastal tide and inundation models, specifically how these data could be more effectively integrated into model construction and performance assessment techniques. It includes a review of numerical wetting and drying algorithms, a method for constructing a seamless digital terrain model including the handling of tidal datums, an investigation into the accuracy of land use / land cover (LULC) based surface roughness parameterization schemes, an application of a cutting edge remotely sensed inundation detection method to assess the performance of a tidal model, and a preliminary investigation into using 3-dimensional airborne laser scanning data to parameterize surface roughness.

A thorough academic review of wetting and drying algorithms employed by contemporary numerical tidal models was conducted. Since nearly all population centers and valuable property are located in the overland regions of the model domain, the coastal models must adequately describe the inundation physics here. This is accomplished by techniques that generally fall into four categories: Thin film, Element removal, Depth extrapolation, and Negative depth. While nearly all wetting and drying algorithms can be classified as one of the four types, each model is distinct and unique in its actual implementation.

The use of spatial elevation data is essential to accurate coastal modeling. Remotely sensed LiDAR is the standard data source for constructing topographic digital terrain models (DTM). Hydrographic soundings provide bathymetric elevation information. These data are combined to form a seamless topobathy surface that is the foundation for distributed coastal models. A three-point inverse distance weighting method was developed in order to account for the spatial

variability of bathymetry data referenced to tidal datums. This method was applied to the Tampa Bay region of Florida in order to produce a seamless topobathy DTM.

Remotely sensed data also contribute to the parameterization of surface roughness. It is used to develop land use / land cover (LULC) data that is in turn used to specify spatially distributed bottom friction and aerodynamic roughness parameters across the model domain. However, these parameters are continuous variables that are a function of the size, shape and density of the terrain and above-ground obstacles. By using LULC data, much of the variation specific to local areas is generalized due to the categorical nature of the data. This was tested by comparing surface roughness parameters computed based on field measurements to those assigned by LULC data at 24 sites across Florida. Using a t-test to quantify the comparison, it was proven that the parameterizations are significantly different. Taking the field measured parameters as ground truth, it is evident that parameterizing surface roughness based on LULC data is deficient.

In addition to providing input parameters, remotely sensed data can also be used to assess the performance of coastal models. Traditional methods of model performance testing include harmonic resynthesis of tidal constituents, water level time series analysis, and comparison to measured high water marks. A new performance assessment that measures a model's ability to predict the extent of inundation was applied to a northern Gulf of Mexico tidal model. The new method, termed the synergetic method, is based on detecting inundation area at specific points in time using satellite imagery. This detected inundation area is compared to that predicted by a time-synchronized tidal model to assess the performance of model in this respect. It was shown

that the synergetic method produces performance metrics that corroborate the results of traditional methods and is useful in assessing the performance of tidal and storm surge models. It was also shown that the subject tidal model is capable of correctly classifying pixels as wet or dry on over 85% of the sample areas.

Lastly, since it has been shown that parameterizing surface roughness using LULC data is deficient, progress toward a new parameterization scheme based on 3-dimensional LiDAR point cloud data is presented. By computing statistics for the entire point cloud along with the implementation of moving window and polynomial fit approaches, empirical relationships were determined that allow the point cloud to estimate surface roughness parameters. A multi-variate regression approach was chosen to investigate the relationship(s) between the predictor variables (LiDAR statistics) and the response variables (surface roughness parameters). It was shown that the empirical fit is weak when comparing the surface roughness parameters to the LiDAR data. The fit was improved by comparing the LiDAR to the more directly measured source terms of the equations used to compute the surface roughness parameters. Future work will involve using these empirical relationships to parameterize a model in the northern Gulf of Mexico and comparing the hydrodynamic results to those of the same model parameterized using contemporary methods.

In conclusion, through the work presented herein, it was demonstrated that incorporating remotely sensed data into coastal models provides many benefits including more accurate topobathy descriptions, the potential to provide more accurate surface roughness parameterizations, and more insightful performance assessments. All of these conclusions were

achieved using data that is readily available to the scientific community and, with the exception of the Synthetic Aperture Radar (SAR) from the Radarsat-1 project used in the inundation detection method, are available free of charge. Airborne LiDAR data are extremely rich sources of information about the terrain that can be exploited in the context of coastal modeling. The data can be used to construct digital terrain models (DTMs), assist in the analysis of satellite remote sensing data, and describe the roughness of the landscape thereby maximizing the cost effectiveness of the data acquisition.

ACKNOWLEDGMENTS

This research is funded in part by NASA Earth Sciences Division, Research Opportunities in Space and Earth Science (ROSES) Grant Number NNX09AT44G. The statements, findings, conclusions, and recommendations expressed herein are those of the authors and do not necessarily reflect the views of NASA.

I sincerely thank Dr. Scott Hagen for the privilege of working in his lab. He has given me the opportunity to rekindle skills that had lain dormant for years and develop new ones that will benefit me for years to come. His flexibility, guidance and most of all his understanding were integral to my success. Like me, he comes from a long line of loyal, hard working people. Intellectual ability is a gift, but it is easily squandered without the work ethic needed to develop and apply it. This value, whether instilled on a farm in Iowa or a construction site in Massachusetts, is the primary driver of success.

I am also appreciative of the support rendered by my committee members, Drs. John Weishampel (Co-Chair), Gour-Tsyh Yeh and Dingbao Wang. Their contributions have significantly improved this work and I look forward to working with them in the future. Also, I would like to thank Dr. Ni-Bin Chang for his contributions in the early stages of this work.

I had the honor of working alongside some excellent students and scientists at the CHAMPS lab including Derek Giardino, Qing Wang, Naeko Takahashi, David Coggin, Hitoshi Tamura, Lillie Thomas, Alfredo Ruiz, Amanda Tritinger and Karim Alizad. Special recognition is warranted for the students and scientists who contributed to my field research. There were some easy days,

but most were filled with oppressive heat, sweat, poison ivy, spiders and mosquitoes. I am eternally grateful to Matt Bilskie, Ammarin Daranpob, Peter Bacopoulos, Daina Smar and Davina Passeri. I have also benefitted immensely from interaction with other departments at UCF, and none more than the Department of Biology. Dr. John Weishampel has given me the benefit of his expertise in a variety of fields and I am very fortunate to have him as my Co-Major Professor on this dissertation. James Angelo was also extremely helpful in the areas of computer programming and statistical analysis. Dr. Tarig Ali, formerly of the UCF Department of Engineering Technology, was integral to my understanding of geospatial data. The computer simulations for this work were conducted on the STOKES high performance computing cluster within the UCF Institute for Simulation and Training. The system administrator, Dr. Sergio Tafur, was most patient and helpful in keeping this system operational and thereby productive for its users.

The cooperation of state agencies through this work is greatly appreciated. In particular, Jenna Wanat from the Apalachicola National Estuarine Research Reserve, Mike Blondin from the Florida Fish and Wildlife Conservation Commission and Arthur Stiles from the Florida Department of Environmental Protection were especially helpful. The Florida Division of Forestry also deserves recognition.

Karen Kebart at the Northwest Florida Water Management District (NWFWMD) and Richard Helfst at Lake County GIS provided the raw LiDAR data. I am also grateful to Ron Bartel and Mark Ihlefeld at the NWFWMD for personally showing me nearly the entire coastline of the Florida Panhandle.

I also wish to thank my colleagues in the professional community for their advice and cooperation throughout my work. In particular, Jesse Feyen and Yuji Funakoshi of NOAA, Hugh Roberts from ARCADIS, Casey Dietrich from the University of Texas, Ethan Kubatko from the Ohio State University, Mike Salisbury from Ardaman & Associates, Alan Zundel from Aquaveo, and Jason Fleming from Seahorse Coastal Consulting. John Atkinson from ARCADIS warrants special acknowledgement as my interactions with him were what sparked the ideas that formed this dissertation and my research direction in general. I am very thankful for our friendship and professional collaborations.

Above all, I am most fortunate to have a loving and supportive family. My time as a Ph.D. student has been anything but easy, both in terms of academic challenges and personal setbacks. I can state with certainty that I would not have been able to endure them without the support of my parents, grandmother, aunts, uncles, cousins, and in-laws. However, most of the support burden fell squarely on the shoulders of my wife, Shannon. Her efforts at work and at home allowed me the freedom to pursue this goal and my success is in large part attributable to her. We are teammates for life.

This dissertation is dedicated to the memory of my grandfather.

STEPHEN JOSEPH CONROY
May 9, 1919 – July 19, 2010

My hero.

TABLE OF CONTENTS

LIST OF FIGURES

LIST OF TABLES

CHAPTER 1. INTRODUCTION

Numerical computer models seek to simulate natural conditions under various scenarios in order to gain insight into the behavior of the systems. The information obtained from model simulations can assist community stakeholders in making decisions that will affect the safety and well-being of the citizens and lands in their charge. However, a model is only as good as the data used to construct it. In the case of coastal circulation and inundation modeling, the water level conditions at the boundaries and the winds over the water surface are used to force the model and are essential to producing accurate results. The models also require spatially distributed topographic and bathymetric elevations as well as surface roughness parameters that describe the terrain. The sources of these data include physical measurements, surveys, output from other models and published data such as land use / land cover. Due to the increasing geographic scale of coastal models, it is becoming practically impossible to manually observe the terrain conditions over the domain and verify the validity of all input data. The underpinning of this dissertation is that airborne Light Detection and Ranging (LiDAR) data are extremely rich sources of information about the terrain that can be exploited in the context of coastal modeling. The data can be used to construct digital terrain models (DTMs), assist in the analysis of satellite remote sensing data, and describe the roughness of the landscape thereby maximizing the cost effectiveness of the data acquisition. Therefore, methods for incorporating several types remotely sensed data into coastal models have been developed, tested and implemented. The most prevalent uses of remotely sensed data in coastal models are for development of the topobathy surface, parameterizing surface roughness, and assessing model performance.

1.1 Hypothesis and Research Objectives

This dissertation seeks to test the following hypothesis:

> *Incorporating remotely sensed data into large-scale coastal tide and inundation models will allow them to produce better results through enhanced parameterization and validation.*

In addition to and in support of testing this hypothesis, the following research questions will also be addressed:

1. Since surface roughness parameters play an important role in the advancement and recession of the wetting front, what is the current state-of-the-art in wetting and drying algorithms employed by numerical tide models?
2. How is the variable nature of tidal datums accounted for in developing coastal inundation models?
3. How well do the surface roughness parameters derived from LULC data describe the actual conditions on the ground?
4. Is assessing the performance of tidal models using remotely sensed snapshots of inundation area a viable means of model validation?
5. How can 3-dimensional LiDAR point cloud data be used to develop more locally accurate surface roughness parameters?

By testing this hypothesis and answering the associated research questions, this dissertation will contribute practically relevant and usable information to the field of coastal tide and inundation

modeling. In particular, the richness of LiDAR data in many phases of coastal modeling will be assessed.

1.2 Wetting and Drying Algorithms

Coastal models typically solve their governing equations over a model domain discretized using a numerical scheme such as the finite difference (FD), finite element (FE) or finite volume (FV) method. These models solve for water levels and velocities as they march forward in time, driven by their boundary and initial conditions. A key element in any model seeking to replicate inundation / recession processes such and astronomic or storm surge tides is the wetting and drying (WD) algorithm employed within the code. Since the governing equations are often the shallow water equations (Kolar *et al.*, 1994) and are only applicable to fluid, the model requires a means for classifying an element as wet or dry. This determination establishes whether or not an element is included in the computations at the current time step. Medeiros and Hagen (2012) conducted a thorough review of WD algorithms used in contemporary numerical tidal flow modeling. Nearly every coastal model, regardless of discretization scheme, has its own unique way of dealing with WD; however, these schemes typically fall into one of the four general categories that are described in CHAPTER 2.

1.3 Digital Terrain Models

Along with the boundary and initial conditions, accurate description of the underlying topobathy surface is emphasized in contemporary coastal models (Westerink *et al.*, 2008). LiDAR data efficiently provide an accurate description of the terrain over large geographic areas. Since the cost of data acquisition is high, it is vital to make the most of the data. While it is readily

apparent to any engineer or scientist how topographic surveys and LiDAR describe the terrain, the bathymetric surface presents some unique challenges, mainly the use of tidal datums during data acquisition. By referencing datums that are computed from the tide record such as Mean Lower Low Water (MLLW) and Mean Sea Level (MSL), two challenges are presented to coastal modelers. First, these datums are often not applicable in inland areas within the model domain. Second, since the datums are computed based on the tidal record, the unique hydrodynamics of each local area causes the orthometric elevation of datums to vary along the coastline. Considering that contemporary models typically include large swaths of coastline, tidal datums can vary significantly within the domain. A method for handling these challenges is presented in CHAPTER 3 along with a repeatable methodology for producing a seamless topobathy digital terrain model.

1.4 Measuring Surface Roughness Parameters in the Field

After topography, surface roughness is the most important spatially distributed parameter in coastal inundation modeling (Straatsma, 2009). Surface roughness in this context refers to three parameters: Manning's n for bottom friction, and effective roughness length, z0, and surface canopy closure fraction for aerodynamic roughness. Currently, the Federal Emergency Management Agency (FEMA) guidance for computing surface roughness parameters relies on published land use / land cover (LULC) data. From field reconnaissance expeditions, it is evident that areas are frequently misclassified by the LULC data. There is also a high degree of variability within areas classified as a particular LULC type. With these two discrepancies in mind, a field measurements campaign was conducted to measure the surface roughness

parameters at 24 sites throughout Florida and compare them to the values assigned by the LULC data. The methodologies and results of this undertaking are presented in CHAPTER 4.

1.5 Model Validation

Once a coastal model has been parameterized, the boundary, surface and initial conditions defined, and simulations run, the performance must be assessed quantitatively. The most common performance assessments for coastal models are harmonic resynthesis of tidal constituents, water level time series analysis, and comparison to high water marks (Bunya *et al.*, 2010). These are all defensible methods that give the modeler excellent insight into the performance of the model. In turn, the modeler is able to draw conclusions about the system based on the model results. However, new methods have been developed based on remotely sensed data that enable modelers to assess the performance of their models in an entirely new way. In particular, using satellite imagery to detect the inundation extent at a specific point in time has enormous potential to assess the performance of coastal models. Modelers are able to time synchronize their simulations to reconstruct the conditions at a particular point in history. The results of the model can then be compared to the inundated area snapshots to determine how well the model predicts the extent of inundation. In CHAPTER 5, the method of Chaouch *et al.*(2011) is applied for the first time to assess the performance of a tidal model of the northern Gulf of Mexico.

1.6 Parameterizing Surface Roughness Using LiDAR

In CHAPTER 4, the accuracy of parameterizing LULC data is investigated. While the LULC method is an automatable process able to compute surface roughness parameters over a large

domain, it is shown to be locally deficient. Therefore, a new method is explored in CHAPTER 6 that uses LiDAR point cloud data to compute the parameters. The LiDAR point cloud provides the modeler with a 3-dimensional description of the terrain and its obstructions. This facilitates the computation of surface roughness based on empirical relationships derived by comparing the field measured data to the LiDAR point cloud (Ritchie, 1996). The ultimate result will be a methodology that is more locally accurate in defining surface roughness parameters yet is still automatable and therefore applicable to model domains of large geographic scale.

1.7 References

Bunya, S., Dietrich, J. C., Westerink, J. J., Ebersole, B. A., Smith, J. M., Atkinson, J. H., . . . Roberts, H. J. 2010. A High-Resolution Coupled Riverine Flow, Tide, Wind, Wind Wave and Storm Surge Model for Southern Louisiana and Mississippi. Part I: Model Development and Validation. *Monthly Weather Review, 138*, 345-377.

Chaouch, N., Temimi, M., Hagen, S. C., Weishampel, J. F., Medeiros, S. C., & Khanbilvardi, R. 2011. A synergetic use of satellite imagery from SAR and optical sensors to improve coastal flood mapping in the Gulf of Mexico. *Hydrological Processes, In Press*. doi: 10.1002/hyp.8268

Kolar, R. L., Westerink, J. J., Gray, W. G., & Luettich, R. A. 1994. Shallow water modeling in spherical coordinates: Equation formulation, numerical implementation, and application. *Journal of Hydraulic Research, 32*(1), 3-24.

Medeiros, S. C., & Hagen, S. C. 2012. Review of wetting and drying algorithms for numerical tidal flow models. *International Journal for Numerical Methods in Fluids, In Press*.

Ritchie, J. C. 1996. Remote sensing applications to hydrology: airborne laser altimeters. *Hydrological Sciences Journal, 41*(4), 625-636.

Straatsma, M. 2009. 3D float tracking: in situ floodplain roughness estimation. *Hydrological Processes, 23*, 201-212. doi: 10.1002/hyp.7147

Westerink, J. J., Luettich, R. A., Feyen, J. C., Atkinson, J. H., Dawson, C., Roberts, H. J., . . . Pourtaheri, H. 2008. A Basin- to Channel-Scale Unstructured Grid Hurricane Storm Surge Model Applied to Southern Louisiana. *Monthly Weather Review, 136*, 833-864.

CHAPTER 2. REVIEW OF WETTING AND DRYING ALGORITHMS FOR NUMERICAL TIDAL FLOW MODELS

The content in this chapter has been accepted for publication as: Medeiros, S. C., & Hagen, S. C. 2012. Review of wetting and drying algorithms for numerical tidal flow models. *International Journal for Numerical Methods in Fluids, In Press*.

2.1 Introduction

In coastal regions worldwide, the flooding and ebbing of the tide is the primary driver of the local ecosystem. All life adapts to its cyclical rhythm. Estuarine plant life naturally migrates to those areas that meet its specific and narrow tolerances for inundation, salinity and soil type (Morris, 2007). Fauna follows shortly behind as it adapts to the patterns dictated by its food sources. These ecological patterns unique to the coast are defined by the behavior of the tides.

The incoming tide (commonly referred to as the flood tide) progressively raises the water level at the coastline and in tidal creeks causing them to overflow into the surrounding tidal marshes. Water levels continue to rise towards a peak at which time flows in the tidal creeks are at their minimum (known as slack tide). After water levels peak, they steadily fall draining the surrounding tidal marshes and exit through tidal creeks (known as ebb tide). The duration of inundation (known as the hydroperiod) is unique to each coastal region, particularly within tidal creek and salt marsh systems, and defines the local characteristics of the ecosystem. The hydroperiod, controlled by the regularity of the tides, can also be influenced by external factors

including freshwater inflows and meteorological conditions such as wind and pressure (especially during extreme events such as hurricanes).

An additional influencing (complicating) factor is sea level rise (SLR) (Morris, 2007). However, the incorporation of sea level rise into coastal models extends beyond simply raising present-day model results as an approximation of increased water surface elevations. Instead, the water surface time series resulting from the tides, river inflow, meteorological effects (storm surge), or any other forcing mechanism is dynamically affected by sea level rise (Titus & Richman, 2001). SLR raises baseline water levels and introduces entirely new bathymetry to the flow. This new bathymetry substantially influences the flow conditions.

The complex physical process of an advancing or receding flood wave presents a non-trivial modeling challenge. As a flood wave inundates a previously dry area, the model must adapt to include these now wet areas into the model. Shortly thereafter, especially in the case of tidal flow modeling, the model must then simulate the receding flood by drying these elements and therefore removing them from the computations. Depending on the scheme, these additions or removals from the computations may be explicit, i.e. elements are literally activated (wetted) or deactivated (dried) within the computational matrix, or implicit, i.e. the dry elements are flagged as “dry” but contain a virtual water level and are still included in the computations. To date, a broad scope review of existing algorithms for addressing the wetting and drying (WD) problem in tidal flow and storm surge inundation modeling has not been conducted.

The issue of WD capability is important to the end-user of any given model as inundation extent and water level provide crucial information to stakeholders, managers and emergency personnel in coastal areas. In the case of storm surge inundation extent, a process that is highly dependent on topography (Horritt & Bates, 2001), an accurate prediction is crucial in order to justify selection of evacuation areas and routes. Another coastal process where an understanding of the wetting front propagation is crucial is the cyclical flooding and ebbing of tidal marshes. The complex ecology of these intertidal zones is highly dependent on a delicate balance of processes simulated by WD algorithms: inundation extent and duration (hydroperiod), and the transport of sediment and nutrients (Donnelly & Bertness, 2001; Morris *et al.*, 2002). The transport of sediment and contaminants is its own specialized modeling field within the study of coastal and riverine processes. Since the fluid is the medium in which both sediments and contaminants are transported, its spatial extent plays a crucial role in the determination of the fate of these constituents. In fact, it is essential that wetting and drying be incorporated into any model seeking to model these processes in environments with moving flow boundaries, such as tidal environments (de Brye *et al.*, 2010; Hardy *et al.*, 2000). Furthermore, on a more fundamental level, WD is essential to the computation of tidal datums such as Mean Sea Level (MSL), Mean Low Water (MLW) and Mean High Water (MHW) (United States Department of Commerce, 2000). It has been shown that these datums vary spatially according to local flow conditions, especially within shallow coastal environments (Meyers III, 2005; Parker *et al.*, 2003). Accurate simulation of WD processes allows researchers to derive these tidal datums that are used heavily for mapping and navigation as well as modeling applications (Medeiros *et al.*, 2011).

A variety of numerical models have been developed to simulate coastal hydrodynamics in one-, two- and three-dimensions. These models employ a diverse set of techniques for solving the governing equations, discretizing the domain, and marching forward in time. The numerical schemes employed in some widely used models can be found in Brufau *et al*. (2002), Chen *et al.* (2003), Deltares (2009), Galland *et al.* (1991), Luettich *et al.* (1992), Luettich & Westerink (2006) and Mellor *et al.* (2002), with particular emphasis on the shallow water equations. While there is great interest in the formulations and discretizations of the shallow water equations, this paper focuses on another aspect of the overall solution algorithm: wetting and drying of computational elements and nodes.

In general, a typical coastal and estuarine hydrodynamic model solves the governing equations over the entire model domain at each time step. However, the equations only apply to those computational elements where a fluid (water) is present. Thus the handling of an element's wet or dry state performs the crucial duty of indicating how or if it is to be included in the computations at the present time step. Figure 2.1 depicts the problem in graphical form for a case with a triangular element spatial discretization. As shown, the WD algorithm is tasked with representing the wetting front within the constraints of the mesh resolution. Various algorithms using unique tactics have been set forth to accomplish this; those with application to tidal circulation modeling will be described in this paper.

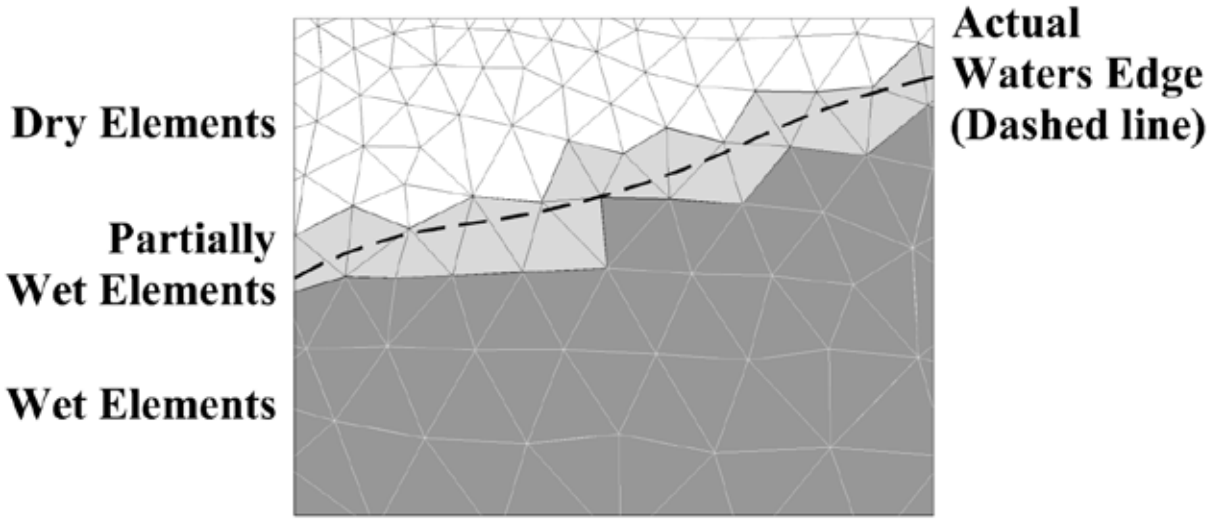

Figure 2.1: Unstructured triangular mesh illustrating wetting front in reality and as seen by numerical model

Accurately capturing the physics of the inundation / recession process has historically been addressed as a computational (WD) problem, to be solved with an algorithm implemented in the computer code and executed in run time. This problem is unique in that it involves a delicate balance of computational efficiency (both processing demand and memory allocation), numerical stability (convergence, spurious oscillations) and scientific accuracy. As with any computer modeling technique, the closer the solution describes the physics, the more computationally intensive it is. Previous reviews of WD algorithms have stressed the computational solutions to the issue, rather than the capture of the physical processes involved (D'Alpaos & Defina, 2007). As stated above, implementing a numerically stable solution that does not introduce spurious noise into the results is indeed important; however, a purely computational remedy that is based loosely or not at all on the physics has the potential to induce artificial damping or dissipation of solution fluctuations. Tchamen & Kahawita (1998) provided an excellent description of the

problems faced by model developers and the generic algorithm used to address them. Balzano (1998) evaluated seven WD schemes implemented in the same model, analyzed the shortcomings evident in the one-dimensional test cases, and proposed three new schemes. D'Alpaos and Defina (2007) also present a general review of WD algorithms as a foundation to their set of two-dimensional shallow flow equations modified to handle partially wet elements (Defina, 2000).

This paper presents a review of WD algorithms in popular coastal and estuarine models based on the shallow water equations. This review is different in scope from previous reviews (listed above) in that the focus is on models typically used to model tidal hydrodynamics and storm surge in contemporary studies. While Balzano (1998) presented a review of WD algorithms in use from 1968-1993, and D'Alpaos & Defina (2007) included more current schemes, a comprehensive review and characterization of contemporary WD algorithms has not been carried out. The models reviewed all operate on structured or unstructured numerical grids that are temporally and spatially constant (i.e. fixed). For the purposes of this paper, moving grid boundary (Lin *et al.*, 2004; Lynch & Gray, 1980; Yeh & Chou, 1979) and adaptive mesh-generation / advancing front (Liang & Borthwick, 2009; Löhner, 1990) approaches are not considered. While highly suited to the problem of wetting and drying, they are omitted here in favor of models that are more commonly applied to tidal circulation modeling. An outcome from this review is a categorization of WD algorithms. Thus, the paper is structured around the four categories identified in the review (please refer to Figure 2.2 for illustrations of these groups): 1) those that specify a thin film of fluid over the entire domain in order to compute the equations of mass and momentum conservation over the entire domain at every time step; 2)

those that employ checking routines to determine if an element or node is wet, dry or potentially one of the two, subsequently removing dry elements from the computational domain; 3) those that extrapolate the fluid depth from wet nodes onto dry nodes and compute the velocities in the newly wet element; and 4) those that allow the model to tolerate negative water depths and permit the simulated water surface to extend below ground. Special emphasis is given to each categories application to specific numeric schemes, namely finite difference (FD), finite element (FE), and finite volume (FV) methods along with their performance in conserving mass and capturing the relevant physics such as the advance and recession of the wetting front. Lastly, a summary is presented along with a brief discussion of future research related to this topic.

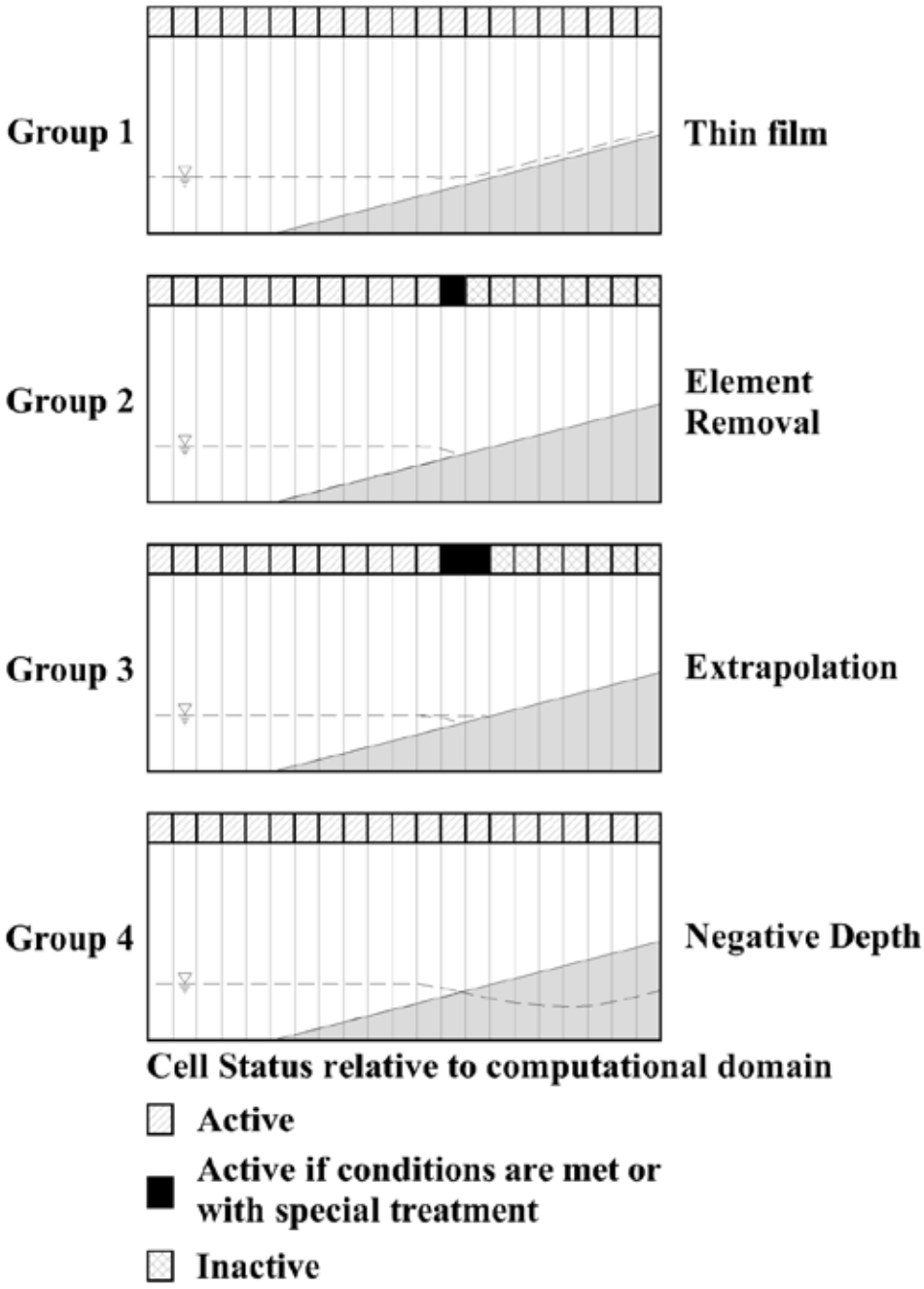

Figure 2.2: Four categories of wetting and drying algorithms

2.2 Thin Film Algorithms

As stated previously, thin film algorithms specify a viscous sub-layer of fluid over the entire computational domain. This allows all nodes, elements and cells to be included in the computational domain at each time step. There is typically a minimum threshold depth that defines the categories of wet or dry in the model, even though there is some fluid present over the entire domain. In some cases, these algorithms employ techniques similar to those of element removal algorithms. However, the manner the constant presence of some fluid in every element within the domain is their defining feature. Please refer to Figure 2.2, Group 1.

In developing their two-dimensional finite element model for river floodplain inundation, Bates & Anderson (1993) applied a modified form of the WD scheme proposed by King & Roig (1988). This scheme operated on a fixed mesh and applied a coefficient α to represent the portion of an element available for flow. This enabled the model to include partially wet elements in the computations and ensured smooth transitions from wet to dry and vice-versa. In order to overcome numerical difficulties (namely undefined derivatives and discontinuities resulting from zero water depths) in the solution procedure, a small, positive α_{min} value was incorporated and represented effectively dry conditions. This model conserves mass globally, i.e. at the domain boundaries and is shown to conserve mass locally to within ±2%. In the test cases presented, the model appears to produce realistic, smooth and continuous representations of the wetting front.

As explained by Oey (2005), the Princeton Ocean Model (POM; Mellor, 2003; Mellor *et al.*, 2002) utilized a variety of approaches to implement WD into their finite difference model. First,

a boundary was defined over which water can never flow, i.e. the cells landward of this boundary must always be dry. Then a region seaward of this boundary was defined where cells can be either wet or dry. This region was intended to simulate marsh and tidal flat areas. In this wet or dry region, cells were defined with a small film of water called with depth H_{dry} (stated as 5 cm) in which the equations of mass and momentum conservation could be solved. The resulting depths were then checked at each cell interface; if the depth dropped below H_{dry} then the velocity was set to zero and the wet or dry state was updated for the next time step. This is one of the simpler, more robust schemes employed; however, it falls into the category of algorithms that require a non-zero depth in every cell, thus solving the equations for all cells at each time step. Xie *et al.* (2004) thoroughly explain this algorithm and apply it to an idealized test case.

In the framework of a one-dimensional discontinuous Galerkin (DG) finite element discretization, Bokhove (2005) presented a WD scheme that sought to preserve the water depth as a positive value. In this model, the WD scheme permitted isolated patches of wet or dry areas, even those that are generated during a simulation such as waves overtopping a dike. In order to resolve discontinuities generated by dry patches that emerge in flat topography such as the recession of water on a tidal flat, the model splits the cells near the boundary. WD algorithms of this type in DG models have also been studied by Ambati (2006). Bunya *et al.* (2009) also developed a WD scheme for a DG shallow water equations model. Similarly, they sought to maintain a positive water depth in the elements and strictly prohibited flux between adjacent dry elements.

Lastly, FVCOM (Chen *et al.*, 2007; Chen *et al.*, 2003) is a finite volume coastal ocean model. The WD algorithm is described as a point treatment incorporating a viscous sublayer of specified thickness (to avoid zero depth and the resulting singularity). The water depth at the nodes is checked against the thickness of the viscous sublayer to determine their state as wet or dry. The cells are subjected to a similar check that incorporates all nodes associated with the cell. If the depth in a cell is less than the thickness of the viscous sublayer, the velocity is set to zero and the cell is subsequently removed from transport computations as well (Chen *et al.*, 2008). FVCOM has been used in WD applications ranging from storm surge (Rego & Li, 2009; Weisberg & Zheng, 2006) to wetland-estuarine-shelf interactions in Massachusetts (Zhao *et al.*, 2010).

2.3 Element Removal Algorithms

Element removal algorithms employ unique (to each model) systems of checks to determine if a cell or element is wet, dry or partially wet. The wet elements are included in the computational domain and the dry ones are not. However, in the case of partially wet elements, further consideration is necessary to determine if the flow conditions at the wetting front are capable of fully wetting a partially wet element. As explained in the examples below, each model approaches this task in a specific manner. Please refer to Figure 2.2, Group 2 for an illustration of this algorithm.

Modifying the earlier model of Falconer and Chen (1991), Lin and Falconer (2004) implemented a WD scheme in their three-dimensional finite difference model. During each time step, a series of drying and flooding checks was performed to determine whether or not to include a particular grid cell in the computational domain. The drying checks were based on a length scale that

describes the bed roughness and were used to determine if a grid cell should be removed from the computational domain by examining the depths at the cell center and each side. To determine if a dry cell is flooded and should be returned to the computational domain, the length scale was used again in comparison with the depths of surrounding grid cells to determine if conditions warrant the flooding of the cell. If so, the cell was returned to the computational domain at the start of the next half time step. The method was validated and tested on an idealized flat tidal bed, an idealized rectangular harbor, and in the Humbert Estuary on the northeast coast of England.

In developing their finite difference storm surge inundation model, Hubbert and McInnes (1999) employed a WD scheme designed to produce smoothly varying results at the wetting front. As in typical WD schemes, the water level in adjacent wet cells determines if a dry cell is eligible to become wet. However, the authors also calculated the potential length of travel of the wetting front in one time step by observing the current velocity in the wet cells. In order for a dry cell to become wet, the water level and the current velocity in the adjacent wet cell must warrant it. The scheme was also applied to the drying of flooded cells as well. This WD scheme was tested on two inundation scenarios in Australia. By varying the grid resolution of the models, the authors showed the danger in artificially wetting dry cells based on water depth criteria alone. In their test cases, large grid cells caused the wetting front to propagate inland beyond a realistic extent when the grid cells were declared wet without the support of the current velocity criteria.

Bates & Hervouet (1999) utilized the finite element model TELEMAC-2D (Galland *et al.*, 1991; J. M. Hervouet, 2000) and began the WD process by characterizing all elements as one of four

types: fully wet, fully dry, partly wet (dam-break type) and partly wet (flooding type). This categorization allowed them to apply an appropriate mass and momentum correction scheme. Once the element subtype was established, all partially wet elements were included in the computations and steps were taken to correct the mass and momentum discrepancies. In the case of momentum, the authors applied the scheme of Hervouet & Janin (1994) which assumed that the change in velocity with respect to time is equal to the water surface slope times the acceleration due to gravity. In some cases, this resulted in spurious results when the water surface slope was nearly flat, such as in the case of an element flooding from the bottom up. In terms of mass conservation, Bates & Hervouet (1999) applied the scheme of Defina *et al.* (1994). This scheme utilizes the bottom topography and water surface elevation to calculate a scaling factor that is applied to the continuity equation. This scaling factor allows for a true representation of the volume of water present on the element. Tests of this method for the simple case of a sinusoidal wave on a sloping beach were presented by Bates (2000). Carniello *et al.* (2005) also employed this scheme in their model of the Venice lagoon in Italy. However, in addition to simulating WD, they coupled their model to a finite volume wind wave model to simulate the combined effects of waves and tide propagation. Defina (2000) referenced and built on this approach by modifying the two-dimensional flow (momentum and continuity) equations to accommodate partially wet elements. The same scaling factor was applied to the continuity equation to preserve mass conservation. The momentum equations were derived in order to account for the subgrid topographic irregularities present in most models and the volume of water (and the subsequent change in water volume) in those elements.

Casulli and Walters (2000) allowed their three-dimensional finite difference / finite volume scheme to incorporate WD "in a natural and straightforward manner (p. 331)," typical of kinetic finite volume models. When the water depths were calculated at each time step, the vertical grid spacing was updated accordingly. If the water depth was zero, then the height of the faces and subsequently the velocity through the faces was also set to zero. Due to the finite volume discretization of the free surface equation, mass is conserved both locally and globally. This was based on earlier work by Casulli and Cheng (Casulli & Cheng, 1992) and also utilized by Zhang *et al.* (Zhang *et al.*, 2004) in the development of their ELCIRC model. While the execution of WD algorithms such as the kinetic energy criteria employed by Lu (Lu, 2003) and the wet-dry tolerance parameter employed by Cea *et al.* (Cea *et al.*, 2006) in this case are innovative in their determination of an element's state, they should still be classified as Element Removal Algorithms.

Ji, Morton and Hamrick (2001) used the Environmental Fluid Dynamics Code (EFDC; Hamrick, 1992) and employed the WD scheme presented by Hamrick (1994) in their analysis of the flooding and drying behavior of Morro Bay, California. As with most finite difference and finite volume models, the key to the WD scheme was the determination of whether or not a cell face was dry based on the water depth in the cell. If a cell face was determined to be dry, the flux was forced to zero.

In Japan, Matsumoto *et al.* (2002) applied a WD approach in their finite element model that used the bubble function (Fortin & Fortin, 1985) for discretization in space and the least-squares bubble function (LSBF) for discretization in time. They employed the minimum depth criteria to

determine whether or not (and how) an element is included in the computations. It was shown to work well as demonstrated in a one-dimensional dam break test case and also a two-dimensional simulation of flow in the Nagaragawa River, Japan.

The finite volume model proposed by Brufau *et al.* (2002) employed a scheme where the wetting front was treated as a boundary where the flow of water was controlled by the difference in both water depth and bottom elevation. In order to maintain mass conservation, the difference in bottom elevation was locally redefined in order to maintain equilibrium. One special case discussed by the authors was the propagation of the wetting front on a dry, adverse slope. In this case, the velocity across the wet/dry cell interface needed to be set to zero or there was a risk of artificially wetting the higher dry cell as a result of the locally redefined bottom elevation difference.

In order to simulate the Quoddy region in the Bay of Fundy, Greenberg *et al.* (Greenberg *et al.*, 2005) adapted the three-dimensional finite element QUODDY model (Lynch & Werner, 1991) to implement a WD scheme. The scheme integrated into the QUODDY model was a relatively simple dry element removal scheme. The model checked the depth at each node of an element and if they were below a certain threshold, the element was considered dry and the velocity at the bottom was set to zero. The authors ran an experiment on an idealized mesh before testing the adapted QUODDY code, termed QUODDY_dry, to the Quoddy region where it proved itself to be a useful tool. (Note: as shown in the above citations, the model was named QUODDY prior to its application in the Quoddy region in the Bay of Fundy.)

One of the most commonly used codes in tidal circulation modeling, the Advanced Circulation (ADCIRC) finite element model (Kolar *et al.*, 1994; Luettich & Westerink, 2006; Luettich *et al.*, 1992) employs a WD algorithm that makes cells active or inactive if the depth exceeds a certain minimum threshold. Dietrich *et al.* (2005) thoroughly explained the evolution of the ADCIRC WD algorithm; only relevant details are presented here. In its first WD algorithm, ADCIRC performed a depth check at each node; if the depth exceeded the minimum threshold depth, the node was activated and participated in the computations. Otherwise, the node was deemed dry and was removed from the computations. In this algorithm there was also a criteria imposed that dictated a node was to remain in its current state for a specified number of time steps before it was allowed to change state. This was implemented in an effort to avoid spurious noise resulting from thin layers of water at or near the threshold depth for rapidly switching a node between wet and dry states (Luettich & Westerink, 1995a, 1995b). Minor updates to this algorithm were introduced in 1999 and included a node state variable (1 for wet, 0 for dry) and also some elemental wetting and drying checks were implemented in order to determine the best method for modifying the node state based on elemental conditions such as the number of wet nodes in the element and whether or not bottom friction or presence of barriers would inhibit the wetting of nodes (Luettich & Westerink, 1999). A subsequent revision in 2004 eliminated the condition that the node must remain in its current state for a specified number of time steps and also addressed the issue of thin films of water creating mass balance errors on steep slopes. The node state condition was determined to be the cause of abnormally slow propagation of flood waves over flat floodplains (a common situation in hurricane storm surge simulations). A new parameter was introduced that forced water to accumulate on a slope prior to flowing. This parameter was applied at the down gradient node within an element and was set to be 120% of

the minimum depth threshold that determines if an element is wet. The 120% value was stated as being an ad hoc selection that had performed well in tests. If the down gradient node had a depth less than this new parameter, then the entire element was declared dry. This new algorithm was determined to perform satisfactorily in test cases, increasing model stability to the point of allowing the time step to double (Dietrich *et al.*, 2005).

Le Dissez *et al.* (2005) proposed a new finite volume hydrodynamic model in which the WD was handled by incorporating a Darcy term into the Navier-Stokes equations along with a phase function *C*. The phase function varied in time according to the prevailing flow conditions. The implementation of the Darcy term was essentially a penalty method (Khadra *et al.*, 2000) that was turned on and off by a coefficient value *K* representing porosity of the element or cell. The value of *K* (and thus the activation of the Darcy term) was controlled by the phase function (i.e. if $C = 1$, then *K* is sufficiently small to make the cell impermeable; if $C < 1$, then *K* is sufficiently large to allow flow into the cell). This approach was shown to work well on both a series of one-dimensional test cases along with a tidal simulation of the Arcachon lagoon. The results showed good agreement with accepted model results that had been validated against field measurements.

Delft3D-FLOW (Deltares, 2009) is a finite difference model commonly used in consulting projects worldwide. Its WD scheme is typical of finite difference models in that a series of checks are performed to determine if a grid point is wet or dry based on the depth of water relative to a threshold value specified by the user. If it is wet, it is included in the computations; if it is dry, it is not. If the water depth at a cell face drops below the threshold (or a specified

fraction of the threshold) then the velocity across that face is set to zero and no momentum or mass transfer occurs. This system, while simple, is robust and effective. Vatvani *et al.* (2002) provided a summary of the WD scheme in Delft3D along with their case study of the Bay of Bengal, India.

Another finite difference model commonly used in consulting and research projects is MIKE 21 developed by DHI (DHI, 2007). This software operates on a rectangular grid and somewhat uniquely specifies two separate flooding and drying depth criteria. This allows the user to specify one coefficient that establishes when a cell is considered flooded (and added to the computations) and another coefficient for when a cell is considered dried (and removed from the computations). The recommended values for the flooding and drying depth criteria 0.2 meters to 0.4 meters and 0.1 meter to 0.2 meters, respectively with a recommended difference between the two parameters of 0.1 meters (DHI, 2007). Bekic *et al.* (Bekic *et al.*, 2006) modify these parameters in order to calibrate their model of the Clyde Estuary in Glasgow, Scotland. MIKE 21 has also been used in many flooding and drying applications including the Bay of Bengal (Madsen & Jakobsen, 2004), Mele Bay and Port Vila in Vanuatu (Klein, 1998), and Oualidia Lagoon in Morocco (Hilmi *et al.*, 2005).

In addition to studies of coastal and estuarine circulation, WD schemes have also been applied to wave overtopping models such as Hu *et al.* (2000). In this case, a one-dimensional model was developed to simulate wave propagation and overtopping over idealized cases such as steps and sloping beaches as well as common coastal structures such as seawalls (sloping, vertical rock

armored). Similar to circulation models, minimum wetting depths along with minimum friction depths (i.e. the minimum depth used to calculate friction losses) were employed to control WD.

2.4 Depth Extrapolation Algorithms

For this set of algorithms, the conditions at the wetting front are given special consideration and play the vital role in advancing the water's edge in the model. In most cases, the depth is extrapolated from wet cells onto dry cells if the conditions warrant. An example of the conditions being too restrictive to allow this is an area where the bottom friction coefficient prevents the advancement of low energy flows. If the depth is able to be extrapolated from a wet cell onto a dry cell, then these new depths are used to compute velocities and the elements or cells are now part of the wet domain (until they become dry, that is). Please refer to Figure 2.2, Group 3 for an illustration of this algorithm.

Lynett *et al.* (2002) used linear extrapolation from the wet region into the dry in the WD scheme of their finite difference model designed to simulate wave runup. The extrapolation process proceeded by locating and analyzing the boundary area between the wet and dry regions. The free surface in the dry region was estimated using one-dimensional linear interpolation and averaging. The interpolation then proceeded to the next level of dry cells, based on the first level of interpolated values in formerly dry cells. The only situation this scheme could not address was a wet region surrounded by dry cells. In this case, the wet area was removed from the computational domain and its water levels were linearly extrapolated as well. This method was validated in both the one- and two-dimensional spaces using an idealized domain and sinusoidal wave forcing.

In the development of their shallow water flooding model, Bradford & Sanders (2002) sought to overcome the limitations of the contemporary WD schemes employed in finite volume methods. In order to address the problem of numerical instabilities generated by very small depths in a partially wet cell as a result of the averaging of depths from wet and dry nodes, a depth tolerance value ε was defined; velocities were only calculated if the depth exceeded this tolerance. This issue was of particular importance in terms of model sensitivity when the bed friction was parameterized using Manning's n. The issue of averaging the depths at the nodes of a partially wet cell also caused artificial leakage into adjacent cells by unrealistically wetting cell faces. This issue was resolved by extrapolating the elevation of the free surface from the neighboring fully wet cell. Lastly, spurious water movement can be induced in cells with sloping bed topographies. To manage this condition, the model did not solve the momentum equations in partially wet cells but rather extrapolated the velocity from the neighboring fully wet cell with the largest water depth.

Begnudelli & Sanders (2006) proposed a geometric method for WD in their finite volume model. They stated that since the finite volume model uses the average depth in a cell applied at the centroid to indicate water volume, this could lead to errors particularly over irregular topography. For example, it is possible that the free surface elevation can be below the topographic elevation of the centroid. To deal with this, they proposed the volume/free-surface relationships (VFR) method to model partially wet cells that differentiated between the free surface elevation and the depth at the centroid. VFRs calculated the elevation of the free surface or average depth (depending on the solution mode, either forward or inverse) after determining the number of wet nodes (for triangular elements, this can be zero, one, two or three). This

approach was tested in the aforementioned paper and also applied in future modeling studies conducted by (Begnudelli & Sanders, 2007; Begnudelli *et al.*, 2008; Sanders, 2007, 2008; Sanders *et al.*, 2008). Please note that the operational version of this model is known as BreZo.

2.5 Negative Depth Algorithms

Negative depth algorithms are closely aligned with porosity schemes. In these cases, the water surface exists below the ground surface, allowing the governing equations to be computed over the entire domain. Areas with negative depths are considered dry. The sub-surface flow conditions are controlled with porosity terms. As the flow depth increases and eventually becomes positive, the wetting of dry cells is simulated. Please refer to Figure 2.2, Group 4 for an illustration of this concept.

Heniche *et al.* (2000) created a WD scheme that relied on the natural extent of the wetting front, i.e. the natural edge where the water surface intersects with the ground surface, a concept that can be easily visualized in a realistic sense. However, the WD scheme in this finite element model allowed the water surface to plunge beneath the topographic surface producing negative water depths. The computations were allowed to proceed by imposing a high friction coefficient in dry areas (i.e. cells with a negative depth), effectively preventing current velocities. In the end, the three test cases proved that mass and momentum are fully conserved in situations of relatively slow and stable wetting front propagation. The authors did concede that this scheme was not well suited to dam break problems.

Using a similar WD concept and the finite element model RMA2 (Donnell, 2008), Nielsen and Apelt (2003) described the class of WD algorithms known as “thin slot”, in particular the form known as marsh porosity. In this WD scheme, flow was allowed to plunge beneath the surface and flow in a low porosity medium. Mass conservation was maintained by transforming the water depth to an equivalent depth. This scheme, applied to four test cases, shows that the selection of WD parameters heavily influences the results.

Similarly to the marsh porosity method, Jiang and Wai (2005) employed a scheme known as the capillary method to their three-dimensional finite element model. This scheme implements a network of capillaries that connect dry cells together just below the minimum water level (i.e. the capillaries are always wet.) This enables the water surface in a dry cell to vary naturally along with that of the nearby wet cells through a modification of the continuity equation but not the momentum equations. Therefore, mass is conserved through the capillaries and since the momentum equations only act on wet cells, momentum is conserved as well. This particular formulation shows great potential in simulating tidal recession from coastal marshes and tidal flats that tend to leave behind wet pools. The method was tested in an idealized case of a basin with varying slope similar to that of LeClerc *et al.* (1990) and also a real application to the Xiamen Estuary in China.

While TELEMAC-2D was previously listed as utilizing an element removal algorithm, newer versions also employ a negative depth scheme (Lang, 2010a, 2010b) with a multitude of options for treating negative depths as they occur including smoothing, establishing a threshold parameter for smoothing, and ensuring positivity.

2.6 Discussion

A variety of schemes have been developed to address WD in coastal hydrodynamic model formulations and codes. A summary of the WD algorithms is presented in Table 2.1: Summary of WD algorithm categories and could serve as a quick reference to a practicing modeler seeking to determine which model (or WD algorithm) to apply to a given research project. The columns represent the most important facets of a WD algorithm from the point of view of a coastal modeler: What popular models use this type of WD algorithm? What numerical schemes employ this type of WD algorithm? How well does it conserve mass globally and locally? How well does it capture the fundamental physics of an advancing/receding wetting front?

Those that specify a thin film of fluid over the entire domain in order to compute the equations of mass and momentum conservation over the entire domain at every time step are computationally more expensive but generally conserve mass and momentum with little or no correction. They also tend to produce smooth solutions at the wetting front. However, this is all predicated on the fact that a fictitious layer of fluid exists over the entire domain, or in the case of some hybrid algorithms, those regions that are eligible to wet and dry. Whether or not this can be classified as truly “capturing the physics” is a matter of perspective.

Algorithms that employ checking routines to determine if an element or node is wet, dry or potentially one of the two and subsequently removing dry elements from the computational domain are the most common and employed in finite difference, finite element and finite volume models. Algorithms of this type save computational cost by not operating on the entire domain at each time step, however, issues concerning the rapid toggling on or off of elements as they

become wet or dry near the wetting front as well as accelerating or dampening the overland flood wave propagation (especially in flat areas) has been an issue, especially in models with implicit solvers. This can be overcome by increasing the spatial resolution of the mesh or by reducing the time step. Furthermore, implementing an explicit solver can also reduce spurious noise at the wetting front. Also, the implementation of discontinuous Galerkin (DG) basis functions within finite element models enforces local mass conservation and produces excellent solutions (although more costly computationally) in a wide variety of problems ranging from bottom up flooding to dam-break scenarios.

Algorithms that extrapolate the fluid depth from wet nodes onto dry nodes and compute the velocities in the newly wet element tend to produce very smooth solutions at the wetting front. However, this occasionally comes at the expense of artificially wetting dry elements, a problem that is managed by sub-algorithms such as VFR (Begnudelli & Sanders, 2006). Extrapolation schemes tend to be used almost exclusively by finite volume models. Mass is conserved using correction schemes as clearly the extrapolation of the water surface introduces new mass into the system. However, the magnitude of this increase is commensurate with that which would exist in reality under the given circumstances; therefore one can state that the scheme realistically conserves mass.

Lastly, WD algorithms that allow the model to tolerate negative water depths and permit the simulated water surface to extend below ground tend to be used exclusively in finite element models. This category of WD algorithms most closely captures the actual physical processes at work since the wetting front does in fact penetrate the ground surface in reality. Also, no mass is

ever artificially introduced into the system (as in thin film and depth extrapolation type algorithms). The implementation of the porosity (both above and below the ground surface) concept shows particular promise in modeling the wetting front in a most natural and intuitive manner.

When discussing the capture of physics, it is essential to make a distinction between a mathematically rigorous treatment of the processes within the model and the smoothness, continuity and realistic appearance of the results. Mathematically rigorous schemes often require damping of numerical instabilities during run-time in order to produce a usable solution. On the other hand, schemes that are more loosely based on the physics tend to produce more natural and realistic looking results. It is up to the modeler to apply his/her judgment in selecting a WD scheme to meet their individual needs and the needs of their project. To that end, more rigorous comparison testing of WD algorithms is required.

In order to facilitate the aforementioned rigorous model testing, accurate benchmark data from reproducible real world events is necessary. This will enable direct, measurable performance tests of a particular model's ability to simulate wetting and drying. Furthermore, it will provide crucial information that will allow WD algorithm developers to correct, refine and establish the scope and applicability of their schemes for real world applications. However, at the present time, these types of data are scarce. High water marks generated during an inundation event and documented after the storm passes are typically readily available but require significant quality control as many factors including meteorological conditions, wind wave influences and human error often negatively impacts the accuracy of these data. Furthermore, they have no time

signature therefore serve only to validate the model in a peak water level context with no indication of the performance of the WD algorithm. Water level time series data is also readily available, but typically only located at established river gauge stations or offshore buoys. This prevents them from assessing how well a model captures the progression of the wetting front as their water level measurements secondarily rely on the topography data to infer the extent of inundation. The most beneficial benchmark data to measure the WD performance of a model would be spatially-accurate time-stamped inundation extents. The development of methods to generate these benchmark data is addressed briefly in the conclusion.

Table 2.1: Summary of WD algorithm categories

Algorithm Category	Examples	Numerical Scheme Applications	Mass Conservation	Physics Capture
Thin Film	POM FVCOM	FE, FV	Adequate, but requires correction after water levels are computed.	Alters the nature of the physics by having thin layer of fluid on "dry" cells, however it produces smooth and realistic wetting fronts.
Element Removal	TELEMAC-2D EFDC ADCIRC Delft3D-FLOW MIKE 21	FE, FD, FV	Dependent on model. Most models conserve mass globally. Newer models using FE Discontinuous Galerkin approach conserve mass locally.	Excellent due to subgrid correction schemes. Tend to perform better on advancing wetting fronts than receding.
Depth Extrapolation	BreZo	FD, FV	Generally yes, with correction procedures required in most cases.	Very good in a wide variety of flow scenarios due to advanced correction schemes such as VFR.
Negative Depth	RMA2	FE	Conserves well on slow moving fronts. Performance dependent on specification of WD parameters.	Same as mass conservation.

2.7 Conclusions and Future Research

Wetting and Drying (WD) algorithms are important to the accurate and useful simulation of overland flooding and inundation. WD is still a non-trivial challenge to numerical modelers in that often times stable, smoothly varying solutions prove to be inaccurate and accurate solutions require very high spatial and temporal resolutions that are computationally costly and frequently unstable. The review conducted herein determined that WD algorithms generally fall into one of four categories: 1) thin film algorithms; 2) element removal algorithms; 3) depth extrapolation

algorithms; and 4) negative depth algorithms. Each scheme has benefits and drawbacks in terms of its applicability to a variety of models, mass conservation both locally and globally, and the capture of the physics.

While this paper presents a review of WD algorithms currently and formerly in use, it could also serve as a starting point for a qualitative comparison between models in terms of their ability to simulate WD over a real domain. This task is non-trivial in that it requires testing of the numerical efficiency of the method as well as its ability to accurately simulate the movement of the wetting front (Leclerc *et al.*, 1990). A study of this type could begin with a comparison of model performance in a still water test for stability such as Liang and Marche (Liang & Marche, 2009), proceed to synthetic test cases for which there are analytical solutions such as the parabolic bowl test case (Thacker, 1981), Leclerc test case (Leclerc *et al.*, 1990) or the quarter-annular harbor (Lynch & Gray, 1978), and conclude with a series of real world scenarios. The latter test requires benchmark data sets that are both temporally and spatially defined. In the case of shallow water equation models, a spatial data set depicting the extent of the inundated area at a particular time would be invaluable. Research into using remotely sensed data to provide this type of benchmark data has been conducted by Richards *et al.* (1987), Hess *et al.* (1990), Smith (1997), Horritt (2001) and Chaouch *et al.* (2011), and has been put into practice by Cobby *et al.* (2003), Mason *et al.* (2003) and Oey *et al.* (2007).

2.8 Acknowledgments

The authors wish to thank Ammarin Daranpob and especially Peter Bacopoulos of the University of Central Florida for their editorial assistance and advice. The authors also wish to thank Jesse

Feyen and Yuji Funakoshi of NOAA CSDL for their assistance. This research is funded in part by NASA Earth Sciences Division, Research Opportunities in Space and Earth Science (ROSES) Grant Number NNX09AT44G. The statements, findings, conclusions, and recommendations expressed herein are those of the authors and do not necessarily reflect the views of NASA.

2.9 References

Ambati, V. R. 2006. *Flooding and drying in discontinuous galerkin discretizations of shallow water equations*. Paper presented at the ECCOMAS CFD 2006, European Conference on Computational Fluid Dynamics, TU Delft, The Netherlands.

Balzano, A. 1998. Evaluation of methods for numerical simulation of wetting and drying in shallow water flow models. *Coastal Engineering, 34*, 83-107.

Bates, P. D. 2000. Development and testing of a subgrid-scale model for moving-boundary hydrodynamic problems in shallow water. *Hydrological Processes, 14*, 2073-2088.

Bates, P. D., & Anderson, M. G. 1993. A two-dimensional finite-element model for river flow inundation. *Proceedings of the Royal Society of London, Series A, 440*, 481-491.

Bates, P. D., & Hervouet, J.-M. 1999. A new method for moving-boundary hydrodynamic problems in shallow water. *Proceedings of the Royal Society of London, Series A, 455*, 3107-3128.

Begnudelli, L., & Sanders, B. F. 2006. Unstructured Grid Finite-Volume Algorithm for Shallow-Water Flow and Scalar Transport with Wetting and Drying. *Journal of Hydraulic Engineering, 132*(4), 371-384.

Begnudelli, L., & Sanders, B. F. 2007. Conservative Wetting and Drying Methodology for Quadrilateral Grid Finite-Volume Models. *Journal of Hydraulic Engineering, 133*(3), 312-322. doi: 10.1061/(ASCE)0733-9429(2007)133:3(312)

Begnudelli, L., Sanders, B. F., & Bradford, S. F. 2008. Adaptive Godunov-Based Model for Flood Simulation. *Journal of Hydraulic Engineering, 134*(6), 714-725.

Bekic, D., Ervine, D. A., & Lardet, P. 2006. *A comparison of one- and two-dimensional model simulation of the Clyde Estuary, Glasgow*. Paper presented at the 7th International Conference on HydroScience and Engineering (ICHE 2006), Philadelphia, PA USA.

Bokhove, O. 2005. Flooding and Drying in Discontinuous Galerkin Finite-Element Discretizations of Shallow-Water Equations. Part 1: One Dimension. *Journal of Scientific Computing, 22 and 23*, 47-82. doi: 10.1007/s10915-004-4136-6

Bradford, S. F., & Sanders, B. F. 2002. Finite-Volume Model for Shalow-Water Flooding of Arbitrary Topography. *Journal of Hydraulic Engineering, 128*(3), 289-298.

Brufau, P., Vàzquez-Cendòn, M. E., & Garcìa-Navarro, P. 2002. A numerical model for the flooding and drying of irregular domains. *International Journal for Numerical Methods in Fluids, 39,* 247-275. doi: 10-1002/fld.285

Bunya, S., Kubatko, E. J., Westerink, J. J., & Dawson, C. 2009. A wetting and drying treatment for the Runge-Kutta discontinuous Galerkin solution to the shalow water equations. *Computer Methods in Applied Mechanics and Engineering, 198,* 1548-1562. doi: 10.1016/j.cma.2009.01.008

Carniello, L., Defina, A., Fagherazzi, S., & D'Alpaos, L. 2005. A combined wind wave-tidal model for the Venice lagoon, Italy. *Journal of Geophysical Research, 110*(F04007), 1-15. doi: 10.1029/2004JF000232

Casulli, V., & Cheng, R. T. 1992. Semi-implicit finite difference methods for three-dimensional shallow water flow. *International Journal for Numerical Methods in Fluids, 15,* 629-648.

Casulli, V., & Walters, R. A. 2000. An unstructured grid, three-dimensional model based on the shallow water equations. *International Journal for Numerical Methods in Fluids, 32,* 331-348.

Cea, L., French, J. R., & Vásquez-Cendón, M. E. 2006. Numerical modelling of tidal flows in complex estuaries including turbulence: An unstructured finite volume solver and experimental validation. *International Journal for Numerical Methods in Engineering, 67,* 1909-1932. doi: 10.1002/nme.1702

Chaouch, N., Temimi, M., Hagen, S. C., Weishampel, J. F., Medeiros, S. C., & Khanbilvardi, R. 2011. A synergetic use of satellite imagery from SAR and optical sensors to improve coastal flood mapping in the Gulf of Mexico. *Hydrological Processes, In Press*. doi: 10.1002/hyp.8268

Chen, C., Huang, H., Beardsley, R. C., Liu, H., Xu, Q., & Cowles, G. 2007. A finite volume numerical approach for coastal ocean circulation studies: Comparisons with finite difference models. *Journal of Geophysical Research, 112*(C03018), 1-34. doi: 10.1029/2006JC003485

Chen, C., Liu, H., & Beardsley, R. C. 2003. An Unstructured Grid, Finite-Volume, Three-Dimensional, Primitive Equations Ocean Model: Application to Coastal Ocean and Estuaries. *Journal of Oceanic and Atmospheric Technology, 20,* 159-186.

Chen, C., Qi, J., Li, C., Beardsley, R. C., Lin, H., Walker, R., & Gates, K. 2008. Complexity of the flooding/drying process in an estuarine tidal-creek salt-marsh system: An application of FVCOM. *Journal of Geophysical Research, 113*(C07052), 1-21. doi: 10.1029/2007/JC004328

Cobby, D. M., Mason, D. C., Horritt, M. S., & Bates, P. D. 2003. Two-dimensional hydraulic flood modelling using a finite-element mesh decomposed according to vegetation and topographic features derived from airborne scanning laser altimetry. *Hydrological Processes, 17*, 1979-2000. doi: 10.1002/hyp.1201

D'Alpaos, L., & Defina, A. 2007. Mathematical modeling of tidal hydrodynamics in shallow lagoons: A review of open issues and applications to the Venice lagoon. *Computers & Geosciences, 33*, 476-496. doi: 10.1016/j.cageo.2006.07.009

de Brye, B., de Brauwere, A., Gourgue, O., Kärnä, T., Lambrechts, J., Comblen, R., & Deleersnijder, E. 2010. A finite-element, multi-scale model of the Scheldt tributaries, river, estuary and ROFI. *Coastal Engineering, 57*, 850-863. doi: 10.1016/j.coastaleng.2010.04.001

Defina, A. 2000. Two-dimensional shallow flow equations for parrtially dry areas. *Water Resources Research, 36*(11), 3251-3264.

Defina, A., D'Alpaos, L., & Matticchio, B. 1994. *A new set of equations for very shallow water and partially dry areas suitable to 2D numerical models*. Paper presented at the Modelling flood propagation over initially dry areas, Milan, Italy.

Deltares. 2009. *Delft-3D-FLOW: Simulation of multi-dimensinal hydrodynamic flows and transport phenomena, including sediments - User Manual*. Delft, The Netherlands: Deltares.

DHI. 2007. *MIKE 21 Flow Model, Hydrodynamic Module, User Guide*.

Dietrich, J. C., Kolar, R. L., & Westerink, J. J. 2005. *Refinements in Continuous Galerkin Wetting and Drying Algorithms*. Paper presented at the Estuarine and Coastal Modeling, Charleston, SC.

Donnell, B. P. 2008. Users Guide to RMA2 WES Version 4.5 (E. R. a. D. C. US Army, W. E. Station & C. a. H. Laboratory, Trans.).

Donnelly, J. P., & Bertness, M. D. 2001. Rapid shoreward encroachment of salt marsh cordgrass in response to accelerated sea-level rise. *Proceedings of the National Academy of Sciences of the United States of America, 98*(25), 14218-14223. doi: 10.1073/pnas.251209298

Falconer, R. A., & Chen, Y. P. 1991. An improved representation of flooding and drying and wind stress effects in a 2-D numerical model. *Proceedings of the Institute of Civil Engineers, Part 2, Research and Theory, 91*, 659-687.

Fortin, M., & Fortin, A. 1985. Newer and Newer elements in Incompressible Flow. *Finite Elements in Fluids, 6*, 171-187.

Galland, J.-C., Goutal, N., & Hervouet, J. M. 1991. TELEMAC: A new numerical model for solving shallow water equations. *Advances in Water Resources, 14*(3), 138-148.

Greenberg, D. A., Shore, J. A., Page, F. H., & Dowd, M. 2005. A finite element circulation model for embayments with drying intertidal areas and its application to the Quoddy region of the Bay of Fundy. *Ocean Modelling, 10*, 211-231. doi: 10.1016/j.ocemod.2004.06.005

Hamrick, J. M. 1992. A three-dimensional Environmental Fluid Dynamics Computer Code: theoretical and computational aspects (Vol. Special Report 317, pp. 63). Williamsburg, VA: The College of William and Mary, Virginia Institute of Marine Science.

Hamrick, J. M. 1994. Application of the EFDC, environmental fluid dynamics computer code to SFWMD Water Conservation Area 2A (pp. 1-126). West Palm Beach, FL: South Florida Water Management District.

Hardy, R. J., Bates, P. D., & Anderson, M. G. 2000. Modeling suspended deposition on a fluvial floodplain using a two-dimensional dynamic finite element model. *Journal of Hydrology, 229*, 202-218.

Heniche, M., Secretan, Y., Boudreau, P., & Leclerc, M. 2000. A two-dimensional finite element drying-wetting shallow water model for rivers and estuaries. *Advances in Water Resources, 23*, 359-372.

Hervouet, J.-M., & Janin, J.-M. 1994. *Finite element algorithms for modelling flood propagation*. Paper presented at the Modelling flood propagation over initially dry areas, Milan, Italy.

Hervouet, J. M. 2000. TELEMAC modelling system: an overview. *Hydrological Processes, 14*, 2209-2210.

Hess, L. L., Melack, J. M., & Simonett, D. S. 1990. Radar detection of flooding beneath the forest canopy: a review. *Internation Journal of Remote Sensing, 11*(7), 1313-1325.

Hilmi, K., Koutitonsky, V. G., Orbi, A., Lakhdar, J. I., & Chagdali, M. 2005. Oualidia lagoon, Morocco: an estuary without a river. *African Journal of Aquatic Science, 30*(1), 1-10.

Horritt, M. S. 2001. Calibration of a 2-dimensional finite element flood flow model using satellite radar imagery. *Water Resources Research, 36*(11), 3279-3291.

Horritt, M. S., & Bates, P. D. 2001. Predicting floodplain inundation: raster-based modelling versus the finite-element approach. *Hydrological Processes, 15*, 825-842.

Hu, K., Mingham, C. G., & Causon, D. M. 2000. Numerical simulation of wave overtopping of coastal structures using the non-linear shalow water equations. *Coastal Engineering, 41*, 433-465.

Hubbert, G. D., & McInnes, K. L. 1999. A Storm Surge Inundation Model for Coastal Planning and Impact Studies. *Journal of Coastal Research, 15*(1), 168-185.

Ji, Z.-G., Morton, M. R., & Hamrick, J. M. 2001. Wetting and Drying Simulation of Estuarine Processes. *Estuarine, Coastal and Shelf Science, 53*, 683-700.

Jiang, Y. W., & Wai, O. W. H. 2005. Drying-wetting approach for 3D finite element sigma coordinate model for estuaries with large tidal flats. *Advances in Water Resources, 28*, 779-792. doi: 10-1016/j.advwatres.2005.02.004

Khadra, K., Angot, P., Parneix, S., & Caltagirone, J.-P. 2000. Fictitious domain approach for numerical modelling of Navier-Stokes equations. *International Journal for Numerical Methods in Fluids, 34*, 651-684.

King, I. P., & Roig, L. C. 1988. *Two-dimensional finite element models for floodplains and tidal flats*. Paper presented at the Proceedings of an International Conference on Computational Methods in Flow Analysis, Okayama, Japan.

Klein, R. 1998. Hydrodynamic Simulation with MIKE21 of Mele Bay and Port Vila, Vanuatu (pp. 63): SOPAC.

Kolar, R. L., Westerink, J. J., Gray, W. G., & Luettich, R. A. 1994. Shallow water modeling in spherical coordinates: Equation formulation, numerical implementation, and application. *Journal of Hydraulic Research, 32*(1), 3-24.

Lang, P. 2010a. TELEMAC modelling system, 2D hydrodynamics, TELEMAC-2D Software, Version 6.0, Reference Manual (pp. 92): EDF-DRD.

Lang, P. 2010b. TELEMAC modelling system, 2D hydrodynamics, TELEMAC-2D software, Version 6.0, User Manual (pp. 118): EDF-DRD.

Le Dissez, A., Sous, D., Vincent, S., Caltagirone, J.-P., & Sottolichio, A. 2005. A novel implicit method for coastal hydrodynamics modeling: application to the Arcachon lagoon. *Comptes Rendus Mecanique, 333*, 796-803.

Leclerc, M., Bellemare, J.-F., Dumas, G., & Dhatt, G. 1990. A finite element model of estuarian and river flows with moving boundaries. *Advances in Water Resources, 13*(4), 158-168. doi: 10.1016/0309-1708(90)90039-7

Liang, Q., & Borthwick, A. G. L. 2009. Adaptive quadtree simulation of shallow water flows with wet-dry fronts over complex topography. *Computers & Fluids, 38*, 221-234. doi: 10.1016/j.compfluid.2008.02.008

Liang, Q., & Marche, F. 2009. Numerical resolution of well-balanced shallow water equations with complex source terms. *Advances in Water Resources, 32*, 873-884. doi: 10.1016/j.advwatres.2009.02.010

Lin, H.-C. J., Cheng, H.-P., Edris, E. V., & Yeh, G.-T. 2004. *Modeling surface and subsurface hydrologic interactions in a south Florida watershed near the Biscayne Bay*. Paper presented at the 15th International Conference on Computational Methods in Water Resources (CMWR XV), Chapel Hill, NC. http://www.sciencedirect.com/science/article/B8G6B-4P40D5C-21/2/e8771eed5921a1eba09dd8c92d2b8e80

Löhner, R. 1990. Progress in Grid Generation via the Advancing Front Technique. *Engineering with Computers, 12*, 186-210.

Lu, Q. 2003. *A three-dimensional modeling of tidal circulation in coastal zones with wetting and drying process*. Paper presented at the International Conference on Estuaries and Coasts, Hangzhou, China.

Luettich, R. A., & Westerink, J. J. 1995a. An Assessment of Flooding and Drying Techniques for Use in the ADCIRC Hydrodynamic Model: Implementation and Performance in One-Dimensional Flows: Department of the Army.

Luettich, R. A., & Westerink, J. J. 1995b. Implementation and Testing of Elemental Flooding and Drying in the ADCIRC Hydrodynamic Model: Department of the Army.

Luettich, R. A., & Westerink, J. J. 1999. Elemental Wetting and Drying in the ADCIRC Hydrodynamic Model: Upgrades and Documentation for ADCIRC Version 34.XX: Department of the Army.

Luettich, R. A., & Westerink, J. J. 2006. ADCIRC: A Paralell Advanced Circulation Model for Oceanic, Coastal and Estuarine Waters. *adcirc.org*. Retrieved from http://adcirc.org/documentv46/ADCIRC_title_page.html

Luettich, R. A., Westerink, J. J., & Scheffner, N. W. 1992. ADCIRC: An advanced three-dimensional circulation model for shelves, coasts, and estuaries, Report 1: Theory and methodology of ADCIRC-2DDI and ADCIRC-3DL (pp. 1-137). Vicksburg, Mississippi: Department of the Army, US Amry Corps of Engineers, Waterways Experiment Station.

Lynch, D. R., & Gray, W. G. 1978. Analytic Solutions for Computer Flow Model Testing. *Journal of the Hydraulics Division, 104*(HY10), 1409-1428.

Lynch, D. R., & Gray, W. G. 1980. Finite Element Simulation of Flow in Deforming Regions. *Journal of Computational Physics, 36*, 135-153.

Lynch, D. R., & Werner, F. E. 1991. Three-dimensional hydrodynamics on finite elements. Part II: Nonlinear time-stepping model. *International Journal for Numerical Methods in Fluids, 12*, 507-533.

Lynett, P. J., Wu, T.-R., & Liu, P. L.-F. 2002. Modeling wave runup with depth-integrated equations. *Coastal Engineering, 46*, 89-107.

Madsen, H., & Jakobsen, F. 2004. Cyclone induced storm surge and flood forecasting in the northern Bay of Bengal. *Coastal Engineering, 51*, 277-296. doi: 10.1016/j.coastaleng.2004.03.001

Mason, D. C., Cobby, D. M., Horritt, M. S., & Bates, P. D. 2003. Floodplain friction parameterization in two-dimensional river flood models using vegetation heights derived from airborne scanning laser altimetry. *Hydrological Processes, 17*, 1711-1732. doi: 10.1002/hyp.1270

Matsumoto, J., Khan, A. A., Wang, S. S. Y., & Kawahara, M. 2002. Shallow Water Flow Analysis with Moving Boundary Technique Using Least-squares Bubble Function. *International Journal of Computational Fluid Dynamics, 16*(2), 129-134.

Medeiros, S. C., Ali, T. A., Hagen, S. C., & Raiford, J. P. 2011. Development of a Seamless Topographic / Bathymetric Digital Terrain Model for Tampa Bay, Florida. *Photogrammetric Engineering and Remote Sensing, 77*(12), 1249-1256.

Mellor, G. L. 2003. Users guide for a three-dimensional, primitive equation, numerical ocean model *Program in Atmospheric and Oceanic Sciences* (pp. 53 pp.): Princeton University.

Mellor, G. L., Hakkinen, S., Ezer, T., & Patchen, R. 2002. A generalization of a sigma coordinate ocean model and an intercomparison of model vertical grids. In N. Pinardi & J. D. Woods (Eds.), *Ocean Forecasting: Conceptual Basis and Applications* (pp. 55-72). New York: Springer.

Meyers III, E. P. 2005. *Review of progress on VDatum, a vertical datum transformation tool*. Paper presented at the Oceans 2005 MTS/IEEE, Washington, DC.

Morris, J. T. 2007. Ecological engineering in intertidal salt marshes. *Hydrobiologia, 577*(1), 161-168. doi: 10.1007/s10750-006-0425-4

Morris, J. T., Sundareshwar, P. V., Nietch, C. T., Kjerfve, B., & Cahoon, D. R. 2002. Responses of coastal wetlands to rising sea level. *Ecology, 83*(10), 2869-2877.

Nielsen, C., & Apelt, C. 2003. Parameters Affecting the Performance of Wetting and Drying in a Two-Dimensional Finite Element Long Wave Hydrodynamic Model. *Journal of Hydraulic Engineering, 129*(8), 628-636. doi: 10.1016/(ASCE)0733-9429(2003)129:8(628)

Oey, L.-Y. 2005. A wetting and drying scheme for POM. *Ocean Modelling, 9*, 133-150.

Oey, L.-Y., Ezer, T., Hu, C., & Muller-Karger, F. E. 2007. Baroclinic tidal flows and inundation processes in Cook Inlet, Alaska: numerical modeling and satellite observations. *Ocean Dynamics, 57*, 205-221. doi: 10.1007/s10236-007-0103-8

Parker, B. B., Hess, K., Milbert, D., & Gill, S. 2003. A national vertical datum transformation tool. *Sea Technology, 44*(9), 10-15.

Rego, J. L., & Li, C. 2009. *On the Receding of Storm Surge along Louisiana's Low-Lying Coast*. Paper presented at the 10th International Coastal Symposium, Lisbon, Portugal.

Richards, J. A., Woodgate, P. W., & Skidmore, A. K. 1987. An explanation of enhanced radar backscattering form flooded forests. *Internation Journal of Remote Sensing, 8*(7), 1093-1100.

Sanders, B. F. 2007. Evaluation of on-line DEMs for flood inundation modeling. *Advances in Water Resources, 30*, 1831-1843.

Sanders, B. F. 2008. Integration of a shallow water model with a local time step. *Journal of Hydraulic Research, 46*(4), 466-475.

Sanders, B. F., Schubert, J. E., & Gallegos, H. A. 2008. Integral formulation of shallow-water equations with anisotropic porosity for urban flood modeling. *Journal of Hydrology, 362*, 19-38.

Smith, L. C. 1997. Satelite remote sensing of river inundation area, stage and discharge: A review. *Hydrological Processes, 11*, 1427-1439.

Tchamen, G. W., & Kahawita, R. A. 1998. Modelling wetting and drying effects over complex topography. *Hydrological Processes, 12*, 1151-1182.

Thacker, W. C. 1981. Some exact solutions to the nonlinear shallow-water wave equations. *Journal of Fluid Mechanics, 107*, 499-508.

Titus, J. G., & Richman, C. 2001. Maps of lands vulnerable to sea level rise: modeled elevations along the US Atlantic and Gulf coasts. *Climate Research, 18*, 205-228. doi: 10.3354/cr018205

United States Department of Commerce. 2000. Tidal datums and their applications. Washington, D.C.: National Oceanic and Atmospheric Administration, National Ocean Service, Center for Operational Oceanographic Products and Services.

Vatvani, D. K., Gerritsen, H., Stelling, G. S., & Krishna Rao, A. V. R. 2002. *Cyclone induced storm surge and flood forecasting system for India*. Paper presented at the International Conference on Solutions to Coastal Disasters, San Diego, CA, USA.

Weisberg, R. H., & Zheng, L. 2006. Hurricane Storm Surge Simulations for Tampa Bay. *Estuaries and Coasts, 29*(6A), 899-913.

Xie, L., Pietrafesa, L. J., & Peng, M. 2004. Incorporation of a Mass-Conserving Inundation Scheme into a Three Dimensional Storm Surge Model. *Journal of Coastal Research, 20*(4), 1209-1223. doi: 10.2112/03-0084R.1

Yeh, G.-T., & Chou, F.-K. 1979. Moving boundary numerical surge model. *Journal of the Waterway, Port, Coastal and Ocean Division, 105*(WW3), 247-263.

Zhang, Y., Baptista, A. M., & Meyers III, E. P. 2004. A cross-scale model for 3D baroclinic circulation in estuary-plume-shelf systems: I. Formulation and skill assessment. *Continental Shelf Research, 24*, 2187-2214. doi: 10.1016/j.csr.2004.07.021

Zhao, L., Chen, C., Vallino, J., Hopkinson, C., Beardsley, R. C., Lin, H., & Lerczak, J. A. 2010. Wetland-estuarine-shelf interactions in the Plum Island Sound and Merrimack River in the Massachusetts coast. *Journal of Geophysical Research, 115*(C10039), 1-13. doi: 10.1029/2009JC006085

CHAPTER 3. DEVELOPMENT OF A SEAMLESS DIGITAL TERRAIN MODEL FOR TAMPA BAY, FLORIDA

The content in this chapter is published as: Medeiros, S. C., Ali, T. A., Hagen, S. C., & Raiford, J. P. 2011. Development of a Seamless Topographic / Bathymetric Digital Terrain Model for Tampa Bay, Florida. *Photogrammetric Engineering and Remote Sensing, 77*(12), 1249-1256.

3.1 Introduction and Background

Airborne Light Detection and Ranging (LiDAR) is rapidly becoming the industry standard for acquisition of topographic data due to its ability to cover large areas accurately and efficiently. It provides the user with an accurate, relatively easy to process and analyze, and cost effective means of describing the topography of large areas; this is especially useful in many engineering and environmental applications (Cobby *et al.*, 2003; Ritchie, 1996). The scientific, engineering and mapping communities have directed significant resources to developing innovative ways to capture, process and utilize LiDAR data.

One of the most promising uses of LiDAR data is its application in constructing Digital Elevation Models (DEMs). These models such as the National Elevation Dataset (Gesch *et al.*, 2002) provide an accurate means of representing the topography over regional scale sections of the Earth's surface. This type of source data is necessary for many engineering and mapping applications, including the generation of nationwide land cover datasets such as the National Land Cover Dataset (NLCD) (Homer *et al.*, 2007). DEMs are also useful in pre/post catastrophe analysis and various forms of water resources modeling due in part to readily available data for all of the coastal United States (Gesch *et al.*, 2002) and the ability to process the data using GIS

(Garbrecht & Martz, 2000). In particular, DEMs derived from LiDAR data are typically resolved enough to capture overland flow characteristics with a high degree of spatial accuracy (Poppenga *et al.*, 2009).

In this paper, LiDAR is used in conjunction with hydrographic survey data to produce a seamless model of the topographic and bathymetric surface associated with the project area (Tampa Bay, Florida, see Figure 3.1). Similar studies have been carried out by Gesch and Wilson (2001) in Tampa Bay, Feyen *et al.* (2006) in North Carolina, and Barnard and Hoover (2009) in southern California.

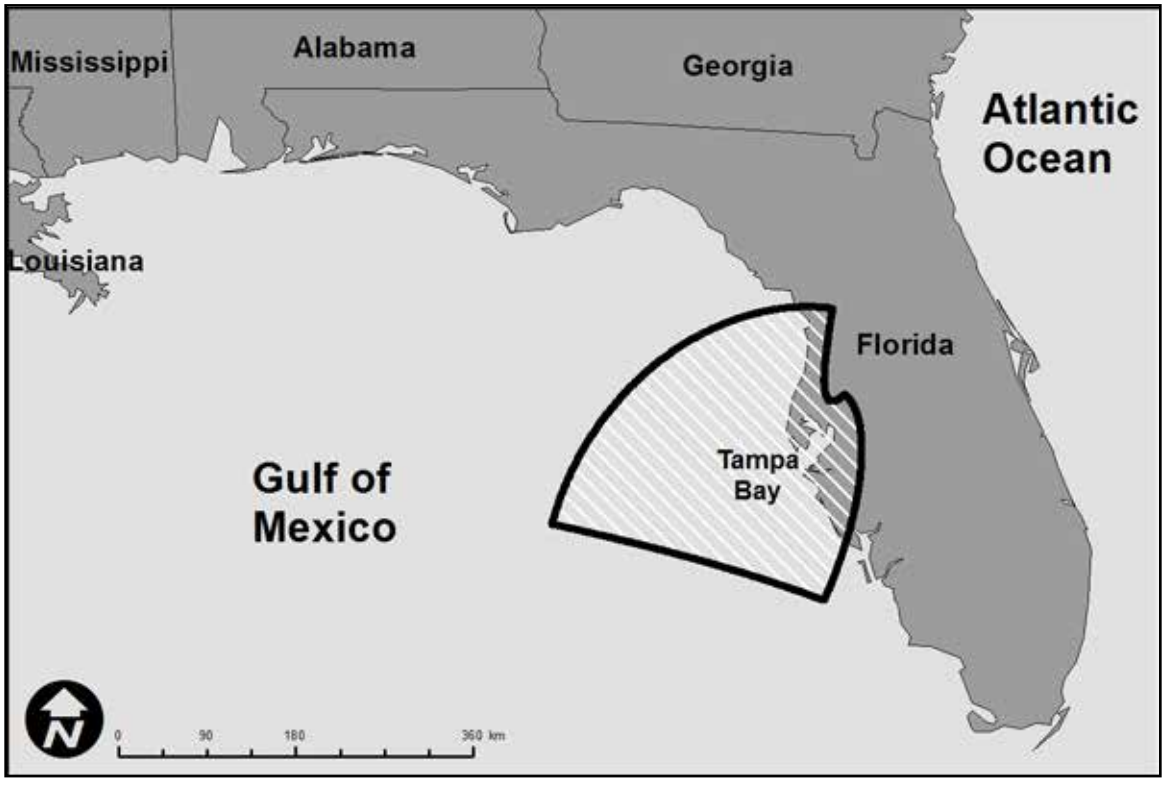

Figure 3.1: Location of Study Area

Before proceeding, it is necessary to define the following terms. These definitions are based on those presented by Maune (2007); however, they are specifically tailored to clarify the material presented herein.

- Digital Elevation Model (DEM) – A digital representation of the terrain consisting of regularly spaced (gridded) elevation data. While it is common for the term DEM to apply to bare-earth representations of terrain, it is used here as the umbrella term for all gridded elevation models;
- Digital Surface Model (DSM) – A gridded first or top surface representation of the terrain. This includes all man-made features (buildings, elevated transportation elements, monuments, etc.) lying on the bare earth; and
- Digital Terrain Model (DTM) – A gridded representation of the bare topographic surface of the Earth. All man-made structural features that are not considered part of the bare-earth surface are removed to expose the underlying terrain. DTMs typically incorporate not only point data, but also other elements such as breaklines and polygon masks in order to generate highly accurate depictions of the terrain.

According to the above-definitions, this paper seeks to produce a DTM of the study area with special consideration given to hydraulically significant features (i.e. barriers and conveyances). This will be accomplished by integrating LiDAR, bathymetric and breakline data. It should be noted that the LiDAR data is delivered as "bare earth" points; it is customary to receive data in this format from the vendor who often uses a combination of proprietary, automatic algorithms such as adaptive LiDAR vegetation point removal (Raber *et al.*, 2002) and manual editing to

filter out non-ground points (Hodgson *et al.*, 2005). Breakline data describe significant linear changes in the terrain surface, such as a riverbank or shoreline. They are used to enforce the location (horizontal and vertical) of these features during interpolation, resulting in more accurate depictions of the terrain (Maune, 2007). The final DTM will be a raster product with 50-foot resolution.

In general, bathymetry or sounding data is referenced to a tidal datum such as Mean Sea Level (MSL), Mean Low Water (MLW) or Mean Lower Low Water (MLLW). For this study, all points (bathymetric and topographic) must be referenced to the North American Vertical Datum of 1988 (NAVD88) per project specifications. The process for obtaining bathymetric data and transforming it to comply with the project's vertical datum requirement are described herein.

The general outline of the procedure used to achieve the end product is: create a bathymetric DTM using hydrographic survey data, create a topographic DTM using LiDAR and various breakline data, and finally create a seamless topobathy DTM of the entire project area. The resulting DTM will be used in a model that simulates hurricane storm surge inundation in the project area. This is a popular and well-suited application of high-resolution DTMs (NOAA, 2007) and an accurate DTM that incorporates topographic and bathymetric data is essential for inundation modeling (Gonzalez *et al.*, 2005).

3.2 Data Acquisition and Processing

The bathymetry data for the project area were obtained from the DVD-ROM entitled Geophysical Data System (GEODAS) for Gridded Bathymetric Data, NGDC Coastal Relief

Model, Volumes 01 – 08, Version 4.1.20 prepared by the National Geophysical Data Center (NGDC). This DVD contains software entitled GEODAS Reader that lets the user specify an area using latitude and longitude and extract bathymetric data. This data is horizontally referenced to the North American Datum of 1983 (NAD83) and the water depths are in meters relative to Mean Sea Level (MSL). Please note that the NDGC data set contains both bathymetric and topographic data; for the purposes of this case study, only "sea cells" were extracted at 6 arc-second resolution. Furthermore, it is also important to note that the NGDC data described above is derived from many independent hydrographic surveys dating back to the 1950's. The raw data from these hydrographic surveys reference different tidal datums such as MLW and MLLW. The use of the NGDC-processed data sets simplifies the datum adjustment process for presented herein; however, the user could apply the presented methodology to each individual hydrographic survey, provided care was taken to identify the datums and make the appropriate adjustments.

Recall that the ultimate goal of the study is to produce a seamless topobathy DTM. In order to accomplish this, all topographic and hydrographic survey data must be referenced to a common datum (NOAA, 2007), in this case NAVD88. Therefore, all bathymetry data must be transformed from MSL to NAVD88. This transformation is nontrivial because MSL varies spatially along the coastline. Fortunately, a software tool called VDatum (Gesch & Wilson, 2001; Meyers III, 2005) is being developed jointly by NOAA's National Geodetic Survey (NGS), Office of Coast Survey (OCS) and Center for Operational Oceanographic Products and Services (CO-OPS). This process is made significantly more efficient and accurate in the coastal regions through the use of this software tool (Gesch & Wilson, 2001) and the authors

acknowledge that VDatum is the best available method for transforming between tidal and orthometric vertical datums. However, this software is currently limited by its geographical coverage; in this case, it can only be used inside Tampa Bay itself leaving a significant portion of the project area untransformed. Therefore, in order to maintain consistency, VDatum will not be used to transform any of the points in this study.

With VDatum's coverage only extending to part of the study area, an interim method of transforming bathymetric data from MSL to NAVD88 based on NOAA Tidal Benchmark Station (TBS) information was adapted from the existing "Interpolation" method of datum conversion (NOAA, 2007). Tidal Benchmark Stations are NOAA-maintained water level stations that have one or more orthometric datums surveyed in at their location. These stations allow for an offset calculation between an orthometric datum and the local tidal datums (MSL, MLLW, etc.). Information derived from the TBSs located inside the study area provides the foundation for transforming the bathymetric data.

3.2.1 Tidal Benchmark Station Data

First, a database containing all tidal benchmark stations maintained by NOAA CO-OPS was obtained. The database contains an entry for each tidal benchmark station and fields listing the station's ID, Latitude, Longitude, and elevations of vertical datums (both tidal and orthometric). Please note that the raw elevations listed in the database are not referenced to any standard vertical datum; they are referenced to a local benchmark established at the station. This fact is not critical to the subject process because the differences (offsets) between tidal and orthometric data (in particular, MSL and NAVD88) are the critical values. With consideration to ease of data

import/export and processing, extraneous fields in the database were deleted and a field containing the offset between MSL and NAVD88 (in meters) was created. This modified database was then imported into ArcGIS using Tools > Add XY Data. Please note that at this point, no ArcToolbox operations can be performed on this data due to its format within ArcGIS; the user must export the data to a shapefile in order to generate an ObjectID field, thereby enabling it for geoprocessing.

Prior to use, the data was pre-processed to simplify the datum conversion. The TBS points were first clipped geographically using a 50-mile buffer around the study area boundary. The 50-mile buffer was employed to provide proper adjustment availability to bathymetry points near the northern and southern extents of the study area. Next, all stations without an elevation value (referenced to the local station benchmark) for NAVD88 were deleted because they could not generate raw offsets between MSL and NAVD88 (i.e. without further processing/calculations). This process resulted in 115 tidal benchmark stations for the project area.

However, further refinement of the TBS data was required in order to remove abnormal and inconsequential data. The primary function of this step was to avoid unrealistic offset values introduced by errors in the TBS data. Stations with abnormally large or small offset values relative to nearby stations were removed from the data set in order to avoid unrealistic offset values. More specifically, a station was removed if its offset value was larger than three times (on an absolute value basis) the value at either of the nearest two stations within 5 kilometers. Three stations were removed for this reason. Furthermore, stations that were located significantly upriver (inland) with no nearby offshore bathymetry points were also removed from

the data set. Nine stations were removed for this reason. Due to the relatively small geographic region and the limited number of potential removals, all candidates were individually inspected to confirm that their removal was reasonable.

After the above-referenced pre-processing, there were 103 Tidal Benchmark Stations remaining, shown in Figure 3.2. The last remaining task is to populate the MSL to NAVD88 offset field using the Field Calculator function in ArcGIS using the following equation (recall that elevations of NAVD88 and MSL are referenced to a local benchmark established at the tidal benchmark station):

$$\left(Elevation\ of\ NAVD88\right) - \left(Elevation\ of\ MSL\right) = Offset \tag{3.1}$$

Refer to Figure 3.3 for a graphical description of this calculation. Table 3.1 contains some examples of TBS offset values.

Figure 3.2: Location of tidal benchmark stations

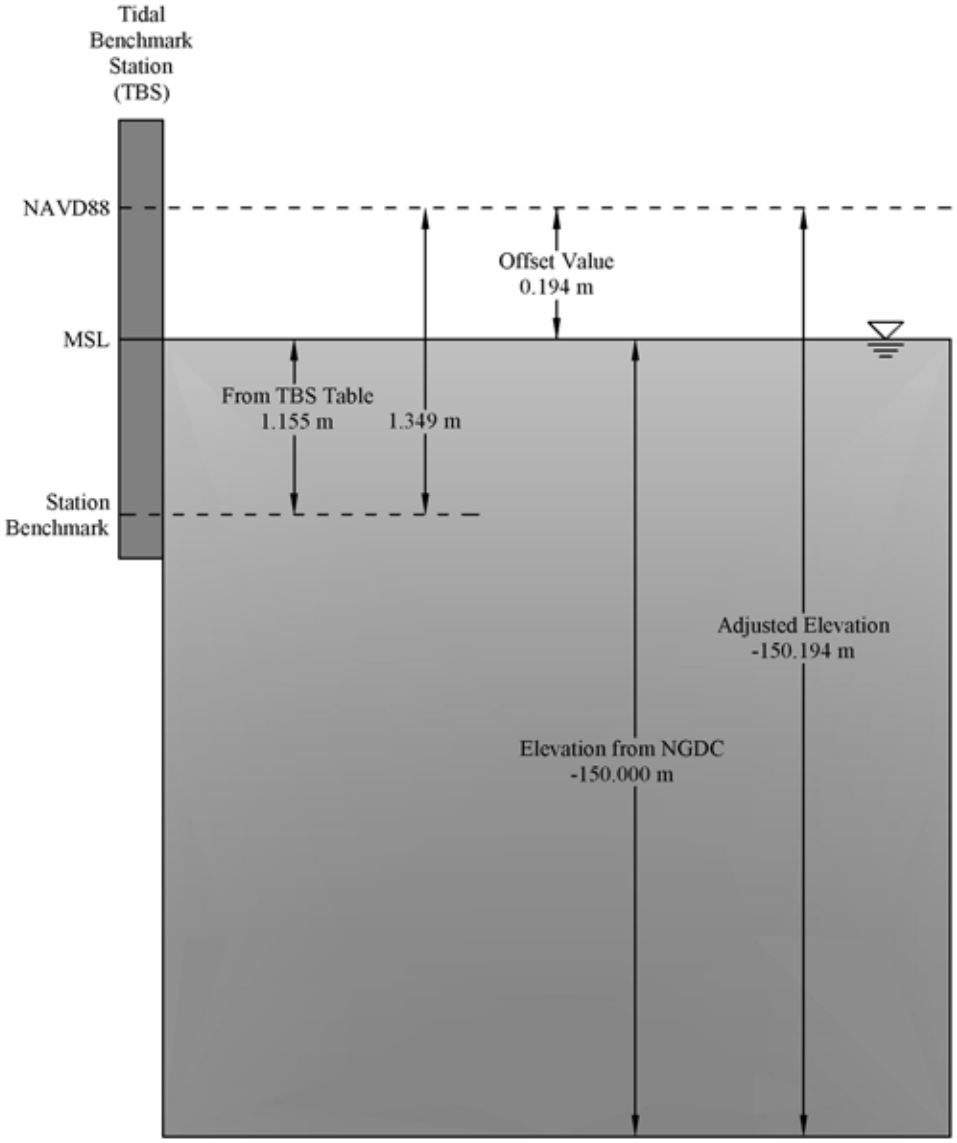

Figure 3.3: Graphical depiction of datum offset implementation (example)

Table 3.1: Tidal benchmark offset examples

Station Number	Station Name	*Elevation of NAVD88 (m)	*Elevation of MSL (m)	Offset Value (m)
8725362	TARPON BAY	1.534	1.350	0.184
8725809	MANASOTA	1.252	1.106	0.146
8726247	BRADENTON, MANATEE RIVER	0.997	0.900	0.097
8726724	CLEARWATER BEACH, GULF OF MEXICO	1.064	0.970	0.094
8727520	CEDAR KEY, GULF OF MEXICO	1.237	1.171	0.066

* Elevations of NAVD88 and MSL are referenced to a local station datum

3.2.2 Adjustment of Bathymetry Points

The next step in the process was to apply this offset to the raw bathymetry points in order to transform them from MSL to NAVD88. The dataset obtained from the NGDC was in the form of a space delimited *.xyz file. This data was converted to a Feature Class in ArcGIS initial download of bathymetry data contained approximately 2.4 million points. The Point Feature Class was then clipped to the boundary of the study; the clipped bathymetry contained approximately 1.5 million points. The XY coordinates were then added to each point in the clipped shapefile in order to continue the datum transformation process.

To summarize the process thus far, we have a point shapefile that contains all bathymetric data points and lists each point's horizontal position (latitude and longitude) and its elevation in meters. We also have a shapefile containing the tidal benchmark stations listing their horizontal position and datum offsets. Before proceeding, we must project these data into a Cartesian

system to enable the subsequent calculations. In this case, the project specifications require the use of State Plane coordinates, in particular Florida State Plane West (NAD83), units of feet.

In order to further reduce the potential for errors generated by incorrect TBS data, a three point nearest neighbor interpolation scheme is applied. The offset applied to each bathymetry point is constructed by using a weighted average of the offsets associated with the three geographically nearest TBSs according to the following formula (Shepard, 1968).

$$o_{avg} = \frac{\sum_{n=1}^{3} o_n / d_n^x}{\sum_{n=1}^{3} 1 / d_n^x} \tag{3.2}$$

Where o_{avg} is the weighted average offset, o_n is the offset associated with station n, and d_n is the distance to station n raised to an exponent x. The selection of the exponent x has been the subject of past research in two-dimensional interpolation of irregularly spaced points. Shepard (1968) recommends an exponent of two for the interpolation associated with general surface mapping (i.e. Inverse Distance Squared Weighting or Reciprocal Distance Squared Weighting). However, in this portion of the methodology, the objective is to reduce the possibility of a single erroneous station dominating the calculation of the offset. As the value of the exponent increases, the relative weight of the closest station is magnified. Therefore, for the purposes of this research, an exponent of one is deemed appropriate.

To generate the values used in Equation (3.2), a table is constructed using the freely available ArcGIS Extension known as Hawth's Tools (www.spatialecology.com/htools/tooldesc.php). In particular, the Distances Between Points (Between Layers) function was used to generate a table (comma delimited text file) consisting of each bathymetry point's ID number, and the ID number and distances of the three (3) closest tidal benchmark stations. The bathymetry points were chosen as the source layer, the tidal benchmark stations were chosen as the target point layer, and "Nearest neighbours" with 3 closest points selected as the Analysis Option. This extension builds a table consisting of each bathymetry point, it's three (3) nearest tidal benchmark stations and the horizontal distances to those stations.

Table Views of the bathymetry points and the nearest tidal benchmark stations are created in ArcGIS and named Bathymetry Table and Nearest TBM Table, respectively. These Table Views are joined yielding a new Table View called the Bathymetry-Nearest TBM Table that lists each bathymetry point, its horizontal and vertical position, and its nearest tidal benchmark stations.

Next, a Table View of the Tidal Benchmark Stations is created, named TBM Stations Table, and joined to the Bathymetry-Nearest TBM Table yielding a new Table View containing each bathymetry point, its horizontal and vertical position, nearest tidal benchmark stations (along with their distances from the point) and their associated offsets. An inverse distance weighted average offset for each bathymetry point is then calculated using Equation (3.2) above and applied by recalculating the POINT_Z attribute. We now have a file that can be used to construct the Bathymetric DEM.

3.2.3 Incorporation of Topographic Data

The major source of topographic data for the project is bare earth LiDAR and breakline products supplied by Woolpert, Inc. as part of the Florida Division of Emergency Management Coastal LiDAR Project. In order to fill in areas in parts of Hillsborough, Hernando, Citrus, Manatee, Pasco and Sarasota counties that are inside of the study area but outside of Woolpert's coverage area, the project team utilized LiDAR and breakline data from the Southwest Florida Water Management District (SWFWMD). Finally, the remaining gaps in the data for the study area were filled using the Florida Fish and Wildlife Conservation Commission (commonly referred to as the FWC) 5-meter resolution DEM. According to the metadata, the FWC DEM was generated from tagged vector contours produced by the Florida Department of Environmental Protection (FDEP) and over 90,000 surface control points. Please refer to Figure 3.4 for a geographical depiction of data sources.

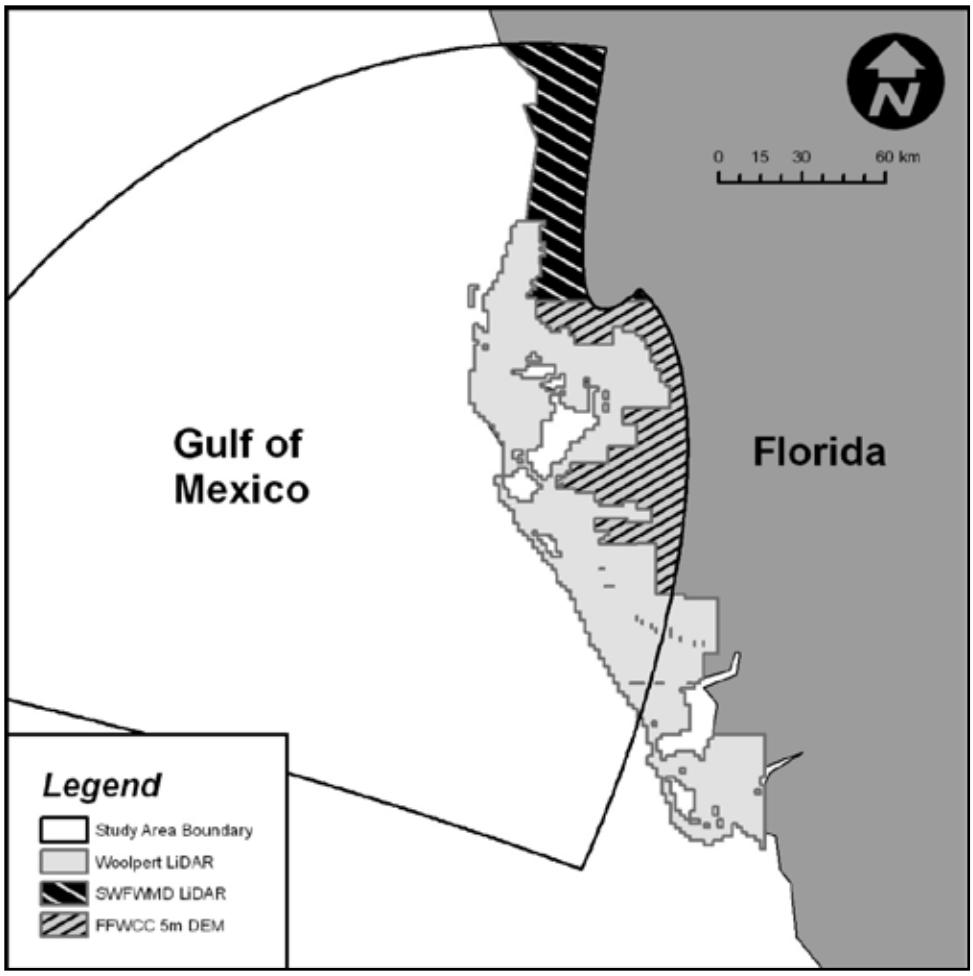

Figure 3.4: Topographic data sources

3.3 Generation of the DTM

In order to create the topographic DTM, the authors employed a framework within the ArcGIS 9.2 environment utilizing an ESRI data structure known as a Terrain Data Set (TDS). A TDS is a multi-resolution, Triangular Irregular Network (TIN) based surface constructed from raw data (LiDAR, SONAR, photogrammetric sources, etc.) and stored as a feature in a geodatabase. A TDS resides inside feature datasets within personal, file and Spatial Database Engine (SDE) geodatabases. The other feature classes in the feature dataset can either participate (i.e. be used

but not stored in the TDS) or be embedded in the TDS, allowing the source data to be archived after the creation of the TDS. This is especially efficient for working with LiDAR data as digital file sizes are routinely one terabyte (TB) or more for county scale projects. In fact, the processed bare earth LiDAR data for a 5000 foot square geographic area can contain approximately 1.1 million points (Coggin, 2008). Another advantage of a TDS is that it gives the user the ability to store and manage vector-based terrain information in the geodatabase. At this point, it is important to acknowledge the size limits for TDSs: two gigabytes (GB) in a personal geodatabase (pGDB); one TB in a file geodatabase (fGDB); and unlimited in an ArcSDE geodatabase.

The workflow for creating the topographic DTM is summarized as follows:

1. Create an fGDB and a feature dataset;
2. Convert LAS (LiDAR) data to a multipoint feature class using ArcGIS 3D Analyst Tools. Note that some of the project LiDAR data was delivered in ASCII 3D format. These data were imported using the ASCII 3D to Feature Class conversion tool.
3. Import the multipoint feature class into the feature dataset along with any other relevant project feature classes such as breaklines and the project area boundary;
4. Build the TDS using the terrain parameters shown in Table 3.2: Terrain Parameters (ESRI, 2008);
5. Extract a Raster DTM (resolution = 50-feet, per project specifications) from the TDS.

Please note that the LiDAR data points for water bodies (Class 9 in the LAS system) required separate extraction and processing. Since the type of airborne LiDAR used in this project cannot accurately depict submerged topography, other means of representing the subsurface terrain of inland water bodies was needed. The project guidelines specified that in the absence of subsurface topographic data for inland water bodies, a depth of 1-foot should be specified. The project team applied this guideline by extracting all Class 9 LAS points separately and then adding the XYZ coordinates to the point attribute table. A new field was added to the attribute table and calculated to be POINT_Z – 1, effectively creating a 1-foot deep water body.

A few narrow gaps were discovered at the edges of the different topographic LiDAR data sets. These were very minor in nature and were treated by edge matching and a low pass filter in ArcGIS. This served to eliminate the significance of the anomalous edges between LiDAR data sets.

Using the data and methodology described above, a land-only terrain surface for the Tampa Bay study area was generated. From this surface, a 50-foot resolution raster DTM was extracted.

The bathymetric DTM was created in a similar manner using the Terrain Dataset technique in ArcGIS 9.2. Using this method, a terrain surface was first created from the bathymetric "mass points" and a raster DEM was then extracted from the terrain surface. Please note that both the shoreline (NOAA Medium Resolution Shoreline, Gulf of Mexico) and study boundary were triangulated as hard clips. The use of the coastline as well as other significant breaklines is an acceptable method to constrain the DTM (Jezek *et al.*, 1999). Table 3.2: Terrain Parameters

(ESRI, 2008) contains a list of the terrain parameters. As described above, a TDS was created and a 50-foot resolution raster DTM was extracted from this surface.

Table 3.2: Terrain Parameters (ESRI, 2008)

Feature Class	Surface Feature Type (SFType)
LiDAR POINTS	Mass point (contains elevations at points or vertices of lines or polygons)
HYDROGRAPHIC FEATURES	Hard Breakline (places TIN triangle edges on line and interprets as distinct break in slope)
ROADS	Hard Breakline
ISLANDS	Hard Fill Value (uses only points in polygon to interpolate elevations for polygon cells)
SOFT FEATURES	Soft Breakline (places triangle edges along line and interprets the terrain as smooth across line)
WATER BODIES	Hard Replace Polygon (areas of constant height)
COASTAL SHORELINE	Hard Breakline
PROJECT AREA	Soft Clip Polygon (define and prevent interpolation across polygon boundaries)

In order to produce the seamless topobathy DTM, the topographic and bathymetric Terrain Data Sets were merged. There was some overlap between the bathymetric and topographic data, but the NOAA medium-resolution shoreline used in this project was employed to clip the bathymetric data. There was a slight elevation disparity at the shoreline (hard breakline) that was treated by rubber sheeting and low pass filtering in ArcGIS to reduce the significance of the anomalous edges. Once the topobathy TDS was complete and issues at the shoreline were resolved as described above, and the seamless topobathy DTM was extracted.

3.4 Results

The results of this study are the DTM raster products to be used in the hurricane storm surge modeling. Figure 3.5 depicts the topographic DTM and captures the prominent riverine features of the area including the Manatee, Little Manatee, Alafia and Hillsborough Rivers. These are all large enough to be considered in the hurricane storm surge model therefore it is essential that they are described by the DTM.

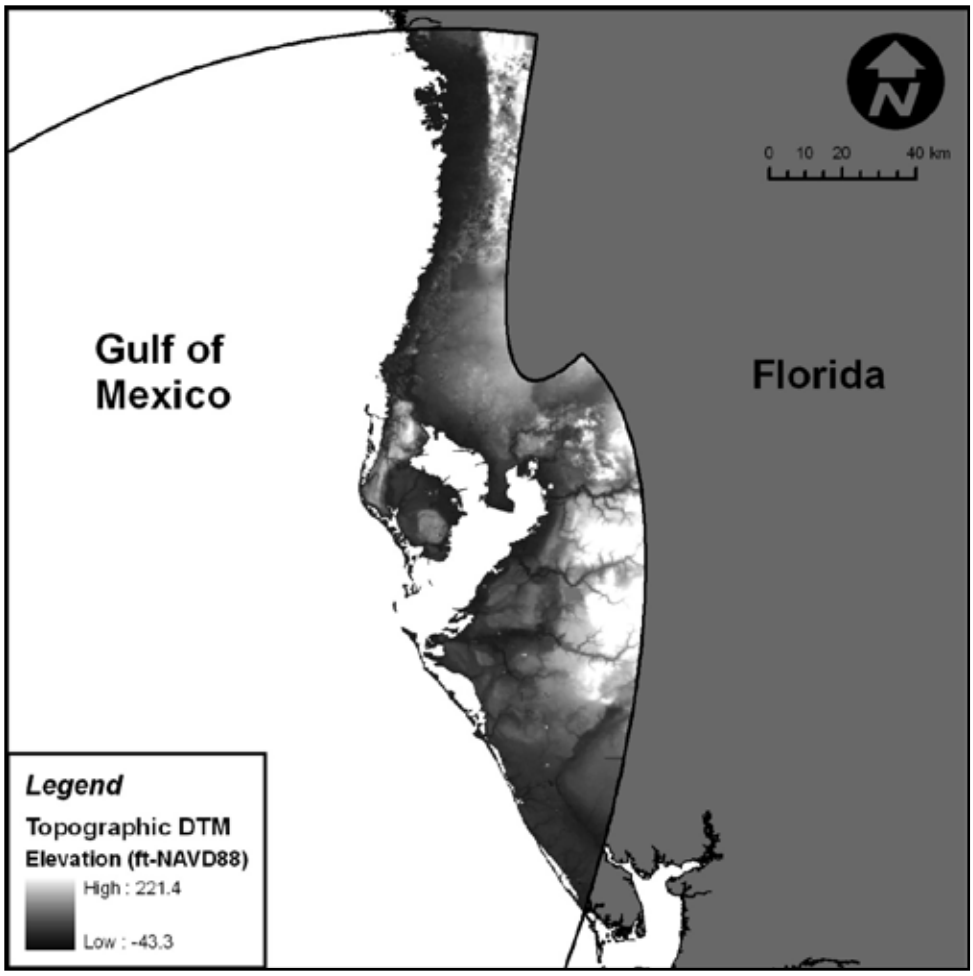

Figure 3.5: Topographic DTM

Figure 3.6 depicts the bathymetric DTM. Although Figure 3.6 covers a much larger area than Figure 3.5, the navigational channels within Tampa Bay and continental shelf are both easily recognized.

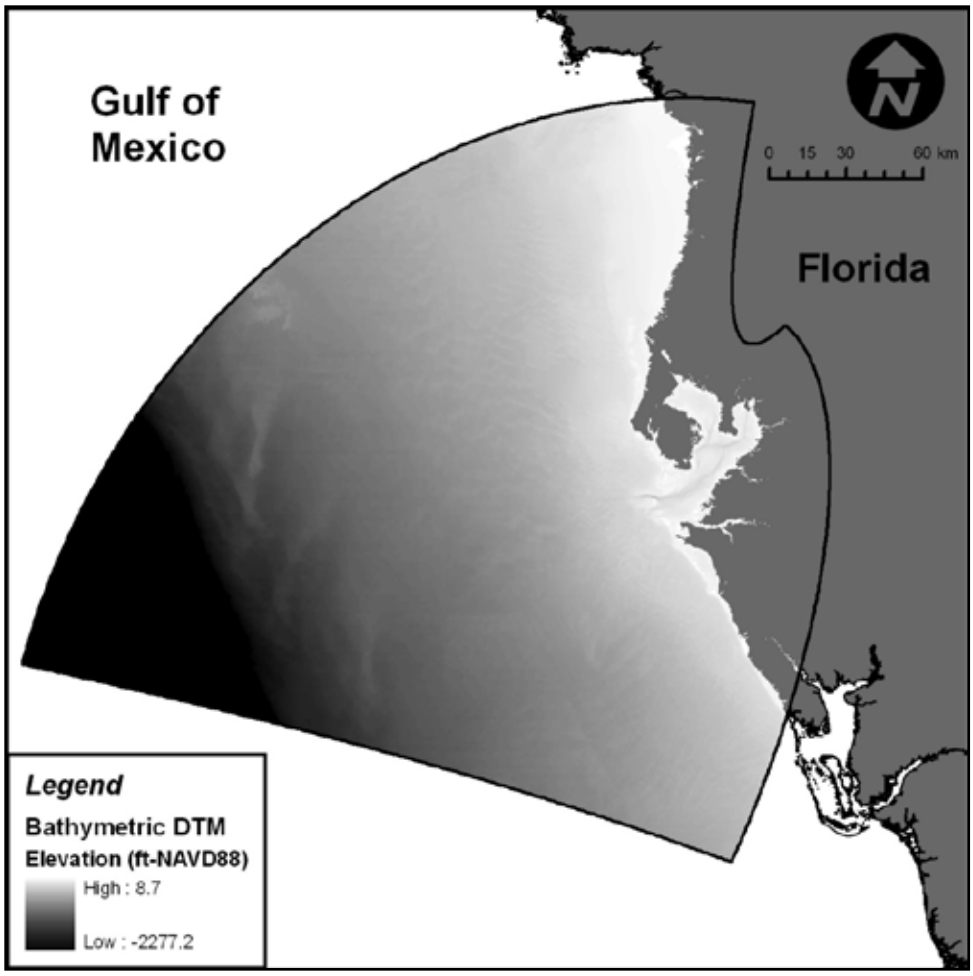

Figure 3.6: Bathymetric DTM

Figure 3.7 depicts the seamless topobathy DTM and it is evident that all of the prominent terrain features present in the topographic and bathymetric DTMs remain. This is a key advantage in using seamless topobathy DTMs in hurricane storm surge modeling. It allows for accurate inundation simulations and also allows the modeler to study the effects of varying the initial water level as a parameter in the model independent of a horizontally predefined coastline boundary (Feyen *et al.*, 2006).

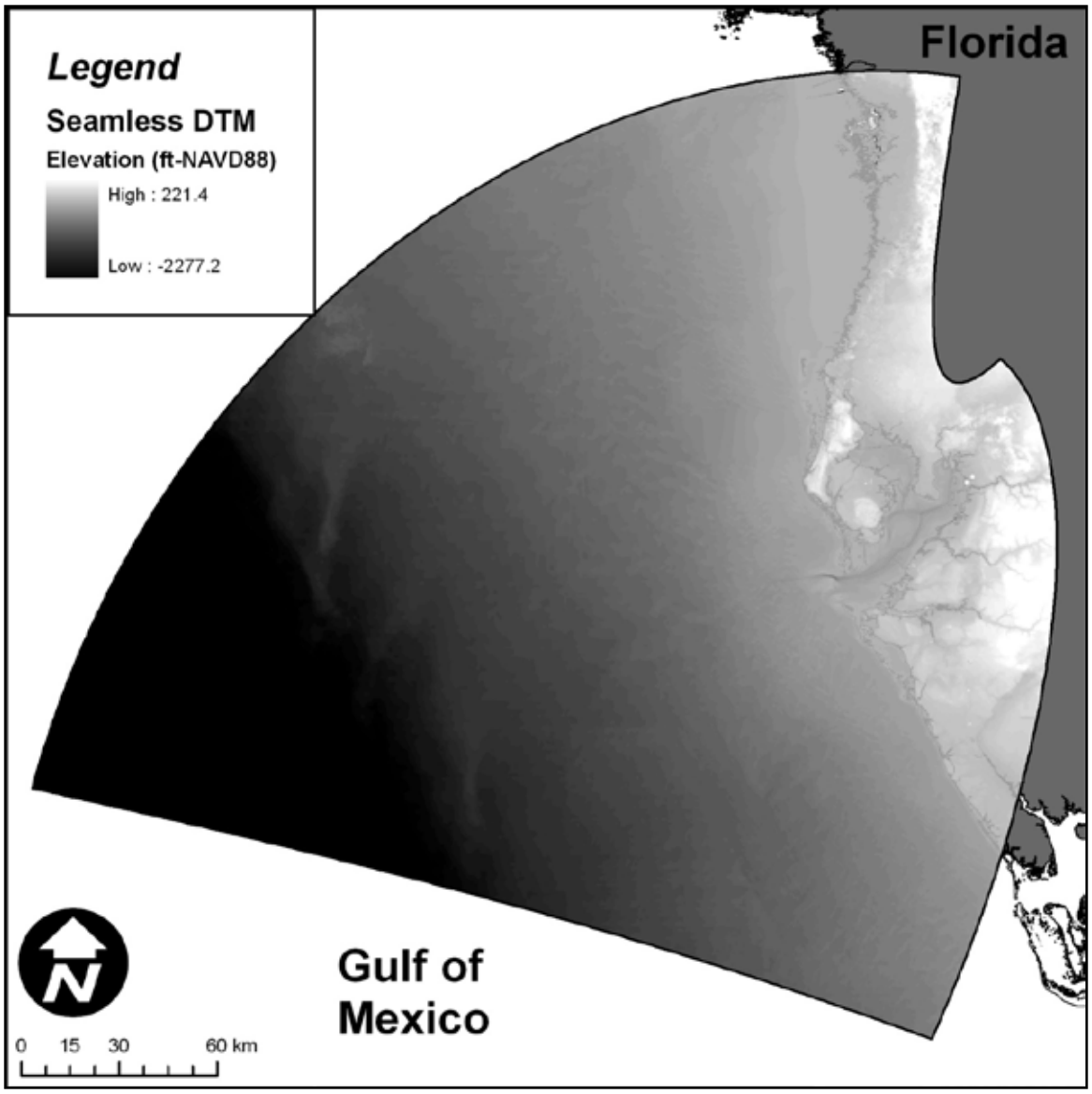

Figure 3.7: Seamless DTM

For the area inside Tampa Bay, the results of the method of bathymetric adjustment presented herein compare favorably to those generated by VDatum. The area covered by VDatum contained a subset of the data consisting of 62,558 points. The average difference in applied offset was 0.061 meters with a range of 0.019 meters to 0.276 meters. The standard deviation

was 0.026 meters. A difference plot of the applied offset values is shown in Figure 3.8. As shown, the differences between the two (2) methods are lower in offshore areas and higher in the estuarine areas as well as areas around the barrier islands (i.e. areas with more complex hydrodynamics).

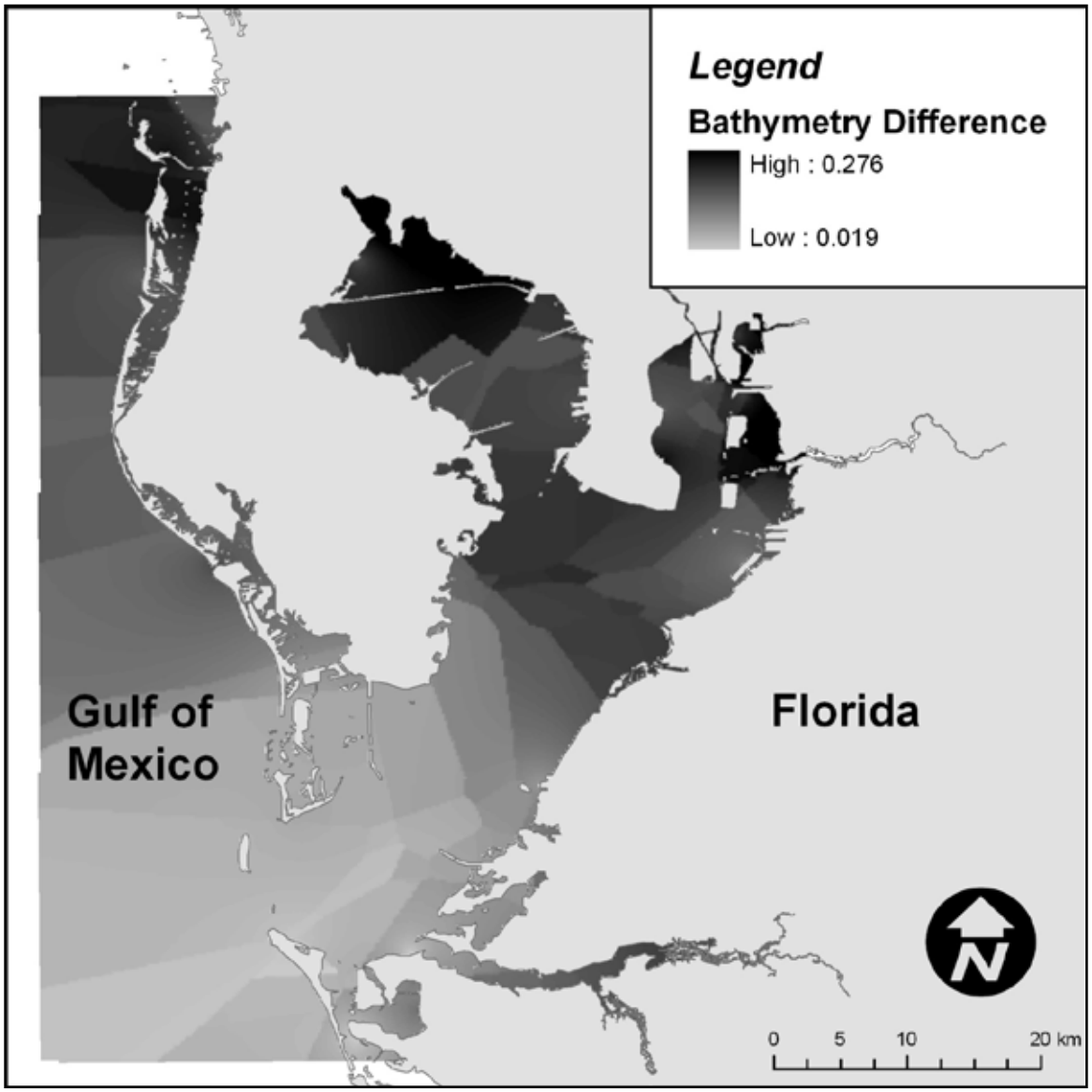

Figure 3.8: Difference between VDatum conversion and method presented herein - Subset of bathymetry data in Tampa Bay, Florida

3.5 Discussion

The method for generating digital terrain models, including the bathymetric adjustment, presented herein does have some limitations. As described above, the method requires significant manual processing of the data to ensure its applicability and accuracy. While this is typically the case for any DTM construction, especially those involving data from multiple sources, the additional step of adjusting the bathymetry adds some complexity to the process. However, the authors made efforts to present the method in an algorithmic manner so it (or parts of it) can be scripted in any number of computer programming languages. Related to the previous description, the time required to complete the method can be significant and it is primarily a function of the number of points being used (either from geographically large or dense data sets). Other aspects that influence time are user skill and computing resources.

In addition to the time and labor based limitations, the method as presented has two (2) inherent geographical limitations: First, tidal benchmark stations located on narrow peninsulas, barrier islands and inshore areas can lead to inaccuracies. In some instances, one of the nearest tidal benchmark stations to a bathymetry point will lie on the opposite side of a significant land barrier, as shown in Figure 3.9. This can lead to the application of an erroneous offset value because the tidal hydrodynamics at the southern most tidal benchmark station are drastically different than the other two (considered representative of the conditions at the bathymetry point), leading to different elevations of MSL (for example). The use of multiple (in this case, three) tidal benchmark station offset values in the weighted average will reduce this effect overall. Also, if the erroneous tidal benchmark station(s) are close to the bathymetry point relative to the others, its effect will not be artificially magnified due to the selection of the exponent in the IDW

formulation. Another means for preventing errors of this nature is the incorporation of barrier methods to the interpolation (Raber & Tullis, 2007) by preventing the selection of a tidal benchmark station located on the opposite side of a "barrier" (in this case, a land mass).

Figure 3.9: Example of Potential Error Induced by Including Tidal Benchmark Stations on Opposite Sides of Significant Land Masses

Similarly, areas with sparse tidal benchmark station coverage present the same error. In this case, the tidal benchmark station(s) may be a substantial distance from the bathymetry point being adjusted and therefore not applicable on a tidal datum basis. This effect can be minimized by possibly selecting fewer tidal benchmark stations to include in the average or imposing

maximum distance criteria to the selection of the stations, thereby focusing on only those stations close to the bathymetry point.

3.6 Conclusions

While other coastal modeling studies such as (Feyen *et al.*, 2006) have integrated LiDAR and bathymetric data, presented herein is a novel approach to generating coastal Digital Terrain Models (DTMs) using the Terrain Data Set structure in ArcGIS. This approach is desirable primarily due to its ability to embed the points in the Terrain Data Set, thereby allowing the large point files to be compressed and archived at an alternate and / or offline storage site. This allows the user to generate end products with varying characteristics such as resolution and interpolation method without having to deal with cumbersome point files. These end products are usable in a variety of engineering and mapping applications; in particular, they are used effectively as a source of topographic data for hydrologic, hydraulic and coastal inundation models. Also presented herein is a method for adjusting bathymetric data from a tidal datum to an orthometric datum. This particular method is useful in two (2) primary capacities: First, it can be used in areas that have yet to be covered by NOAA's VDatum product. This includes areas outside of the United States, provided there are accurately surveyed tidal stations in the region. Second, the method can be used to verify the results of a VDatum conversion to ensure that the results are reasonable.

3.7 Acknowledgments

The authors would like to thank Jesse Feyen of NOAA's Coast Survey Development Laboratory for his guidance regarding VDatum as well as providing data regarding the Tidal Benchmark

Stations. Funding for this project was provided through a Services contract with Woolpert, Inc., to assist them with their work with the Florida Division of Emergency Management under SLOSH Task Order Contract No. 07-HS-34-14-00-22-469. This research is also funded in part by NASA Earth Sciences Division, Research Opportunities in Space and Earth Science (ROSES) Grant Number NNX09AT44G. The statements, findings, conclusions, and recommendations expressed herein are those of the authors and do not necessarily reflect the views of NASA.

3.8 References

Barnard, P. L., & Hoover, D. 2009. A seamless, high-resolution, coastal digital elevation model (DEM) for southern California. In U. S. G. Survey (Ed.).

Cobby, D. M., Mason, D. C., Horritt, M. S., & Bates, P. D. 2003. Two-dimensional hydraulic flood modelling using a finite-element mesh decomposed according to vegetation and topographic features derived from airborne scanning laser altimetry. *Hydrological Processes, 17*, 1979-2000. doi: 10.1002/hyp.1201

Coggin, D. W. 2008. LiDAR in coastal storm surge modeling: Modeling linear raised features *Master's Thesis* (pp. 140 pp). Orlando, FL: University of Central Florida.

ESRI. 2008. ArcGIS 9.2 Desktop Help: Terrain dataset concepts Retrieved September 23, 2009, from http://webhelp.esri.com/arcgisdesktop/9.2/index.cfm?TopicName=Terrain_dataset_concepts&anchor=anchor types of feature class data sources

Feyen, J. C., Hess, K., Spargo, E., Wong, A., White, S., Sellars, J., & Gill, S. 2006. *Development of a Continuous Bathymetric/Topographic Unstructured Coastal Flooding Model to Study Sea Level Rise in North Carolina*. Paper presented at the 9th International Conference on Estuarine and Coastal Modeling.

Garbrecht, J., & Martz, L. W. 2000. *Digital Elevation Model Issues in Water Resources Modeling.* Paper presented at the Hydrologic and Hydraulic Modeling Support with Geographical Information Systems, Redlands, CA.

Gesch, D., Oimoen, M., Greenlee, S. K., Nelson, C., Steuck, M., & Tyler, D. 2002. The National Elevation Dataset. *Photogrammetric Engineering and Remote Sensing, 68*(1), 5-11.

Gesch, D., & Wilson, R. 2001. Development of a Seamless Multisource Topographic / Bathymetric Elevation Model for Tampa Bay. *Marine Technology Society Journal, 35*(4), 58-64.

Gonzalez, F. I., Titov, V. V., Mofjeld, H. O., Venturato, A. J., Simmons, R. S., Hansen, R., . . . Walsh, T. J. 2005. Progress in NTHMP Hazard Assessment. *Natural Hazards, 35*(1), 89-110. doi: 10.1007/s11069-004-2406-0

Hodgson, M. E., Jensen, J. R., Raber, G. T., Tullis, J. A., Davis, B. A., Thompson, G., & Schuckman, K. 2005. An evaluation of Lidar-derived elevation and terrain slope in leaf-off conditions. *Photogrammetric Engineering and Remote Sensing, 71*(7), 817-823.

Homer, C., Dewitz, J., Fry, J., Coan, M., Hossain, N., Larson, C., . . . Wickham, J. 2007. Completion of the 2001 National Land Cover Database for the Conterminous United States. *Photogrammetric Engineering and Remote Sensing, 73*(4), 337-341.

Jezek, K. C., Liu, H., Zhao, Z., & Li, B. 1999. Improving a digital elevation model of Antarctica using radar remote sensing data and GIS techniques. *Polar Geography, 23*(3), 185-200.

Maune, D. F. (Ed.). (2007). *Digital Elevation Model Technologies and Applications: The DEM Users Manual, 2nd Edition* (2nd ed.). Bethesda, MD: American Society for Photogrammetry and Remote Sensing.

Meyers III, E. P. 2005. *Review of progress on VDatum, a vertical datum transformation tool*. Paper presented at the Oceans 2005 MTS/IEEE, Washington, DC.

NOAA. 2007. Topographic and Bathymetric Data Considerations: Datums, Datum Conversion Techniques, and Data Integration. Part II of A Roadmap to a Seamless Topobathy Surface: National Oceanic and Atmospheric Administration.

Poppenga, S. K., Worstell, B. B., Stoker, J. M., & Greenlee, S. K. 2009. Comparison of Surface Flow Features from Lidar-Derived Digital Elevation Models with Historical Elevation and Hydrography Data for Minnehaha County, South Dakota (pp. 24): United States Geological Survey.

Raber, G. T., Jensen, J. R., Schill, S. R., & Schuckman, K. 2002. Creation of digital terrain models using an adaptive lidar vegetation point removal process. *Photogrammetric Engineering and Remote Sensing, 68*(12), 1307-1315.

Raber, G. T., & Tullis, J. A. 2007. Rapid assessment of storm-surge inundation after hurricane katrina utilizing a modified distance interpolation approach. *GIScience & Remote Sensing, 44*(3), 220-236.

Ritchie, J. C. 1996. Remote sensing applications to hydrology: airborne laser altimeters. *Hydrological Sciences Journal, 41*(4), 625-636.

Shepard, D. 1968. *A two-dimensional interpolation function for irregularly spaced data.* Paper presented at the 23rd ACM National Conference.

CHAPTER 4. COMPARISON OF SURFACE ROUGHNESS PARAMETERS DERIVED FROM LAND COVER DATA AND FIELD MEASUREMENTS

The content in this chapter is under review and in revision as: Medeiros, S. C., Hagen, S. C., & Weishampel, J. F. 2012. Comparison of floodplain surface roughness parameters derived from land cover data and field measurements. *Journal of Hydrology, In Revision*.

4.1 Introduction

The propagation of overland inundation is heavily influenced by the roughness of the terrain surface. It is the most important parameter, after topography, that influences overland flow patterns (M. Straatsma, 2009). Drag forces exerted on the flow by above-ground obstructions in the floodplain such as trees, grasses, bushes and structures serve to dissipate hydraulic energy and the momentum of the flood wave. These obstructions also modify wind characteristics, an important forcing mechanism in hurricane storm surge modeling. In finite element schemes, these phenomena are parameterized and implemented in the form of bottom friction coefficients (Strelkoff *et al.*, 2009) such as Manning's n, along with coefficients that represent the surface canopy closure and effective roughness length (aerodynamic roughness). This study focuses on the parameterization of surface roughness in 2-dimensional, depth integrated models where according to Morvan *et al.* (2008) "roughness is a model of the physical processes that are omitted" (p. 191) from the governing equations. Two prominent examples of this type of model are TELEMAC-2D (Galland *et al.*, 1991; Hervouet, 2000) and ADCIRC (Luettich & Westerink, 2006; Luettich *et al.*, 1992).

Many studies consider bottom friction to be a calibrated model parameter (Mailapalli *et al.*, 2008); however, more and more researchers are constructing models that seek to describe the physics of the processes as purely as possible, with no calibrated or tuned friction parameters (Atkinson *et al.*, 2011; Bacopoulos *et al.*, 2009; Cobby *et al.*, 2003; Mason *et al.*, 2003; Westerink *et al.*, 2008). Please note that in this context, the terms "calibrated" or "tuned" refer to those models where bottom friction is adjusted using automated optimization algorithms in an effort to improve model results with respect to observed data. All modeling requires some level of engineering judgment and the manual adjustment of bottom friction parameters, within generally accepted ranges, is herein not considered "calibration". Fortunately, many studies have been conducted to assist the modeler in selecting and adjusting bottom friction parameters based on the conditions of the domain.

Past investigations into the determination of the bottom friction coefficient at actual sites throughout the world typically follow one of two methods:

1. Measure flow velocity and topographic conditions (depth and cross-sectional area); or
2. Measure topographic conditions and physical characteristics (heights, widths, etc.) of obstacles that impede flow.

Both methodologies then rely on established equations, usually empirical (Burguete *et al.*, 2007), to compute bottom friction.

Following the first method, research has been conducted by Harun-ur-Rashid (1990), Bakry *et al.* (1992), Vieux and Farajalla (1994), Myers *et al.* (1999), Sepaskhah and Bondar (2002), Stephan

and Gutknecht (2002), Mailapalli *et al.* (2008), Aricó *et al.* (2009), among others. Studies of this type employ numerical models that use the topographic data as input and measured flows as initial and boundary conditions. The value for the roughness coefficient is then calibrated to match recorded water levels. Xu and Wright (1995) took this methodology from the rivers and floodplains into the nearshore regions of the Middle Atlantic Bight and tested roughness models with emphasis on grain, ripple and sediment motion roughness. Li and Zhang (2001) simplified the analytical model of Yu and Singh (1989), producing a methodology that relies on measurements of the advancing water front over crop fields and is therefore able to compute Manning's n without measurements of the water surface elevation. Straatsma (2009) employed a 3-dimensional float tracking apparatus along with Acoustic Doppler Current Profiler (ADCP) data to provide the field measurements that were then used to derive roughness values using the Chézy equation. This general method and its derivative innovations provide a counterpoint to the method presented herein.

Direct measurement of bottom friction coefficient in the field has been applied most notably by Arcement and Schneider (1989). In this study, the method of Petryk and Bosmajian (1975) was adapted with the vegetation density of the trees and the soil grain size distribution measured directly, along with estimations of Manning's n values to account for microtopography (Strelkoff *et al.*, 2000), non-living obstacles (debris, stumps, boulders, etc) and low lying vegetation. De Doncker *et al.* (2009) was able to compute Manning's n as a function of the amount of biomass (measured in grams per square meter) in a river channel. The contribution of the soil to the overall roughness has also been a topic of research, largely from an irrigation perspective. Limerinos (1970) developed a method which was employed by Arcement and Schneider (1989)

based on percentiles of the soil grain size distribution, following Strickler (1923). B. Gomez (1993) used flow measurements and profile photography to compute the roughness of stable armored gravel beds without relying on characteristic grain size. J. A. Gomez *et al.* (2005) employed the chain method of Saleh (1993) to measure the roughness of the soil.

For parameterizing overland flow models in practice, researchers and engineers rely on published results of the above-referenced work coupled with engineering judgment. Barnes (1967) and Arcement and Schneider (1989) provide photos of river reaches and floodplains where Manning's n has been computed to provide the engineer with a reference image for comparison to his/her project area. There are also references that provide tables of value ranges for different types of channels and floodplains, most notably those found in textbooks such as Chow (1959), French (1985) and Chow *et al.* (1988). Jakubis (2000) provides a list of recommended values from the literature. However, almost unanimously, the authors caution the application of published values to actual field situations.

In the case of hurricane storm surge inundation models, the roughness of the terrain surface exerts drag forces not only on the inundating flood wave, but also the prevailing winds that drive overland flows. In numerical models of this type, the winds serve as a forcing mechanism that transfers momentum to the water column by a stress (drag) applied at the air-sea interface. Frequently, the wind velocities are derived from meteorological models that produce spatially and temporally dynamic wind fields that assume open-ocean conditions (i.e. no obstacles above the ground or water surfaces). Wind forcing to the inundation model is usually comprised of observed data assimilated to the domain; Cardone and Cox (2009) describe this process in detail.

However, above-ground obstacles upwind of a particular point serve to reduce the effective wind velocity at that point. As a result, parameters describing the canopy closure coverage and horizontal wind velocity reduction have been developed and applied to capture this effect (Westerink *et al.*, 2008). Efforts to measure these parameters in the field mirror those of bottom friction coefficient. Analogous to the first methodology presented previously, researchers place anemometers throughout a field site or wind tunnel and measure the spatial variability of the wind field, followed by the computation of the corresponding roughness length based on average vegetation density and/or height (Sullivan & Greeley, 1993). Direct measurement of these parameters has been carried out by Lettau (1969) and improved upon by (Macdonald *et al.*, 1998). Lookup tables of these values intended to assist practicing engineers with parameter selection are presented by Wieringa (1993), Simiu and Scanlan (1996) and Tieleman (2003). For engineering practice in the United States, the primary source for these values is the Federal Emergency Management Agency Multi-Hazard Loss Estimation Methodology manual (FEMA, 2006) which draws heavily from the work referenced above.

An automated parameterization scheme is required in order to implement these parameters in hurricane storm surge inundation models due to their typically large geographic scope. The direct measurement of surface roughness parameters at this scale is prohibitively expensive, if not impossible (Vieux & Farajalla, 1994). Since it is not feasible to compute the surface roughness parameters based on field measurements over the entire domain, modelers currently rely on land use / land cover (LULC) maps derived from remotely sensed data. Each LULC class has associated surface roughness parameter values; these values are then interpolated onto the mesh nodes and are incorporated into the model computations (Bunya *et al.*, 2010; Westerink

et al., 2008). While the accuracy and resolution of the published LULC data are progressing (Homer *et al.*, 2007), the *in-situ* conditions often differ significantly. This is especially true when one considers the needs of individual user groups. Biologists and planners rely on these data to conduct research and enhance decision making within a spatial framework; in fact, the LULC was initially used for assessing land use changes, modeling nutrient and pesticide loads in runoff, and assessing biodiversity and habitat preference (Vogelmann *et al.*, 1998). However, for engineers or modelers that are concerned with the physical effect that terrain obstructions have on inundation flow or hurricane winds, the published data are sub-optimal and a more accurate description is necessary. While previous studies such as Werner *et al.* (2005) have demonstrated that reliance on values from the literature can be problematic, a direct comparison of surface roughness parameters based on LULC data and *in-situ* measurements has not been carried out.

The research presented herein demonstrates this discrepancy by comparing the surface roughness characteristics computed based on field measurements and those assigned by the LULC method. This comparison is conducted for 24 sites in Florida and the results along with the associated statistics show that the *in-situ* surface roughness parameters can differ substantially from those assigned by the LULC method.

4.2 Field Measurement Methods

Field measurements were conducted by a four person team at 24 sites on public land in Florida's Volusia, Lake and Franklin Counties from August 2010 to August 2011. More specifically, the field measurement sites were located in the Lake Monroe (LKMO), Seminole Forest (SEMF) and Hilochee (HILO) Wildlife Management Areas (WMA) and also the Apalachicola National

Estuarine Research Reserve (ANER) as shown in Figure 4.1. For clarity, these areas will be referred to as "locations" to distinguish them from the "sites" where the actual measurements took place. The 1992 and 2006 National Land Cover Dataset (NLCD) (Homer *et al.*, 2007; Vogelmann *et al.*, 2001) along with the 2006 Coastwatch Change Analysis Program (C-CAP; National Oceanic and Atmospheric Administration, 1995 - present) classifications for each site are shown in Table 4.1. The sites were selected in order to capture the common LULC types typical of Florida's Gulf coast, as shown in Table 4.2.

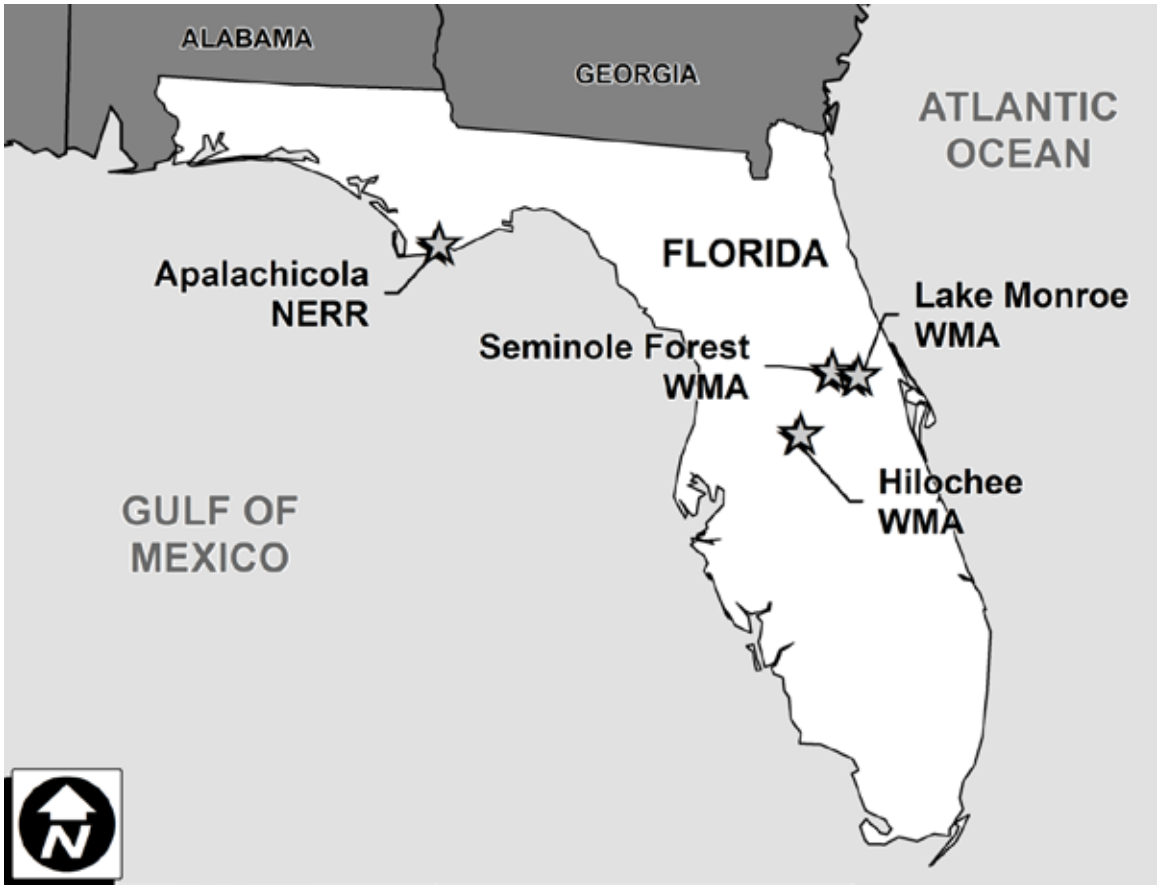

Figure 4.1: Field measurement site locations

Table 4.1: Land use / land cover classifications of field measurement sites

Site	1992 NLCD	2006 NLCD	2006 C-CAP
ANER-01	31 - Bare rock/sand	24 - Developed, high intensity (67%) 31 - Barren land (33%)	2 – High-intensity developed (66%) 20 – Bare land (34%)
ANER-02	31 - Bare rock/sand	31 - Barren land	20 – Bare land
ANER-03	42 - Evergreen forest	52 - Shrub/scrub (58%) 71 - Grassland/herbaceous (42%)	8 – Grassland (53%) 12 – Scrub/shrub (47%)
ANER-04	31 - Bare rock/sand	24 - Developed, high intensity	2 – High-intensity developed (89%) 20 – Bare land (11%)
ANER-05	91 - Woody wetland	90 - Woody wetlands	13 – Palustrine forested wetland (1%) 14 – Palustrine scrub/shrub wetland (99%)
ANER-06	31 - Bare rock/sand	31 - Barren land	20 – Bare land
ANER-07	91 - Woody wetland	52 - Shrub/scrub (74%) 90 - Woody wetlands (26%)	12 – Scrub/shrub (79%) 20 – Bare land (21%)
ANER-08	33 – Transitional (24%) 71 – Grassland (50%) 42 - Evergreen forest (26%)	31 - Barren land	12 – Scrub/shrub (26%) 20 – Bare land (74%)
ANER-09	31 - Bare rock/sand	31 - Barren land	20 – Bare land
ANER-10	42 - Evergreen forest	95 - Emergent herbaceous wetlands	12 – Scrub/shrub (8%) 18 – Estuarine emergent wetland (92%)
HILO-01	71 - Grassland	90 - Woody wetlands	13 – Palustrine forested wetland (21%) 14 – Palustrine scrub/shrub wetland (79%)
HILO-02	42 - Evergreen forest	90 - Woody wetlands	13 – Palustrine forested wetland
HILO-03	91 - Woody wetland	90 - Woody wetlands	13 – Palustrine forested wetland
LKMO-01	42 - Evergreen forest	90 - Woody wetlands	13 – Palustrine forested wetland
LKMO-02	71 - Grassland	21 - Developed, open space	5 – Developed open space (88%) 14 – Palustrine scrub/shrub wetland (12%)
LKMO-03	71 - Grassland (85%) 85 – Rec. grass (15%)	21 - Developed, open space	13 – Palustrine forested wetland
LKMO-04	92 - Herbaceous wetland	90 - Woody wetlands (92%) 95 - Emergent herbaceous wetlands (8%)	14 - Palustrine scrub/shrub wetland (97 %) 15 – Palustrine emergent wetland (3%)
SEMF-01	92 - Herbaceous wetland (94%) 11 - Open water (6%)	52 - Shrub/scrub	10 – Evergreen forest (20%) 12 – Scrub/shrub (80%)

Table 4.1: Land use / land cover classifications of field measurement sites

Site	1992 NLCD	2006 NLCD	2006 C-CAP
SEMF-02	42 - Evergreen forest (68%) 51 - Shrub land (29%) 92 - Herbaceous wetland (3%)	52 - Shrub/scrub (70%) 42 - Evergreen forest (30%)	10 – Evergreen forest (62%) 12 – Scrub/shrub (38%)
SEMF-03	91 - Woody wetland	52 - Shrub/scrub	12 – Scrub/shrub
SEMF-04	31 - Bare rock/sand	81 - Pasture hay (93%) 42 - Evergreen forest (7%)	7 – Pasture/hay
SEMF-05	91 - Woody wetland (88%) 33 - Transitional (12%)	52 - Shrub/scrub	12 – Scrub/shrub
SEMF-06	33 - Transitional (91%) 23 - Commercial (9%)	71 - Grassland/herbaceous (61%) 52 - Shrub/scrub	4 – Low-intensity developed (93%) 7 – Pasture/hay (7%)
SEMF-07	42 - Evergreen forest (68%) 91 - Woody wetland (32%)	42 - Evergreen forest	10 – Evergreen forest

Table 4.2: Land Use / Land Cover distribution within 20 km of Florida's Gulf coast shoreline

2006 NLCD Class	Percent of Land Area in Gulf Coastal Florida
52 - Shrub/Scrub	23%
82 - Cultivated Crops	16%
71 - Grassland Herbaceous	15%
42 - Evergreen Forest	13%
41 - Deciduous Forest	12%
81 - Pasture Hay	7%
90 - Woody Wetlands	4%
21 - Developed, Open Space	3%
43 - Mixed Forest	2%
22 - Developed, Low Intensity	2%
95 - Emergent Herbaceous Wetlands	1%
31 - Barren Land	1%
23 - Developed Medium Intensity	1%
24 - Developed, High Intensity	0%

*** LULC Class Open Water was removed prior to computing percentages**

Each rectangular field measurement site measured 30 meters by 15 meters following Arcement and Schneider (1989) with the long edge running East-West as shown in Figure 4.2. Site candidates were randomly plotted within the boundaries of the location and the field research team navigated to the site candidates using handheld Global Positioning Systems (GPS). Site candidates were discarded if they were: located in areas closed by management staff; located in open water; inaccessible due to excessively dense understory vegetation; or deemed unsafe. Possible reasons for declaring a site unsafe include an excessive amount of stinging insects, poisonous plants or the presence of large broken tree limbs precariously suspended in the canopy. The team leader (corresponding author of this paper) also selected sites in order to achieve a range of surface roughness conditions typical in coastal areas in the southeastern United States at risk from hurricane storm surge including bare earth (e.g. parking lot, mowed grass field), areas of continuous or patchy tall grass and dense tree coverage. Once the site was established, it was demarcated using stakes and string aligned with magnetic compasses and measuring tapes. The coordinates for the site corners were obtained with handheld GPS in the Universal Transverse Mercator (UTM) projection and the World Geodetic System datum of 1984 (WGS84).

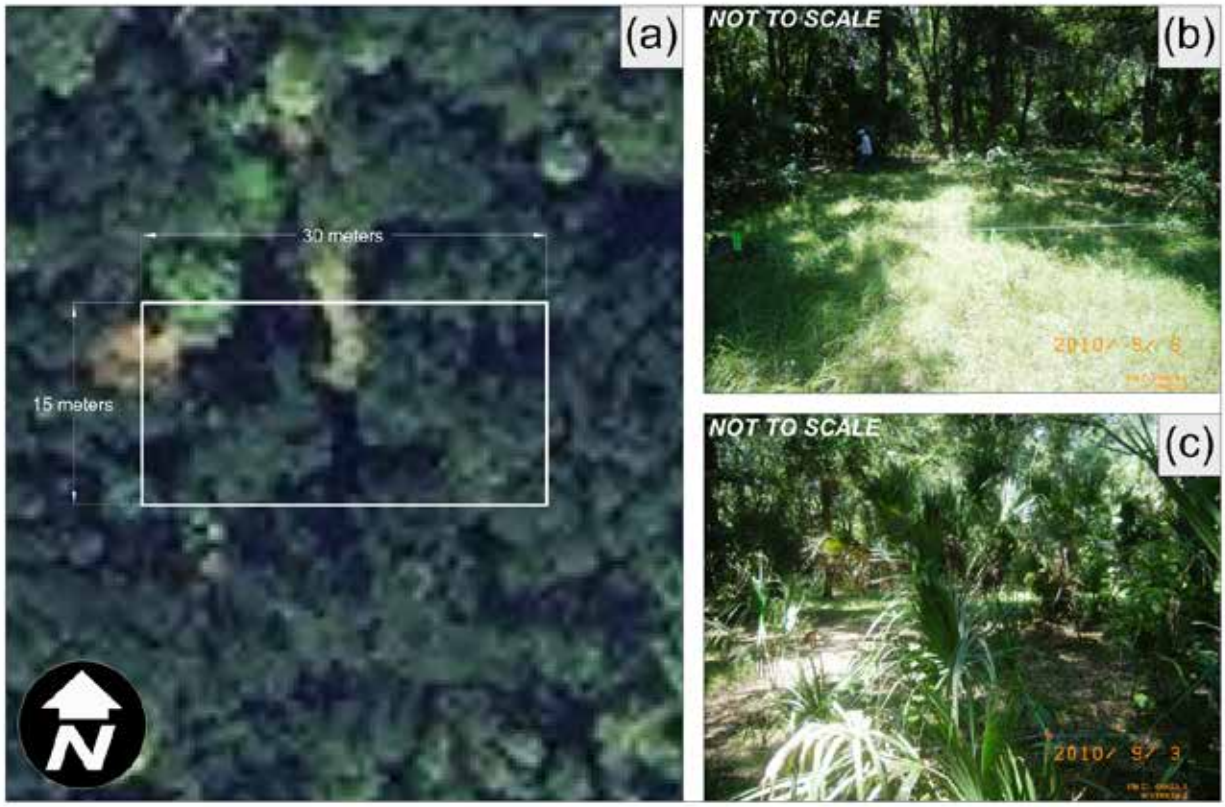

Figure 4.2: Site layout example: (a) Aerial view of site boundary; (b) Ground level view of site, looking south; (b) Ground level view of site, looking west

With the site boundary established, each member of the team independently estimated the bottom friction coefficients associated with each of the following: microtopography or relatively small undulations in the terrain within the site along with the presence of any depressions or conveyances; obstructions such as large rocks, stumps and debris; and low lying vegetation such as grasses, shrubs and seedlings. These estimations are taken according to the descriptions found in Table 3 and Figures 6 through 20 of Arcement and Schneider (1989) and are necessary for computing Manning's n. The team leader instructed the participants on the estimation techniques and tested their aptitude on demonstration sites prior to obtaining actual study data.

Each team member independently estimated the surface canopy coverage at nine locations on site: the four site corners; the midpoint of each site boundary edge; and the exact center of the site. Estimations were obtained using a moosehorn measurement tool. This tool uses a mirror oriented to allow the researcher to see directly above him/her, assisted by vertical and horizontal leveling bubbles visible when looking into the device. Once the instrument is leveled, the researcher estimated the percentage of the field of view that is obscured by canopy.

The team then measured the dimensions of all above-ground obstructions present on the site. Obstructions were classified into three categories: trees, low lying vegetation and obstacles. Trees were defined by species and the presence of a defined trunk. Saplings and trees less than approximately 1 meter in height were classified as low lying vegetation. Low lying vegetation also included shrubs, clumps of tall grasses and short palmetto clusters. Obstacles included stumps, dead trees, logs and debris. A photograph of each obstruction was taken with a GPS enabled camera (thereby also recording the geographic position). A reflector was attached to each subject obstruction being photographed in order to differentiate it from its surroundings.

For trees, the team obtained the following measurements: diameter of the trunk at breast height (D_{BH}); total height, taken with a laser hypsometer independently by two participants; height to the lowest significant branch (defined as the lowest branch that contributes to the canopy formation), taken with measuring tape or laser hypsometer independently by two participants (note that the two researchers taking this measurement also independently selected the lowest significant branch in addition to measuring its height); and width of the tree's canopy in both north-south and east-west directions. For trees with split trunks or clusters of like trees that share

the same canopy, the diameters were measured and combined using a modified circle packing method. The cluster diameter was computed according to the following equation:

$$for \begin{cases} N < 3, D_0 = \sum D_n \\ N = 3, D_0 = \sum D_1, D_2 \\ N > 3, D_0 = 2.91 D_{avg} + 0.107 \sum D_n \end{cases} \quad (4.1)$$

where N = number of trees in the cluster; D_0 = the minimum cluster diameter (m); D_n = individual D_{BH} of trees in the cluster; D_1, D_2 = the largest and second largest D_{BH} in the cluster, respectively; and D_{avg} = average D_{BH} in the cluster. For the case of $N > 3$, the work of Huang *et. al.* (2002) was adapted. This work applies a heuristic algorithm to solve the problem of determining the minimum radius of a cluster of unequal circles. A testing data set consisting of a group of circles with unequal radii and their corresponding minimum cluster radius was presented. This data set was used here to develop the multiple regression function. This function describes the diameter of a cluster of unequal circles based on the average diameter and sum of the diameters of the trees in the cluster.

For low lying vegetation, the team obtained the following measurements: total height taken with measuring tape; total width of the vegetation in the north-south and east-west directions. In some instances, multiple plants in contact or in close proximity to one another were grouped and measured as one. Low lying vegetation was given a blaze orange backdrop for the photograph in order to distinguish it from its surroundings. The species of the vegetation was also recorded.

The measurements for obstacles were identical to those of low lying vegetation, except that instead of species, a brief description of the obstacle was recorded.

Lastly, a topsoil sample of approximately 1.5 to 2 kilograms was taken from an open area as close as possible to the center of the site. The research team first removed any extraneous materials (e.g., leaf litter) from the sample site and then proceeded to remove the soil sample to a depth of approximately 10 centimeters. The sample was subjected to a sieve analysis in order to determine the grain size distribution of the topsoil according to ASTM Standard C136-06. The sieve stack consisted of the following mesh sizes: #10 (2.000 mm); #16 (1.180 mm); #20 (0.850 mm); #40 (0.425 mm); #60 (0.250 mm); #100 (0.150 mm); and #200 (0.075 mm). This set is suitable for the medium sands typical of Florida topsoil.

4.3 Calculations

The measurements taken in the field provided a data set that required careful processing, with the computation of each parameter requiring a unique approach to the utilization of the field measured data. The process for calculating each surface roughness parameter is presented in detail below.

4.3.1 Determining Manning's n

The determination of the bottom friction coefficient Manning's n proceeded according to methodology established by Arcement and Schneider (1989). While the general methodology was closely followed, some modifications were implemented. Please note that the term *R* appears in several places throughout the Manning's n computation process. This value

represents the hydraulic radius, which for floodplains is equal to the flood depth. While it is widely known that Manning's n is sensitive to the depth of flow, for the purposes of this research, the flood depth is assumed to be 1 meter. This value was chosen because it represents a reasonable base value to develop Manning's n coefficients that will in turn be varied with depth within numerical tidal and storm surge models. For example, the ADCIRC model employs a hybrid bottom friction formulation that computes an adjusted bottom friction coefficient based on Manning's n and flow depth at each time step (Luettich & Westerink, 2006).

The modifications to the Manning's equation proposed by Petryk and Bosmajian (1975) were used, given in the following form for SI units:

$$n = n_0 \left[1 + (Veg_d)\frac{C_*}{2g} R^{2/3}\right]^{1/2} \tag{4.2}$$

where n = Manning's n for the sample area at the specified flow depth; n_0 = base or boundary roughness Manning's n associated with all drag forces except those caused by trees; Veg_d = Vegetation density (m^2/m^3), or the fraction of the cross-sectional flow area occupied by tree trunks; C_* = Effective bulk drag coefficient of vegetation; R = hydraulic radius (m); g = acceleration due to gravity (m/s^2). The effective bulk drag coefficient of vegetation, C_*, is computed based on Figure 4 in Arcement and Schneider (1989).

The computation of the base Manning's n consists of summing the contributions from the topsoil (n_b), microtopography or surface irregularities (n_1), obstacles in the flood plain (n_3) and low lying vegetation (n_4):

$$n_o = \left(n_b + n_1 + n_2 + n_3 + n_4\right) m \tag{4.3}$$

Please note that m and n_2 are neglected as they are artifacts from the method's original application to channels. The n_2 term is neglected because it represents the contribution from the variance of the shape and size of the flow cross-section to the overall friction coefficient; this value is assumed to be zero because a floodplain is considered to be an infinitely wide, consistent cross-section. Also, m is a parameter that remains from this equation's original application to channels; it represents a correction factor accounting for the sinuosity or meandering of the channel. In the case of a floodplain, m = 1.0 because the length of the flow path and valley length are equal (Arcement & Schneider, 1989).

The value for the friction coefficient of the topsoil was calculated based on the following equation (Limerinos, 1970) modified for SI units (Marcus *et al.*, 1992):

$$n_b = \frac{0.1129 R^{1/6}}{1.16 + 2.0 \log\left(\frac{R}{d_{84}}\right)} \tag{4.4}$$

where d_{84} = the 84th percentile diameter from the *in-situ* soil sample (m). Aberle and Smart (2003) showed that grain size percentile method for computing bottom friction, as employed

here, is ineffective when the flow depth is of the same order of magnitude as the grain size. This is the case on steep, rocky slopes such as mountain streams. However, in the case of coastal circulation and hurricane storm surge models, the soil types are typically fine to medium grained sands with flow depths multiple orders of magnitude greater than grain size. Therefore, this method is sufficient for this application. Also, sites or sections of sites that contained asphalt were given the Manning's n value of 0.013 (Chow, 1959).

The average estimates of n_1, n_3, and n_4 obtained by the participants on each site were also used in the calculation of n_0. Obvious outliers caused by recording errors were discarded from the averages; these were identified by computing the *z-score* of each estimation (Mendenhall & Sincich, 2007) according to the following formula:

$$z = \frac{y - \bar{y}}{s} \tag{4.5}$$

where y = participant estimated value; $\bar{y}$ = the mean estimated value (in this case the average estimate from the four participants); and s = standard deviation of estimates from the four participants. Estimates with *z-scores* greater than 2 were discarded.

Vegetation density was computed using the "Direct Technique" of Arcement and Schneider (1989):

$$Veg_d = \frac{R\sum D_{BH}}{Rwl} \tag{4.6}$$

where R = hydraulic radius (m); D_{BH} = diameter at breast height of tree trunk (m); w = width of site (m); l = length of site (m).

4.3.2 Determining Surface Canopy Coverage

The surface canopy coverage for the site is computed by averaging the estimation taken by each participant at each location. The *z-score* criteria for identifying and discarding outliers presented in Section 3.1 were also used here. The coverage percentages for all 9 measurement locations (C_p) are averaged to determine the canopy coverage fraction for the site (C_s).

4.3.3 Determining Effective Roughness Length

The effective roughness length is an anisotropic parameter that reduces the horizontal velocity of the wind at a given point. The wind velocity reduction experienced at any given point will be different based on the wind direction due to differing upwind land cover characteristics. To provide a usable parameter to storm surge inundation modelers, the effective roughness lengths for 12 wind directions were computed based on the following formula (Lettau, 1969):

$$z_0 = 0.5 \frac{H \bar{S}}{A} \tag{4.7}$$

where H = average height of all trees, low lying vegetation and obstacles (m); $\bar{S}$ = average frontal or silhouette area "seen" by the wind from each direction (m^2); A = total land area occupied by the roughness elements or the area of the field measurement site. The formulas for each term are presented below.

$$H = \frac{\sum_{1}^{N} H_n}{N} \tag{4.8}$$

$$S = \frac{\sum_{1}^{N_t} S_t + \sum_{1}^{N_l} S_l + \sum_{1}^{N_o} S_o}{N} \tag{4.9}$$

$$A = \frac{wl}{N} \tag{4.10}$$

where H_n = height of individual roughness element (m); N = total number of roughness elements; N_t = number of trees; N_l = number of low lying vegetation elements; and N_o = number of obstacles. Special consideration is given to the frontal or silhouette area. Similar to Jasinski and Crago (1999), the frontal profile for trees is assumed to be a half-ellipsoid on a post and is calculated as follows:

$$S_t = \left(H_{SB} D_{BH}\right) + F_{FA} \frac{\pi \left(H_T - H_{SB}\right)\left(D_c/2\right)}{2} \tag{4.11}$$

where S_t = silhouette area of tree (m^2); H_{SB} = height to the lowest significant branch (m); D_{BH} = diameter at breast height (m); F_{FA} = fraction of frontal area occupied by leaves and branches, as opposed to empty space; H_T = total height of tree (m); and D_c = diameter of canopy (direction dependent, m). The frontal areas of low lying vegetation and obstacles are computed in similar fashion:

$$S_l = F_{FA} \frac{p\left(H_l\right)\left(D_l/2\right)}{2} \tag{4.12}$$

$$S_o = F_{FA} \frac{p\left(H_o\right)\left(D_o/2\right)}{2} \tag{4.13}$$

where S_l = silhouette area of low lying vegetation element (m^2); H_l = height of low lying vegetation element (m); D_l = diameter of low lying vegetation element (m); S_o = silhouette area of obstacle (m^2); H_o = height of obstacle (m); and D_o = diameter of obstacle (m). As shown, low lying vegetation elements and obstacles are approximated as half-ellipses. The value of F_{FA} is assumed to be 0.5 for all types of vegetation and obstacles (FEMA, 2006).

In order to account for the directional dependency of the frontal area, the team measured diameters in the north-south and east-west directions for each roughness element in the field. These diameters form the basis of an elliptical interpolation scheme that computes the frontal area facing each of the 12 directions of the effective roughness parameter. An example is shown in Figure 4.3. The interpolated, intermediate diameters are calculated as follows, based on the inherent properties of an ellipse (Clynch & Garfield, 2006):

$$D_c = 2\sqrt{\frac{a^2}{1+\left(\frac{a^2}{b^2}-1\right)\sin^2 f}} \tag{4.14}$$

where D_c = diameter of tree canopy (m); a = semi-major axial radius of the tree canopy (m); b = semi-minor axial radius of the tree canopy (m); and f = angle measured from the east-west line (radians).

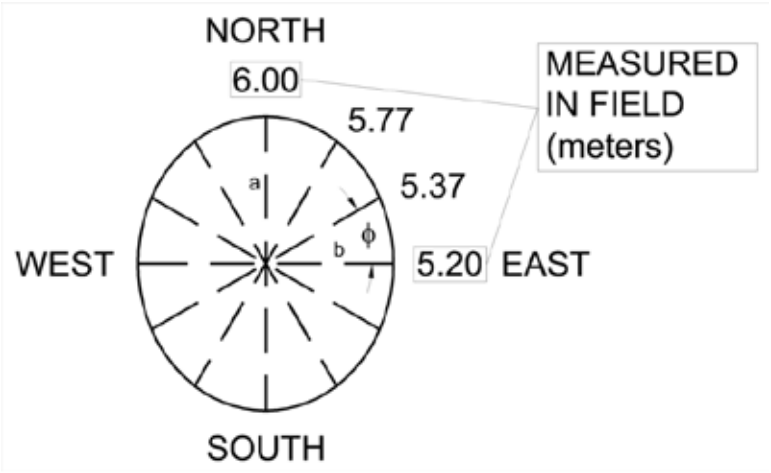

Figure 4.3: Elliptical interpolation of tree canopy parameter

4.3.4 Determining parameters assigned by NLCD

A recent storm surge inundation study by Bunya *et al.* (2010) using the ADCIRC model (Luettich & Westerink, 2006; Luettich *et al.*, 1992) is taken to be the current state of the art for applying surface roughness parameters based on LULC data. Although multiple LULC schemes are presented in that work, only the 1992 NLCD (Vogelmann *et al.*, 2001) is used here. While 1992 data may seem outdated, it is the only data set presented in Bunya *et al.* (2010) that provides a ubiquitous set of classes and their respective surface roughness parameters. The others are state specific and would not provide a consistent parameterization for comparison. These data are delivered as a raster product with 30 meter resolution and cover the entire

conterminous United States. Manning's n values are taken from Table 5 in Bunya *et al.* (2010). Effective roughness length values are taken from Table 9 in Bunya *et al.* (2010). For the field measurement sites where multiple LULC classes are present within a site, an average value is used, weighted by area. No quantitative comparison of surface canopy coverage was performed as further research is yet to be done on the incorporation of fractional values into overland inundation models. In spite of this, the surface canopy coverage results are presented for completeness.

4.3.5 Comparison of parameters derived from the two methods

In order to compare the results from the two parameterization methods, the LULC method was assumed to be the predictor and the field measurement method was assumed to be the ground truth or observed value. Manning's n values were compared based on the Root Mean Square Error (RMSE) according to the following formula:

$$RMSE = \sqrt{N^{-1} \sum_{i=1}^{N} \left(P_i - O_i \right)^2} \tag{4.15}$$

where N = the number of comparisons (in this case, 24); P_i = the predicted (assigned by NLCD) value for the ith site; and O_i = the observed (computed based on field measurements) value. Manning's n values are also compared to a range of values based on in-situ conditions at each site, guided by Chow (1959).

The effective roughness length used RMSE as the basis for comparison. Since the NLCD assigns a single value to a LULC class (rather than one for each direction), the average of the

field measured values (in the 12 directions) was used for comparison purposes. Effective roughness length values are also compared to a range of values based on in-situ conditions at each site and guided by Wieringa (1993) and Simiu and Scanlan (1996) as presented by FEMA (2006).

Lastly, a single sample *t-test* was applied to the absolute errors to determine the overall effectiveness of the NLCD method in selecting Manning's n and effective roughness length. This standard statistical test evaluated the null hypothesis that the mean of the absolute errors is zero (Mendenhall & Sincich, 2007). A two-tailed approach at a 95% confidence interval (α = 0.05) was used.

4.4 Results

The results for Manning's n, calculated versus assigned according to NLCD Land Cover class, are shown in Table 4.3. As stated on the summary line, the RMSE of the predicted values is 0.083. As the RMSE is similar in magnitude to the predicted and observed values of Manning's n, this represents a significant parameterization error for physically based models desiring to capture the physics of overland flow without automatic calibration. In fact, from the perspective of Manning's n, a RMSE of this magnitude can be considered approximately equivalent to erroneously parameterizing a High Density Residential area as Bare Rock/Sand. Compared to values published in the literature, the LULC method was within range on 25.0% of the sites, while the field measured values were within range on 50% of the sites.

Table 4.3: Comparison of Manning's n values computed from field measurements and those assigned by 1992 NLCD

Site	*Manning's n*			*Range from literature based on in-situ conditions*
	NLCD	*Field*	*Error*	
ANER-01	0.040	0.035	0.005	0.020 – 0.050
ANER-02	0.040	0.024	0.016	0.035 – 0.070
ANER-03	0.180	0.029	0.151	0.040 – 0.080
ANER-04	0.040	0.013	0.027	0.013
ANER-05	0.140	0.046	0.094	0.070 – 0.160
ANER-06	0.040	0.032	0.008	0.020 – 0.035
ANER-07	0.140	0.031	0.109	0.040 – 0.080
ANER-08	0.089	0.023	0.066	0.035 – 0.070
ANER-09	0.040	0.022	0.018	0.018 – 0.030
ANER-10	0.180	0.050	0.130	0.040 – 0.100
HILO-01	0.035	0.043	-0.008	0.030 – 0.050
HILO-02	0.180	0.030	0.150	0.035 – 0.060
HILO-03	0.140	0.035	0.105	0.040 - 0080
LKMO-01	0.180	0.031	0.149	0.050 – 0.080
LKMO-02	0.035	0.045	-0.010	0.035 – 0.055
LKMO-03	0.034	0.050	-0.016	0.070 – 0.160
LKMO-04	0.035	0.041	-0.006	0.050 – 0.110
SEMF-01	0.034	0.037	-0.003	0.022 – 0.035
SEMF-02	0.144	0.061	0.083	0.045 – 0.110
SEMF-03	0.140	0.052	0.088	0.035 – 0.070
SEMF-04	0.040	0.045	-0.005	0.035 – 0.065
SEMF-05	0.135	0.055	0.081	0.045 – 0.095
SEMF-06	0.095	0.017	0.079	0.025 – 0.055
SEMF-07	0.167	0.047	0.121	0.040 – 0.080
RMSE			**0.083**	

The aerodynamic roughness values for surface canopy coverage and effective roughness length are presented in Table 4.4 and Table 4.5, respectively. The maximum computed canopy coverage was 73% in a heavily forested area. The NLCD assigned effective roughness length values have a RMSE of 1.244 meters. This is well within the magnitude of the predicted and observed values and in fact exceeds the average of the field measured values, making this an unacceptable level of error. From the perspective of effective roughness length, a RMSE of this magnitude can be considered approximately equivalent to twice the error that would result from erroneously parameterizing Shrub Land as Evergreen Forest. Compared to values published in the literature, the NLCD data was within range on 12.5% of the sites, while the field measured values were within range on 20.8% of the sites.

Table 4.4: Surface canopy values computed from field measurements

Site	***Canopy Coverage***	***Site***	***Canopy Coverage***	***Site***	***Canopy Coverage***
ANER-01	0.00	ANER-09	0.00	LKMO-04	0.43
ANER-02	0.00	ANER-10	0.08	SEMF-01	0.15
ANER-03	0.04	HILO-01	0.00	SEMF-02	0.00
ANER-04	0.00	HILO-02	0.15	SEMF-03	0.17
ANER-05	0.13	HILO-03	0.00	SEMF-04	0.02
ANER-06	0.00	LKMO-01	0.73	SEMF-05	0.00
ANER-07	0.12	LKMO-02	0.25	SEMF-06	0.20
ANER-08	0.23	LKMO-03	0.63	SEMF-07	0.02

Table 4.5: Comparison of effective roughness values computed from field measurements and those assigned by 1992 NLCD

	Effective Roughness Length (m)			
Site	***NLCD***	***Field***	***Error***	***Range from literature based on in-situ conditions***
ANER-01	0.090	0.039	0.052	0.010 – 0.100
ANER-02	0.090	0.003	0.087	0.008 – 0.030
ANER-03	0.720	0.097	0.623	0.180 – 0.240
ANER-04	0.090	0.000	0.090	0.0002 – 0.0005
ANER-05	0.550	1.945	-1.395	0.900 – 1.000
ANER-06	0.090	0.004	0.087	0.0040 – 0.016
ANER-07	0.550	0.921	-0.371	0.650 – 0.800
ANER-08	0.252	0.100	0.152	0.170 – 0.240
ANER-09	0.090	0.011	0.080	0.004 – 0.015
ANER-10	0.720	1.182	-0.462	0.650 – 1.000
HILO-01	0.040	0.140	-0.100	0.02 – 0.06
HILO-02	0.720	0.689	0.031	0.650 – 0.800
HILO-03	0.550	0.195	0.355	0.350 – 0.450
LKMO-01	0.720	0.124	0.596	0.070 – 0.20
LKMO-02	0.040	0.187	-0.147	0.045 – 0.055
LKMO-03	0.041	4.658	-4.617	1.700 – 2.300
LKMO-04	0.110	3.399	-3.289	1.500 – 2.200
SEMF-01	0.103	0.962	-0.859	0.450 – 0.550
SEMF-02	0.530	0.039	0.491	0.250 – 0.400
SEMF-03	0.550	0.196	0.354	0.350 – 0.450
SEMF-04	0.090	0.610	-0.520	0.450 – 0.600
SEMF-05	0.506	0.061	0.445	0.200 – 0.450
SEMF-06	0.200	0.461	-0.261	0.500 – 1.000
SEMF-07	0.666	0.321	0.345	0.400 – 0.500
RMSE			**1.244**	

The absolute errors for the predicted and observed Manning's n and effective roughness lengths were compared using a single sample *t-test*. The results of this test, using a two-tailed approach

and a 95% confidence interval (a = 0.05), are shown in Table 4.6 for Manning's n and effective roughness length, respectively. As shown in Table 5, the 95% confidence intervals for Manning's n and effective roughness length are 0.039 – 0.088 and 0.165 meters – 1.152 meters, respectively. Therefore, we reject the null hypothesis that the mean absolute error is zero for both parameters. This indicates that the Manning's n and effective roughness length values predicted by LULC method were significantly different than those measured in the field.

Table 4.6: Results of a two tailed t-test (95% confidence) on the absolute errors of the surface roughness values assigned by 1992 NLCD to those computed from field measurements

	Absolute Error	
Statistic	***Manning's n***	z_0
Mean	0.064	0.659
Standard Deviation	0.054	1.078
Number of Observations	24	24
Degrees of Freedom	23	23
Standard Error	0.011	0.220
t statistic	5.766	2.993
p value	0.000	0.006
alpha	0.05	0.05
alpha/2	0.025	0.025
Confidence Interval	0.025	0.493
Lower Confidence Limit	0.039	0.165
Upper Confidence Limit	0.088	1.152

Lastly, the errors in all parameters were not equal across the different LULC types encountered in the field. As shown in Table 4.7, the 1992 NLCD does a reasonable job at predicting Manning's n for Bare Rock / Sand, Grassland and Herbaceous Wetland areas but does an especially poor job predicting Manning's n for Evergreen Forest and Woody Wetland Areas. In

terms of effective roughness length, the results are generally poor but contrary to the results of the Manning's n comparison, the 1992 NLCD data did a poor job predicting the values for Grassland and Herbaceous Wetland areas.

Table 4.7: Results of the comparison between surface roughness parameters assigned by 1992 NLCD to those computed from field measurements, broken down by LULC class

*1992 NLCD Class**		*Number of Sites*	*Manning's n RMSE*	*z_0 RMSE (meters)*
31	Bare Rock / Sand	6	0.015	0.225
33	Transitional	2	0.072	0.214
42	Evergreen Forest	6	0.133	0.469
71	Grassland	3	0.012	2.667
91	Woody Wetland	5	0.096	0.712
92	Herbaceous Wetland	2	0.005	2.403

*** For sites where more than one LULC class is present, the dominant class is used**

4.5 Discussion

The selection of techniques for direct measurement of roughness, especially for bottom friction, required a delicate balance of considerations including budget, available equipment, applicability, and scale. Kouwen and Fathi-Moghadam (2000) present an excellent work detailing the measurement of drag measurements on four species of conifer trees. Järvelä (2002, 2005) conducted flume experiments where both and non-submerged vegetation density were important factors in computing roughness, primary as a function of velocity. Baptist *et al.* (2007) induced equations describing the flow resistance due to vegetation that were refined using genetic programming and tested on both synthetic and actual laboratory testing data. Hutoff *et al.* (2007) developed an analytical solution to the problem of flow through submerged vegetation. This method reduces the vegetation density to a field of identical rigid cylinders in

order to apply a standard drag force term. All of these methods increased the understanding of the flow processes at work when fluid flows through vegetation; however, they are not necessarily applicable to large scale parameterizations of highly mixed vegetation in variable flow fields influenced by outside factors such as wind and pressure, yet. These methods are without a doubt a step in this direction but the authors selected the method of Arcement and Schneider (1989) because it was developed for field conditions, is widely used in the United States and it contributed significantly to the development of the bottom friction lookup tables based on LULC data, as presented in Bunya *et al.* (2010) and Dietrich *et al.* (2011).

There are systematic factors concerning the field measurements and the associated computations that must be noted. The field measurements themselves contain systematic errors and in the case of Manning's *n*, rely on human estimates of surface roughness conditions. Furthermore, the computations of Manning's *n* and effective roughness length are based on empirically derived equations.

The primary sources of uncertainty in the field measurements are the estimations of the Manning's n components and surface canopy. Using the guidance provided in Arcement and Schneider (1989), in particular Table 3 of that report, the participants were all working from the same framework to estimate n_1, n_3 and n_4'. The participant estimates did differ but not to any significant degree. The average of the standard deviations for each parameter on each site are 0.0035, 0.0047 and 0.0032 for n_1, n_3 and n_4', respectively. This was computed by determining the variance of each set of estimations (i.e. among the participants) on each site and computing the standard deviation of the set consisting of those values across all sites. The average standard

deviation for the surface canopy estimates, computed in a similar manner was approximately 13%. This is reasonable considering the nature of the measurement and equipment used. On average, the estimations among the participants are reasonable and errors are managed by discarding outliers and averaging as explained in Section 3.1.

Some field measurements were carried out with equipment that has inherent systematic and random errors. Canopy diameters were measured using measuring tapes; on small vegetation this error was minimal as the participants could accurately determine the extents. However, for trees, the process involved determining the extent of the canopy visually and positioning beneath it. It is estimated that the canopy diameter measurements for tall trees could vary as much as plus or minus 0.5 meters. An error bar of this magnitude does not significantly impact the computation of effective roughness length because for tall trees, their height tends to be the dominant factor and also they tend to have large diameters thereby minimizing the percentage of the measured diameter affected by the error.

The heights of the trees were measured using a laser hypsometer. Uncertainty in this measurement is influenced by the participant's judgment as to the location of the top of the tree. It is also influenced by the ability for the laser to accurately range the distance to the tree being measured; this is a problem in dense forests where the line of sight from the participant to the tree trunk is often obstructed. This source of uncertainty is minimized by taking two height measurements for each tree and averaging the result. These same sources of uncertainty are also present in the measurement of height to significant branch (H_{SB}). Throughout this research campaign, the tree height measurements and significant branch heights taken by the two

participants differed by 0.64 and 0.35 meters, respectively. These differences are minor and any error is minimized by averaging the two prior to the computations. There is also the added uncertainty due to the participant's selection of the significant branch, i.e the lowest branch that contributes to the canopy. Due to the averaging of measurements from two participants, this error is also minimized.

There is also error in the comparison of results due to the use of handheld GPS technology to locate sites in the field. The handheld GPS used in this research has an accuracy of 2 – 5 meters depending on the conditions (3 meters was common). This may lead to spatially inaccurate classification of a sites LULC class and subsequently it's associated surface roughness parameters. Since the resolution of the 1992 NLCD data is 30 meters, this error may be significant. However, this error is mitigated by using an area weighted average of the surface roughness parameters within a site.

The equations used to convert the field measurements into surface roughness parameters are largely empirical in nature. This is especially true of Equations (4.2), (4.4) and (4.7). However, these equations are established in the literature and the studies that have occurred in this field since they were published. In the absence of a true physical measure of friction, or more fundamental, of energy loss, these equations are acceptable. They do, however, contain some variables whose values must be assumed in order to perform the computations.

Most obviously, the value of hydraulic radius, R, was assumed to be one meter. Recall that for a flood plain, R is equal to the depth of flooding. This is a realistic value for the primary

application of this research to hurricane storm surge modeling. However, hurricane storm surges can range from fractions of a meter (on the order of one foot) to several meters such as those experienced in Mississippi during Hurricane Katrina (Knabb *et al.*, 2011). Even considering this sensitivity to the assumed parameter of flood depth, coastal hydrodynamic models such as ADCIRC (Luettich & Westerink, 2006; Luettich *et al.*, 1992) convert the specified Manning's n to a minimum bottom friction coefficient that varies quadratically with depth. Therefore, assuming a flood depth of one meter is reasonable for the parameterization of hurricane storm surge models.

The basis of the selection of surface roughness parameters using the NLCD data is the identification of the sites LULC classification. The 1992 NLCD classes for the sites used in this research are shown in Table 4.1. It is worth noting that coastal inundation modelers apply distance or area weighted interpolation schemes that factor in not only the LULC class at the exact location of a computational point, but include those in the surrounding area in as well. This minimizes the adverse effects of small pockets of a particular LULC class surrounded by a different one (Atkinson *et al.*, 2011). However, the inherent variability within each LULC class, along with misclassification errors, still presents a problem for physics-based modelers. The interpolation schemes employed in practice serve to smooth out, but not eliminate, the errors associated with the LULC method for assigning surface roughness parameters. Another source of uncertainty in the results presented herein is the time elapsed between the acquisition of the remotely sensed data used to classify the LULC of the 1992 NLCD and the field measurements taken to compute competing surface roughness parameters. While this is certainly true as shown in Table 4.1, at its root, the primary contention of this research is not that the 1992 NLCD data

are inaccurate, but rather that it was not designed to describe the surface roughness of the terrain and therefore does a sub-optimal job at doing so. Since 1992 NLCD data are the basis for parameterizing contemporary hurricane storm surge models, they make a good candidate for comparison. Even as LULC classifications become more accurate, the problem of the inherent variability within the LULC classes remains and therefore the unique roughness of the terrain at any given point in the domain will by definition be homogenized due to the categorical nature of LULC classes.

Even with these sources of uncertainty, only in a few cases were the field measured roughness parameters drastically different from the range given in the literature. This is to be expected since the ranges given in the literature require a significant amount of judgment and experience to apply, whereas computing the roughness values based on field measurements is a fairly straight forward procedure. It is interesting to note that the roughness parameters associated with LULC classes, regardless of scheme, were all generated based on the values published in the literature. This demonstrates how much the in-situ roughness associated with a particular LULC class can vary from the "typical" conditions used to assign the parameters.

4.6 Conclusions

In order to investigate the accuracy of assigning surface roughness parameters based on NLCD land cover classes, parameters were computed based on field measurements taken at 24 sites in Florida. The computed parameters were Manning's n bottom friction coefficient, surface canopy coverage, and effective roughness length. These three surface roughness parameters play a significant role in the modeling of tidal and storm surge flow over land.

The results of the study indicate that while parameterizing surface roughness using NLCD land cover data may be the best available practice at present, it is deficient. The inherent variability within land cover classes and misclassification errors in terms of their engineering properties renders this methodology sub-optimal. Furthermore, while detection and classification methods have increased in efficiency and accuracy in recent years, areas can still be incorrectly classified, leading to erroneous local roughness parameterizations. Perhaps engineers and modelers would be better served by parameterizing surface roughness based on the physical structure of the terrain and the obstructions lying on it. However, typical coastal model domain sizes prohibit field campaigns sufficient in scope to properly parameterize the entire region of interest.

Therefore, an alternative approach may be to mine remotely sensed data such as airborne LiDAR (especially since the application of LiDAR is already required for FEMA coastal inundation digital elevation models) to describe the terrain roughness and compute the corresponding surface roughness parameters which will facilitate applying the methodology at a regional or geographical scale. Work on this topic has been initiated by Menenti and Ritchie (1994), Straatsma and Middelkoop (2007) and Straatsma (2008) who were all able to develop parameterization schemes without reliance on categorical data such as LULC. However, work remains to be done to fully develop a method for parameterizing surface roughness, both bottom friction and aerodynamic roughness that is applicable to large scale hydrodynamic modeling. With that capability, a comparison between identical coastal inundation models, one parameterized using LULC data and one parameterized based on the physical terrain roughness described using remotely sensed data could be performed. This comparison would determine whether or not model performance is improved by a more physically-based parameterization of

surface roughness. The mining of LiDAR data may also provide a means to easily parameterize fractional surface canopy coverage over a model domain and lead to its implementation in coastal inundation models, further reducing the uncertainty in this important parameter.

4.7 Acknowledgments

The authors wish to thank Matt Bilskie, Peter Bacopoulos, Ammarin Daranpob, Daina Smar, Davina Passeri for assisting with the field measurements. We also wish to thank the Florida Fish and Wildlife Conservation Commission, the Florida Division of Forestry, and the Florida Department of Environmental Protection for facilitating the field work on the lands in their charge. We are also deeply grateful to James Angelo for his advice on the presentation of the statistical results. This study is funded in part under NASA Grant Number NNX09AT44G. The statements, findings, conclusions, and recommendations expressed herein are those of the authors and do not necessarily reflect the views of NASA.

4.8 References

Aberle, J., & Smart, G. M. 2003. The influence of roughness structure on flow resistance on steep slopes. *Journal of Hydraulic Research, 41*(3), 259-269. doi: 10.1080/00221680309499971

Arcement, G. J., & Schneider, V. R. 1989. Guide for Selecting Manning's Roughness Coefficients for Natural Channels and Flood Plains (pp. 67).

Aricó, C., Nasello, C., & Tucciarelli, T. 2009. Using unsteady-state water level data to estimate channel roughness and discharge hydrograph. *Advances in Water Resources, 32*, 1223-1240. doi: 10.1016/j.advwatres.2009.05.001

Atkinson, J. H., Roberts, H. J., Hagen, S. C., Zou, S., Bacopoulos, P., Medeiros, S. C., . . . Cobell, Z. 2011. Deriving frictional parameters and performing historical validation for an ADCIRC storm surge model of the Florida gulf coast. *Florida Watershed Journal, 4*(2), 22-27.

Bacopoulos, P., Funakoshi, Y., Hagen, S. C., Cox, A. T., & Cardone, V. J. 2009. The role of meteorological forcing on the St. Johns River (Northeastern Florida). *Journal of Hydrology, 369*, 55-70.

Bakry, M. F., Gates, T. K., & Khattab, A. F. 1992. Field-measured hydraulic resistance characteristics in vegetation-infested canals. *Journal of Irrigation and Drainage Engineering, 118*(2), 256-274.

Baptist, M. J., Babovic, V., Rodríguez Uthurburu, J., Keijzer, M., Uittenbogaard, R. E., Mynett, A., & Verway, A. 2007. On inducing equations for vegetation resistance. *Journal of Hydraulic Research, 45*(4), 435-450. doi: 10.1080/00221686.2007.9521778

Barnes, H. H. 1967. Roughness Characteristics of Natural Channels: U.S. Geological Survey.

Bunya, S., Dietrich, J. C., Westerink, J. J., Ebersole, B. A., Smith, J. M., Atkinson, J. H., . . . Roberts, H. J. 2010. A High-Resolution Coupled Riverine Flow, Tide, Wind, Wind Wave and Storm Surge Model for Southern Louisiana and Mississippi. Part I: Model Development and Validation. *Monthly Weather Review, 138*, 345-377.

Burguete, J., Garcìa-Navarro, P., Murillo, J., & Garcìa-Palacìn, I. 2007. Analysis of the friction term in the one-dimensional shallow-water model. *Journal of Hydraulic Engineering, 133*(9), 1048-1063. doi: 10.1061/(ASCE)0733-9429(2007)133:9(1048)

Cardone, V. J., & Cox, A. T. 2009. Tropical cyclone wind field forcing for surge models: critical issues and sensitivities. *Natural Hazards, 51*, 29-47. doi: 10.1007/s11069-009-9369-0

Chow, V. T. 1959. *Open-channel hydraulics*. New York: McGraw-Hill Book Co.

Chow, V. T., Maidment, D. R., & Mays, L. W. 1988. *Applied Hydrology*: McGraw-Hill, Inc.

Clynch, J. R., & Garfield, N. 2006, March 22, 2011. Equations of an Ellipse, from http://www.gmat.unsw.edu.au/snap/gps/clynch_notes.htm

Cobby, D. M., Mason, D. C., Horritt, M. S., & Bates, P. D. 2003. Two-dimensional hydraulic flood modelling using a finite-element mesh decomposed according to vegetation and topographic features derived from airborne scanning laser altimetry. *Hydrological Processes, 17*, 1979-2000. doi: 10.1002/hyp.1201

De Doncker, L., Troch, P., Verhoven, R., Bal, K., Meire, P., & Quintelier, J. 2009. Determination of the Manning roughness coefficient influenced by vegetation in the river Aa and Biebrza river. *Environmental Fluid Mechanics, 9*, 549-567. doi: 10.1007/s10652-009-9149-0

Dietrich, J. C., Westerink, J. J., Kennedy, A. B., Smith, J. M., Jensen, R. E., Zijlema, M., . . . Cobell, Z. 2011. Hurricane Gustav (2008) waves and storm surge: Hindcast, synoptic analysis and validation in southern Louisiana. *Monthly Weather Review, 139*, 2488-2522. doi: 10.1175/2011MWR3611.1

FEMA. 2006. Multi-hazard Loss Estimation Methodology - Hurricane Model - HAZUS MH MR3 (pp. 598 pp.). Washington, D.C.

French, R. H. 1985. *Open Channel Hydraulics*. New York: McGraw-Hill.

Galland, J.-C., Goutal, N., & Hervouet, J. M. 1991. TELEMAC: A new numerical model for solving shallow water equations. *Advances in Water Resources, 14*(3), 138-148.

Gomez, B. 1993. Roughness of stable, armored gravel beds. *Water Resources Research, 29*(11), 3631-3642.

Gomez, J. A., Vanderlinden, K., & Nearing, M. A. 2005. Spatial variability of surface roughness and hydraulic conductivity after disk tillage: implications for runoff variability. *Journal of Hydrology, 311,* 143-156. doi: 10.1016/j.jhydrol.2005.01.014

Harun-ur-Rashid, M. 1990. Estimation of Manning's roughness coefficient for basin and border irrigation. *Agricultural Water Management, 18,* 29-33.

Hervouet, J. M. 2000. TELEMAC modelling system: an overview. *Hydrological Processes, 14,* 2209-2210.

Homer, C., Dewitz, J., Fry, J., Coan, M., Hossain, N., Larson, C., . . . Wickham, J. 2007. Completion of the 2001 National Land Cover Database for the Conterminous United States. *Photogrammetric Engineering and Remote Sensing, 73*(4), 337-341.

Huang, W. Q., Li, Y., Gerard, S., Li, C. M., & Xu, R. C. 2002. *A 'Learning From Human' heuristic for solving unequal circle packing problem.* Paper presented at the First International Workshop on Heuristics, Beijing, China.

Huthoff, F., Augustijn, D. C. M., & Hulscher, S. J. M. H. 2007. Analytical solution of the depth-averaged flow velocity in case of submerged rigid cylindrical vegetation. *Water Resources Research, 43*(W06413). doi: 10.1029/2006WR005625

Jakubis, M. 2000. A contribution to determination of the roughness coefficient of drainage and irrigation channels with clopes reinforced and grassing. *Journal of the International Comission on Irrigation and Drainage, 49*(3), 41-54.

Järvelä, J. 2002. Flow resistance of flexible and stiff vegetation: a flume study with natural plants. *Journal of Hydrology, 269*(1-2), 44-54. doi: 10.1016/S0022-1694(02)00193-2

Järvelä, J. 2005. Effect of submerged flexible vegetatin on flow structure and resistance. *Journal of Hydrology, 307,* 233-241. doi: 10.1016/j.jhydrol.2004.10.013

Jasinski, M. F., & Crago, R. D. 1999. Estimation of vegetation aerodynamic roughness of natural regions using frontal area density determined from satellite imagery. *Agricultural and Forest Meteorology, 94,* 65-77.

Knabb, R. D., Rhome, J. R., & Brown, D. P. 2011. Tropical Cyclone Report, Hurricane Katrina, 23-30 August 2005 (N. H. Center, Trans.): National Oceanographic and Atmospheric Administration.

Kouwen, N., & Fathi-Moghadam, M. 2000. Friction factors for coniferous trees along rivers. *Journal of Hydraulic Engineering, 126*(10), 732-740.

Lettau, H. 1969. Note on Aerodynamic Roughness-Parameter Estimation on the Basis of Roughness-Element Description. *Journal of Applied Meteorology, 8*, 828-832.

Li, Z., & Zhang, J. 2001. Calculation of field Manning's roughness coefficient. *Agricultural Water Management, 49*, 153-161.

Limerinos, J. T. 1970. Determination of the Manning coefficient from measured bed roughness in natural channels (pp. 47).

Luettich, R. A., & Westerink, J. J. 2006. ADCIRC: A Paralell Advanced Circulation Model for Oceanic, Coastal and Estuarine Waters. *adcirc.org*. Retrieved from http://adcirc.org/documentv46/ADCIRC_title_page.html

Luettich, R. A., Westerink, J. J., & Scheffner, N. W. 1992. ADCIRC: An advanced three-dimensional circulation model for shelves, coasts, and estuaries, Report 1: Theory and methodology of ADCIRC-2DDI and ADCIRC-3DL (pp. 1-137). Vicksburg, Mississippi: Department of the Army, US Amry Corps of Engineers, Waterways Experiment Station.

Macdonald, R. W., Griffiths, R. F., & Hall, D. J. 1998. An improved method for the estimation of surface roughness of obstacle arrays. *Atmospheric Environment, 32*(11), 1857-1864.

Mailapalli, D. R., Raghuwanshi, N. S., Singh, R., Schmitz, G. H., & Lennartz, F. 2008. Spatial and temporal variation of Manning's roughness coefficient in furrow irrigation. *Journal of Irrigation and Drainage Engineering, 134*(2), 185-192. doi: 10.1061/(ASCE)0733-9437(2008)134:2(185)

Marcus, W. A., Roberts, K., Harvey, L., & Tackman, G. 1992. An evaluation of methods for estimating Manning's n in small mountain streams. *Mountain Research and Development, 12*(3), 227-239.

Mason, D. C., Cobby, D. M., Horritt, M. S., & Bates, P. D. 2003. Floodplain friction parameterization in two-dimensional river flood models using vegetation heights derived from airborne scanning laser altimetry. *Hydrological Processes, 17*, 1711-1732. doi: 10.1002/hyp.1270

Mendenhall, W., & Sincich, T. 2007. *Statistics for engineering and the sciences* (5th Edition ed.). Upper Saddle River, NJ: Prentice Hall, Inc.

Menenti, M., & Ritchie, J. C. 1994. Estimation of effective aerodynamic roughness of Walnut Gulch watershed with laser altimeter measurements. *Water Resources Research, 30,* 1329-1337.

Morvan, H., Knight, D., Wright, N., Tang, X., & Crossley, A. 2008. The concept of roughness in fluvial hydraulics and its formulation in 1D, 2D and 3D numerical simulation models. *Journal of Hydraulic Research, 46*(2), 191-208. doi: 10.1080I00221686.2008.9521855

Myers, W. R. C., Knight, D. W., Lyness, J. F., Cassells, J. B., & Brown, F. 1999. Resistance coefficients for inbank and overbank flows. *Proceedings of the Institution of Civil Engineers, Water, Maritime and Energy, 136*(2), 105-115.

National Oceanic and Atmospheric Administration, C. S. C. 1995 - present. The Coastal Change Analysis Program (C-CAP) Regional Land Cover. Charleston, SC: NOAA Coastal Services Center.

Petryk, S., & Bosmajian III, G. 1975. Analysis of flow through vegetation. *Journal of the Hydraulics Division, 101*(HY7), 871-884.

Saleh, A. 1993. Soil roughness measurement: chain method. *Journal of Soil and Water Conservation, 48*(6), 527-529.

Sepaskhah, A. R., & Bondar, H. 2002. Estimation of Manning roughness coefficient for bare and vegetated furrow irrigation. *Biosystems Engineering, 82*(3), 351-357. doi: 10.1006/bioe.2002.0076

Simiu, E., & Scanlan, R. H. 1996. *Wind effects on structures: fundamentals and applications to design*. New York: John Wiley.

Stephan, U., & Gutknecht, D. 2002. Hydraulic resistance of submerged flexible vegetation. *Journal of Hydrology, 269*, 27-43.

Straatsma, M. 2009. 3D float tracking: in situ floodplain roughness estimation. *Hydrological Processes, 23*, 201-212. doi: 10.1002/hyp.7147

Straatsma, M., & Middelkoop, H. 2007. Extracting structural characteristics of herbaceous floodplain vegetation under leaf-off conditions using airborne laser scanner data. *International Journal of Remote Sensing, 28*(11), 2447-2467.

Straatsma, M. W. 2008. Quantitative mapping of hydrodynamic vegetation density of floodplain forests under leaf-off conditions using airborne laser scanning. *Photogrammetric Engineering and Remote Sensing, 74*(8), 987-998.

Strelkoff, T. S., Clemmens, A. J., & Bautista, E. 2000. *Field-parameter estimation for surface irrigation management and design*. Paper presented at the Watershed Management 2000 Science and Engineering Technology for the New Millenium, Fort Collins, CO.

Strelkoff, T. S., Clemmens, A. J., & Bautista, E. 2009. Estimation of soil and crop hydraulic properties. *Journal of Irrigation and Drainage Engineering, 135*(5), 537-555. doi: 1O.106l/(ASCE)IR.l943-4774.0000088

Strickler, A. 1923. Beiträge zur Frage der Geschwindigkeitsformel und der Rauhligkeitszahlen für Ströme, Kanäle und Geschlossene Leitungen. *Mitt. des Eidgenössischen Amtes für Wasser-wirtschaft, 16*.

Sullivan, R., & Greeley, R. 1993. Comparison of aerodynamic roughness measured in a field experiment and in a wind tunnel simulation. *Journal of Wind Engineering and Industrial Aerodynamics, 48*, 25-50.

Tieleman, H. W. 2003. Roughness estimation for wind-load simulation experiments. *Journal of Wind Engineering and Industrial Aerodynamics, 91*, 1163-1173. doi: 10.1016/S0167-6105(03)00058-8

Vieux, B. E., & Farajalla, N. S. 1994. Capturing the essential spatial variability in distributed hydrologcal modelling: hydraulic roughness. *Hydrological Processes, 8*, 221-236.

Vogelmann, J. E., Howard, S. M., Yang, L., Larson, C. R., Wylie, B. K., & Van Driel, N. 2001. Completion of the 1990s National Land Cover Data Set for the conterminous United States from Landsat thematic mapper data and ancillary data sources. *Photogrammetric Engineering and Remote Sensing, 67*, 650-652.

Vogelmann, J. E., Sohl, T. L., Campbell, P. V., & Shaw, D. M. 1998. Regional land cover characterization using LANDSAT thematic mapper data and ancillary data sources. *Environmental Monitoring and Assessment, 51*, 415-428.

Werner, M. G. F., Hunter, N. M., & Bates, P. D. 2005. Identifiability of distributed floodplain roughness values in flood extent estimation. *Journal of Hydrology, 314*, 139-157. doi: 10.1016/j.jhydrol.2005.03.012

Westerink, J. J., Luettich, R. A., Feyen, J. C., Atkinson, J. H., Dawson, C., Roberts, H. J., . . . Pourtaheri, H. 2008. A Basin- to Channel-Scale Unstructured Grid Hurricane Storm Surge Model Applied to Southern Louisiana. *Monthly Weather Review, 136*, 833-864.

Wieringa, J. 1993. Representative roughness parameters for homogeneous terrain. *Boundary Layer Meteorology, 63*, 323-363.

Xu, J. P., & Wright, L. D. 1995. Tests of bed roughness models using field data from the Middle Atlantic Bight. *Continental Shelf Research, 15*(11/12), 1409-1434.

Yu, F. X., & Singh, V. P. 1989. Analytical model for border irrigation. *Journal of Irrigation and Drainage, 115*(6), 982-998.

CHAPTER 5. ASSESSING THE PERFORMANCE OF A NORTHERN GULF OF MEXICO TIDAL MODEL USING SATELLITE IMAGERY

The content in this chapter is under review as: Medeiros, S.C., Hagen, S.C., Temimi, M., Feyen, J.C., Chaouch, N., Weishampel, J.F., Funakoshi, Y., Khanbilvardi, R. 2012. Assessing the performance of a northern Gulf of Mexico tidal model using satellite imagery. *Hydrological Processes, In Review*.

5.1 Introduction

Accurate simulation of the tides is the foundation for any study involving modeling of coastal hydrodynamics. Developing an accurate tidal simulation provides the basis for validating model skill before incorporating more complex processes in the coastal hydrodynamics model such as river inflow, wind, atmospheric pressure, and surface waves. Using this strategy for developing an accurate comprehensive coastal circulation model, the first step is to test the performance of the model in accurately reproducing the local tidal signal.

The assessment of a model's performance will herein be referred to as its skill (Warner *et al.*, 2005), where skill is typically measured by comparing model output to observed data. The most basic comparison is to perform a resynthesis of observed harmonic tide constituents. It is critical to note that such comparison of harmonic tide constituents is only attainable at constantly submerged locations since the harmonic tide constituents are derived from, and represent, a constantly wetted tide signal. As such, gages are installed and maintained off of piers or jettys, measure continuous water levels, perform harmonic analysis on those measured water levels and report the harmonic tide constituents (Parker, 2007). Historical harmonic tide constituents can

be obtained from gages situated within a model's interior, and compared to harmonic tide constituents derived from water level time series computed by the model. In the United States and its territories, this information is available from the National Oceanic and Atmospheric Administration Center for Operational Oceanographic Products and Services (NOAA CO-OPS, http://tidesandcurrents.noaa.gov/). In the event that the subject gage is not maintained by NOAA CO-OPS and/or does not provide harmonic constituents, the historic water level time series can be decomposed (Foreman *et al.*, 1995; Schureman, 1941). One tool for completing this type of analysis is the T_TIDE software package (Pawlowicz *et al.*, 2002).

Additional historical data such as observed water level time series and measured high water marks are also used to validate storm surge models, such as done for model hindcasts in the northern Gulf of Mexico (Westerink *et al.* (2008), Bunya *et al.* (2010) and Dietrich *et al.* (2011)). Comparison to historical high water marks is a limited assessment as it only considers the maximum water level predicted by the model at a given location without providing a skill measure of when the maximum water level occurred. Also, high water mark measurements can be affected by processes such as short wave run-up, as well as by the subjective selection of the actual high water mark elevation(Atkinson *et al.*, 2011).

An assessment of model skill that incorporates both spatial and temporal factors is required in order to examine not only the ability of the model to predict water levels at specific locations, but also the ability of the model to predict the spatial extent of inundated area. This is important for modeling the flooding and drying of tidal flats during ecological studies, projecting the condition

of evacuation/access routes during and after major storms, and assessing the availability of estuarine navigational access.

Nearly all contemporary coastal circulation models employ a numerical wetting and drying (WD) algorithm to simulate the physics of an advancing or receding flood wave. A review of these algorithms is provided by Medeiros and Hagen (2012). WD is a crucial component of models seeking to simulate the astronomic tide. It has been shown that the flooding and ebbing of the tide within coastal marshes can significantly affect the amplitude and phase of the astronomic tide. WD is also needed to simulate the rate of flood and ebb of non-cyclical events such as storm surge (Medeiros *et al.*, 2009). However, the means to test the performance of WD in large scale distributed models are limited, particularly the prediction of the extent of inundation.

Recent advances in the use of remotely sensed data to detect inundated area have taken steps toward this end. In particular, studies conducted by Horritt *et al.* (2001) and Chaouch *et al.* (2011) have used Synthetic Aperture Radar to detect inundated area. The method developed by Horritt *et al.* (2001) was tested by Cobby *et al.* (2003) and Mason *et al.* (2003) in river flood scenarios. The primary difference between the method of Horritt *et al.* (2001) and Chaouch *et al.* (2011) is the former computes the inundation extent as a vector feature (line) using a statistical active contour model where the latter computes a raster representation of cells as wet or dry. In this paper, the method of Chaouch *et al.* (2011), herein referred to as the "synergetic method", has been used to validate an operational tidal model.

A summary of the approach proposed by Chaouch *et al.* (2011) is provided in subsequent section. Further details are provided in Chaouch *et al.* (2011). The synergetic method uses a change detection approach to analyze Radarsat-1 data, in particular the backscatter values. The development of the synergetic method employed a novel approach for identifying the area subject to tidal fluctuations *a priori* and applying the change detection algorithm within that pre-defined band of land area. Masking out the areas that were either always dry or always wet significantly increased the accuracy of the method. The method was validated synoptically by comparing the predictions of inundated area with historic aerial imagery in the Apalachicola region of the Florida panhandle (location shown in Figure 5.1). Please note that herein the term synoptic refers to the conditions at a specific point in time.

This paper expands the previous study by Chaouch *et al.* (2011) and applies the synergetic method to assess the performance of a tidal model of the northern Gulf of Mexico in simulating coastal inundation. First, the performance of the model in continuously submerged regions is assessed by harmonic analysis and comparison of model output to time synchronized tide gage measurements over four separate time periods in the years 2003 and 2004. Then model performance in regions that wet and dry is assessed by comparing the inundated area generated by the model to the inundated area detected using the synergetic method over four areas within the domain during the same time periods as were evaluated for the time series analysis.

5.2 Model Description

For tidal calculation, the two-dimensional, depth-integrated Advanced Circulation (ADCIRC) code (Luettich & Westerink, 2006; Luettich *et al.*, 1992) is used. ADCIRC solves the shallow

water equations in their barotropic form expressed in spherical coordinates (Kolar, Westerink, Gray, *et al.*, 1994). In order to avoid the spurious numerical noise common to finite element solutions of the shallow water equations (Gray, 1982), they are reformulated into a Generalized Wave Continuity equation (GWCE) (Lynch & Gray, 1979). This reformulation contains a combination of a time differentiated form of the primitive continuity equation and a spatially differentiated form of the primitive, conservative momentum equations, to which is added the primitive continuity equation multiplied by a constant τ_0 that is constant in time but (optionally) variable in space. This is followed by the transformation of the advective terms of the GWCE into their non-conservative form (Kolar, Westerink, Cantekin, *et al.*, 1994).

The model is based on the Western North Atlantic Tidal (WNAT) model domain that extends eastward from the 60° west meridian to the North and South American coastlines, incorporating the Atlantic Ocean, Caribbean Sea and the Gulf of Mexico (see

Figure 5.1). In order to produce accurate results, the model boundary must be established well outside the Gulf of Mexico to allow adequate spatial extent for the propagation of non-linear model physics through the Caribbean Sea, into the Gulf and up to the focus area (Blain *et al.*, 1994). The model focuses on the Apalachicola area and was constructed as part of a Federal Emergency Management Agency (FEMA) map modernization study of Franklin, Jefferson and Wakulla (FWJ) counties in Florida (Gangai *et al.*, 2011). This model, herein referred to as FWJ, was selected for its high resolution in the Apalachicola, Florida region with node spacing of 30 to 50 meters in the river channels and bank areas and 250 to 300 meters in the floodplains (see Figure 2). Detailed descriptions of the model development, including the sources of topography,

bathymetry, surface roughness parameterization and tidal validation at four stations located in the focus area of the mesh, including Apalachicola, can be found in Coggin *et al.* (2011), Salisbury *et al.* (2011) and Atkinson *et al.* (2011).

Figure 5.1: Tidal model domain and tide gage station locations (inset)

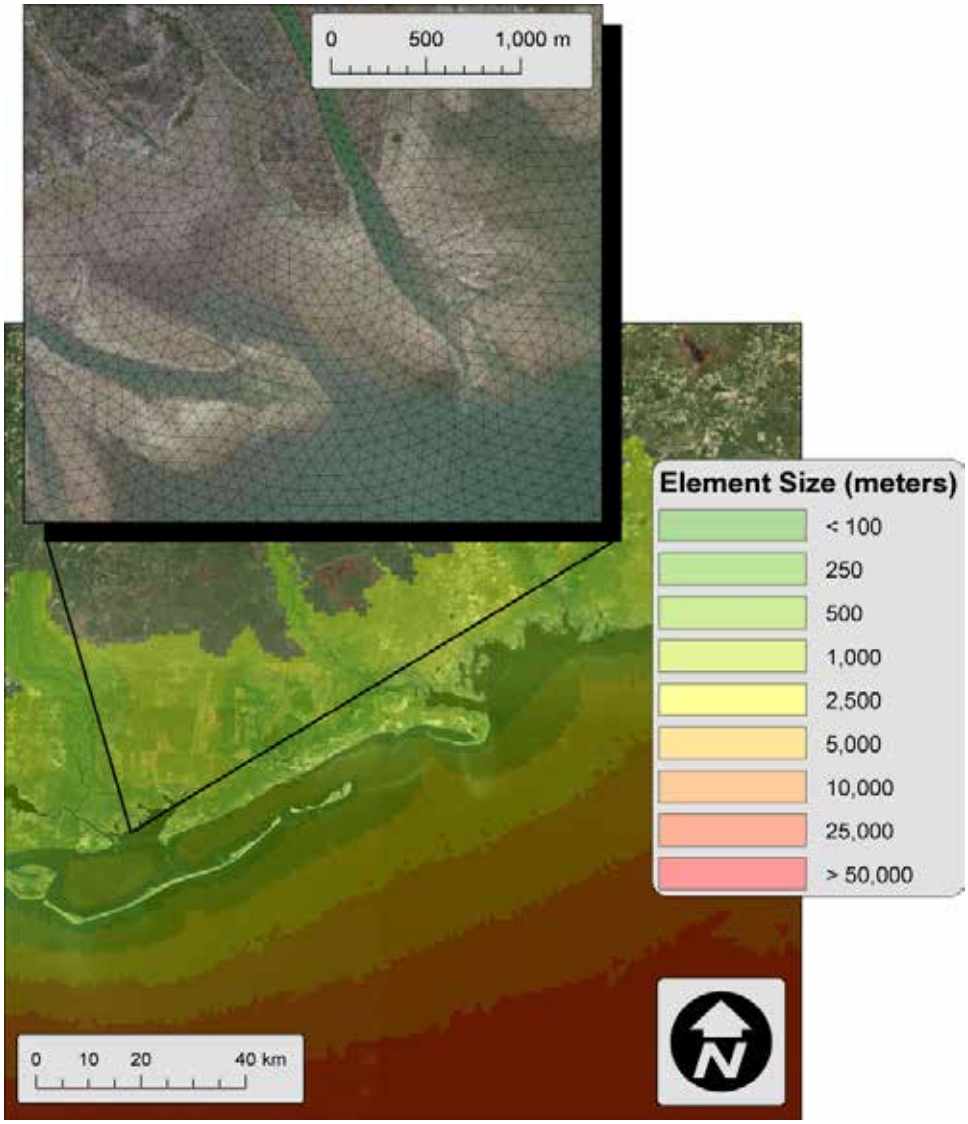

Figure 5.2: Mesh resolution in the tidal model focus area

For the research conducted herein, the model is forced at the open ocean boundary using ten tidal constituents (STEADY, K_1, O_1, Q_1, M_2, S_2, N_2, K_2, M_4 and M_6). Eight tidal potential terms were also included (K_1, O_1, P_1, Q_1, M_2, S_2, N_2 and K_2). These terms were derived from the FES.95.2 tidal database (Jones & Davies, 2008) No other forcing such as river inflow, winds or pressures

were considered. A one second time step was used over a 45 day simulation that included a ten day spin up. Also, an initial water level adjustment, specific to each simulated time period, was implemented to account for the seasonal steric effects that cause swelling or contraction of the Gulf of Mexico (Westerink *et al.*, 2008). This adjustment is necessary to account for water level changes due to thermal and atmospheric pressure effects that are particularly pronounced in the central northern Gulf of Mexico (Turner, 1991).

The harmonic boundary forcing and tidal potential terms (amplitude and phase) were unmodified for the simulations used to analyze the resynthesized tidal signal from the model output and historic gage station constituents. For the simulations used to produce water level time series comparisons and the wet/dry output image for comparison to the synergetic method, the tidal nodal factors and equilibrium arguments (Schureman, 1941) were adjusted to synchronize the model output with the synergetic method snapshot times discussed in the next section.

5.3 Validation Methodology

The tidal model is validated using three methods for skill measure: harmonic analysis, synoptic water level time series and spatial extent of inundation. The first two methods are common in coastal modeling and will give insight into model skill at specific locations within the model interior. The third method is a novel approach that tests not only the model's ability to capture the astronomic tide at specific locations, but also its ability to accurately predict the spatial extent of inundation at specific moments in time. These methods are able to focus in on three characteristics of the model: the resolution of the finite element mesh in key areas, the

description of the terrain processed by the model, and the wetting and drying algorithm used within the numerical code.

The harmonic analysis is conducted at three National Ocean Service (NOS) tide gage stations within the model domain: Apalachicola, FL 8728690; Panama City, FL 8729108; and Cedar Key, FL 8727520 (see Figure 5.1). Twenty-three constituents are harmonically analyzed over the final 30 days of a 45 day ADCIRC simulation (Luettich Jr. & Westerink, 2010). These constituents are resynthesized to form the predicted tidal signal at each station. NOS provides 37 harmonic constituents at each station that are derived by decomposing the observed tidal signal over an entire epoch (NOAA/NOS/CO-OPS, http://tidesandcurrents.noaa.gov/). These constituents are resynthesized to form the theoretical tidal signal at each station. For brevity, only the eight most dominant constituents in terms of amplitude (excluding the Solar Annual and Solar Semi-Annual) at the Apalachicola station are shown in Table 5.1 along with their associated frequencies and amplitudes (Foreman *et al.*, 1995; Pawlowicz *et al.*, 2002).

Table 5.1: Dominant tidal constituents in Apalachicola region

Constituent Name	Description	Frequency (cycles hour^{-1})	Amplitude (meter)
K_1	Lunar diurnal	0.04178075	0.130
M_2	Principal lunar semidiurnal	0.08051140	0.116
O_1	Lunar diurnal	0.03873065	0.112
P_1	Solar diurnal	0.04155259	0.043
S_2	Principal solar semidiurnal	0.08333333	0.037
Q_1	Larger lunar elliptic diurnal	0.03721850	0.023
N_2	Larger lunar elliptic semidiurnal	0.07899925	0.018
K_2	Lunisolar semidiurnal	0.08356149	0.016

Following Willmott (1981), the results of the harmonic analysis are assessed both visually and quantitatively beginning with the model skill measure presented by Warner *et al.* (2005):

$$Skill = 1 - \frac{\sum \left| H_{model} - H_{obs} \right|^2}{\sum \left(\left| H_{model} - \overline{H_{obs}} \right| + \left| H_{obs} - \overline{H_{obs}} \right| \right)^2} \tag{5.1}$$

where H_{model} is the water surface elevation computed by the tidal model at a specific time (meter); H_{obs} is the observed water surface elevation at a tide gage station (meter); and $\overline{H_{obs}}$ is the mean observed water surface elevation over the comparison period (meter). A skill value approaching unity indicates a well performing model.

The water level time series at each station is also used to assess the performance of the tidal model. The water level time series is analyzed at the Apalachicola station over the four time periods that coincide with the remotely sensed data snapshots (see Table 5.2). The performance of the model is again assessed visually and also using the model skill measure of Equation (5.1) over a 15 day period of time extending from seven days prior to and seven days after the remotely sensed data snapshot time. Furthermore, the root mean square error (RMSE) for both the harmonic analysis and the 15 day water level time series is computed according to the following formula:

$$RMSE = \sqrt{\frac{\sum \left(H_{model} - H_{obs} \right)^2}{N}} \tag{5.2}$$

where N is the number of observations. The normalized RMSE (NRMSE) is also presented to account for the tidal range when assessing the impact of an error. The RMSE is normalized using the range of water surface elevations present at the tide gage during the relevant time period as follows:

$$NRMSE = \frac{RMSE}{H_{obs-\max} - H_{obs-\min}} \tag{5.3}$$

Lastly, the model performance is assessed based on the areal extent of the inundated area at a specific historic time. The processing of the remotely sensed data to determine the inundated area is described in detail by Chaouch *et al.* (2011). Four 10 km square areas within the boundary of one Radarsat scene were selected as candidates for skill assessment. The four areas were selected because they contained extensive tidal flats and barrier islands, and also because they represent the major population and recreation centers within the study area. The spatial resolution of Radarsat images is 25m. They were acquired in the same mode, standard mode, with consistent observation geometry. The assessment areas are labeled A through D running from west to east as shown in Figure 5.3 respectively representing Apalachicola, Carrabelle / Dog Island, Ochlockonee Bay and Apalachee Bay. An example of the raw output from the synergetic method is shown in Figure 5.4. Within these areas, it was necessary to convert the output from the model into a geo-referenced image that was time synchronized with the Radarsat data.

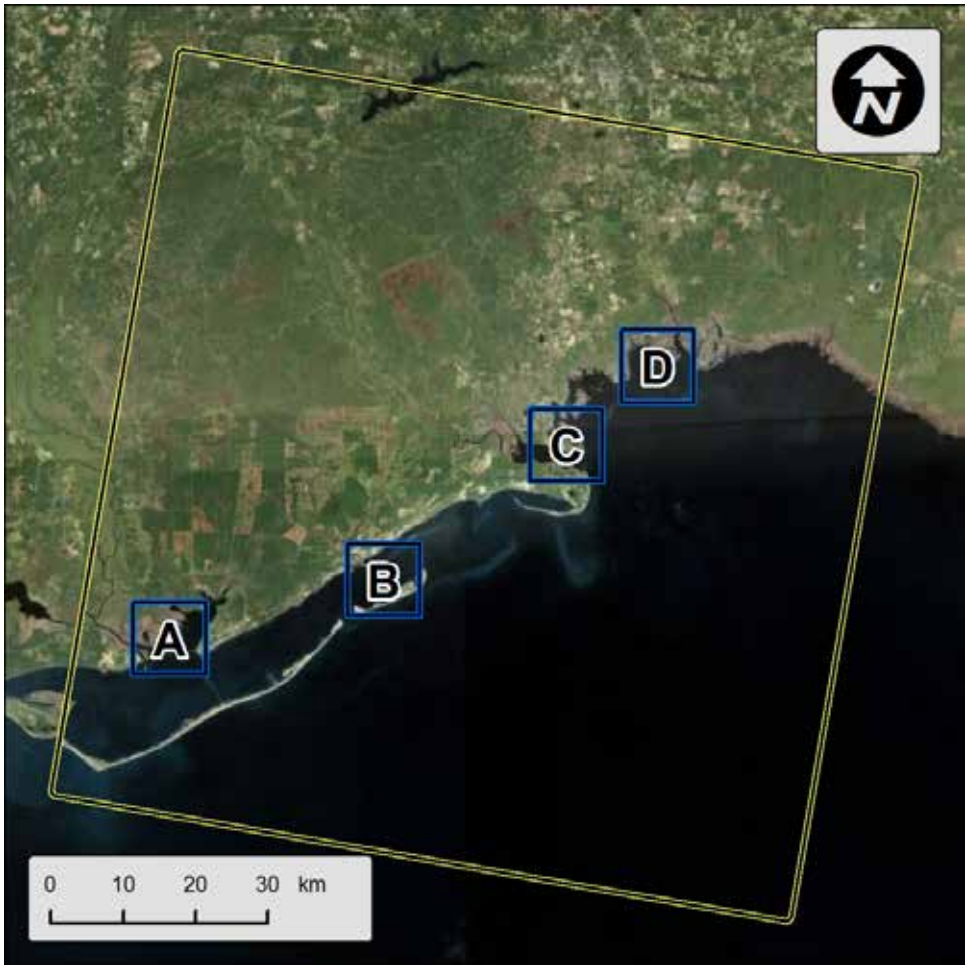

Figure 5.3: Synergetic method assessment areas (blue) within the Radarsat snapshot boundary (yellow)

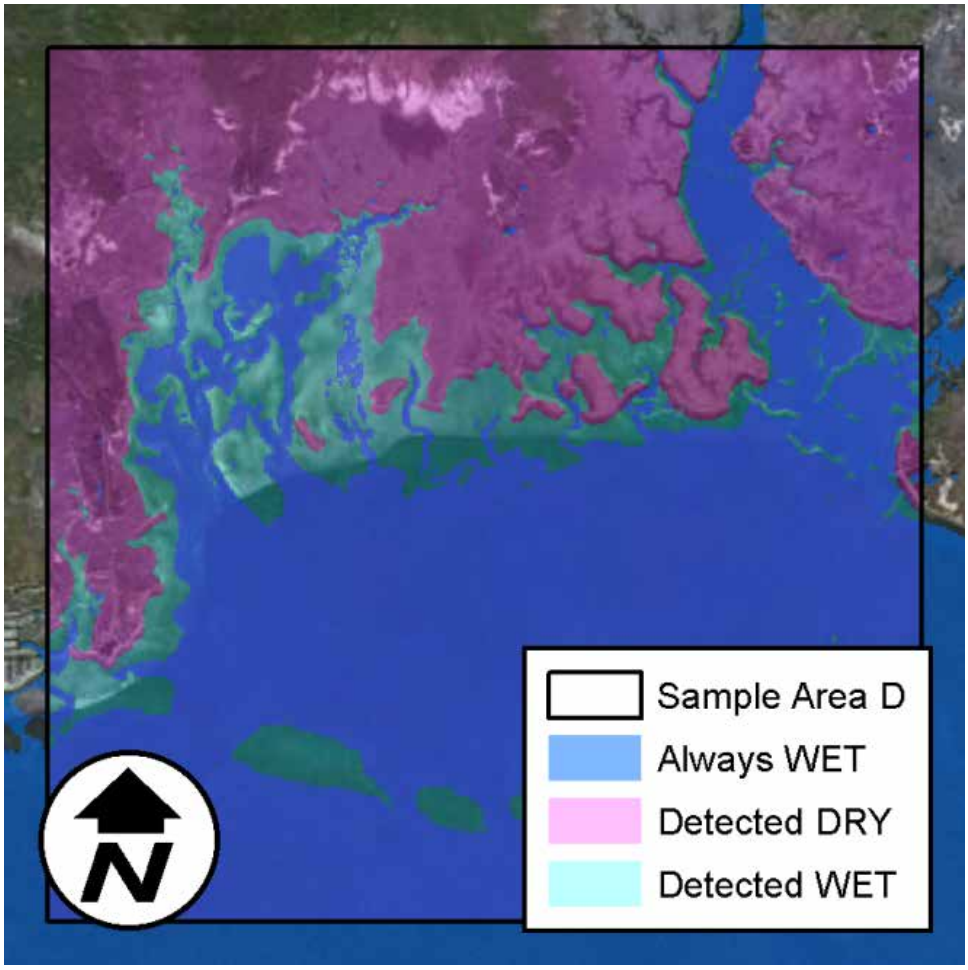

Figure 5.4: Inundation detection output delivered by the synergetic method

As stated previously, the model was simulated over four specific time periods to align with the Radarsat data and to provide a time synchronized comparison of predicted versus observed inundated area. The model produces output consisting of the elevation of the water surface at each computational point at pre-specified time intervals. In this case, the model produced output every 300 time steps or every 5 minutes for the period of time that included the specific time of the Radarsat snapshot. The output set corresponding to the exact time of the Radarsat snapshot

is extracted from the model and converted to a set of spatially distributed XYZ points with the Z value representing the water surface elevation. This set of points is converted to a one channel raster image at the same resolution of the Radarsat snapshot where the pixels are classified as either dry or wet. The two images are then compared and model performance is assessed quantitatively using the Probability of Detection (POD) method (Marzban, 1998; Williams *et al.*, 2002).

The two images are compared and two POD values are computed: one for the areas that should be dry (according to the Radarsat data) and one for the areas that should be wet. POD is computed following Chaouch *et al.* (2011):

$$POD = \frac{A}{(A+C)} \tag{5.4}$$

Where A = the number of pixels correctly classified as class X (either wet or dry) and C = the pixels of class X that have not been classified as class X. The hit rate, or overall classification skill of the model, is also used to measure performance. The hit rate is simply the percentage of the total number of pixels within the subarea that were classified correctly (Makkeasorn *et al.*, 2009) and is equivalent to the average POD, weighted by the number of wet or dry pixels. Higher POD and hit rate indicate better model performance.

Table 5.2: Simulation time period information

Simulation	Simulation Start	Radarsat Snapshot	Simulation End
1	21 Dec 2002	20 Jan 2003	4 Feb 2003
2	18 Aug 2003	17 Sept 2003	2 Oct 2003
3	2 Feb 2004	3 Mar 2004	18 Mar 2004
4	25 Jun 2004	25 Jul 2004	9 Aug 2004

5.4 Results and Discussion

As shown in Figure 5.5, the model performs well when reproducing the resynthesized tidal signal at the three NOS tide gage stations. The peaks and troughs of the tidal signal are captured and the model appears to be in phase. This is corroborated by the high skill and low RMSE and NRMSE results presented in Table 5.3. For example, at the Apalachicola station, the model produces a skill value of 0.97, a RMSE of less than 6 centimeters, and a NRMSE of 6.7%. Furthermore, the results fall within expectations as the model has 30 to 60 meter resolution near the Apalachicola station in contrast to 4 and 4-6 kilometer resolutions at the Panama City and Cedar Key stations respectively. Therefore the model should be more accurate at this location.

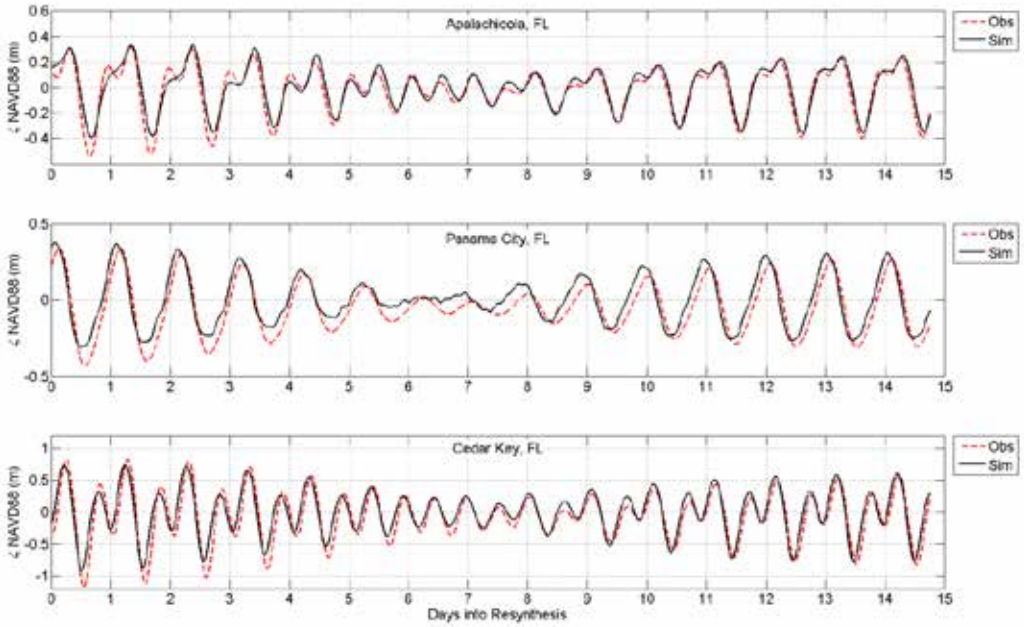

Figure 5.5: Tidal resynthesis plots

Table 5.3: Quantitative assessment of harmonic resynthesis results

Station	Skill	RMSE (meter)	NRMSE %
Apalachicola	0.97	0.058	6.7
Panama City	0.94	0.079	10.3
Cedar Key	0.95	0.164	8.2

The historic water level time series comparisons for the Apalachicola station are shown in Figure 5.6. Only the Apalachicola station lies within both the focus area and Radarsat snapshot boundary; therefore NOS stations in Panama City and Cedar Key are omitted.

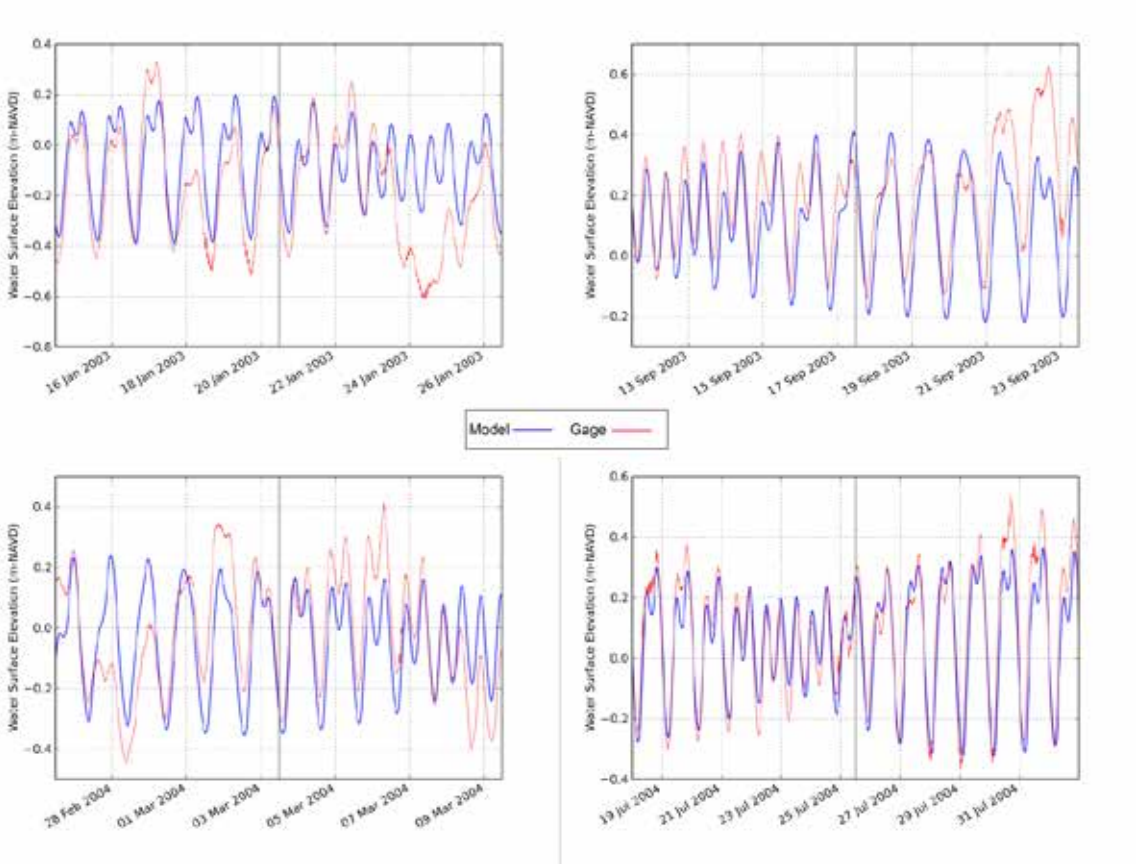

Figure 5.6: Water level time series for the Apalachicola tide gage station at the times of the Radarsat snapshots. The bold vertical line indicates the synergetic method snapshot time.

Table 5.4: Quantitative assessment of synoptic simulations during the four time periods corresponding to the Radarsat snapshots at the Apalachicola tide gage station

Date	Skill	RMSE (meter)	NRMSE %
20 January 2003	0.79	0.175	18.6
17 September 2003	0.83	0.138	17.7
3 March 2004	0.77	0.162	18.9
25 July 2004	0.96	0.074	8.2

Assessing the performance of the model with respect to measured water level time series indicates that there are likely non-astronomic tide forcing mechanisms involved such as riverine inflow and meteorological (wind and pressure) effects, especially during the 20 January 2003 and 3 March 2004 time periods. This is apparent in Figure 5.6 (a) through (c) in the highly non-cyclical nature of the observed tide. At multiple times, such as 24 January 2003, 23 September 2003 and 6 March 2004 the observed tide displays sustained rising or falling trends that are likely caused by ambient winds. The skill measures in Table 5.3 and Table 5.4 corroborate this. To investigate this further, the wind and river inflow conditions during the relevant time periods were examined and are presented in Figure 5.7 and Figure 5.8, respectively.

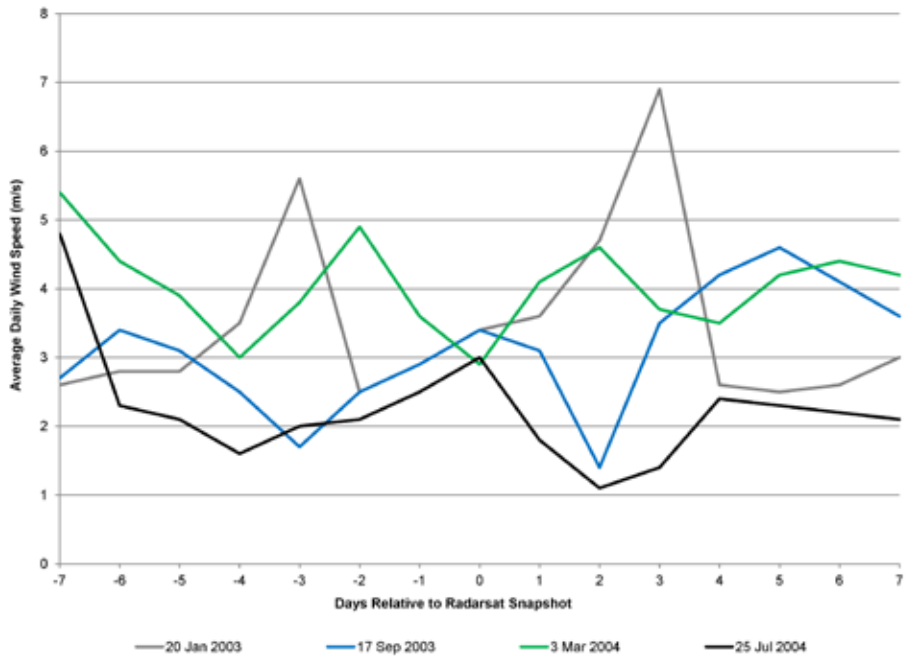

Figure 5.7: Average daily wind speed at Apalachicola Municipal Airport

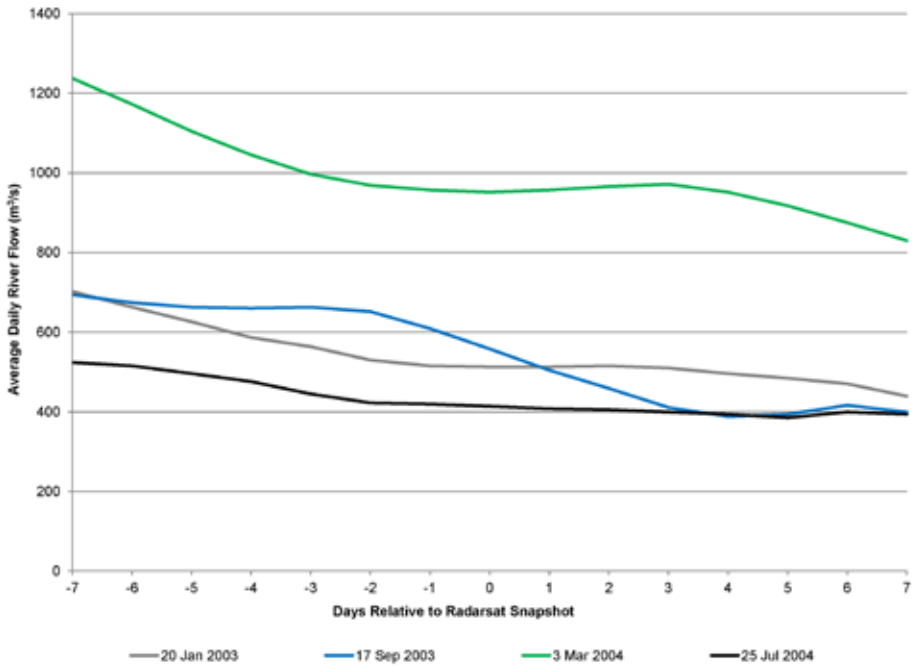

Figure 5.8: Average daily flow for the Apalachicola River

Average daily wind conditions at the Apalachicola Municipal Airport were obtained from the NOAA National Climatic Data Center (NOAA, 2012). Average daily flows for the Apalachicola River (USGS Station No. 02359170) were obtained from the USGS National Water Information System (USGS, 2012). As shown in Figure 5.7, although the wind conditions are highly variable, the 25 July 2004 time period had the lowest overall wind influence. The winds during the 20 January 2003 and 3 March 2004 time periods are generally more intense. In Figure 5.8, the 25 July 2004 time period clearly has the least riverine influence and the 3 March 2004 has the greatest. These results corroborate the water surface elevation results and demonstrate the likelihood that the deviations from the historical data are likely due to these missing model forcings. Furthermore, in general, a model that has a high skill in terms of harmonic resynthesis and less in synoptic comparisons is usually missing physics active during the synoptic

comparisons. The high skill in the harmonic resynthesis indicates that the model resolution, surface roughness parameterization, and topographic / bathymetric description are likely sufficient as these factors have been shown to influence tidal flooding and recession (Bates & Hervouet, 1999; Medeiros *et al.*, 2011; Medeiros *et al.*, 2009; Westerink *et al.*, 1992). Therefore, the error in the synoptic comparisons must be due to the absence of additional forcing mechanisms as described above. The results of the synoptic inundation area comparisons are shown in Figure 5.9 through Figure 5.12. The POD and Hit Rate values are shown in Table 5.5.

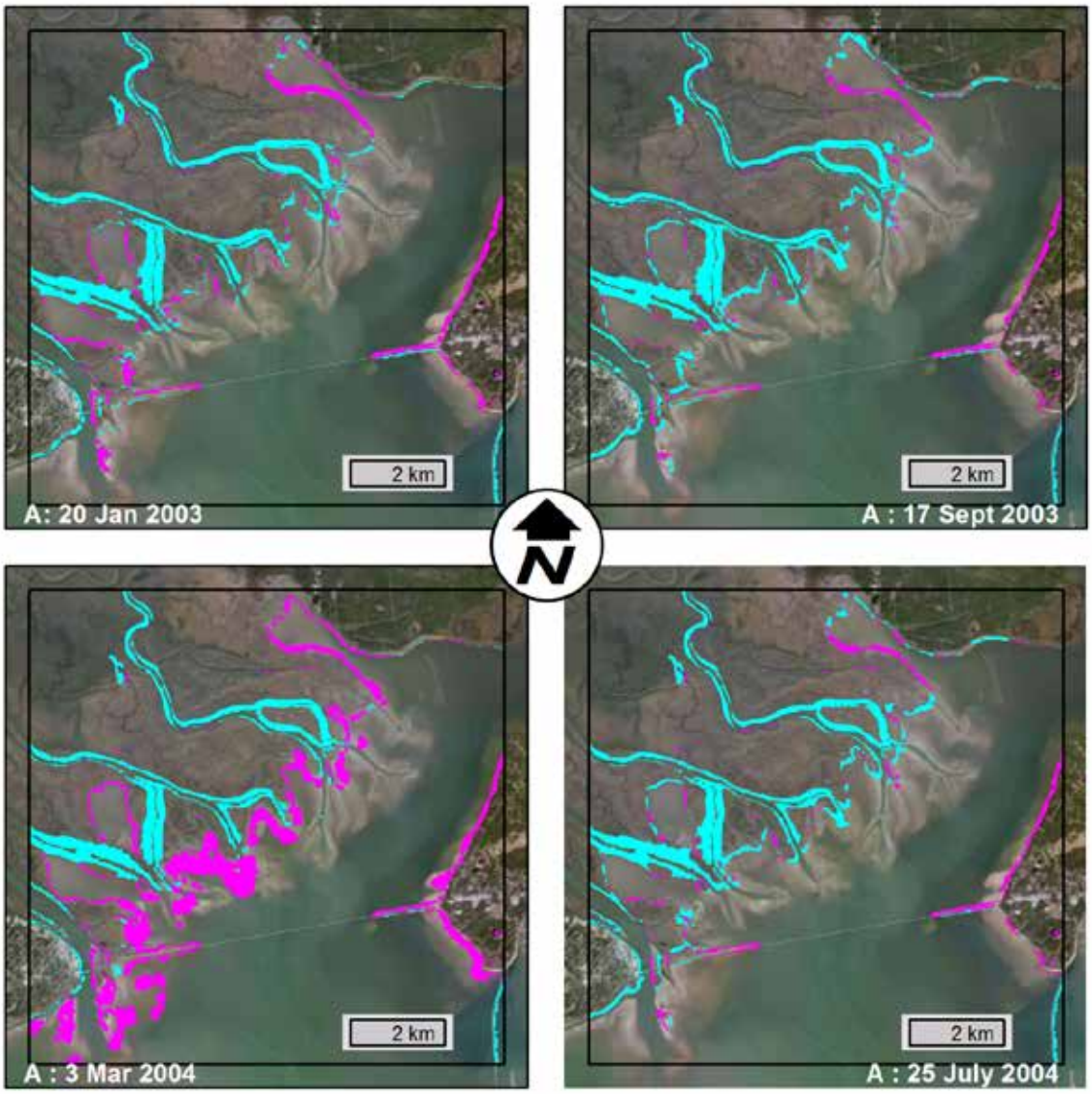

Figure 5.9: Synoptic inundation results for Area A (Apalachicola). Areas incorrectly predicted as DRY shown in magenta; Areas incorrectly predicted as WET shown in cyan. All other areas within the square boundary were correct.

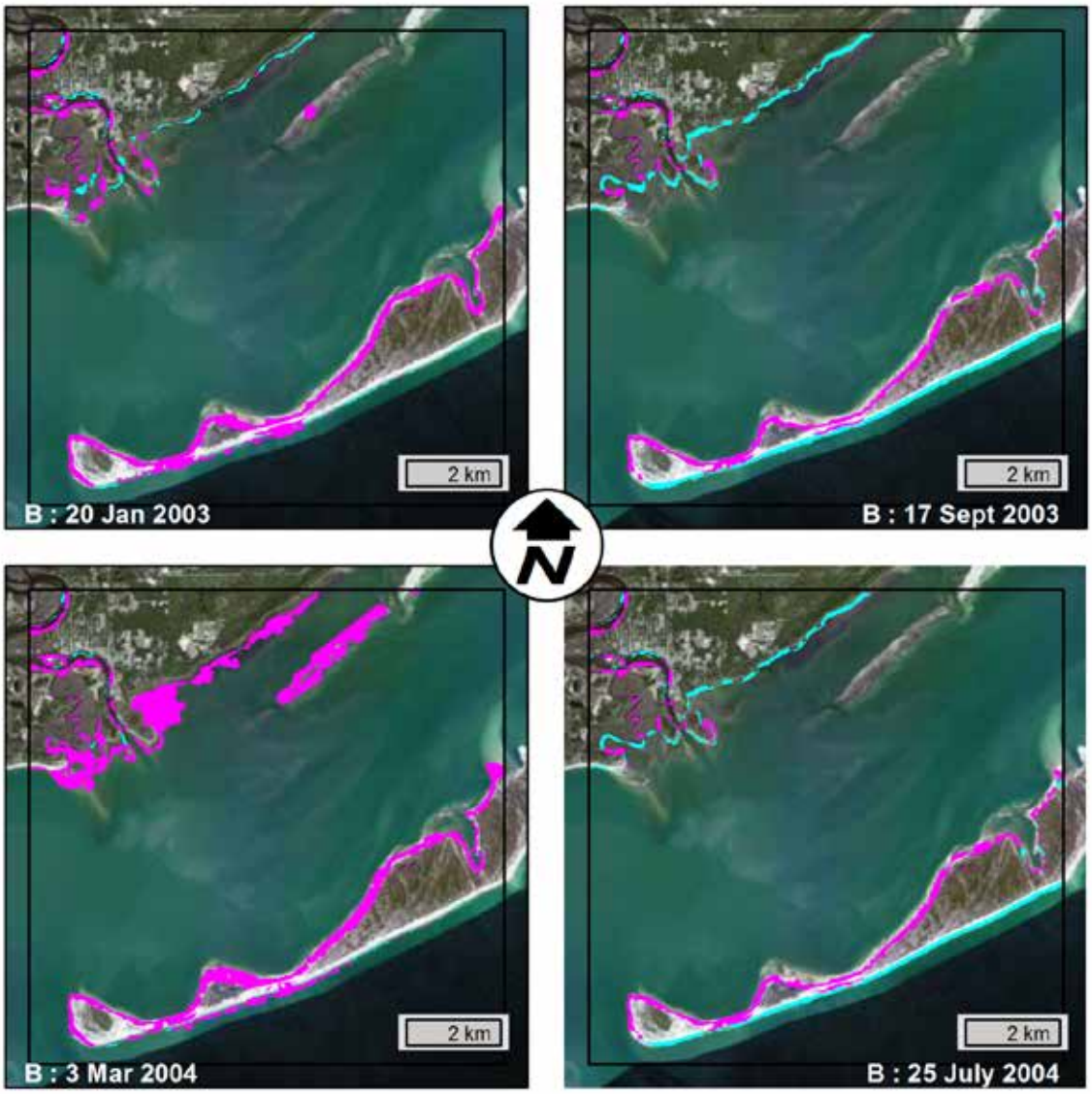

Figure 5.10: Synoptic inundation results for Area B (Carrabelle / Dog Island). Areas incorrectly predicted as DRY shown in magenta; Areas incorrectly predicted as WET shown in cyan. All other areas within the square boundary were correct.

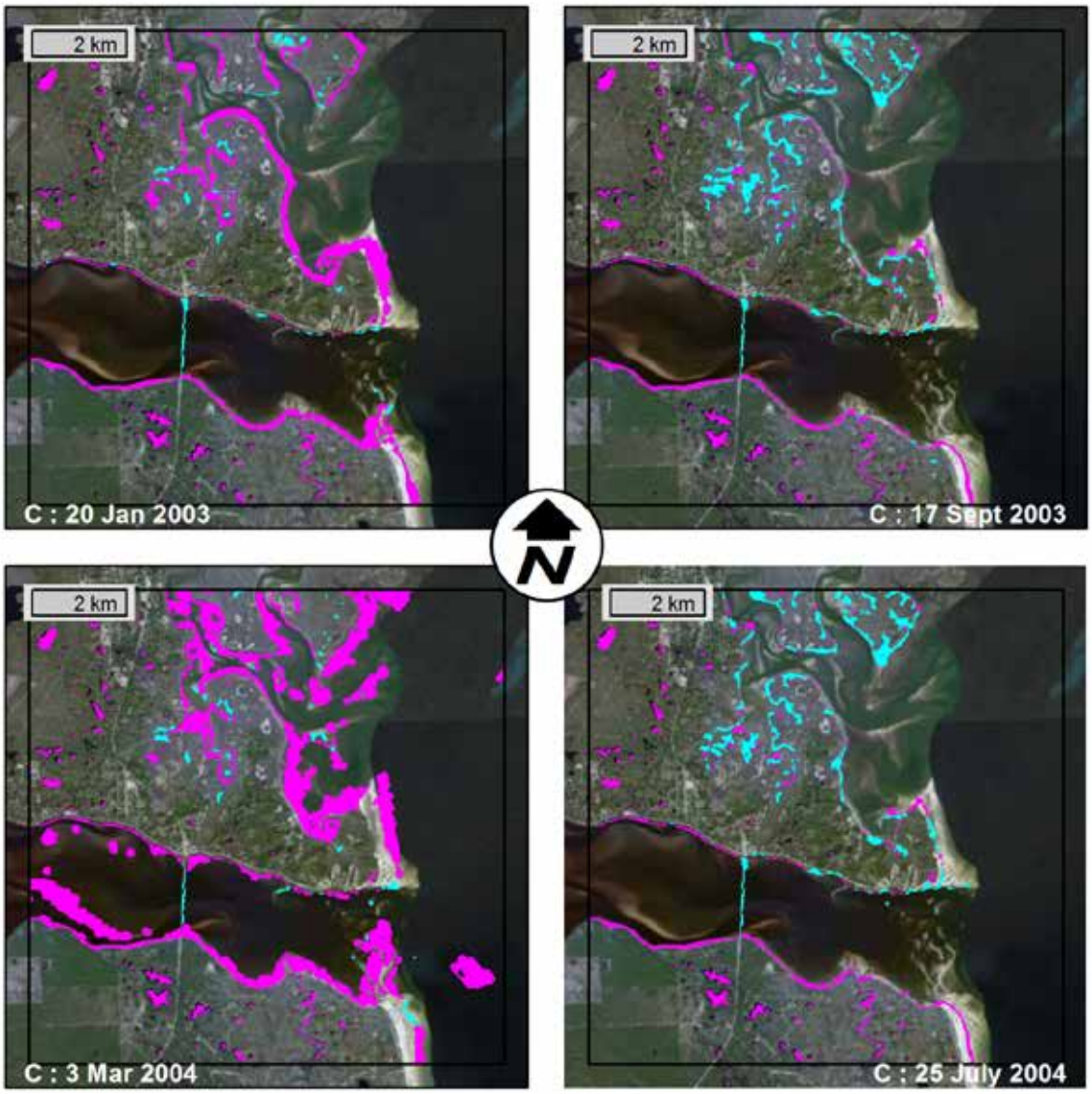

Figure 5.11: Synoptic inundation results for Area C (Ochlockonee Bay). Areas incorrectly predicted as DRY shown in magenta; Areas incorrectly predicted as WET shown in cyan. All other areas within the square boundary were correct.

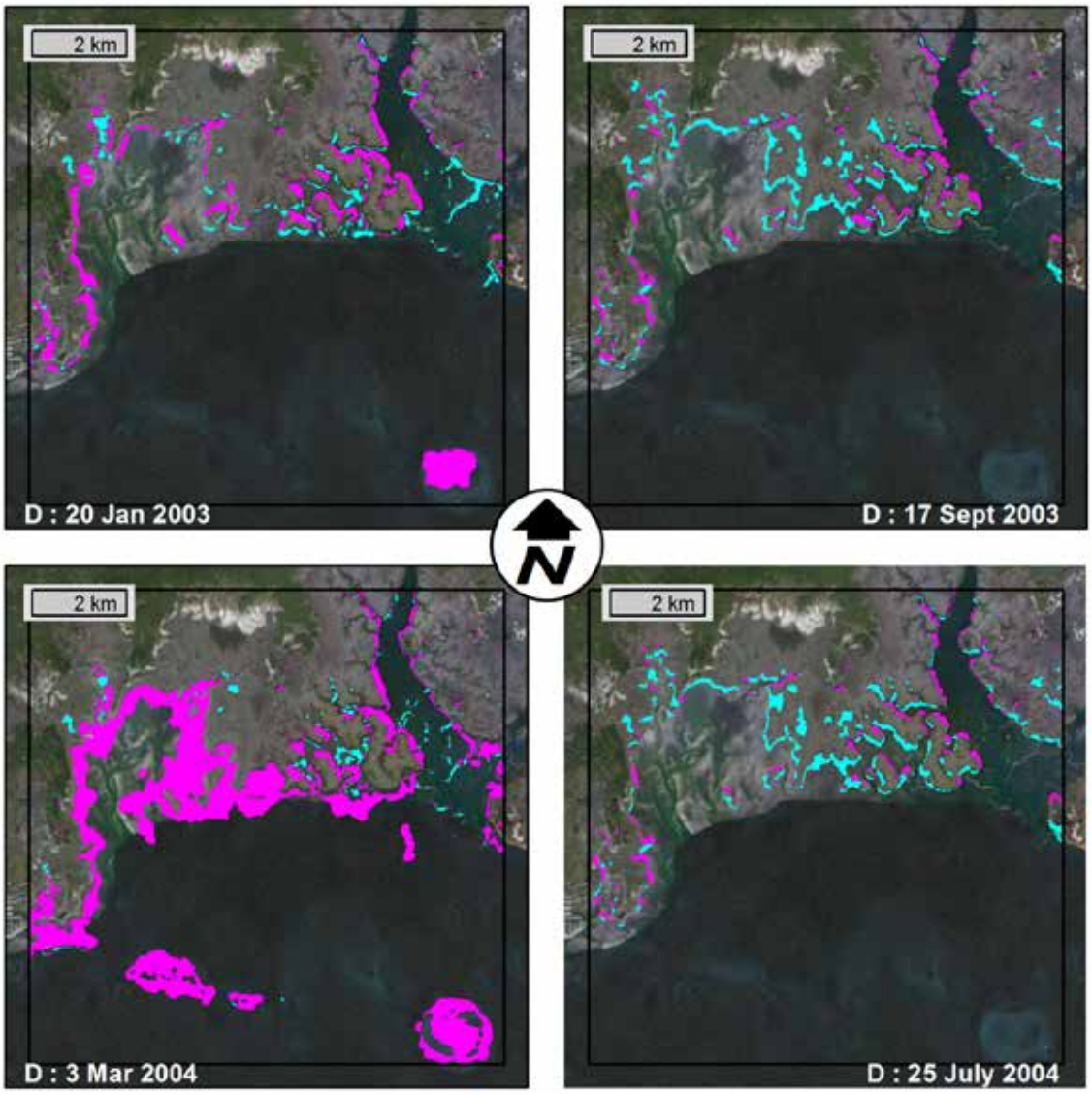

Figure 5.12: Synoptic inundation results for Area D (Apalachee Bay). Areas incorrectly predicted as DRY shown in magenta; Areas incorrectly predicted as WET shown in cyan. All other areas within the square boundary were correct.

Table 5.5: Probability of Detection (POD) and Hit Rate statistics for the inundated area comparison

Area	Date	POD dry	POD wet	Hit Rate
A	20 January 2003	88.8%	96.6%	93.3%
A	17 September 2003	86.8%	98.1%	93.3%
A	3 March 2004	90.0%	88.8%	89.3%
A	25 July 2004	87.6%	97.8%	93.5%
B	20 January 2003	97.5%	96.1%	96.4%
B	17 September 2003	91.1%	97.7%	96.5%
B	3 March 2004	99.4%	92.2%	93.6%
B	25 July 2004	92.4%	97.7%	96.7%
C	20 January 2003	99.0%	90.9%	94.5%
C	17 September 2003	95.6%	96.3%	96.0%
C	3 March 2004	99.0%	79.2%	88.4%
C	25 July 2004	95.5%	96.5%	96.1%
D	20 January 2003	96.5%	94.7%	95.3%
D	17 September 2003	93.0%	97.9%	96.4%
D	3 March 2004	98.2%	81.8%	87.5%
D	25 July 2004	93.4%	98.4%	96.8%

All time periods produce hit rates greater than 85%. The model consistently performs best during the 25 July 2004 time period according to the water level time series and inundation area comparisons. This is also the time period with the least amount of meteorological or riverine influence; therefore, this result is within expectations for reasons described previously. This result also serves to validate the decision to omit the meteorological and riverine inflow forcings for the purposes of establishing the applicability of the synergetic method in this context. With those forcings included, the model should be more accurate (provided the input data were representative of the conditions); however, in order to demonstrate the applicability of the synergetic method, it is beneficial to carefully and intentionally accept discrepancies between the observed data and model results to determine if the synergetic method agrees with traditional

performance assessment techniques. The synergetic method does in fact produce results that agree with traditional assessment methods; simulations with weak quantitative skill values were also weaker in the synergetic method assessment.

Out of the four time periods studied, 3 March 2004 had the lowest water level measured at the Apalachicola station (see Table 5.6). The majority of the error in this time period is incorrectly predicting areas as dry.

Table 5.6: Water levels (m-NAVD88) at the Apalachicola station

Date	Observed Water Level	Modeled Water Level	Difference
20 January 2003	-0.060	0.047	0.107
17 September 2003	0.241	0.387	0.146
3 March 2004	-0.234	-0.277	-0.043
25 July 2004	0.276	0.234	-0.042

One possible reason for the discrepancy in model results compared to ground truth is the issue of topographic description. Having already established that the description of the topographic / bathymetric surface is essential to an accurate model, it must be noted that the FWJ model is largely based on airborne laser scanning data acquired in 2006. It is possible that the LiDAR data over-predicts the elevation in these salt marsh areas due to the emergent vegetation and water level conditions. Focusing on this issue, it is immediately apparent that the synergetic method not only quantitatively assesses the performance of the model in a novel way, but it also yields information that spatially identifies potential problem areas in the model. These problem

areas could be improved during model development by adding resolution and/or improving the topobathy description.

5.5 Conclusions

A recently developed method for detecting inundated area based on synergistically integrated remotely sensed data was applied to assess the performance of a tidal model of the northern Gulf of Mexico. The objective was to demonstrate the applicability of the synergetic method and its agreement with traditional performance assessment methodologies such as harmonic resynthesis and water level time series analysis. A harmonic analysis simulation along with synoptic simulations spanning four specific historical time periods were conducted to test the performance of the tidal model.

The results indicate that the model is able to accurately reproduce the astronomic tides. The harmonic resynthesis produces model skill measures of 0.94 or greater and normalized root mean square errors of 10.3% or less. On a water level time series basis, the model skill exceeded 0.77 in all cases and had normalized root mean square errors of 18.9% or less. The weakest performance occurs during time periods of significant non-astronomic tide influence. The model is able to reproduce the extent of inundation within four sample areas inside the focus region (area of highest resolution) of the model domain and produces hit rate values of greater than 85% in all tests. The comparisons of synoptic inundation areas generally agree with the results of the traditional performance assessment measures and should continue to be used in concert with one another. The results also suggest that there may be topographical discrepancies in the ADCIRC

model, particularly in salt marsh areas. These possible errors are illuminated by the synergetic method, especially during periods of low water.

As the applicability of the synergetic method has been validated herein, it would benefit modelers to apply it as validation protocol in conjunction with traditional methods. However, the synergetic method is limited by the spatial and temporal availability of Radarsat data. It is also not available to the general public at this time. This method shows significant promise in advancing the development of inundation models if it can be widely implemented. This is particularly true in storm surge applications because Radarsat data are unaffected by cloud cover or day/night restrictions. It would be relevant for governmental agencies to task satellites for acquiring data during tropical cyclone activity and make use of the data in real time for the monitoring of these extreme events. The advancements in wetting and drying algorithm development and testing, hindcast simulation validation, and post-storm assessments that would be made possible would result in scientific advances within the modeling community. Also, the emergency management community would benefit from access to observed flooding conditions during major coastal events.

5.6 Acknowledgments

This study is funded in part under NASA Grant Number NNX09AT44G. The statements, findings, conclusions, and recommendations expressed herein are those of the authors and do not necessarily reflect the views of NASA. Computer simulations were carried out on the high performance computing cluster STOKES at the University of Central Florida, Institute for Simulation and Training (System Administrator: Sergio Tafur, Ph.D.) The two lead authors were

also given a tour of the focus area by Mr. Ron Bartel of the Northwest Florida Water Management District and this paper benefitted immensely from this local knowledge.

5.7 References

Atkinson, J. H., Roberts, H. J., Hagen, S. C., Zou, S., Bacopoulos, P., Medeiros, S. C., . . . Cobell, Z. 2011. Deriving frictional parameters and performing historical validation for an ADCIRC storm surge model of the Florida gulf coast. *Florida Watershed Journal, 4*(2), 22-27.

Bates, P. D., & Hervouet, J.-M. 1999. A new method for moving-boundary hydrodynamic problems in shallow water. *Proceedings of the Royal Society of London, Series A, 455*, 3107-3128.

Blain, C. A., Westerink, J. J., Luettich, R. A., & Scheffner, N. W. 1994. ADCIRC: An advanced three-dimensional circulation model for shelves, coasts, and estuaries, Report 4: Hurricane storm surge modeling using large domains. Vicksburg, Mississippi.

Bunya, S., Dietrich, J. C., Westerink, J. J., Ebersole, B. A., Smith, J. M., Atkinson, J. H., . . . Roberts, H. J. 2010. A High-Resolution Coupled Riverine Flow, Tide, Wind, Wind Wave and Storm Surge Model for Southern Louisiana and Mississippi. Part I: Model Development and Validation. *Monthly Weather Review, 138*, 345-377.

Chaouch, N., Temimi, M., Hagen, S. C., Weishampel, J. F., Medeiros, S. C., & Khanbilvardi, R. 2011. A synergetic use of satellite imagery from SAR and optical sensors to improve coastal flood mapping in the Gulf of Mexico. *Hydrological Processes, In Press*. doi: 10.1002/hyp.8268

Cobby, D. M., Mason, D. C., Horritt, M. S., & Bates, P. D. 2003. Two-dimensional hydraulic flood modelling using a finite-element mesh decomposed according to vegetation and topographic features derived from airborne scanning laser altimetry. *Hydrological Processes, 17*, 1979-2000. doi: 10.1002/hyp.1201

Coggin, D. W., Hagen, S. C., & Salisbury, M. B. 2011. A digital elevation model for Franklin, Wakulla and Jefferson counties, Florida. *Florida Watershed Journal, 4*(2), 5-10.

Dietrich, J. C., Westerink, J. J., Kennedy, A. B., Smith, J. M., Jensen, R. E., Zijlema, M., . . . Cobell, Z. 2011. Hurricane Gustav (2008) waves and storm surge: Hindcast, synoptic analysis and validation in southern Louisiana. *Monthly Weather Review, 139*, 2488-2522. doi: 10.1175/2011MWR3611.1

Foreman, M. G. G., Crawford, W. R., & Marsden, R. F. 1995. De-tiding: Theory and Practice. In D. R. Lynch & A. M. Davies (Eds.), *Coastal and Estuarine Studies, 47, Quantitative Skill Assessment for Coastal Ocean Studies* (pp. 203-239). Washington, DC: AGU Press.

Gangai, J., Hagen, S. C., & Bartel, R. 2011. An overview of a FEMA coastal inundation study for the Big Bend region of Florida. *Florida Watershed Journal, 4*(2), 1-4.

Gray, W. G. 1982. Some inadequacies of finite element models as simulators of two-dimensional circulation. *Advances in Water Resources, 5*(3), 171-177.

Horritt, M. S., Mason, D. C., & Luckman, A. J. 2001. Flood boundary delineation from Synthetic Aperture Radar imagery using a statistical active contour model. *Internation Journal of Remote Sensing, 22*(13), 2489-2507. doi: 10.1080/0143116011690

Jones, J. E., & Davies, A. M. 2008. Storm surge computations for the west coast of Britain using a finite element model (TELEMAC). *Ocean Dynamics, 58*, 337-363. doi: 10.1007/s10236-008-0140-y

Kolar, R. L., Westerink, J. J., Cantekin, M. E., & Blain, C. A. 1994. Aspects of nonlinear simulations using shallow-water models based on the wave continuity equation. *Computers and Fluids, 23*(3), 523-538.

Kolar, R. L., Westerink, J. J., Gray, W. G., & Luettich, R. A. 1994. Shallow water modeling in spherical coordinates: Equation formulation, numerical implementation, and application. *Journal of Hydraulic Research, 32*(1), 3-24.

Luettich Jr., R. A., & Westerink, J. J. 2010, April 1, 2010. ADCIRC User's Manual - v49 Retrieved February 20, 2012, from http://adcirc.org/documentv49/ADCIRC_title_page.html

Luettich, R. A., & Westerink, J. J. 2006. ADCIRC: A Paralell Advanced Circulation Model for Oceanic, Coastal and Estuarine Waters. *adcirc.org*. Retrieved from http://adcirc.org/documentv46/ADCIRC_title_page.html

Luettich, R. A., Westerink, J. J., & Scheffner, N. W. 1992. ADCIRC: An advanced three-dimensional circulation model for shelves, coasts, and estuaries, Report 1: Theory and methodology of ADCIRC-2DDI and ADCIRC-3DL (pp. 1-137). Vicksburg, Mississippi: Department of the Army, US Amry Corps of Engineers, Waterways Experiment Station.

Lynch, D. R., & Gray, W. G. 1979. A wave equation model for finite element tidal computations. *Computers and Fluids, 7*, 207-228.

Makkeasorn, A., Chang, N. B., & Li, J. 2009. Seasonal change detection of riparian zones with remote sensing images and genetic programming in a semi-arid watershed. *Journal of Environmental Management, 90*, 1069-1080.

Marzban, C. 1998. Scalar Measures of Performance in Rare-Event Situations. *Weather and Forecasting, 13*(3), 753-763. doi: 10.1175/1520-0434(1998)013<0753:smopir>2.0.co;2

Mason, D. C., Cobby, D. M., Horritt, M. S., & Bates, P. D. 2003. Floodplain friction parameterization in two-dimensional river flood models using vegetation heights derived

from airborne scanning laser altimetry. *Hydrological Processes, 17*, 1711-1732. doi: 10.1002/hyp.1270

Medeiros, S. C., Ali, T. A., Hagen, S. C., & Raiford, J. P. 2011. Development of a Seamless Topographic / Bathymetric Digital Terrain Model for Tampa Bay, Florida. *Photogrammetric Engineering and Remote Sensing, 77*(12), 1249-1256.

Medeiros, S. C., & Hagen, S. C. 2012. Review of wetting and drying algorithms for numerical tidal flow models. *International Journal for Numerical Methods in Fluids, In Press*.

Medeiros, S. C., Takahashi, N., Wang, Q., & Hagen, S. C. 2009. *Hurricane storm surge simulation for a coastal riverine system using a high resolution unstructured mesh with detailed surface characteristics.* Paper presented at the 33rd IAHR Congress: Water Engineering for a Sustainable Environment, Vancouver, BC, Canda.

NOAA. 2012. National Climatic Data Center Retrieved 03/11/2012, from http://www.ncdc.noaa.gov/oa/ncdc.html

NOAA/NOS/CO-OPS. NOAA Tides & Currents, Harmonic Constutuents Retrieved January 25, 2012, from http://tidesandcurrents.noaa.gov/station_retrieve.shtml?type=Harmonic+Constituents

Parker, B. B. 2007. Tidal Analysis and Prediction (C. f. O. O. P. a. S. National Ocean Service, Trans.). Silver Spring, MD: U.S. Department of Commerce, National Oceanic and Atmospheric Administration.

Pawlowicz, R., Beardsley, R. C., & Lentz, S. 2002. Classical tidal harmonic analysis including error estimates in MATLAB using T_TIDE. *Computers and Geosciences, 28*, 929-937.

Salisbury, M. B., Hagen, S. C., Coggin, D. W., Bacopoulos, P., Atkinson, J. H., & Roberts, H. J. 2011. Unstructured mesh development for the Big Bend region (Florida). *Florida Watershed Journal, 4*(2), 11-14.

Schureman, P. 1941. Manual of harmonic analysis and prediction of tides (C. a. G. Survey, Trans.). Washington, DC: U.S. Department of Commerce.

Turner, R. E. 1991. Tide gauge records, water level rise, and subsidence in the northern Gulf of Mexico. *Estuaries and Coasts, 14*(2), 139-147. doi: 10.2307/1351687

USGS. 2012. National Water Information System Retrieved 03/121/2012, from http://waterdata.usgs.gov/nwis/

Warner, J. C., Geyer, W. R., & Lerczak, J. A. 2005. Numerical modeling of an estuary: A comprehensive skill assessment. *Journal of Geophysical Research, 110*(C05001), 13 pp.

Westerink, J. J., Luettich, R. A., Baptista, A. M., Scheffner, N. W., & Farrar, P. 1992. Tide and Storm Surge Predictions Using Finite Element Model. *Journal of Hydraulic Engineering, 118*(10), 1373-1390.

Westerink, J. J., Luettich, R. A., Feyen, J. C., Atkinson, J. H., Dawson, C., Roberts, H. J., . . . Pourtaheri, H. 2008. A Basin- to Channel-Scale Unstructured Grid Hurricane Storm Surge Model Applied to Southern Louisiana. *Monthly Weather Review, 136*, 833-864.

Williams, R. N., Michael, K. J., Pendlebury, S., & Crowther, P. 2002. An automated image analysis system for determining sea-ice concentration and cloud cover from AVHRR images of the Antarctic. *International Journal of Remote Sensing, 23*(4), 611-625. doi: 10.1080/01431160010025989

Willmott, C. J. 1981. On the validation of models. *Physical Geography, 2*(2), 184-194.

CHAPTER 6. COMPUTING SPATIALLY DISTRIBUTED SURFACE ROUGHNESS PARAMETERS USING LIDAR POINT CLOUD DATA

6.1 Introduction

Tidal and storm surge modeling in coastal areas provides key decision makers with information that allows them to most effectively protect life and property. This life and property is almost always located in the overland regions of the model, therefore the model must have sufficient resolution and be parameterized as accurately as possible in these locations. This paper focuses on the latter requirement.

The framework for this investigation is two-dimensional depth integrated tidal and storm surge simulations using models such as the Advanced Circulation Model for Oceanic, Coastal and Estuarine Waters (ADCIRC; Luettich & Westerink, 2006; Luettich *et al.*, 1992) and TELEMAC-2D (Galland *et al.*, 1991; Hervouet, 2000). Recent studies using these models in this context have been conducted by Hagen *et al.* (2011), Dietrich *et al.*(2011), Bunya *et al.* (2010), Jones *et al.* (Jones *et al.*, 2009), Jones and Davies (2008), Westerink *et al.* (2008), and Coughlan *et al.* (2007). In terms of developing models of this type, surface roughness is the most important input parameter for inundation models after topography (M. Straatsma, 2009) as they influence wind velocity and overland flow (Ritchie, 1996). The surface roughness parameters most often used in contemporary tidal and storm surge modeling are Manning's *n* (bottom friction), surface canopy closure (reduction of vertical wind effects) and effective roughness length (also known as z_0, reduction of horizontal wind effects). The current methodology for specifying surface

roughness parameters across large scale distributed models, especially in the United States, relies heavily on published land use / land cover data such as Coastal Change Analysis Project (C-CAP; National Oceanic and Atmospheric Administration, 1995 - present) and the National Land Cover Dataset (Homer *et al.,* 2007; Vogelmann *et al.,* 2001). This method is useful mainly because it is easily automatable, straightforward to apply; and scientifically defensible; these are important attributes as model scope and resolution increases. However, it has been shown by Medeiros *et al.* (2012) that this method is locally deficient due to the variability of surface roughness within each LULC class, misclassification errors within the LULC data, and errors arising from parameterizing a continuous variable (roughness) using discrete look-up tables. Therefore, a new method for computing these parameters would be beneficial.

Past research into the translation of field conditions into numerical model parameters is extensive. While they have made excellent contributions to our understanding of roughness within natural flow fields, microscale studies investigating the drag forces and flow resistance in and around individual roughness elements, or very small patches of roughness elements, such as Hutoff *et al.* (2007), Wilson *et al.* (Wilson *et al.*, 2003), Stephan and Gutknecht (2002) are not considered here in order to focus on large scale parameterization techniques involving remotely sensed data. In particular, studies that investigated methods for using remotely sensed data to describe above-ground vegetation are especially relevant.

The term “remotely sensed data” can refer to essentially any data acquired by means other than direct measurement but is typically used to describe data acquired from aircraft or orbiting satellites. Remotely sensed data, especially those acquired via satellite, have proven to be

effective in describing the properties of the ground surface and vegetation. In a hybrid approach, Straatsma and Baptist (2008) fused LiDAR with multispectral data in order to enhance the parameterization of spatially distributed Chézy bottom friction coefficient in a floodplain However, 3-dimensional LiDAR point cloud data have been shown to contain abundant descriptive information about the landscape (Wang & Tseng, 2010). In fact, Hyyppä and Hyyppä (1999) demonstrated that LiDAR point cloud data outperformed various optical remotely sensed data (SPOT, Landsat Thematic Mapper) for extracting measureable attributed from vegetation (Raber *et al.*, 2002). Therefore, 3-dimensional LiDAR point cloud data will be used to construct the parameterization model proposed herein. To further refine the scope, large footprint or full waveform LiDAR studies such as Drake *et al.* (2002), Hollaus *et al.* (2011) are not considered because small footprint LiDAR is overwhelming more prevalent in tidal and storm surge modeling and it is also more effective for measuring the characteristics of trees , a significant contributor to surface roughness in coastal regions.

First, it is appropriate to note that term airborne laser scanning, or ALS, is synonymous with both laser altimetry and Light Detection and Ranging, or LiDAR (Coggin, 2008). While the extraction object surfaces is one of the most beneficial uses of the 3-dimensional LiDAR point cloud (Vosselman *et al.*, 2004), in terms of computing hydrodynamic model roughness parameters, measureable vegetation characteristics such as height and frontal area are essential (Mason *et al.*, 2003). In fact, much of the earliest work in this field focused on establishing that LiDAR could be used to measure vegetation and forest characteristics accurately and efficiently (Lim *et al.*, 2003). Nelson *et al.* (1984) present one of the earliest studies using airborne laser scanning (ALS) to determine vegetation properties, in particular the characteristics of a forest

canopy. In particular, that study was able to establish a relationship between canopy closure (a relevant surface roughness parameter) and the penetration capability of the airborne laser. Menenti and Ritchie (1994) also used ALS to estimate a surface roughness parameter. In that study, an empirical relationship between the mean vegetation height and standard deviation of vegetation height was able to estimate the effective roughness length, z_0, at the watershed scale. De Vries *et al.* (2003) applied a similar and slightly more advanced technique, also to compute z_0 based on the relationship between obstruction height, frontal area and planimetric area developed by Lettau (1969). The standard deviation of LiDAR elevations was also used by Davenport *et al.* (2000) and Hopkinson *et al.* (2004) to estimate measured vegetation height; this methodology was adapted parameterize roughness for river flood modeling by Cobby *et al.* (2001). Weltz *et al.* (1994) used ALS not only to estimate vegetation heights, but also to distinguish between different plant communities. Ritchie (1996) further explored the application of this technology to hydrologic studies, including the measurement of surface roughness. Straatsma and Middelkoop (2007) present some shortcomings of LiDAR data in terms of computing hydrodynamic roughness including the lack stem stiffness information and the land cover dependence of the empirical relationships.

As stated previously, any method for computing surface roughness parameters for large scale, distributed coastal hydrodynamic models must also be automatable in order to be practical. Two primary criteria must be satisfied in order to meet this requirement: First, it must be relatively straightforward to translate the mathematics behind the method into computer code. This leads the researcher to use the simplest possible mathematical model to describe the empirical relationships between the LiDAR point cloud and the ground truth data (Kraus & Rieger, 1999).

Second, the source data required by the method must be available over the applicable areas of the model domain.

This paper proposes a method that uses 3-dimensional LiDAR point cloud data, tiled into pixels that slightly exceed the resolution of the hydrodynamic model mesh, to parameterize surface roughness. While comparing the vegetation characteristics to LiDAR data at the tile or plot level (i.e. on a defined patch of terrain) has been done in the past (see Kato *et al.* (2007) for a listing of previous studies), the research presented herein is unique because it takes the derived vegetation characteristics and uses them to compute surface roughness parameters directly. The field measured surface roughness terms from 24 test sites in Florida are used to derive the empirical relationships through multi-variate regression.

6.2 Methodology

The general methodology followed herein is as follows: establishment of test sites that have both LiDAR point cloud data and field measurements, tabulating field measurements and subsequent surface roughness parameter computation results (response variables), pre-processing point cloud data, computing statistics from point cloud data (predictor variables), and multi-variate regression analysis to determine preliminary relationships between the predictor and response variables.

6.2.1 Test Sites

This study uses the LiDAR data and field measured surface roughness terms associated with 24 test sites in Florida. These sites are located in Volusia, Lake and Franklin counties and are all

located within land cover classes that are prevalent in the coastal, storm surge prone regions of Florida. A map showing the location of the test sites is included as Figure 4.1 and a summary of the test sites along with their land cover classes is presented in Table 4.1. A detailed description of the field measurements process and surface roughness calculations are presented in Sections 4.2 and 4.3, respectively; only relevant details are reiterated here.

The sites are rectangular, measuring 30 meters in the east-west direction and 15 meters in the north-south, following Arcement and Schneider (1989). In order to become a candidate for inclusion in the study, 3-dimensional LiDAR point cloud data must be available on the site. The entire population of sites was chosen to represent a range of roughness conditions present in surge prone regions of Florida. The number of LiDAR points on each site is shown in Table 6.1.

Table 6.1: LiDAR point cloud densities for test sites

Site	Total Points	Total Point Density (pts/meter^2)	Ground Points	Ground Point Density (pts/meter^2)	Non-Ground Points	Non-Ground Point Density (pts/meter^2)
ANER-01	2271	5.05	560	1.24	1711	3.80
ANER-02	1567	3.48	646	1.44	921	2.05
ANER-03	1663	3.70	270	0.60	1393	3.10
ANER-04	1573	3.50	464	1.03	1109	2.46
ANER-05	2486	5.52	266	0.59	2220	4.93
ANER-06	1540	3.42	528	1.17	1012	2.25
ANER-07	2368	5.26	363	0.81	2005	4.46
ANER-08	1793	3.98	385	0.86	1408	3.13
ANER-09	1520	3.38	711	1.58	809	1.80
ANER-10	2193	4.87	306	0.68	1887	4.19
HILO-01	1306	2.90	292	0.65	1014	2.25
HILO-02	697	1.55	15	0.03	682	1.52
HILO-03	2059	4.58	59	0.13	2000	4.44
LKMO-01	556	1.24	154	0.34	402	0.89
LKMO-02	342	0.76	184	0.41	158	0.35
LKMO-03	358	0.80	72	0.16	286	0.64
LKMO-04	335	0.74	73	0.16	262	0.58
SEMF-01	1971	4.38	569	1.26	1402	3.12
SEMF-02	2194	4.88	143	0.32	2051	4.56
SEMF-03	578	1.28	168	0.37	410	0.91
SEMF-04	652	1.45	317	0.70	335	0.74
SEMF-05	648	1.44	236	0.52	412	0.92
SEMF-06	2439	5.42	401	0.89	2038	4.53
SEMF-07	2366	5.26	414	0.92	1952	4.34

6.2.2 Response Variables

The surface roughness parameters computed from field measurements are the response variables in the multi-variate regression. These parameters, along with their multi-variate regression variable identifier are as follows:

- y_1 = Manning's n;
- y_2 = Surface canopy closure fraction; and
- y_3 = Effective roughness length, z_0.

The terms in the equations used to compute the surface roughness parameters are also considered response variables. These terms, along with their multi-variate regression variable identifier are as follows:

- y_4 = Manning's n_1, roughness associated with microtopography;
- y_5 = Manning's n_3, roughness associated with obstacles in the floodplain;
- y_6 = Manning's n_4', roughness associated with low-lying vegetation in the floodplain;
- y_7 = Manning's n_b, base roughness associated with soil;
- y_8 = Veg_d, Vegetation density of trees;
- y_9 = H, average height of all measured obstructions;
- y_{10} = S, average frontal or silhouette area of all measured obstructions; and
- y_{11} = A, average planimetric area of all measured obstructions.

6.2.3 Pre-Processing LiDAR Point Cloud Data

The pre-classified (ground and non-ground) LiDAR data were delivered in LAS format version 1.3 (ASPRS, 2010). For this project, the data were obtained from the Northwest Florida Water Management District (NWFWMD), Lake County Geographic Information Systems (GIS) Department, and United States Geological Survey Center for LiDAR Information Coordination

and Knowledge (USGS CLICK; http://lidar.cr.usgs.gov/). The following steps were carried out in order to prepare the LiDAR for the multivariate regression:

1. All data were projected into the Universal Transverse Mercator (UTM) system, referencing the World Geodetic System 1984 (WGS 84) datum. The points on the ANER sites lie in UTM Zone 16 North. All others lie in UTM Zone 17 North;
2. All elevation (Z) data were adjusted to units of meters referencing the North American Vertical Datum of 1988 (NAVD88);
3. The LiDAR data were converted into ASCII text with the X (easting), Y (northing), Z (elevation) and Class fields persisting using LAStools, specifically las2txt.exe;
4. The de-trended heights of the non-ground points were computed using LAStools. In summary, LAStools, specifically lasheight.exe, computes a triangular irregular network (TIN) from the ground points and uses the resulting surface to compute the height of the non-ground points;
5. The LiDAR data was remapped to a local coordinate system. The southwestern-most point was defined as the origin and the X and Y values for all other points were adjusted to reference this origin;
6. The LiDAR is divided into ground and non-ground data sets based on the LAS Class value. Ground points are Class 2.

An example of the LiDAR point cloud for a test site is shown in Figure 6.1.

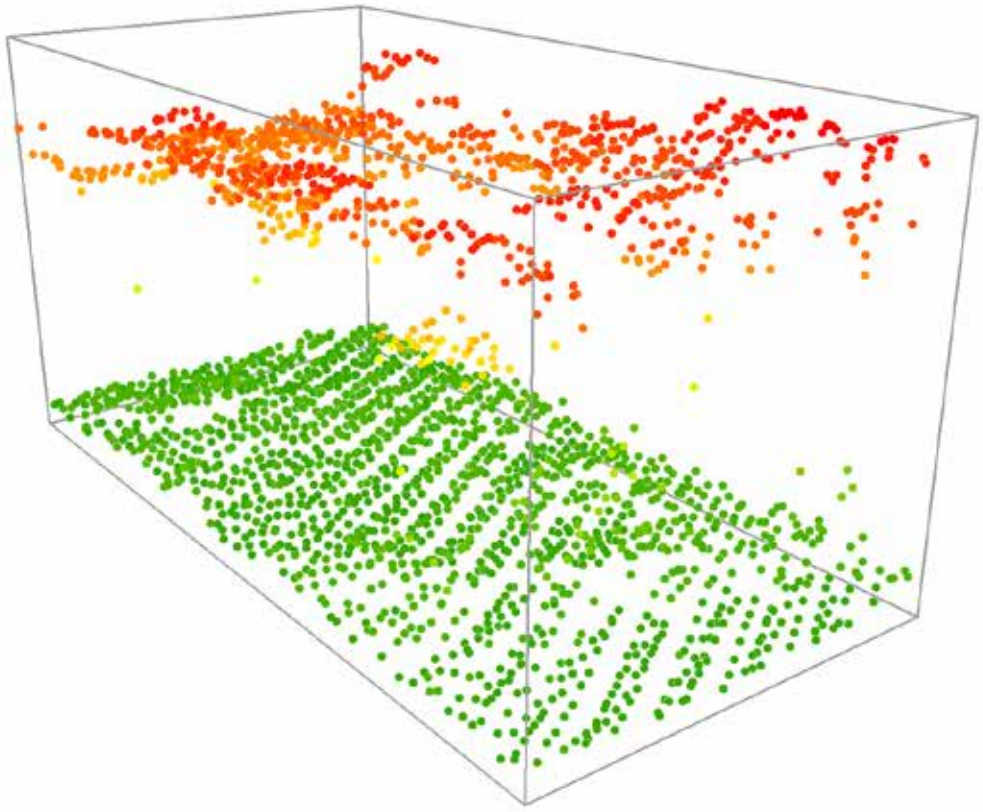

Figure 6.1: Example of LiDAR point cloud data

6.2.4 Predictor Variables

The statistics derived from the LiDAR point cloud serve as the predictor variables in the multi-variate regression analysis. The predictor variables are computed for each site as explained below.

- x_1 = Ground point fraction, ratio of ground points to total points on a site;
- x_2 = Non-ground point fraction, ratio of non-ground points to total points on a site, or one minus the ground point fraction;

- $x_3 = \sigma_{gz}^2$, or variance of ground point elevations, given by the following equation:

$$\sigma_{gz}^2 = \frac{\sum_{i=1}^{k_g} \left(Z_{gi} - \mu_{gz}\right)^2}{k_g} \tag{6.1}$$

where k_g = number of ground points; Z_{gi} = the elevation of the ith ground point (meter NAVD88); μ_{gz} = the mean elevation of the ground points (meter NAVD88);

- $x_4 = \sigma_{gz}$, or standard deviation of ground point elevations, defined as the square root of the variance of ground point elevations;
- $x_5 = \mu_{ngh}$, or mean of the non-ground point heights (meter);
- $x_6 = \sigma_{ngh}^2$, or variance of non-ground point heights, given by the following equation:

$$\sigma_{ngh}^2 = \frac{\sum_{i=1}^{k_{ng}} \left(h_{ngi} - \mu_{ngh}\right)^2}{k_{ng}} \tag{6.2}$$

where k_{ng} = number of non-ground points; h_{ngi} = height of the ith non-ground point (meter).

- $x_7 = \sigma_{ngh}$, or standard deviation of non-ground point heights, defined as the square root of the variance of non-ground point heights;

- $x_8 = c_v$, or coefficient of variation of non-ground point heights, defined as the ratio of the standard deviation to the mean, given by the following equation:

$$c_v = \frac{s_{ngh}}{m_{ngh}} \tag{6.3}$$

- x_9 = 2 meter plus point fraction, ratio of non-ground points with a height greater than or equal to 2 meters to total points on a site;
- x_{10} = 2 meter plus non-ground point fraction, ratio of non-ground points with a height greater than or equal to 2 meters to the number of non-ground points on a site;

Predictor variable x_{11} requires special consideration. A moving window approach was applied to determine the local maximum heights within the site. This technique is effective when the site has many surface discontinuities and a simple arithmetic mean of non-ground point heights is insufficient. (Hollaus *et al.*, 2010; M. Straatsma & Middelkoop, 2007). The site was divided into 1-meter square, non-overlapping pixels. Within each pixel, the maximum non-ground point height was extracted and stored. Refer to Figure 6.2 for a depiction of an example moving window. Predictor variable x_{11} is the mean of the moving window maximum non-ground point heights.

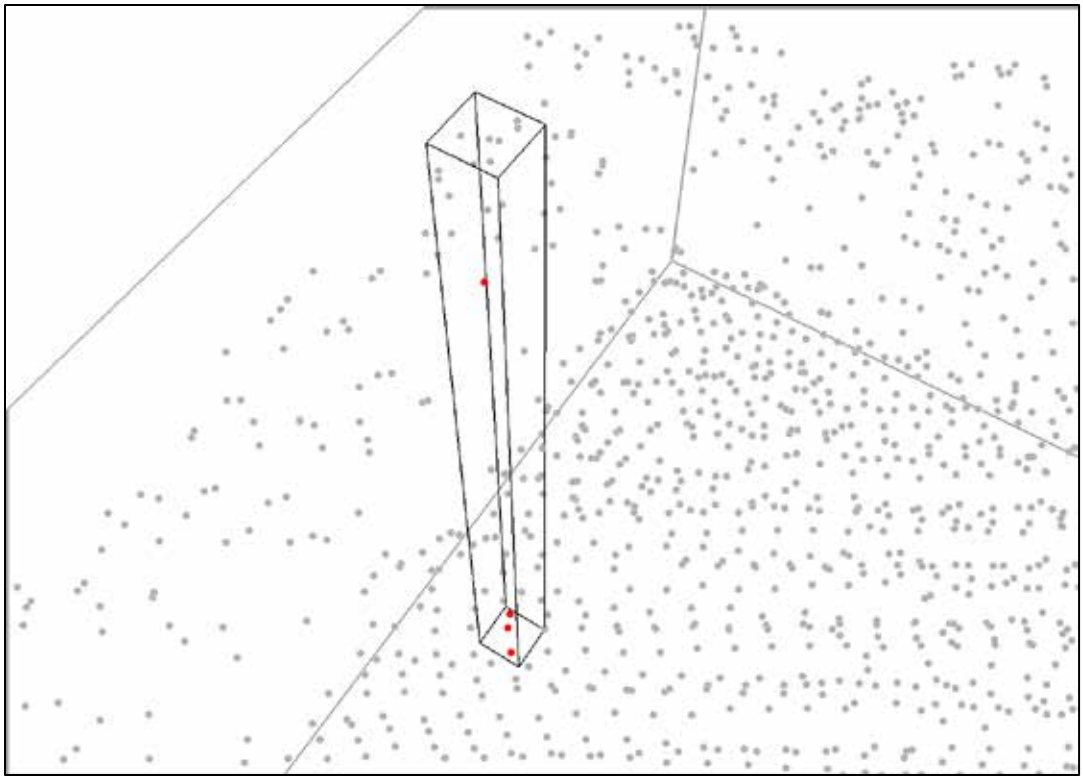

Figure 6.2: Example of moving window processing. Non-ground points within the moving window are enlarged and shown in red.

Predictor variable x_{12} also requires special consideration. In order to extract a surrogate for frontal or silhouette area, the site was divided into 1 meter wide stripes in both east-west and north-south orientations. The non-ground points within each stripe were temporarily extracted from the population for processing. The non-ground points within the stripe were assumed to lie along an axis defined as the stripe center line; in reality they deviate slightly (+/- 0.5 meters) from this axis. The stripe points now form a scatter set with a pseudo abscissa defined as its local X or Y coordinate (depending on the orientation of the stripe) and a pseudo ordinate defined as its height.

A least squares polynomial fitting routine was applied to the points in the stripe. This routine began with a first degree or linear fit and increased the degree of the fitted polynomial by one, with a maximum degree equal to six. The coefficient of determination, commonly denoted as R^2, was computed for the polynomial of each degree. The polynomial with the maximum R^2 was used for further processing.

The area beneath the winning polynomial from the fitting routine was then computed. While it is possible to integrate the winning polynomial over the interval from the minimum pseudo ordinate to the maximum pseudo ordinate, this results in negative areas being included into the computation as a result of the polynomial function dropping below zero in some instances. This is physically impossible; therefore, a primitive area computation was carried out using the following equation:

$$A_{stripe} = \sum_{x=o_{\min}}^{o_{\max}} a_v;\ a_v = \begin{cases} f(x)\Delta x & for\ f(x)\Delta x > 0 \\ 0 & for\ f(x)\Delta x \le 0 \end{cases} \tag{6.4}$$

where $o_{\min}$ = the minimum pseudo ordinate (meter); $o_{\max}$ = the maximum pseudo ordinate (meter); a_v = the area beneath the polynomial at x (meter^2); $f(x)$ = the fitting polynomial; Δx = the x increment for the area calculation. For this research, Δx = 0.1 meters (10 centimeters). A depiction of a stripe area calculation is shown in Figure X. The green area is the area considered to be an obstruction; the gray area is neglected in the area computation. The stripe area was then converted to a unit area using the following formula:

$$A_{unit} = \frac{A_{stripe}}{\left(o_{\max} - o_{\min}\right)} \tag{6.5}$$

Predictor variable x_{12} is equal to the mean unit area computed from all stripes (in both orientations) on the site. For the test sites used in this study, there are 14 stripes in the east-west orientation and 29 stripes in the north-south orientation.

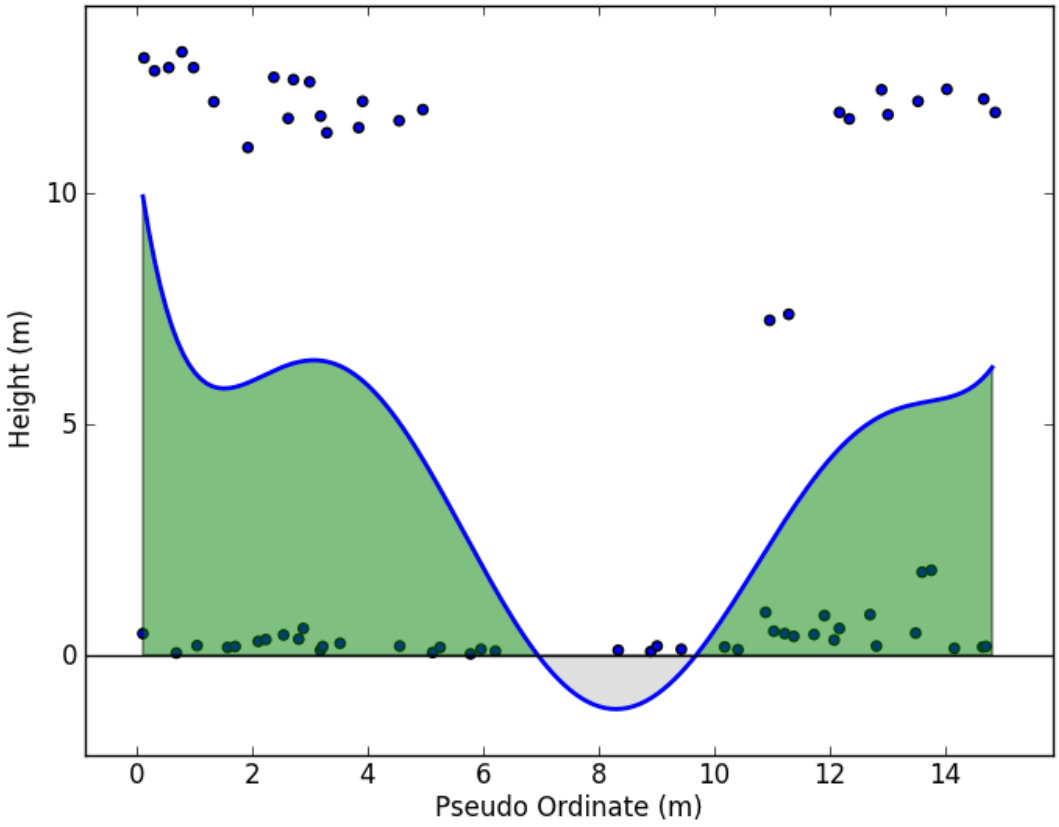

Figure 6.3: Stripe frontal area calculation. Blue dots represent non-ground points. Blue line is the best fit polynomial. Green (positive) area is used in the computation while gray (negative) area is neglected.

6.2.5 Multi-Variate Regression

A brute force multi-variate regression analysis was conducted to determine which predictor variable(s) explained the variability in the response variables. Up to six predictor variables were considered for each response variable with all possible combinations considered. The multi-variate regression was carried out using the open source statistical software package R (R Development Core Team, 2011).

6.3 Results and Discussion

The coefficient of determination (R^2) for each response variable is shown in Figure 6.4. As shown, the fit between the predictor variables and the surface roughness parameters as well as their individual terms is generally weak. The fit quality increases as the number of predictors increases, although the slope of the line decreases as the number of predictors increases. This indicates that six predictors are approaching the optimal amount, although investigation into additional predictors would be beneficial.

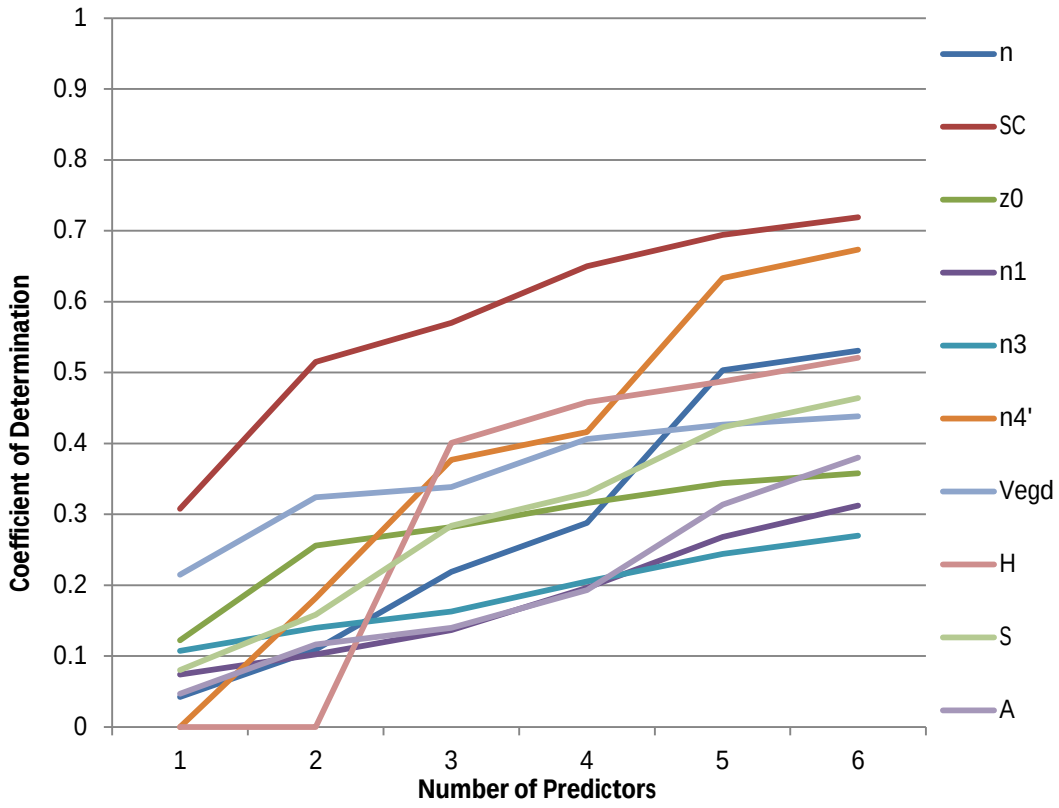

Figure 6.4: Multi-variate regression results

For effective roughness length, z_0, it is clear from Figure 6.4 that the fit is substantially better for the three terms that appear in the equation than for z_0 itself. For Manning's n, only n_4' is substantially better than n in terms of fit. The n_1, n_3, n_b and Veg_d terms all perform worse, especially as the number of predictors increases. This indicates that perhaps more descriptive LiDAR statistics (predictor variables) should be investigated. One explanation for the weak fit is that the process being modeled is highly non-linear, as many natural systems are. Therefore, the application of a complex, non-linear model will likely produce better results. In order to pursue this strategy, the variables that provide the most information must be identified.

Figure 6.5 depicts the frequency of use of all the predictor variables. As shown, the best predictor variables are the variance of the ground point elevations, mean of non-ground point heights, variance of non-ground point heights, 2 meter plus point fraction, and polynomial fit unit area. These are likely to be the variables that will contribute most to a non-linear model. Also evident from Figure 6.5 is that the variances of the ground point elevations as well as non-ground point heights appear to be more effective than their respective standard deviations.

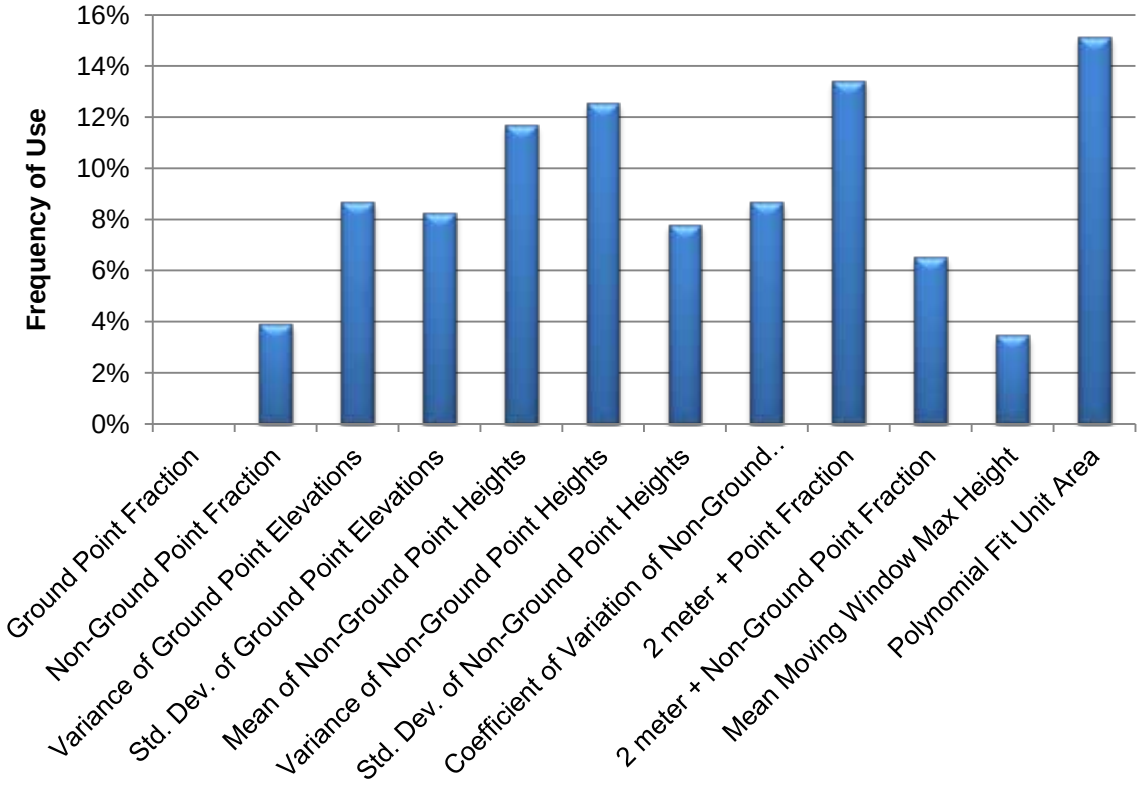

Figure 6.5: Frequency of use for predictor variables

6.4 Conclusions and Future Work

The major finding from this preliminary investigation is that the prediction of surface roughness parameters based on LiDAR point cloud data is a highly complex process. Surface canopy appears to estimatable based on multi-variate regression alone. In terms of the predictor variables derived from the LiDAR statistics, the variance of the ground point elevations, mean of non-ground point heights, variance of non-ground point heights, 2 meter plus point fraction, and polynomial fit unit area contribute most effectively to the estimation of surface roughness parameters.

In terms of future work, an investigation into more descriptive LiDAR statistics (predictor variables) would be beneficial. One these new predictors have been tested in multi-variate regression, complex mathematical models such as neural networks, genetic programming and random forests should be investigated as it is clear that the relationship between the surface roughness parameters and their associated measureable characteristics is highly non-linear. Also, a hydrodynamic test where LiDAR based parameterization technique is applied to a model that has been parameterized using traditional methods (constant bottom friction, LULC) is appropriate, if not necessary to fully establish LiDAR based surface roughness parameterization as a valid technique.

Once these tasks are successfully completed, coastal modelers will be able to construct topographic digital elevation models and establish physically-based surface roughness using the same readily available dataset.

6.5 References

Arcement, G. J., & Schneider, V. R. 1989. Guide for Selecting Manning's Roughness Coefficients for Natural Channels and Flood Plains (pp. 67).

ASPRS. 2010. LAS Specification, Version 1.3 - R11 (pp. 18pp). Bethesda, Maryland.

Bunya, S., Dietrich, J. C., Westerink, J. J., Ebersole, B. A., Smith, J. M., Atkinson, J. H., . . . Roberts, H. J. 2010. A High-Resolution Coupled Riverine Flow, Tide, Wind, Wind Wave and Storm Surge Model for Southern Louisiana and Mississippi. Part I: Model Development and Validation. *Monthly Weather Review, 138*, 345-377.

Cobby, D. M., Mason, D. C., & Davenport, I. J. 2001. Image processing of airborne scanning laser altimetry data for improved river flood modeling. *ISPRS Journal of Photogrammetry and Remote Sensing, 56*, 121-138.

Coggin, D. W. 2008. LiDAR in coastal storm surge modeling: Modeling linear raised features *Master's Thesis* (pp. 140 pp). Orlando, FL: University of Central Florida.

Coughlan, C., Vincent, C. E., Dolphin, T. J., & Rees, J. M. 2007. Effects of tidal stage on the wave climate inshore of a sandbank. *Journal of Coastal Research, SI 50*((Proceedings of the 9th International Coastal Symposium)), 751-756.

Davenport, I. J., Bradbury, R. B., Anderson, G. Q. A., Hayman, G. R. F., Krebs, J. R., Mason, D. C., . . . Veck, N. J. 2000. Improving bird population models using airborne remote sensing. *Internation Journal of Remote Sensing, 21*(13/14), 2705-2717.

De Vries, A. C., Kustas, W. P., Ritchie, J. C., Klaassen, W., Menenti, M., Rango, A., & Prueger, J. H. 2003. Effective aerodynamic roughness estimated from airborne laser altimeter measurements of surface features. *International Journal of Remote Sensing, 24*(7), 1545-1558.

Dietrich, J. C., Westerink, J. J., Kennedy, A. B., Smith, J. M., Jensen, R. E., Zijlema, M., . . . Cobell, Z. 2011. Hurricane Gustav (2008) waves and storm surge: Hindcast, synoptic analysis and validation in southern Louisiana. *Monthly Weather Review, 139*, 2488-2522. doi: 10.1175/2011MWR3611.1

Drake, J. B., Dubayah, R. O., Clark, D. B., Knox, R. G., Blair, J. B., Hofton, M. A., . . . Prince, S. 2002. Estimation of tropical forest structural characteristics using large-footprint lidar. *Remote Sensing of Environment, 79*(2-3), 305-319.

Galland, J.-C., Goutal, N., & Hervouet, J. M. 1991. TELEMAC: A new numerical model for solving shallow water equations. *Advances in Water Resources, 14*(3), 138-148.

Hagen, S. C., Bacopoulos, P., Cox, A. T., & Cardone, V. J. 2011. Hydrodynamics of the 2004 Florida Hurricanes. *journal of Coastal Research, In Press*. doi: 10.2112/JCOASTRES-D-10-00170.1

Hervouet, J. M. 2000. TELEMAC modelling system: an overview. *Hydrological Processes, 14*, 2209-2210.

Hollaus, M., Aubrecht, C., Höfle, B., Steinnocher, K., & Wagner, W. 2011. Roughness mapping on various vertical scales based on full-waveform laser scanning data. *Remote Sensing, 3*, 503-523. doi: 10.3390/rs3030503

Hollaus, M., Mandlburger, G., Pfiefer, N., & Mücke, W. 2010. *Land cover dependent derivation of digital surface models from airborne laser scanning data*. Paper presented at the IAPRS, Saint-Mandé, France.

Homer, C., Dewitz, J., Fry, J., Coan, M., Hossain, N., Larson, C., . . . Wickham, J. 2007. Completion of the 2001 National Land Cover Database for the Conterminous United States. *Photogrammetric Engineering and Remote Sensing, 73*(4), 337-341.

Hopkinson, C., Lim, K., Chasmer, L. E., Treitz, P., Creed, I. F., & Gynan, C. 2004. Wetland grass to plantation forest - estimating vegetation height form the standard deviation of lidar frequency distributions. *International Archives of Photogrammetry, Remote Sensing and Spatial Information Sciences, XXXVI*(8/W2), 288-294.

Huthoff, F., Augustijn, D. C. M., & Hulscher, S. J. M. H. 2007. Analytical solution of the depth-averaged flow velocity in case of submerged rigid cylindrical vegetation. *Water Resources Research, 43*(W06413). doi: 10.1029/2006WR005625

Hyyppä, H., & Hyyppä, J. 1999. Comparing the accuracy of laser scanner with other optical remote sensing data sources for stand attribute retrieval. *The Photogrammetric Journal of Finland, 16*(2), 5-15.

Jones, J. E., & Davies, A. M. 2008. Storm surge computations for the west coast of Britain using a finite element model (TELEMAC). *Ocean Dynamics, 58*, 337-363. doi: 10.1007/s10236-008-0140-y

Jones, J. E., Hall, P., & Davies, A. M. 2009. An inter-comparison of tidal solutions computed with a range of unstructured grid models of the Irish and Celtic Sea Regions. *Ocean Dynamics, 59*, 997-1023. doi: 10.1007/s10236-009-0225-2

Kato, A., Schreuder, G. F., Calhoun, D., Schiess, P., & Stuetzle, W. 2007. *Digital surface model of tree canopy structure from LiDAR data through implicit surface reconstruction*. Paper presented at the ASPRS 2007 Annual Conference, Tampa, Florida.

Kraus, K., & Rieger, W. 1999. *Processing of laser scanning data for wooded areas.* Paper presented at the Photogrammetric Week '99, Heidelberg, Germany.

Lettau, H. 1969. Note on Aerodynamic Roughness-Parameter Estimation on the Basis of Roughness-Element Description. *Journal of Applied Meteorology, 8*, 828-832.

Lim, K., Treitz, P., Wulder, M., St-Onge, B., & Flood, M. 2003. LiDAR remote sensing of forest structure. *Progress in Physical Geography, 27*(1), 88-106.

Luettich, R. A., & Westerink, J. J. 2006. ADCIRC: A Paralell Advanced Circulation Model for Oceanic, Coastal and Estuarine Waters. *adcirc.org*. Retrieved from http://adcirc.org/documentv46/ADCIRC_title_page.html

Luettich, R. A., Westerink, J. J., & Scheffner, N. W. 1992. ADCIRC: An advanced three-dimensional circulation model for shelves, coasts, and estuaries, Report 1: Theory and methodology of ADCIRC-2DDI and ADCIRC-3DL (pp. 1-137). Vicksburg, Mississippi: Department of the Army, US Amry Corps of Engineers, Waterways Experiment Station.

Mason, D. C., Cobby, D. M., Horritt, M. S., & Bates, P. D. 2003. Floodplain friction parameterization in two-dimensional river flood models using vegetation heights derived from airborne scanning laser altimetry. *Hydrological Processes, 17*, 1711-1732. doi: 10.1002/hyp.1270

Medeiros, S. C., Hagen, S. C., & Weishampel, J. F. 2012. Comparison of floodplain surface roughness parameters derived from land cover data and field measurements. *Journal of Hydrology, In Revision*.

Menenti, M., & Ritchie, J. C. 1994. Estimation of effective aerodynamic roughness of Walnut Gulch watershed with laser altimeter measurements. *Water Resources Research, 30*, 1329-1337.

National Oceanic and Atmospheric Administration, C. S. C. 1995 - present. The Coastal Change Analysis Program (C-CAP) Regional Land Cover. Charleston, SC: NOAA Coastal Services Center.

Nelson, R., Krabill, W., & Maclean, G. 1984. Determining forest canopy characteristics using airborne laser data. *Remote Sensing of Environment, 15*, 201-212.

R Development Core Team. 2011. R: A language and environment for statistical computing. Vienna, Austria. Retrieved from http://www.R-project.org

Raber, G. T., Jensen, J. R., Schill, S. R., & Schuckman, K. 2002. Creation of digital terrain models using an adaptive lidar vegetation point removal process. *Photogrammetric Engineering and Remote Sensing, 68*(12), 1307-1315.

Ritchie, J. C. 1996. Remote sensing applications to hydrology: airborne laser altimeters. *Hydrological Sciences Journal, 41*(4), 625-636.

Stephan, U., & Gutknecht, D. 2002. Hydraulic resistance of submerged flexible vegetation. *Journal of Hydrology, 269*, 27-43.

Straatsma, M. 2009. 3D float tracking: in situ floodplain roughness estimation. *Hydrological Processes, 23*, 201-212. doi: 10.1002/hyp.7147

Straatsma, M., & Middelkoop, H. 2007. Extracting structural characteristics of herbaceous floodplain vegetation under leaf-off conditions using airborne laser scanner data. *International Journal of Remote Sensing, 28*(11), 2447-2467.

Straatsma, M. W., & Baptist, M. J. 2008. Floodplain roughness parameterization using airborne laser scaning and spectral remote sensing. *Remote Sensing of Environment, 112,* 1062-1080.

Vogelmann, J. E., Howard, S. M., Yang, L., Larson, C. R., Wylie, B. K., & Van Driel, N. 2001. Completion of the 1990s National Land Cover Data Set for the conterminous United States from Landsat thematic mapper data and ancillary data sources. *Photogrammetric Engineering and Remote Sensing, 67*, 650-652.

Vosselman, G., Gorte, B. G. H., Sithole, G., & Rabbani, T. 2004. Recognising structure in laser scanner point clouds. *International Archives of Photogrammetry, Remote Sensing and Spatial Information Sciences, 46*(8/W2), 33-38.

Wang, M., & Tseng, Y.-H. 2010. Automatic segmentation of Lidar data into coplanar point clusters using an octree-based split-and-merge algorithm. *Photogrammetric Engineering and Remote Sensing, 76*(4), 407-420.

Weltz, M. A., Ritchie, J. C., & Fox, H. D. 1994. Comparison of laser and field measurements of vegetation height and canopy cover. *Water Resources Research, 30*(5), 1311-1319.

Westerink, J. J., Luettich, R. A., Feyen, J. C., Atkinson, J. H., Dawson, C., Roberts, H. J., . . . Pourtaheri, H. 2008. A Basin- to Channel-Scale Unstructured Grid Hurricane Storm Surge Model Applied to Southern Louisiana. *Monthly Weather Review, 136*, 833-864.

Wilson, C. A. M. E., Stoesser, T., Bates, P. D., & Batemann Pinzen, A. 2003. Open channel flow through different forms of submerged flexible vegetation. *Journal of Hydraulic Engineering, 129*(11), 847-853. doi: 10.1061/(ASCE)0733-9429(2003)129:11(847)

CHAPTER 7. CONCLUSION

The objective of this dissertation was to investigate the use of remotely sensed data in coastal tide and inundation models, specifically how these data could be more effectively integrated into model construction and performance assessment techniques. To this end, remotely sensed data were acquired, processed, assimilated and applied in a coastal modeling framework.

The work began with a thorough academic review of wetting and drying algorithms employed by contemporary numerical tidal models. Since nearly all population centers and valuable property are located in the overland regions of the model domain, the coastal models must adequately describe the inundation physics here. This is accomplished by techniques that generally fall into four categories: Thin film, Element removal, Depth extrapolation, and Negative depth. While nearly all wetting and drying algorithms can be classified as one of the four types, each model is distinct and unique in its actual implementation.

The use of spatial elevation data is essential to accurate coastal modeling. Remotely sensed LiDAR is the standard data source for constructing topographic digital terrain models (DTM). Hydrographic soundings provide bathymetric elevation information. These data are combined to form a seamless topobathy surface that is the foundation for distributed coastal models. A three-point inverse distance weighting method was developed in order to account for the spatial variability of bathymetry data referenced to tidal datums. This method was applied to the Tampa Bay region of Florida in order to produce a seamless topobathy DTM.

Remotely sensed data also contributes to the parameterization of surface roughness. It is used to develop land use / land cover (LULC) data that is in turn used to specify spatially distributed bottom friction and aerodynamic roughness parameters across the model domain. However, these parameters are continuous variables that are a function of the size, shape and density of the terrain and above-ground obstacles. By using LULC data, much of the variation specific to local areas is generalized due to the categorical nature of the data. This was tested by comparing surface roughness parameters computed based on field measurements to those assigned by LULC data at 24 sites across Florida. Using a t-test to quantify the comparison, it was proven that the parameterizations are significantly different. Taking the field measured parameters as ground truth, it can therefore be stated that parameterizing surface roughness based on LULC data is deficient.

In addition to providing input parameters, remotely sensed data can also be used to assess the performance of coastal models. Traditional methods of model performance testing include harmonic resynthesis of tidal constituents, water level time series analysis, and comparison to measured high water marks. All of these methods give modelers excellent insight into the skill of the model. A new performance assessment that measures a model's ability to predict the extent of inundation was applied to a northern Gulf of Mexico tidal model. The new method, termed the synergetic method, is based on detecting inundation area at specific points in time using satellite imagery. This detected inundation area is compared to that predicted by a time-synchronized tidal model to assess the performance of model in this respect. It was shown that the synergetic method produces performance metrics that corroborate the results of traditional methods and is useful in assessing the performance of tidal and storm surge models. It was also

shown that the subject tidal model is capable of correctly classifying pixels as wet or dry on over 85% of the sample areas.

Lastly, since it has been shown that parameterizing surface roughness using LULC data is deficient, progress toward a new parameterization scheme based on 3-dimensional LiDAR point cloud data is presented. By computing statistics for the entire point cloud along with the implementation of moving window and polynomial fit approaches, empirical relationships were determined that allow the point cloud to estimate surface roughness parameters. A multi-variate regression approach was chosen to investigate the relationship(s) between the predictor variables (LiDAR statistics) and the response variables (surface roughness parameters). It was shown that the empirical fit is weak when comparing the surface roughness parameters to the LiDAR data. The fit was improved by comparing the LiDAR to the more directly measured source terms of the equations used to compute the surface roughness parameters. Future work will involve using these empirical relationships to parameterize a model in the northern Gulf of Mexico and comparing the hydrodynamic results to those of the same model parameterized using contemporary methods.

In conclusion, through the work presented herein, it was demonstrated that incorporating remotely sensed data into coastal models provides many benefits including more accurate topobathy descriptions, the potential to provide more accurate surface roughness parameterizations, and more insightful performance assessments. All of these conclusions were achieved using data that is readily available to the scientific community and, with the exception of the Synthetic Aperture Radar (SAR) from the Radarsat-1 project used in the inundation

detection method, are available free of charge. Airborne LiDAR data are extremely rich sources of information about the terrain that can be exploited in the context of coastal modeling. The data can be used to construct digital terrain models (DTMs), assist in the analysis of satellite remote sensing data, and describe the roughness of the landscape thereby maximizing the cost effectiveness of the data acquisition.

APPENDIX A: FIELD DATA FOR SITE ANER-01

----- General Information ---------
Site ID = ANER-01
Team Leader = MEDEIROS
Participants = SMAR, PASSERI, DARANPOB
Date = 8/8/2011
Arrival Time = 8:30 AM
Arrival Weather = PARTLY CLOUDY, WARM
Departure Time = 9:30 AM
Departure Weather = PARTLY CLOUDY, HOT
Datum = WGS84
Coordinate System = UTM16N
Site Photo Looking East = 3
Site Photo Looking North = 10
Site Photo Looking West = 7
Site Photo Looking South = 5
Site Photos Looking at the Ground = 11,12,13

----- Site Boundary GPS Coordinates ---------

POINT_NAME	EASTING	NORTHING	PHOTO_ID
WEST CENTER	718773.3	3290417.3	2
EAST CENTER	718806.1	3290418	8
NORTH WEST	718773.2	3290423.2	4
SOUTH WEST	718772.1	3290411.1	1
NORTH EAST	718802.1	3290429.3	6
SOUTH EAST	718808.6	3290411.8	9

----- Surface Canopy Estimates ---------

NW	NC	NE	W	C	E	SW	SC	SE
0	0	0	0	0	0	0	0	0
0	0	0	0	0	0	0	0	0
0	0	0	0	0	0	0	0	0
0	0	0	0	0	0	0	0	0

----- Manning's n Component Estimates ---------

n1	n3	n4_PRIME
0.002	0.02	0.001
0	0.02	0.001
0.001	0.025	0.001

0.001 0.015 0.001

----- Low Lying Vegetation Measurements ---------

PHOTO_NS	PHOTO_EW	EASTING	NORTHING	DIM_NS	DIM_EW	HEIGHT	DESC

----- Tree Measurements ---------

PHOTO	EASTING	NORTHING	DBH	HT1	HT2	HT_SB1	HT_SB2	DIM_NS	DIM_EW	DESC

----- Obstacle Measurements ---------

PHOTO	EASTING	NORTHING	DIM_NS	DIM_EW	HEIGHT	DESC
14	718782	3290414.1	3.53	3.37	2.07	WOOD SLAT FENCE
15	718784.4	3290415.7	6.67	6.48	2.19	WOOD SLAT FENCE
16	718795.7	3290413.7	10.65	17.14	2.1	WOOD SLAT FENCE
17	718791.8	3290418.6	15	12.1	0.14	CURB & SIDEWALK
18	718777.4	3290413.4	8.7	7.42	0.14	CURB & SIDEWALK

----- Soil Water Content ---------

CONTAINER_ID	MASS_CONTAINER	MASS_CONTAINER_MOISTSAMPLE	MASS_CONTAINER_DRYSAMPLE
20	50.4	148.8	145.5
A3(5)	50	163.6	159.5
A2(3)	50.5	141.7	137.9

----- Soil Grain Size Distribution ---------

SIEVE_OPENING	MASS_RETAINED
2	129
1.18	13.2
0.85	14.2
0.425	101.8
0.25	710.3
0.15	249.1
0.075	30.2
0	12.3


ANER-01_01


ANER-01_2A


ANER-01_02


ANER-01_03


ANER-01_04


ANER-01_05


ANER-01_06


ANER-01_07


ANER-01_08

ANER-01_09

ANER-01_10

ANER-01_11

ANER-01_12

ANER-01_13

ANER-01_14

ANER-01_15

ANER-01_16

ANER-01_17

ANER-01_18

APPENDIX B: FIELD DATA FOR SITE ANER-02

----- General Information ---------
Site ID = ANER-02
Team Leader = MEDEIROS
Participants = DARANPOB, PASSERI, SMAR
Date = 8/8/2011
Arrival Time = 9:40 AM
Arrival Weather = PARTLY CLOUDY, RAIN TO THE WEST
Departure Time = 11:0 AM
Departure Weather = PARTLY CLOUDY, HOT, RAIN PASSED WEST
Datum = WGS84
Coordinate System = UTM16N
Site Photo Looking East = 10
Site Photo Looking North = 7
Site Photo Looking West = 5
Site Photo Looking South = 2
Site Photos Looking at the Ground = 11,12

----- Site Boundary GPS Coordinates ---------

POINT_NAME	EASTING	NORTHING	PHOTO_ID
WEST CENTER	718784.3	3290581.4	9
EAST CENTER	718812	3290584.7	4
NORTH WEST	718783.3	3290591.8	1
SOUTH WEST	718783.1	3290575.8	8
NORTH EAST	718811.6	3290591.5	3
SOUTH EAST	718811.8	3290577.3	6

----- Surface Canopy Estimates ---------

NW	NC	NE	W	C	E	SW	SC	SE
0	0	0	0	0	0	0	0	0
0	0	0	0	0	0	0	0	0
0	0	0	0	0	0	0	0	0
0	0	0	0	0	0	0	0	0

----- Manning's n Component Estimates ---------

n1	n3	n4_PRIME
0.005	0	0.005
0.003	0	0.005
0.005	0.001	0.001
0.003	0.001	0.003

----- Low Lying Vegetation Measurements ---------

PHOTO_NS	PHOTO_EW	EASTING	NORTHING	DIM_NS	DIM_EW	HEIGHT	DESC
	13	718813.6	3290582.9	0.8	1.1	0.4	ROSEMARY
	14	718810.5	3290579.1	1.2	1.5	0.85	GRASS
	15	718808.8	3290579.4	0.67	0.7	0.4	ROSEMARY
	16	718811	3290578.5	0.9	0.7	0.7	GRASS
	17	718809.4	3290579.1	1.1	1	0.9	ROSEMARY + GRASS
	18	718809.3	3290582.8	0.7	1.1	0.5	ROSEMARY + GRASS
	19	718807.9	3290584	0.6	1	0.4	ROSEMARY
	20	718806	3290588.6	0.55	0.4	0.4	ROSEMARY
	21	718802.8	3290588.5	0.6	0.9	0.35	?
	22	718801.9	3290588.8	0.6	0.6	0.6	ROSEMARY
	23	718803.1	3290586.4	0.6	0.7	0.4	ROSEMARY
	24	718804.8	3290582.1	1.45	1.6	0.65	GRASS
27	25,26	718805.1	3290577.5	1.1	1.3	0.65	GRASS
29	28	718804	3290578.4	2.7	2.1	0.65	BUSH WITH THORNS
	30	718801.3	3290577.7	0.8	1.3	0.65	ROSEMARY
	31	718797.4	3290574.6	0.5	0.4	0.4	ROSEMARY
	32	718793.2	3290582.5	1.3	1.2	0.7	ROSEMARY, MOSTLY DEAD
	33	718789.9	3290585.8	1.2	1.4	0.65	ROSEMARY
	34	718787.8	3290580.8	0.55	0.6	0.45	ROSEMARY
	35	718790.9	3290577.2	0.45	0.75	0.5	ROSEMARY
	36	718784.7	3290577.7	1.25	0.8	0.6	ROSEMARY
	37	718785.4	3290583.9	1.1	0.85	0.35	ROSEMARY
	38	718784.5	3290584.5	1.1	0.9	0.45	ROSEMARY

----- Tree Measurements ---------

PHOTO	EASTING	NORTHING	DBH	HT1	HT2	HT_SB1	HT_SB2	DIM_NS	DIM_EW	DESC

----- Obstacle Measurements ---------

PHOTO	EASTING	NORTHING	DIM_NS	DIM_EW	HEIGHT	DESC

----- Soil Water Content ---------

CONTAINER_ID	MASS_CONTAINER	MASS_CONTAINER_MOISTSAMPLE	MASS_CONTAINER_DRYSAMPLE
A2(4)	49.7	123	121.4
A4(T)	50.5	156.6	154.3
D1	49.7	172.6	168.7

----- Soil Grain Size Distribution ---------

SIEVE_OPENING	MASS_RETAINED
2	0.2
1.18	0.2
0.85	256.5
0.425	729.4
0.25	116.9
0.15	38.5
0.075	2.1
0	0.1

ANER-02_01

ANER-02_02

ANER-02_03

ANER-02_04

ANER-02_05

ANER-02_06

ANER-02_07

ANER-02_08

ANER-02_09

ANER-02_10

ANER-02_11

ANER-02_12

ANER-02_13

ANER-02_14

ANER-02_15

ANER-02_16

ANER-02_17

ANER-02_18

ANER-02_19

ANER-02_20

ANER-02_21

ANER-02_22

ANER-02_23

ANER-02_24

ANER-02_25

ANER-02_26

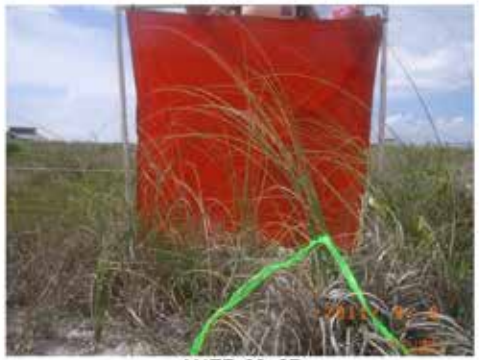

ANER-02_27

ANER-02_28

ANER-02_29

ANER-02_30

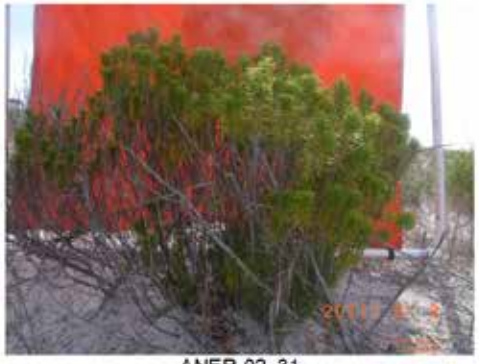

ANER-02_31

ANER-02_32

ANER-02_33

ANER-02_34

ANER-02_35

ANER-02_36

ANER-02_37

ANER-02_38

APPENDIX C: FIELD DATA FOR SITE ANER-03

----- General Information ---------
Site ID = ANER-03
Team Leader = MEDEIROS
Participants = PASSERI, SMAR, DARANPOB
Date = 8/8/2011
Arrival Time = 12:5 PM
Arrival Weather = PARTLY CLOUDY, HOT, SLIGHT BREEZE
Departure Time = 2:15 PM
Departure Weather = RAIN, T STORM
Datum = UTM16N
Coordinate System = WGS84
Site Photo Looking East = 5
Site Photo Looking North = 2
Site Photo Looking West = 10
Site Photo Looking South = 7
Site Photos Looking at the Ground = 11,12

----- Site Boundary GPS Coordinates ---------

POINT_NAME	EASTING	NORTHING	PHOTO_ID
WEST CENTER	718182.4	3290141.8	4
EAST CENTER	718209.8	3290143.5	9
NORTH WEST	718210.6	3290152.8	8
SOUTH WEST	718181.4	3290138.1	3
NORTH EAST	718180.6	3290149.4	6
SOUTH EAST	718214.4	3290141.2	1

----- Surface Canopy Estimates ---------

NW	NC	NE	W	C	E	SW	SC	SE
0	0	0	5	0	0	30	0	0
0	0	0	0	0	0	20	0	0
0	0	0	0	0	0	75	0	0
0	0	0	0	0	0	20	0	0

----- Manning's n Component Estimates ---------

n1	n3	n4_PRIME
0.006	0.001	0.008
0.003	0.001	0.01
0.007	0.003	0.006
0.002	0.002	0.005

----- Low Lying Vegetation Measurements ---------

PHOTO_NS	PHOTO_EW	EASTING	NORTHING	DIM_NS	DIM_EW	HEIGHT	DESC
13	14	718209.1	3290138	5.9	5.7	1.3	GALBERRY
15	16	718206.7	3290133	0.6	0.65	0.6	PAW PAW
17	18	718206.3	3290138.9	0.9	0.95	0.75	PAW PAW
20	19	718205.5	3290139.8	1.4	1	0.55	ROSEMARY + PAW PAW
22	21	718202.6	3290137.2	0.8	0.5	0.6	PAW PAW
24	23	718201.8	3290137.5	0.5	0.8	0.55	PAW PAW
26	25	718203.4	3290139.4	1.1	0.9	0.65	ROSEMARY + PAW PAW
28	27	718202.2	3290143.7	1.1	0.9	0.6	PAW PAW
30	29	718208.4	3290142.3	1.7	1.5	0.8	PAW PAW MOSTLY DEAD
32	31	718211.6	3290143.6	1.1	0.9	0.6	PAW PAW MOSTLY DEAD
34	33	718208	3290150	1.1	1	0.4	PAW PAW MOSTLY DEAD
	35	718201.8	3290152.3	0.7	0.8	0.45	PAW PAW
	36	718207	3290147.8	0.6	0.45	0.45	ROSEMARY
38	37	718204.4	3290144.7	1.9	1.4	0.75	ROSEMARY
40	39	718197.8	3290134.7	1.5	1.7	0.5	PAW PAW + ROSEMARY
42	41	718194.6	3290136.2	1.5	1.6	0.45	PAW PAW
	43	718198.3	3290136.8	2.5	1.2	0.6	PAW PAW CLUSTER
	44	718194.1	3290144.8	1.4	1.4	0.4	PAW PAW
	45	718195.2	3290145.7	2.4	1.1	0.6	PAW PAW
	46	718196.3	3290142	1.7	1.3	0.6	PAW PAW
	47	718196.7	3290148.5	1.7	1.8	1	ROSEMARY
	48	718197.9	3290146.1	1.1	1.4	0.45	ROSEMARY + PAW PAW
	49	718194.3	3290152.5	1.4	1.7	0.6	ROSEMARY + PAW PAW
	50	718193.2	3290150	1.75	1.3	0.55	ROSEMARY + PAW PAW
	51	718191.1	3290146.9	1.2	1.1	0.65	PAW PAW
	52	718191.7	3290145.3	1	0.7	0.55	PAW PAW
	53	718190.5	3290140.1	1	1.4	0.55	PAW PAW
	54	718190.7	3290143.2	0.7	1.4	0.6	PAW PAW + DOG FENNEL
	55	718190.8	3290148.1	0.8	1	0.45	ROSEMARY
	56	718189.7	3290152.4	0.8	0.7	0.5	ROSEMARY

	57	718190.5	3290152.4	1.3	2.1	0.5	ROSEMARY
	58	718188.7	3290149.3	0.7	0.55	0.4	ROSEMARY
	59	718184.6	3290150.4	0.85	0.8	0.55	PAW PAW
	60	718185.2	3290148.3	1.8	2.5	0.7	PAW PAW
	61	718187.4	3290145.3	2.1	2.3	0.65	PAW PAW
	62	718188.3	3290143.1	1.6	2.2	0.7	ROSEMARY
	63	718187.8	3290139.4	0.65	0.55	0.55	PAW PAW
	64	718185.9	3290137.2	1	0.8	0.5	ROSEMARY
	65	718188.1	3290136.3	0.7	0.5	0.4	ROSEMARY
67	66	718181.1	3290139.6	5.5	4.2	1.1	MIXED CLUSTER
	67A	718185.2	3290135.4	1.3	1.2	0.75	MIXED CLUSTER

----- Tree Measurements ---------

PHOTO	EASTING	NORTHING	DBH	HT1	HT2	HT_SB1	HT_SB2	DIM_NS	DIM_EW	DESC
68	718186.7	3290140	59	12.8	13	2	4	11.3	10	SAND PINE
69	718181.7	3290135.3	40	14.7	11.6	4.4	4	6.1	3.3	SAND PINE

----- Obstacle Measurements ---------

PHOTO	EASTING	NORTHING	DIM_NS	DIM_EW	HEIGHT	DESC
70	718190.4	3290156.1	0.9	2	0.2	LOG
71	718176.3	3290134	1.3	0.8	0.25	LOG

----- Soil Water Content ---------

CONTAINER_ID	MASS_CONTAINER	MASS_CONTAINER_MOISTSAMPLE	MASS_CONTAINER_DRYSAMPLE
A1(3)	50.2	136.2	132.4
17	51	174.8	169.2
101	50.4	150.1	145.5

----- Soil Grain Size Distribution ---------

SIEVE_OPENING	MASS_RETAINED
2	0.1
1.18	0.2
0.85	0.4
0.425	559.4
0.25	599.7
0.15	42.6
0.075	2.1
0	0.1

ANER-03_01

ANER-03_02

ANER-03_03

ANER-03_04

ANER-03_05

ANER-03_06

ANER-03_07

ANER-03_08

ANER-03_09

ANER-03_10

ANER-03_11

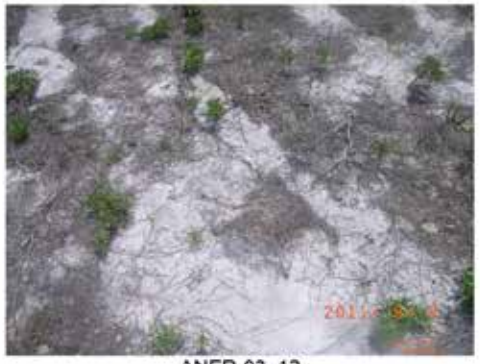

ANER-03_12

ANER-03_13

ANER-03_14

ANER-03_15

ANER-03_16

ANER-03_17

ANER-03_18

ANER-03_19

ANER-03_20

ANER-03_21

ANER-03_22

ANER-03_23

ANER-03_24

ANER-03_25

ANER-03_26

ANER-03_27

ANER-03_28

ANER-03_29

ANER-03_30

ANER-03_31

ANER-03_32

ANER-03_33

ANER-03_34

ANER-03_35

ANER-03_36

ANER-03_37

ANER-03_38

ANER-03_39

ANER-03_40

ANER-03_41

ANER-03_42

ANER-03_43

ANER-03_44

ANER-03_45

ANER-03_46

ANER-03_47

ANER-03_48

ANER-03_49

ANER-03_50

ANER-03_51

ANER-03_52

ANER-03_53

ANER-03_54

ANER-03_55

ANER-03_56

ANER-03_57

ANER-03_58

ANER-03_59

ANER-03_60

ANER-03_61

ANER-03_62

ANER-03_63

ANER-03_64

ANER-03_65

ANER-03_66

ANER-03_67

ANER-03_67A

ANER-03_68

ANER-03_69

ANER-03_70

ANER-03_71

APPENDIX D: FIELD DATA FOR SITE ANER-04

----- General Information ---------
Site ID = ANER-04
Team Leader = MEDEIROS
Participants = SMAR, DARANPOB, PASSERI
Date = 8/8/2011
Arrival Time = 2:50 PM
Arrival Weather = DRIZZLE, SUN EMERGING
Departure Time = 3:30 PM
Departure Weather = OVERCAST, MUGGY
Datum = UTM16N
Coordinate System = WGS84
Site Photo Looking East = 10
Site Photo Looking North = 7
Site Photo Looking West = 8
Site Photo Looking South = 9
Site Photos Looking at the Ground = 6

----- Site Boundary GPS Coordinates ---------

POINT_NAME	EASTING	NORTHING	PHOTO_ID
WEST CENTER	716501.5	3288054.9	5
EAST CENTER	716532.2	3288057	4
NORTH WEST	716502.4	3288065.1	2
SOUTH WEST	716499.2	3288048.4	1
NORTH EAST	716530.9	3288065	3
SOUTH EAST	716532.3	3288050.2	NP

----- Surface Canopy Estimates ---------

NW	NC	NE	W	C	E	SW	SC	SE
0	0	0	0	0	0	0	0	0
0	0	0	0	0	0	0	0	0
0	0	0	0	0	0	0	0	0
0	0	0	0	0	0	0	0	0

----- Manning's n Component Estimates ---------

n1	n3	n4_PRIME
0	0	0
0	0	0
0	0	0
0	0	0

----- Low Lying Vegetation Measurements ---------

PHOTO_NS	PHOTO_EW	EASTING	NORTHING	DIM_NS	DIM_EW	HEIGHT	DESC

----- Tree Measurements ---------

PHOTO	EASTING	NORTHING	DBH	HT1	HT2	HT_SB1	HT_SB2	DIM_NS	DIM_EW	DESC

----- Obstacle Measurements ---------

PHOTO	EASTING	NORTHING	DIM_NS	DIM_EW	HEIGHT	DESC

----- Soil Water Content ---------

CONTAINER_ID	MASS_CONTAINER	MASS_CONTAINER_MOISTSAMPLE	MASS_CONTAINER_DRYSAMPLE

----- Soil Grain Size Distribution ---------

SIEVE_OPENING	MASS_RETAINED
2	2
1.18	4
0.85	16
0.425	160
0.25	359
0.15	160
0.075	100
0	99

ANER-04_01

ANER-04_02

ANER-04_03

ANER-04_04

ANER-04_05

ANER-04_06

ANER-04_07

ANER-04_08

ANER-04_09

ANER-04_10

APPENDIX E: FIELD DATA FOR SITE ANER-05

----- General Information ---------
Site ID = ANER-05
Team Leader = MEDEIROS
Participants = SMAR, DARANPOB, PASSERI
Date = 8/8/2011
Arrival Time = 4:0 PM
Arrival Weather = OVERCAST, MUGGY, BUGGY
Departure Time = 6:20 PM
Departure Weather = SAME
Datum = UTM16N
Coordinate System = WGS84
Site Photo Looking East = 4
Site Photo Looking North = 10
Site Photo Looking West = 8
Site Photo Looking South = 5
Site Photos Looking at the Ground = 11,12

----- Site Boundary GPS Coordinates ---------

POINT_NAME	EASTING	NORTHING	PHOTO_ID
WEST CENTER	713830.5	3286918	2
EAST CENTER	713861.2	3286914.9	7
NORTH WEST	713831.9	3286928.2	3
SOUTH WEST	713829.3	3286909.4	1
NORTH EAST	713858.6	3286925.6	6
SOUTH EAST	713858.9	3286909	9

----- Surface Canopy Estimates ---------

NW	NC	NE	W	C	E	SW	SC	SE
20	15	0	0	0	30	5	20	10
50	5	1	0	0	0	0	5	40
50	15	40	0	0	0	5	15	30
30	40	0	0	0	20	0	5	10

----- Manning's n Component Estimates ---------

n1	n3	n4_PRIME
0.005	0.005	0.01
0.006	0.004	0.02
0.004	0.005	0.02
0.005	0.015	0.025

----- Low Lying Vegetation Measurements ---------

PHOTO_NS	PHOTO_EW	EASTING	NORTHING	DIM_NS	DIM_EW	HEIGHT	DESC
14	13	713837.3	3286913.5	3.8	10.8	1.6	GALBERRY
16	15	713840.4	3286919.7	3.55	1.3	2	GALBERRY
18	17	713840.9	3286919.8	3.1	2.9	1.4	GALBERRY
20	19	713841.9	3286924.7	0.9	1.1	1	GALBERRY
22	21	713848.9	3286925.5	1.6	1.8	1.2	GALBERRY
24	23	713852.4	3286925.2	1.2	8.7	1.8	PAW PAW
26	25	713856.2	3286921.3	4.4	4.5	1.6	PAW PAW
	27	713852.6	3286915.7	1.3	3.2	1.9	PAW PAW

----- Tree Measurements ---------

PHOTO	EASTING	NORTHING	DBH	HT1	HT2	HT_SB1	HT_SB2	DIM_NS	DIM_EW	DESC
40	713835.4	3286913.2	17	15.6	18.9	11.9	12	2.6	2.4	SAND PINE
41	713836.4	3286918.7	19	19.8	16	10.1	10.5	2.9	5	SAND PINE
42	713833.5	3286916.2	26	16.1	17.5	10.2	10.1	2.9	4.2	SAND PINE
43	713838.3	3286913.5	12.5	14.8	12.7	10.1	11.4	3.5	1.8	SAND PINE
44	713840	3286912.3	19.25	15.6	17.1	11.3	11.7	3.4	4.5	SAND PINE
45	713833.7	3286919.6	22.7	13.4	12.5	11	11.1	3.3	3.5	SAND PINE
46	713836.9	3286918.1	7.2	6.5	6	4	2.7	1.9	1.6	SAND PINE
47	713836.1	3286920.6	14	9.9	11.4	8.1	7.5	2.9	2	SAND PINE
48	713835.6	3286928.3	23	13.3	14.6	7.4	10.6	3.25	3.6	SAND PINE
49	713843.7	3286930	24.2	14.7	15.8	9.6	9.9	5.65	5.04	SAND PINE
50	713845.6	3286926.6	18.5	13.1	14.5	8.4	8.5	4.5	3.4	SAND PINE
51	713847.5	3286927.3	20	12.7	14	9.9	9.9	2.2	3.4	SAND PINE
53	713850	3286923	24.3	15.2	16.8	9.5	10.1	3.8	3.7	SAND PINE
54	713852.4	3286923.7	16.7	13.2	13.8	9.5	10.2	3.6	3.7	SAND PINE
56	713859.1	3286926.6	20.5	11	10.4	7.4	7.5	2.6	2.15	SAND PINE
57	713857	3286923.8	14.2	11.9	13.1	9.5	9.4	2.3	3.5	SAND PINE
58	713854.9	3286920	13.9	11.8	12.8	8.9	10	1.6	3.6	SAND PINE
59	713855.7	3286920.3	13.1	10.2	10.9	8	7.8	3.3	2.2	SAND PINE
60	713854.6	3286920.9	16.8	9.3	12.5	8.9	8.9	2.8	2.9	SAND PINE

61	713853.9	3286917.9	14.3	12	11.5	8.2	9	2.1	2.05	SAND PINE
62	713855.2	3286917.3	12.5	10.9	11.5	8.5	9	3	2.5	SAND PINE
63	713855.7	3286921	12.2	8.1	9.2	6.1	8	2.1	1.9	SAND PINE
64	713858.9	3286919.5	16.3	11.4	11	8.5	8.3	3	2.3	SAND PINE
65	713856.3	3286917.3	16.2	11.7	12.8	7.6	8.5	3.65	2.9	SAND PINE
66	713856.9	3286915.8	16.6	12.4	11.6	8.2	8.1	3.4	2.6	SAND PINE
67	713856	3286919.7	13.1	9.8	10.7	8.2	8.8	1.1	1.4	SAND PINE
68	713856.3	3286918.2	15.1	11.2	10.3	8.2	9.2	3.6	4	SAND PINE
69	713852.6	3286913.2	19.9	14.1	15.2	9.6	9	2.95	4.5	SAND PINE
70	713844.7	3286920.1	27.7	11.8	13.1	9.3	9.6	2.9	3.7	SAND PINE

----- Obstacle Measurements ---------

PHOTO	EASTING	NORTHING	DIM_NS	DIM_EW	HEIGHT	DESC
30	713839.8	3286919.7	3.8	1.1	0.1	LOG
31	713836.9	3286919.7	3.1	2.9	0.25	BRANCH
32	713836.4	3286918.7	0.05	0.05	1.05	DEAD TREE
33	713834.5	3286920.3	0.3	0.9	0.1	LOG
34	713837.4	3286908.6	0.7	2.3	0.07	RAILROAD TIE
35	713835.8	3286921.5	0.22	0.22	4	DEAD TREE
36	713843.8	3286922.9	0.4	0.25	3.75	DEAD TREE
37	713835.5	3286923.7	0.9	0.5	7.1	DEAD CLUSTER OF TREES
38,39	713841.2	3286921.6	0.15	0.15	11.1	DEAD TREE
52	713850.8	3286924.6	0.13	0.13	6.7	DEAD TREE
55	713856.2	3286924.1	0.12	0.12	6.1	DEAD TREE
71	713840.5	3286913	0.11	0.11	0.74	STUMP

----- Soil Water Content ---------

CONTAINER_ID	MASS_CONTAINER	MASS_CONTAINER_MOISTSAMPLE	MASS_CONTAINER_DRYSAMPLE
102	49.8	122.6	112.8
19	50.4	126	115.9
103	50.5	129.6	117.7

----- Soil Grain Size Distribution ---------

SIEVE_OPENING	MASS_RETAINED
2	15.3
1.18	16.8
0.85	14.6
0.425	156.8
0.25	818
0.15	119.6
0.075	9.8
0	1.1

ANER-05_01

ANER-05_02

ANER-05_03

ANER-05_04

ANER-05_05

ANER-05_06

ANER-05_07

ANER-05_08

ANER-05_09

ANER-05_10

ANER-05_11

ANER-05_12

ANER-05_13

ANER-05_14

ANER-05_15

ANER-05_16

ANER-05_17

ANER-05_18

ANER-05_19

ANER-05_20

ANER-05_21

ANER-05_22

ANER-05_23

ANER-05_24

ANER-05_25

ANER-05_26

ANER-05_27

ANER-05_28

ANER-05_29

ANER-05_30

ANER-05_31

ANER-05_32

ANER-05_33

ANER-05_34

ANER-05_35

ANER-05_36A

ANER-05_36

ANER-05_37

ANER-05_38

ANER-05_40

ANER-05_41

ANER-05_42

ANER-05_43

ANER-05_44

ANER-05_45

ANER-05_46

ANER-05_47

ANER-05_48

ANER-05_49

ANER-05_50

ANER-05_51

ANER-05_52

ANER-05_53

ANER-05_54

ANER-05_55

ANER-05_56

ANER-05_57

ANER-05_58

ANER-05_59

ANER-05_60

ANER-05_61

ANER-05_62

ANER-05_63

ANER-05_64

ANER-05_65

ANER-05_66

ANER-05_67

ANER-05_68

ANER-05_69

ANER-05_70

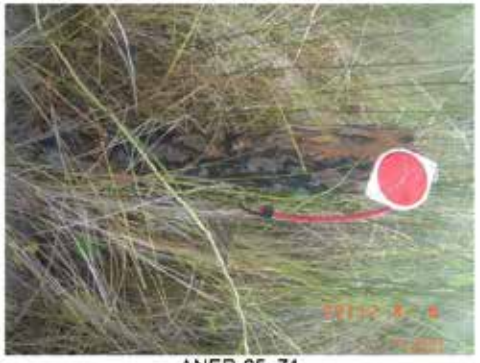

ANER-05_71

APPENDIX F: FIELD DATA FOR SITE ANER-06

----- General Information ---------
Site ID = ANER-06
Team Leader = MEDEIROS
Participants = SMAR, DARANPOB, PASSERI
Date = 8/9/2011
Arrival Time = 8:20 AM
Arrival Weather = PARTLY CLOUDY
Departure Time = 9:23 AM
Departure Weather = T-STORM APPROACHING, DRIZZLE
Datum = UTM16N
Coordinate System = WGS84
Site Photo Looking East = 2
Site Photo Looking North = 3
Site Photo Looking West = 5
Site Photo Looking South = 8
Site Photos Looking at the Ground = 11,12,13

----- Site Boundary GPS Coordinates ---------

POINT_NAME	EASTING	NORTHING	PHOTO_ID
WEST CENTER	717500	3289199.8	9
EAST CENTER	717529.9	3289201.6	7
NORTH WEST	717501.8	3289209.6	1
SOUTH WEST	717502.4	3289191.5	3A
NORTH EAST	717530.2	3289209.6	6
SOUTH EAST	717533.5	3289193	4

----- Surface Canopy Estimates ---------

NW	NC	NE	W	C	E	SW	SC	SE
0	0	0	0	0	0	0	0	0
0	0	0	0	0	0	0	0	0
0	0	0	0	0	0	0	0	0
0	0	0	0	0	0	0	0	0

----- Manning's n Component Estimates ---------

n1	n3	n4_PRIME
0.015	0	0.006
0.011	0	0.005
0.008	0.001	0.005
0.015	0.001	0.005

----- Low Lying Vegetation Measurements ---------

PHOTO_NS	PHOTO_EW	EASTING	NORTHING	DIM_NS	DIM_EW	HEIGHT	DESC
	14	717516.7	3289206.2	0.6	0.7	0.96	GRASS
	15	717513.6	3289207.1	0.9	0.7	0.9	GRASS
	16	717525.5	3289206.4	0.8	1.7	0.7	GRASS
	17	717522.1	3289200.8	0.9	0.7	0.9	GRASS
	18	717517.7	3289202.3	0.85	0.95	0.65	GRASS
	19	717514.4	3289196.7	1	0.9	0.85	GRASS
	20	717514.1	3289197.3	0.6	0.8	0.9	GRASS
	21	717508.7	3289198.1	0.65	0.7	0.7	GRASS
	22	717505.2	3289198.6	1.2	1.1	0.95	GRASS
	23	717504.1	3289197.4	1.3	1.5	1	GRASS
	24	717502.3	3289193.3	0.6	1.1	1.1	GRASS
	25	717505	3289195.2	0.4	0.6	0.85	GRASS
	26	717510.6	3289197.2	0.9	0.8	0.55	GRASS

----- Tree Measurements ---------

PHOTO	EASTING	NORTHING	DBH	HT1	HT2	HT_SB1	HT_SB2	DIM_NS	DIM_EW	DESC

----- Obstacle Measurements ---------

PHOTO	EASTING	NORTHING	DIM_NS	DIM_EW	HEIGHT	DESC

----- Soil Water Content ---------

CONTAINER_ID	MASS_CONTAINER	MASS_CONTAINER_MOISTSAMPLE	MASS_CONTAINER_DRYSAMPLE
A3(5)	50	157	154.3
20	50.4	134.5	132.6
A2(3)	50.5	159.5	157.2

----- Soil Grain Size Distribution ---------

SIEVE_OPENING	MASS_RETAINED
2	7.1
1.18	2.1
0.85	1.9
0.425	60.3
0.25	864.1
0.15	413.3
0.075	19.1
0	1.7

ANER-06_01

ANER-06_02

ANER-06_3A

ANER-06_03

ANER-06_04

ANER-06_05

ANER-06_06

ANER-06_07

ANER-06_08

ANER-06_09

ANER-06_11

ANER-06_12

ANER-06_13

ANER-06_14

ANER-06_15

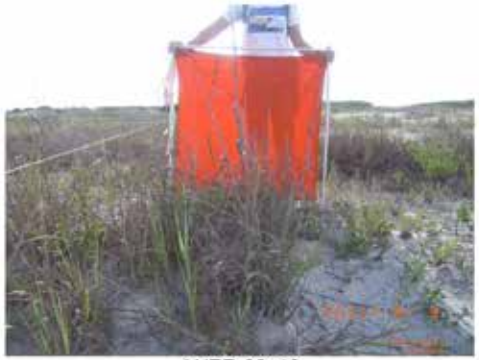

ANER-06_16

ANER-06_17

ANER-06_18

ANER-06_19

ANER-06_20

ANER-06_21

ANER-06_22

ANER-06_23

ANER-06_24

ANER-06_25

ANER-06_26

APPENDIX G: FIELD DATA FOR SITE ANER-07

----- General Information ---------
Site ID = ANER-07
Team Leader = MEDEIROS
Participants = SMAR, PASSERI, DARANPOB
Date = 8/10/2011
Arrival Time = 8:50 AM
Arrival Weather = PARTLY CLOUDY, HOT
Departure Time = 10:25 AM
Departure Weather = SAME
Datum = UTM16N
Coordinate System = WGS84
Site Photo Looking East = 8
Site Photo Looking North = 9
Site Photo Looking West = 2
Site Photo Looking South = 6
Site Photos Looking at the Ground = 11,12,13,14

----- Site Boundary GPS Coordinates ---------

POINT_NAME	EASTING	NORTHING	PHOTO_ID
WEST CENTER	717603.6	3289724.5	10
EAST CENTER	717634.7	3289726.3	3
NORTH WEST	717609.6	3289732.6	5
SOUTH WEST	717602.7	3289715.2	7
NORTH EAST	717630	3289735.2	4
SOUTH EAST	717635.7	3289717.1	1

----- Surface Canopy Estimates ---------

NW	NC	NE	W	C	E	SW	SC	SE
60	0	0	45	40	10	0	0	0
15	0	0	40	20	0	0	0	0
25	0	0	25	45	1	0	0	0
5	0	0	35	45	5	0	0	0

----- Manning's n Component Estimates ---------

n1	n3	n4_PRIME
0.011	0.001	0.006
0.005	0.003	0.007
0.01	0.003	0.005
0.006	0.001	0.006

----- Low Lying Vegetation Measurements ---------

PHOTO_NS	PHOTO_EW	EASTING	NORTHING	DIM_NS	DIM_EW	HEIGHT	DESC
16	15	717607.5	3289728	15	7	1	CONTINUOUS PATCH OF GALBERRY, SOUTHERN FOX GRAPE
18	17	717612.8	3289732.4	1.4	4.3	1.45	GREENBRIAR OVER DEAD BUSH
20	19	717619.9	3289730.1	2	2.2	1	GREENBRIAR OVER DEAD BUSH
	21	717615.6	3289729.4	1	0.75	0.6	DAD WAX MYRTLE
	22	717621.2	3289732.2	0.6	0.5	0.6	WAX MYRTLE
23A	23	717626.9	3289729.9	1.35	2.05	1.05	GREENBRIAR OVER DEAD BUSH
26	25	717632.7	3289733.1	5.5	5.4	1.3	GREENBRIAR, PAW PAW, DEAD PINE
28	27	717635.9	3289722.7	6.3	5.6	1.4	HOLE WITH PAW PAW, GREENBRIAR, DEAD SAPLINGS
30	29	717624.5	3289724	7.5	9	0.766666666666667	MIXED CLUSTER WITH PAW PAW, FERNS, GREENBRIAR

----- Tree Measurements ---------

PHOTO	EASTING	NORTHING	DBH	HT1	HT2	HT_SB1	HT_SB2	DIM_NS	DIM_EW	DESC
32	717603.5	3289725.7	43.5	15.3	16.1	10.6	10.4	6.3	4	SAND PINE
33	717608.2	3289723.4	22.5	13.6	13.6	11.8	11.1	2.9	1.3	SAND PINE
34	717607.1	3289724.9	31.8	13.9	13.3	5.4	5.4	6.65	6.5	SAND PINE
35	717609.7	3289725.2	5	4.1	3.9	2.7	2.7	1	1.4	SAND PINE
36	717607.5	3289727.7	35.3	14.1	12.6	8.1	8.3	7.8	7.9	SAND PINE
37	717625.9	3289723.7	39.7	15.4	17.6	9.7	9.5	6.1	5.9	SAND PINE
38	717622.9	3289727	6.3	4.1	3.1	1.7	2.9	1.6	1.9	SAND PINE
39	717625.7	3289722.5	3.2	3.1	3.1	2	2	1	1.3	SAND PINE
40	717627.8	3289722.8	34.1	10.9	11.4	4.1	4.1	7.6	6.5	SAND PINE
41	717623.8	3289722.7	6.5	4.9	5.1	2.2	4.5	1.7	1.9	SAND PINE
42	717625.9	3289722.8	3	2.4	2.4	1.7	1.7	1.1	0.7	SAND PINE WITH GREENBRIAR
43	717627.8	3289723.1	20.8	12.4	17.1	8.1	8	4.4	4.6	SAND PINE
44	717629.3	3289728.4	24.5	11.3	10.2	8.4	6.9	6.2	6.4	SAND PINE
45	717630.1	3289730.3	2.5	2.25	2.25	1.35	1.35	0.75	0.65	SAND PINE WITH GREENBRIAR

----- Obstacle Measurements ---------

PHOTO	EASTING	NORTHING	DIM_NS	DIM_EW	HEIGHT	DESC
24	717324.9	3289732.9	0.4	0.3	1.5	DEAD PINE SAPLING
31	717621	3289724.8	2.4	2.3	1.4	DEAD BUSH

----- Soil Water Content ---------

CONTAINER_ID	MASS_CONTAINER	MASS_CONTAINER_MOISTSAMPLE	MASS_CONTAINER_DRYSAMPLE
D1	49.7	159.9	155.1
A4(T)	50.5	146.8	143
A2(4)	49.8	161.3	156.6

----- Soil Grain Size Distribution ---------

SIEVE_OPENING	MASS_RETAINED
2	3.5
1.18	4.2
0.85	5
0.425	882.6
0.25	239.6
0.15	117
0.075	4.3
0	0

ANER-07_01

ANER-07_02

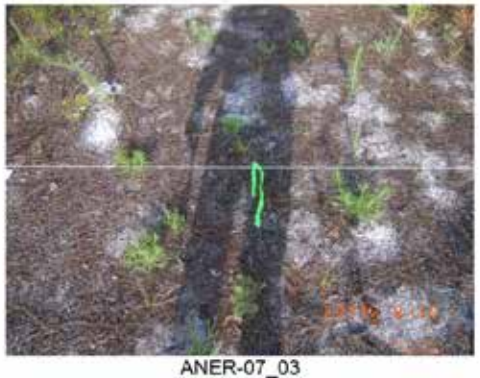

ANER-07_03

ANER-07_04

ANER-07_05

ANER-07_06

ANER-07_07

ANER-07_08

ANER-07_09

ANER-07_10

ANER-07_11

ANER-07_12

ANER-07_13

ANER-07_14

ANER-07_15

ANER-07_16

ANER-07_17

ANER-07_18

ANER-07_19

ANER-07_20

ANER-07_21

ANER-07_22

ANER-07_23

ANER-07_23A

ANER-07_24

ANER-07_25

ANER-07_26

ANER-07_27

ANER-07_28

ANER-07_29

ANER-07_30

ANER-07_31

ANER-07_32

ANER-07_33

ANER-07_34

ANER-07_35

ANER-07_36

ANER-07_37

ANER-07_38

ANER-07_39

ANER-07_40

ANER-07_41

ANER-07_42

ANER-07_43

ANER-07_44

ANER-07_45

APPENDIX H: FIELD DATA FOR SITE ANER-08

----- General Information ---------
Site ID = ANER-08
Team Leader = MEDEIROS
Participants = SMAR, DARANPOB, PASSERI
Date = 8/10/2011
Arrival Time = 11:35 AM
Arrival Weather = MOSTLY CLOUDY, T-STORMS TO THE SW
Departure Time = 12:30 PM
Departure Weather = OVERCAST, WARM
Datum = UTM16N
Coordinate System = WGS84
Site Photo Looking East = 10
Site Photo Looking North = 9
Site Photo Looking West = 13A
Site Photo Looking South = 11,12
Site Photos Looking at the Ground = 4,5

----- Site Boundary GPS Coordinates ---------

POINT_NAME	EASTING	NORTHING	PHOTO_ID
WEST CENTER	716486.7	3289027.9	2
EAST CENTER	716518.9	3289031	7
NORTH WEST	716485.2	3289037.5	1
SOUTH WEST	716489.8	3289019.7	3
NORTH EAST	716516.9	3289037.5	8
SOUTH EAST	716514.8	3289021.7	6

----- Surface Canopy Estimates ---------

NW	NC	NE	W	C	E	SW	SC	SE
0	30	0	0	90	0	0	0	85
40	0	0	0	85	0	0	0	60
40	0	0	0	90	0	0	0	85
50	0	0	0	85	0	0	0	80

----- Manning's n Component Estimates ---------

n1	n3	n4_PRIME
0.001	0.001	0.002
0.005	0.001	0.002
0.002	0.003	0.007
0.008	0.003	0.001

----- Low Lying Vegetation Measurements ---------

PHOTO_NS	PHOTO_EW	EASTING	NORTHING	DIM_NS	DIM_EW	HEIGHT	DESC
14	13	716503.8	3289020.6	1.1	1.4	0.5	ROSEMARY
	15	716504.1	3289020	0.55	0.5	0.45	ROSEMARY
18	17	716506.8	3289031.7	2.3	2.3	1.5	BURNT BUSH
20	19	716506.8	3289033.6	4.3	2.9	1.5	BURNT BUSH
	21	716502.7	3289036.6	1.1	1.6	1.1	BURNT BUSH
24	23	716501.5	3289027.6	1.5	2.6	1.1	BURNT BUSH
26	25	716499.8	3289032.8	2.2	1.4	0.9	BURNT BUSH
28	27	716494.4	3289020.1	1.5	2.5	0.75	ROSEMARY REGROWING
29		716492.6	3289018.5	0.7	0.85	0.75	ROSEMARY REGROWING
30		716497.1	3289021.7	0.4	0.9	0.7	ROSEMARY REGROWING
	31	716491.1	3289024.6	1.35	1.4	0.9	ROSEMARY REGROWING
33	32	716487.9	3289024	0.5	0.7	0.7	ROSEMARY REGROWING
35	34	716490	3289027.1	1	1	0.7	ROSEMARY REGROWING
	36	716492.1	3289025.9	1.6	1.8	1.1	ROSEMARY REGROWING
	37	716490	3289028	0.7	0.9	0.5	?
39	38	716489.6	3289032.3	1.6	2	1.15	DEAD BUSH
	40	716490.1	3289034.2	2	1.7	1.1	ROSEMARY REGROWING

----- Tree Measurements ---------

PHOTO	EASTING	NORTHING	DBH	HT1	HT2	HT_SB1	HT_SB2	DIM_NS	DIM_EW	DESC
44	716506.3	3289032.6	69.5	17.6	15.1	7	6.2	10.9	11.6	SAND PINE

----- Obstacle Measurements ---------

PHOTO	EASTING	NORTHING	DIM_NS	DIM_EW	HEIGHT	DESC
41	716506.8	3289031.4	1.2	0.9	0.45	BURNT LOG
42	716501.2	3289030.1	0.8	1.4	0.25	BURNT TWISTED LOG
43	716488.2	3289035	0.95	1.55	0.2	PILE OF DEAD LOGS

----- Soil Water Content ---------

CONTAINER_ID	MASS_CONTAINER	MASS_CONTAINER_MOISTSAMPLE	MASS_CONTAINER_DRYSAMPLE
17	51	137.9	134.2
A1(3)	50.3	161.1	156.7
101	50.4	163.3	157.9

----- Soil Grain Size Distribution ---------

SIEVE_OPENING	MASS_RETAINED
2	2.2
1.18	3.2
0.85	3.3
0.425	169
0.25	1067.8
0.15	91.2
0.075	2
0	0

ANER-08_01

ANER-08_02

ANER-08_03

ANER-08_04

ANER-08_05

ANER-08_06

ANER-08_07

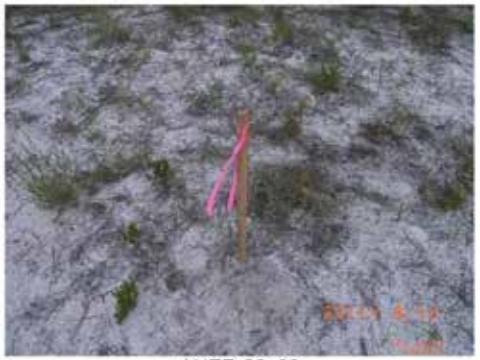

ANER-08_08

ANER-08_09

ANER-08_10

ANER-08_11

ANER-08_12

ANER-08_13A

ANER-08_13

ANER-08_14

ANER-08_15

ANER-08_17

ANER-08_18

ANER-08_19

ANER-08_20

ANER-08_21

ANER-08_23

ANER-08_24

ANER-08_25

ANER-08_26

ANER-08_27

ANER-08_28

ANER-08_29

ANER-08_30

ANER-08_31

ANER-08_32

ANER-08_33

ANER-08_34

ANER-08_35

ANER-08_36

ANER-08_37

ANER-08_38

ANER-08_39

ANER-08_40

ANER-08_41

ANER-08_42

ANER-08_43

ANER-08_44

APPENDIX I: FIELD DATA FOR SITE ANER-09

----- General Information ---------
Site ID = ANER-09
Team Leader = MEDEIROS
Participants = PASSERI, DARANPOB, SMAR
Date = 8/10/2011
Arrival Time = 1:50 PM
Arrival Weather = OVERCAST, BREEZY
Departure Time = 2:20 PM
Departure Weather = OVERCAST, BREEZY
Datum = UTM16N
Coordinate System = WGS84
Site Photo Looking East = 8
Site Photo Looking North = 5
Site Photo Looking West = 10
Site Photo Looking South = 9
Site Photos Looking at the Ground = 11,12

----- Site Boundary GPS Coordinates ---------

POINT_NAME	EASTING	NORTHING	PHOTO_ID
WEST CENTER	719055.6	3290596	7
EAST CENTER	719084.8	3290599.9	3
NORTH WEST	719051.7	3290604.2	1
SOUTH WEST	716054.7	3290586.7	6
NORTH EAST	719081.5	3290604.2	2
SOUTH EAST	719081.8	3290590	4

----- Surface Canopy Estimates ---------

NW	NC	NE	W	C	E	SW	SC	SE
0	0	0	0	0	0	0	0	0
0	0	0	0	0	0	0	0	0
0	0	0	0	0	0	0	0	0
0	0	0	0	0	0	0	0	0

----- Manning's n Component Estimates ---------

n1	n3	n4_PRIME
0.005	0	0.002
0.005	0.001	0.001
0.01	0	0.001
0.005	0	0.002

----- Low Lying Vegetation Measurements ---------

PHOTO_NS	PHOTO_EW	EASTING	NORTHING	DIM_NS	DIM_EW	HEIGHT	DESC
	13	719078.8	3290592.7	0.6	1.2	0.7	GRASS
	14	719073.9	3290593.8	1.9	1.8	1.7	GRASS
	15	719067.9	3290599	0.7	0.8	0.65	GRASS
	16	719067.9	3290600.2	0.7	0.6	1	GRASS
18	17	719063	3290602.3	2.4	3.2	1.8	GRASS
21	19,20	719052.3	3290599	2.1	2.2	1.8	GRASS
23	22	719056.3	3290599	1.7	1.8	2	GRASS

----- Tree Measurements ---------

PHOTO	EASTING	NORTHING	DBH	HT1	HT2	HT_SB1	HT_SB2	DIM_NS	DIM_EW	DESC

----- Obstacle Measurements ---------

PHOTO	EASTING	NORTHING	DIM_NS	DIM_EW	HEIGHT	DESC

----- Soil Water Content ---------

CONTAINER_ID	MASS_CONTAINER	MASS_CONTAINER_MOISTSAMPLE	MASS_CONTAINER_DRYSAMPLE
102	50.3	158.9	155.6
103	50.3	175.9	172.1
19	50.2	174.6	170.6

----- Soil Grain Size Distribution ---------

SIEVE_OPENING	MASS_RETAINED
2	6.4
1.18	0.9
0.85	1.2
0.425	105.4
0.25	926.2
0.15	327.3
0.075	10.4
0	0

ANER-09_01

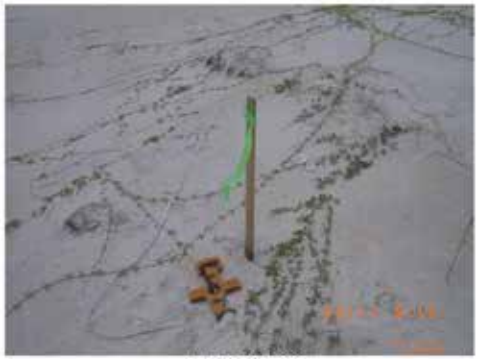

ANER-09_02

ANER-09_03

ANER-09_04

ANER-09_05

ANER-09_06

ANER-09_07

ANER-09_08

ANER-09_09

ANER-09_10

ANER-09_11

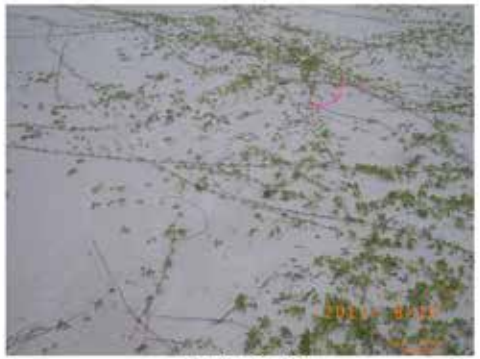

ANER-09_12

ANER-09_13

ANER-09_14

ANER-09_15

ANER-09_16

ANER-09_17

ANER-09_18

ANER-09_19

ANER-09_20

ANER-09_21

ANER-09_22

ANER-09_23

APPENDIX J: FIELD DATA FOR SITE ANER-10

----- General Information ---------
Site ID = ANER-10
Team Leader = MEDEIROS
Participants = SMAR, PASSERI, DARANPOB
Date = 8/11/2011
Arrival Time = 9:0 AM
Arrival Weather = MOSTLY CLOUDY, HOT HUMID
Departure Time = 10:30 AM
Departure Weather = PARTLY CLOUDY, HOT HUMID
Datum = UTM16N
Coordinate System = WGS84
Site Photo Looking East = 10
Site Photo Looking North = 2
Site Photo Looking West = 5
Site Photo Looking South = 7
Site Photos Looking at the Ground = 11,12

----- Site Boundary GPS Coordinates ---------

POINT_NAME	EASTING	NORTHING	PHOTO_ID
WEST CENTER	704987.5	3294917.8	9
EAST CENTER	705020.3	3294917.5	4
NORTH WEST	704988	3294924	8
SOUTH WEST	704988.2	3294912	1
NORTH EAST	705018.7	3294920.9	6
SOUTH EAST	705015.3	3294911.9	3

----- Surface Canopy Estimates ---------

NW	NC	NE	W	C	E	SW	SC	SE
0	0	0	2	6	15	25	0	40
0	0	0	10	5	0	35	0	20
0	10	0	10	5	0	35	0	25
0	0	0	5	10	0	5	0	40

----- Manning's n Component Estimates ---------

n1	n3	n4_PRIME
0.002	0.001	0.02
0.02	0.004	0.025
0.005	0.003	0.025
0.001	0.003	0.025

----- Low Lying Vegetation Measurements ---------

PHOTO_NS	PHOTO_EW	EASTING	NORTHING	DIM_NS	DIM_EW	HEIGHT	DESC
SEE GROUND PHOTOS	11,12	SITE CENTER	SITE CENTER	15	30	1.56	333333333333SPARTINA, JUNCUS

----- Tree Measurements ---------

PHOTO	EASTING	NORTHING	DBH	HT1	HT2	HT_SB1	HT_SB2	DIM_NS	DIM_EW	DESC
13	705014.4	3294906	33.5	19.1	16.4	10.9	12.6	5.6	6.8	SAND PINE
14	705009.4	3294910.8	33	16.6	17.6	10.9	11.1	5	5.1	SAND PINE
15	705003.5	3294911	33	17.4	17.4	13.4	12.2	7	7	SAND PINE
16	704997.5	3294915.2	30	14.8	14.8	10.2	11.1	7.4	5.3	SAND PINE
17	704995.9	3294915.8	37	13.6	13.6	9.8	12.3	9.4	7.8	SAND PINE

----- Obstacle Measurements ---------

PHOTO	EASTING	NORTHING	DIM_NS	DIM_EW	HEIGHT	DESC
18	705005.7	3294922.8	0.1	0.1	0.79	SKINNY STUMP

----- Soil Water Content ---------

CONTAINER_ID	MASS_CONTAINER	MASS_CONTAINER_MOISTSAMPLE	MASS_CONTAINER_DRYSAMPLE
101	50.5	108.5	62
D1	49.7	105.1	61.2
A1(3)	50.2	129	65.7

----- Soil Grain Size Distribution ---------

SIEVE_OPENING	MASS_RETAINED
2	2.4
1.18	81.5
0.85	68.4
0.425	88.8
0.25	68.1
0.15	69.6
0.075	29.7
0	30.3

ANER-10_01

ANER-10_02

ANER-10_03

ANER-10_04

ANER-10_05

ANER-10_06

ANER-10_07

ANER-10_08

ANER-10_09

ANER-10_10

ANER-10_11

ANER-10_12

ANER-10_13

ANER-10_14

ANER-10_15

ANER-10_16

ANER-10_17

ANER-10_18

APPENDIX K: FIELD DATA FOR SITE HILO-01

----- General Information ---------
Site ID = HILO-01
Team Leader = MEDEIROS
Participants = DARANPOB, BACOPOULOS, BILSKIE
Date = 11/12/2010
Arrival Time = 8:45 AM
Arrival Weather = COOL, PARTLY CLOUDY, BREEZY
Departure Time = 1:10 PM
Departure Weather = WARM, PARTLY CLOUDY
Datum = WGS84
Coordinate System = UTM17N
Site Photo Looking East = 11
Site Photo Looking North = 2
Site Photo Looking West = 4,6
Site Photo Looking South = 8
Site Photos Looking at the Ground = 12,13,14

----- Site Boundary GPS Coordinates ---------

POINT_NAME	EASTING	NORTHING	PHOTO_ID
WEST CENTER	428760.3	3136467.4	10
EAST CENTER	428792.1	3136469.1	5
NORTH WEST	428763.1	3136479.1	9
SOUTH WEST	428761.4	3136465.2	1
NORTH EAST	428790.8	3136479.5	7
SOUTH EAST	428794	3136462.3	3

----- Surface Canopy Estimates ---------

NW	NC	NE	W	C	E	SW	SC	SE
0	0	0	0	0	0	0	0	0
0	0	0	0	0	0	0	0	0
0	0	0	0	0	0	0	0	0
0	0	0	0	0	0	0	0	0

----- Manning's n Component Estimates ---------

n1	n3	n4_PRIME
0.005	0	0.02
0.005	0.004	0.017
0.004	0.002	0.022
0.006	0.003	0.024

----- Low Lying Vegetation Measurements ---------

PHOTO_NS	PHOTO_EW	EASTING	NORTHING	DIM_NS	DIM_EW	HEIGHT	DESC
16	15	428764.6	3136464.3	2.8	2.7	1.95	GRASS, SEE PHOTO
	17	428762.2	3136467.4	1.8	1.1	1.7	GRASS, SEE PHOTO
	18	428764.9	3136465.8	1.4	1	1.6	GRASS + ROSEMARY?
	19	428763.8	3136470.2	2.4	1.8	1.9	GRASS + THORNS
	20	428765.2	3136471.1	3.9	4.5	1.8	GRASS + THORNS
	21	428765.5	3136474.8	2.2	3.7	1.55	YELLOW FLOWER STAGGERBRUSH
22		428762.8	3136478.5	0.9	1.3	1.4	YELLOW FLOWER STAGGERBRUSH
23		428763.9	3136477.2	1.2	1.1	1.3	YELLOW FLOWER STAGGERBRUSH
24		428763.6	3136477.8	1.3	1.3	1.6	YELLOW FLOWER STAGGERBRUSH
	25	428766.1	3136477.2	0.9	1.4	0.95	YELLOW FLOWER STAGGERBRUSH
	26	428769.3	3136476.6	1.1	0.8	1.4	DOG FENNEL
	27	428769	3136474.7	1.3	1.5	1.3	DOG FENNEL + STAGGERBRUSH + GRASS
	28	428769.6	3136471.7	1.1	2.6	1.6	DOG FENNEL + STAGGERBRUSH + GRASS
	29	428767.7	3136471.7	1.1	1.5	1.3	THORNS + STAGGERBRUSH
	30	428767.7	3136471.4	0.9	1.5	1.7	GRASS + THORNS
	31	428767.1	3136470.1	1.2	1.1	1	GRASS + THORNS
	32	428766.3	3136468	1.6	0.9	1.3	GRASS + THORNS
	33	428767.6	3136468.6	1.5	1.4	1.4	GRASS + THORNS + STAGGERBRUSH
	34	428766	3136465.5	2.2	1.6	1.5	GRASS + THORNS + STAGGERBRUSH
	35	428764.6	3136466.8	2.9	1.7	1.6	GRASS + THORNS + STAGGERBRUSH
	36	428768.4	3136463.4	0.9	1.4	1.6	THORNS + GRASS
37		428770.3	3136464.3	1.5	1.7	1.2	GRASS+ STAGGERBRUSH
38		428770.6	3136463	1.4	1.9	1.5	GRASS + DOG FENNEL + STAGGERBRUSH + THORNS
	39	428772	3136464.9	1.5	1.7	1.65	GRASS + DOG FENNEL + STAGGERBRUSH
	40	428771.2	3136465.2	1.2	1.8	1.6	GRASS
	41	428772	3136464.3	1.8	1.3	1.6	STAGGERBRUSH
42		428768.2	3136465.5	0.7	1.2	1.8	GRASS
	43	428767.1	3136466.4	0.5	0.6	1.5	GRASS
	44	428768.7	3136467.4	1.1	0.7	1.7	GRASS
45		428769	3136469.2	3.2	3.4	1.5	THORN

46		428768.8	3136474.4	0.8	0.7	1.6	GRASS
47		428767.4	3136474.4	1	1	1.5	STAGGERBRUSH + GRASS
48		428769.3	3136473.5	2.3	1.6	1.4	STAGGERBRUSH + GRASS
49		428765.8	3136475.7	0.8	0.9	1.5	GRASS
	50	428769.3	3136475.7	0.8	1.5	1.4	GRASS
	51	428769.6	3136475	1.2	1.3	1.3	GRASS
52		428771	3136476.6	2.2	1.5	1.4	GRASS
53		428770.7	3136475.6	3.8	2.8	1.5	GRASS
54		428773.4	3136475.3	1.3	2	1.45	GRASS
55		428774.2	3136476.2	2.9	3	1.4	GRASS + STAGGERBRUSH
56		428776.7	3136475	3.3	2.7	1.4	STAGGERBRUSH + THORNS
	57	428775.3	3136471.6	1.9	1.6	1.5	GRASS
	58	428773.1	3136472.9	2.2	1.7	1.2	THORNS + GRASS + STAGGERBRUSH
59		428770.4	3136472	2	2.5	1.3	GRASS (2 TYPES)
60		428771.7	3136472.3	1.6	1.7	1.4	GRASS
	61	428773.4	3136470.7	1.7	1.1	1.5	GRASS
	62	428772.5	3136467.9	1.3	0.7	1.5	GRASS
	63	428772	3136465.8	3.8	2.2	1.4	THORN + STAGGERBRUSH + GRASS
64		428769.5	3136465.2	0.7	1.1	1.4	GRASS + DOG FENNEL
	65	428772.5	3136464.3	1.1	0.9	2	GRASS
66		428774.4	3136463.9	2	1.9	1.5	GRASS + DOG FENNEL + STAGGERBRUSH
67		428774.7	3136463.3	1.8	1.9	1.6	GRASS
68	69	428776.6	3136469.2	3.5	5.1	1.9	GRASS + DOG FENNEL
71	70	428776.4	3136469.8	2.9	2.7	1.6	GRASS?
72		428775.8	3136470.1	1.1	0.9	1.6	DOG FENNEL
74	73	428781	3136475.6	5.7	7.8	1.4	GRASS + STAGGERBRUSH + DOG FENNEL
75		428781.8	3136472.5	2	1.9	1.4	STAGGERBRUSH + GRASS
76		428780.4	3136468.2	1.1	1.2	1.2	GRASS + STAGGERBRUSH + DOG FENNEL
77		428780.2	3136471	1.2	1.1	1.3	GRASS + STAGGERBRUSH + DOG FENNEL
78		428781.8	3136465.7	1.8	1.9	1.4	GRASS + STAGGERBRUSH + DOG FENNEL
79		428778.2	3136467.3	2.7	3.2	1.6	MAINLY DOG FENNEL
80		428781.2	3136463.6	2.6	2	1.4	DOG FENNEL + STAGGERBRUSH + GRASS
81		428783.9	3136464.5	2	2.5	1.3	GRASS
82		428783.1	3136466.6	1.5	1.4	1.4	GRASS + STAGGERBRUSH
83		428784	3136467.3	1.4	1.1	1.2	GRASS + STAGGERBRUSH
84		428783.7	3136468.2	1.9	2.9	1.5	GRASS + STAGGERBRUSH + DOG FENNEL
85	86	428782.1	3136472.8	2	2.2	1.8	GRASS + STAGGERBRUSH
87		428784.3	3136473.4	3.2	1.8	1.6	GRASS + DOG FENNEL
88		428786.1	3136466.3	1.4	1.6	1.65	GRASS + STAGGERBRUSH

89		428782.6	3136467	1.2	2.3	1.1	GRASS
90		428788	3136466	0.6	0.6	0.9	GRASS
	91	428787.2	3136467.9	0.8	0.7	1.1	GRASS
	92	428786.1	3136468.2	1.3	1.3	1.6	DOG FENNEL
93		428786.7	3136465.4	1.8	1.2	1.4	STAGGERBRUSH
94		428791.3	3136462.3	1.1	1.3	1	STAGGERBRUSH + GRASS
	95	428791	3136464.4	1.2	1.2	1	STAGGERBRUSH
96		428791.3	3136466	2.1	2.6	1.5	STAGGERBRUSH + DOG FENNEL
97		428787.5	3136466	1.5	2.2	1.4	GRASS + STAGGERBRUSH
98		428787	3136466.9	0.4	0.6	1.2	STAGGERBRUSH
	99	428784.5	3136469.1	1.6	1.3	1.1	STAGGERBRUSH + GRASS
	100	428792.2	3136476.4	1.2	0.9	0.9	GRASS
	101	428789.5	3136476.5	0.8	0.8	1.2	GRASS + STAGGERBRUSH
	102	428792.2	3136477.7	1.8	0.8	1.1	GRASS
103		428790.8	3136475.8	0.8	0.7	1	STAGGERBRUSH + GRASS
105	104	428788.3	3136472.5	5.6	7.8	2	LRG CLSTR GRASS+STAGGERBRUSH+DOG FENNEL

----- Tree Measurements ---------

PHOTO	EASTING	NORTHING	DBH	HT1	HT2	HT_SB1	HT_SB2	DIM_NS	DIM_EW	DESC

----- Obstacle Measurements ---------

PHOTO	EASTING	NORTHING	DIM_NS	DIM_EW	HEIGHT	DESC

----- Soil Water Content ---------

CONTAINER_ID	MASS_CONTAINER	MASS_CONTAINER_MOISTSAMPLE	MASS_CONTAINER_DRYSAMPLE
B4(5)	50.6	155.7	151.1
A4(3)	50.4	182.9	176.9
A-4(4)	50.4	159.8	155.5

----- Soil Grain Size Distribution ---------

SIEVE_OPENING	MASS_RETAINED
2	1.4
1.18	2.1
0.85	8.4
0.425	245.9
0.25	550.2
0.15	221
0.075	109.2
0	26.1

HILO-01_1

HILO-01_2

HILO-01_3

HILO-01_4

HILO-01_5

HILO-01_6

HILO-01_7

HILO-01_8

HILO-01_9

HILO-01_10

HILO-01_11

HILO-01_12

HILO-01_13

HILO-01_14

HILO-01_15

HILO-01_16

HILO-01_17

HILO-01_18

HILO-01_19

HILO-01_20

HILO-01_21

HILO-01_22

HILO-01_23

HILO-01_24

HILO-01_25

HILO-01_26

HILO-01_27

HILO-01_28

HILO-01_29

HILO-01_30

HILO-01_31

HILO-01_32

HILO-01_33

HILO-01_34

HILO-01_35

HILO-01_36

HILO-01_37

HILO-01_38

HILO-01_39

HILO-01_40

HILO-01_41

HILO-01_42

HILO-01_43

HILO-01_44

HILO-01_45

HILO-01_46

HILO-01_47

HILO-01_48

HILO-01_49

HILO-01_50

HILO-01_51

HILO-01_52

HILO-01_53

HILO-01_54

HILO-01_55

HILO-01_56

HILO-01_57

HILO-01_58

HILO-01_59

HILO-01_60

HILO-01_61

HILO-01_62

HILO-01_63


HILO-01_64


HILO-01_65


HILO-01_66


HILO-01_67


HILO-01_68


HILO-01_69


HILO-01_70


HILO-01_71


HILO-01_72

HILO-01_73

HILO-01_74

HILO-01_75

HILO-01_76

HILO-01_77

HILO-01_78

HILO-01_79

HILO-01_80

HILO-01_81

HILO-01_82

HILO-01_83

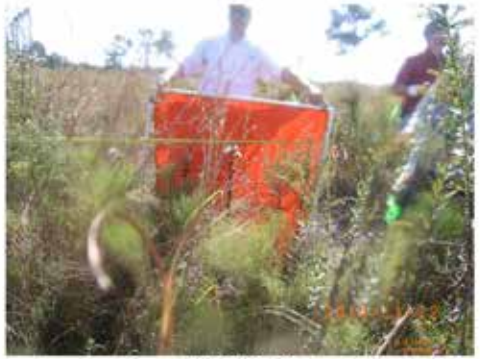

HILO-01_84

HILO-01_85

HILO-01_86

HILO-01_87

HILO-01_88

HILO-01_89

HILO-01_90

HILO-01_91

HILO-01_92

HILO-01_93

HILO-01_94

HILO-01_95

HILO-01_96

HILO-01_97

HILO-01_98

HILO-01_99

HILO-01_100

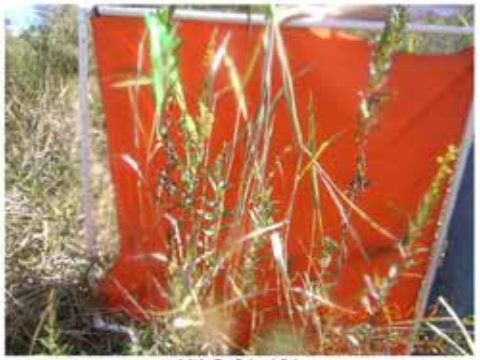

HILO-01_101

HILO-01_102

HILO-01_103

HILO-01_104

HILO-01_105

APPENDIX L: FIELD DATA FOR SITE HILO-02

----- General Information ---------
Site ID = HILO-02
Team Leader = MEDEIROS
Participants = DARANPOB, BACOPOULOS, BILSKIE
Date = 11/19/2010
Arrival Time = 8:40 AM
Arrival Weather = COOL, CLEAR
Departure Time = 12:50 PM
Departure Weather = WARM, CLEAR
Datum = WGS84
Coordinate System = UTM17N
Site Photo Looking East = 3
Site Photo Looking North = 4
Site Photo Looking West = 6
Site Photo Looking South = 9
Site Photos Looking at the Ground = 10,11,12,13

----- Site Boundary GPS Coordinates ---------

POINT_NAME	EASTING	NORTHING	PHOTO_ID
WEST CENTER	427496.5	3138157.6	2
EAST CENTER	427526.8	3138160.4	7
NORTH WEST	427501	3138169.2	1
SOUTH WEST	427497.3	3138153.6	3B
NORTH EAST	427526	3138171.5	8
SOUTH EAST	427529.7	3138155.5	5

----- Surface Canopy Estimates ---------

NW	NC	NE	W	C	E	SW	SC	SE
75	0	15	5	40	70	0	0	20
20	0	5	0	20	60	0	0	15
0	0	10	0	5	40	0	0	15
10	0	5	5	5	60	0	0	20

----- Manning's n Component Estimates ---------

n1	n3	n4_PRIME
0.003	0.006	0.005
0.002	0.002	0.004
0.002	0.003	0.004
0.003	0.021	0.005

----- Low Lying Vegetation Measurements ---------

PHOTO_NS	PHOTO_EW	EASTING	NORTHING	DIM_NS	DIM_EW	HEIGHT	DESC
15	14	427502.5	3138154.4	1.75	1.6	1.7	WAX MYRTLE
	17	427497.3	3138154.2	0.4	0.35	1.1	WAX MYRTLE
19	18	427498.4	3138156.9	1.3	0.6	1	PAW PAW (BURNT)
22	21	427500.4	3138163.7	1.2	1.3	1	PAW PAW (BURNT)
24	23	427496.6	3138166.5	1.77	0.7	1.16	PAW PAW (BURNT)
25	26	427503.9	3138166.4	3.8	2.75	1.6	PAW PAW (BURNT) + WAX MYRTLE
30	31	427506.9	3138165.8	0.5	1.65	1.43	WAX MYRTLE
33	32	427505	3138169.2	2.7	2.1	1.35	PAW PAW (BURNT)
35	34	427506.9	3138162.7	1.4	1.4	1.1	PAW PAW (BURNT)
36	37	427501.7	3138161.5	0.65	1.9	0.8	?
38,39B	39	427504.7	3138160.6	0.9	1.7	1.3	PAW PAW
42	41	427504.1	3138154.4	0.65	0.5	0.8	PAW PAW
43	44	427504.1	3138154.1	0.26	0.3	0.8	PAW PAW
	45	427504.1	3138154.7	1.4	1.25	1.5	WAX MYRTLE (ALMOST A TREE)
46B	46	427505.8	3138156	0.5	1.2	1.07	PAW PAW (BURNT)
52	53	427513.1	3138158.7	1.95	2	0.85	WAX MYRTLE (BURNT)
	54	427513.7	3138158.7	1.25	0.95	0.9	PAW PAW (BURNT)
56	55	427512.9	3138160.2	2.1	2.2	0.9	PAW PAW (BURNT)
57		427511.5	3138159.3	0.1	0.75	1.2	PAW PAW (BURNT)
58		427510.7	3138159.9	0.65	1.1	1.1	PAW PAW (BURNT)
59		427510.2	3138159.9	0.3	0.7	0.9	PAW PAW (BURNT)
60		427507.7	3138160.6	0.9	1	0.9	PAW PAW (BURNT)
61	62	427510.4	3138163.3	1.6	1.7	1.15	PAW PAW (BURNT)
	63	427512.6	3138163.3	0.6	0.5	0.8	WAX MYRTLE
65	64	427515.9	3138160.8	1.3	1.1	1.5	WAX MYRTLE + PAW PAW
67	66	427514	3138163.6	1.3	1.35	1	WAX MYRTLE
70	69	427509.4	3138165.5	1.9	1.6	1	BURNT PAW PAW
71B	71	427511.3	3138167.6	2.1	2.9	1.2	BURNT PAW PAW + WAX MYRTLE
74	73	427512.4	3138167.9	2.9	1.5	0.85	BURNT PAW PAW + WAX MYRTLE
	78	427522.9	3138155.2	0.5	0.4	1.15	WAX MYRTLE

83	84	427523.8	3138158.9	1.9	1.1	1.6	WAX MYRTLE
85	86	427524	3138157.1	2	0.8	1.7	WAX MYRTLE
89	90	427523.5	3138157.1	1.1	0.8	1.4	WAX MYRTLE
91	92	427524.3	3138161.7	1	1.1	1.9	WAX MYRTLE
94	93	427513.1	3138156.8	2.1	2.1	1.2	LEANING WAX MYRTLE
99	98	427527	3138157.1	1.3	1.5	1.4	WAX MYRTLE
100	101	427530	3138158.6	1.6	0.65	1.2	LEANING SAND PINE
102B	103B	427524.9	3138159.2	0.9	0.7	1	BURNT WAX MYRTLE
104	105	427526	3138161.4	1.3	0.9	1.4	BURNT WAX MYRTLE
106		427522.2	3138162.6	0.6	0.8	1.2	BURNT WAX MYRTLE
107		427524.6	3138159.5	1.2	1	1.2	BURNT WAX MYRTLE
108	109	427521.3	3138162	2.1	2	1.2	BURNT WAX MYRTLE
110	111	427521.9	3138160.8	1.3	1	1.1	BURNT WAX MYRTLE
112	113	427520.5	3138164.8	1	0.7	1	BURNT WAX MYRTLE
116		427524.6	3138162	0.5	1.2	1.2	BURNT WAX MYRTLE
117		427524.3	3138164.5	0.85	0.9	1.3	BURNT WAX MYRTLE
118		427525.4	3138163.2	1.1	1.8	1.9	BURNT WAX MYRTLE
	127	427521.6	3138163.3	1.8	0.8	1	BURNT WAX MYRTLE
	128	427521.6	3138168.5	2.3	1.8	1.9	BURNT WAX MYRTLE
	129	427518.1	3138172.5	2.2	1.5	1.5	BURNT WAX MYRTLE
	130	427520	3138174.6	0.6	1	0.8	BURNT WAX MYRTLE
143		427525.2	3138170	2.2	0.7	0.8	BURNT WAX MYRTLE

----- Tree Measurements ---------

PHOTO	EASTING	NORTHING	DBH	HT1	HT2	HT_SB1	HT_SB2	DIM_NS	DIM_EW	DESC
68	427512.9	3138160.5	31.5	19.7	22.3	12	10.3	5.5	5	SAND PINE
75	427520.2	3138158.6	8	4.6	4.7	0.3	0.35	1.8	2.4	WAX MYRTLE
76	427521.8	3138157.1	1.5	2.85	2.87	0.52	0.52	0.6	0.6	WAX MYRTLE
77	427521.8	3138156.2	1	2.2	2.2	0.6	0.59	1.3	0.9	WAX MYRTLE
79	427522.1	3138161.1	13.3	7.6	7.8	4.8	4.7	1.4	1.4	SAND PINE
80	427525.9	3138155.5	5	5.9	5.9	3.9	3.6	0.7	0.9	SAND PINE
81	427523.5	3138158	10.5	10.2	9.6	6.4	6.2	1.2	1.6	SAND PINE
82	427524.8	3138157.1	10.5	13.7	10.3	4.9	4.8	2.9	2	SAND PINE
87	427521.9	3138161.4	4.5	8.5	8.6	6.2	5.6	1.2	1.2	SAND PINE
88	427523.8	3138157.7	2	2.65	2.67	0.6	0.6	1	0.8	WAX MYRTLE
95	427522.4	3138158	10	10	9.5	3.9	4.3	1.7	2	SAND PINE
96	427521.3	3138163.3	9.1	8.7	7.7	0.36	0.7	2.9	2.7	WAX MYRTLE
97	427525.4	3138158.9	3	2.54	2.56	0.9	0.93	1	1	WAX MYRTLE
102	427530.6	3138162	6	10.6	11.4	6.5	6	1.7	0.8	SAND PINE

103	427523	3138160.8	7.7	10.5	9.8	1.4	1.45	2.3	2.2	WAX MYRTLE
114	427519.4	3138159.9	10.3	6.1	5.7	0.75	0.62	2.7	2	WAX MYRTLE
115	427521.1	3138161.4	4.5	2.92	2.86	0.5	1.25	1.2	1.4	WAX MYRTLE
119	427528.1	3138161.7	2	2.82	2.77	1.8	1.8	1.7	1.6	WAX MYRTLE
120	427526.2	3138161.7	6.2	7.8	8.3	1.75	1.79	2.3	2	WAX MYRTLE
121	427527.6	3138166	2	2.48	2.47	1.18	1.16	0.7	0.9	WAX MYRTLE
122	427528.4	3138162.9	1	2.07	2	1.23	1.2	0.8	0.5	WAX MYRTLE
123	427527	3138162.3	12.6	6.5	6.8	1.7	1.56	2.8	3.1	WAX MYRTLE
124	427527.6	3138165.1	3	2.9	2.6	1.24	1.24	1.8	1.5	WAX MYRTLE
125	427527.4	3138169.7	10.1	6.7	6.6	0.9	0.5	2.7	2.5	WAX MYRTLE
126	427524.6	3138162.6	4.3	5.5	5.8	1.7	1.7	1.8	2.1	WAX MYRTLE
131132	427522.2	3138169.4	7.2	6.2	7.9	1.05	1.05	1.8	1.8	WAX MYRTLE
133	427520.6	3138168.2	33.1	25.4	26.1	14.1	13.3	4.9	5.1	SAND PINE
134	427523.5	3138168.2	10.7	6.8	5.9	1.29	1.3	2.4	2.6	WAX MYRTLE
135	427523.3	3138172.2	9.7	9.4	8.5	1.39	1.4	2.9	2.8	WAX MYRTLE
136	427522.7	3138167.2	2	2.85	2.94	1.58	1.65	1	1.4	WAX MYRTLE
137	427520.3	3138169.7	3	6.4	5	1.45	1.42	1.5	1.7	WAX MYRTLE
138	427523	3138167.2	1.5	2	2.1	1.13	1.12	1.2	0.5	BURNT WAX MYRTLE
139	427523	3138171.6	8	8.6	8.1	5.8	5.5	1.1	1.5	WAX MYRTLE
140	427527.9	3138170	6	7	7.3	2.9	4.4	1.4	1.3	WAX MYRTLE
141	427523.3	3138168.8	5	6.5	7.1	2.1	1.78	1.4	1.5	WAX MYRTLE
142	427524.9	3138171.5	11.4	5.9	5.3	1.54	1.2	2.4	2.4	WAX MYRTLE
144	427527.9	3138173.4	2	2.17	2.2	1.3	1.3	1.5	1.4	WAX MYRTLE
145	427526	3138170.6	2	2.5	2.5	0.77	0.7	1.15	1.1	WAX MYRTLE
146	427531.2	3138174	3	3.4	3.45	1.2	1.46	1.3	0.3	SAND PINE

----- Obstacle Measurements ---------

PHOTO	EASTING	NORTHING	DIM_NS	DIM_EW	HEIGHT	DESC
16	427499	3138154.8	4.7	2.27	0.64	DEAD TREE ON GROUND
20	427498.7	3138161.9	2.4	2.8	0.13	BURNT BRANCH
27	427507.2	3138167.3	1.4	0.32	0.23	LOG
28	427506.1	3138165.2	2.2	2	0.27	LOG
29	427504.7	3138164.3	0.243	0.243	7.55	DEAD TREE
40	427503.1	3138155.4	0.22	0.22	0.1	STUMP
47	427508.8	3138158.1	0.65	0.85	0.09	STUMP
48	427506.4	3138160.6	0.4	0.4	0.17	STUMP
49	427506.9	3138159.3	0.4	0.4	0.14	STUMP
50	427509.6	3138157.8	0.75	1.9	0.1	LOG
51	427511.5	3138155.6	0.75	0.8	0.21	STUMP
72	427509.1	3138167	0.34	0.3	0.08	STUMP

----- Soil Water Content ---------

CONTAINER_ID	MASS_CONTAINER	MASS_CONTAINER_MOISTSAMPLE	MASS_CONTAINER_DRYSAMPLE
A3(1)	50.6	178.1	162.7
A3(2)	50.1	168.4	150.7
A3(4)	50.3	164.9	152.1

----- Soil Grain Size Distribution ---------

SIEVE_OPENING	MASS_RETAINED
2	4.9
1.18	9.2
0.85	38.6
0.425	399.3
0.25	366.9
0.15	103.3
0.075	24.8
0	7.2

HILO-02_1

HILO-02_2

HILO-02_3

HILO-02_3B

HILO-02_4

HILO-02_5

HILO-02_6

HILO-02_7

HILO-02_8

HILO-02_9

HILO-02_10

HILO-02_11

HILO-02_12

HILO-02_13

HILO-02_14

HILO-02_15

HILO-02_16

HILO-02_17

HILO-02_18

HILO-02_19

HILO-02_20

HILO-02_21

HILO-02_22

HILO-02_23

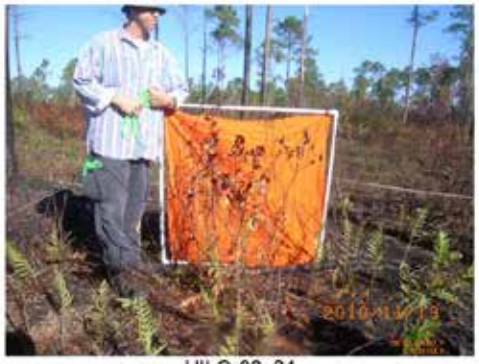

HILO-02_24

HILO-02_25

HILO-02_26

HILO-02_27

HILO-02_28

HILO-02_29

HILO-02_30

HILO-02_31

HILO-02_32

HILO-02_33

HILO-02_34

HILO-02_35

HILO-02_36

HILO-02_37

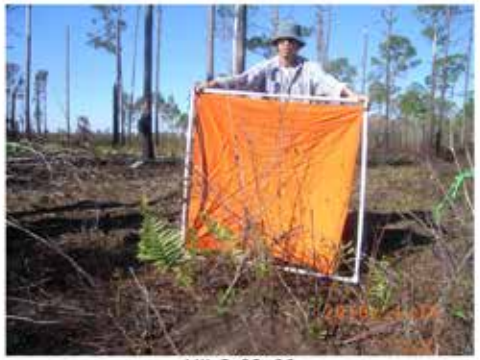

HILO-02_38

HILO-02_39

HILO-02_39B

HILO-02_40

HILO-02_41

HILO-02_42

HILO-02_43

HILO-02_44

HILO-02_45

HILO-02_46

HILO-02_46B

HILO-02_47X

HILO-02_47

HILO-02_48

HILO-02_49

HILO-02_50

HILO-02_51

HILO-02_52

HILO-02_53

HILO-02_54

HILO-02_55

HILO-02_56

HILO-02_57

HILO-02_58

HILO-02_59

HILO-02_60

HILO-02_61

HILO-02_62

HILO-02_63

HILO-02_64

HILO-02_65

HILO-02_66

HILO-02_67

HILO-02_68

HILO-02_69

HILO-02_70

HILO-02_71

HILO-02_71B

HILO-02_72

HILO-02_73

HILO-02_74

HILO-02_75

HILO-02_76


HILO-02_77


HILO-02_78


HILO-02_79


HILO-02_80


HILO-02_81


HILO-02_82


HILO-02_83


HILO-02_84


HILO-02_85

HILO-02_86

HILO-02_87

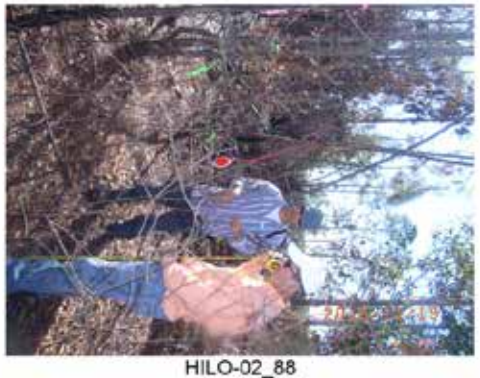

HILO-02_88

HILO-02_89

HILO-02_90

HILO-02_91

HILO-02_92

HILO-02_93

HILO-02_94


HILO-02_95


HILO-02_96


HILO-02_97


HILO-02_98


HILO-02_99


HILO-02_100


HILO-02_101


HILO-02_102


HILO-02_103

HILO-02_102B

HILO-02_103B

HILO-02_104

HILO-02_105

HILO-02_106

HILO-02_107

HILO-02_108

HILO-02_109

HILO-02_110

HILO-02_111

HILO-02_112

HILO-02_113

HILO-02_114

HILO-02_115

HILO-02_116

HILO-02_117

HILO-02_118

HILO-02_119


HILO-02_120


HILO-02_121


HILO-02_122


HILO-02_123


HILO-02_124


HILO-02_125

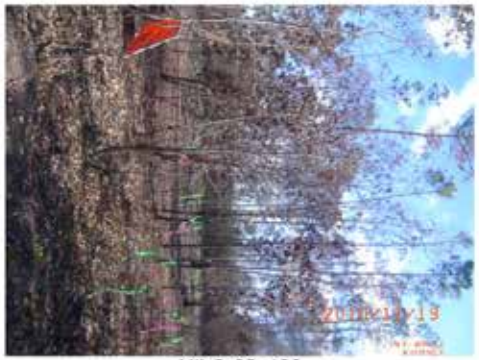
HILO-02_126


HILO-02_127


HILO-02_128

HILO-02_129

HILO-02_130

HILO-02_131

HILO-02_132

HILO-02_133

HILO-02_134

HILO-02_135

HILO-02_136

HILO-02_137


HILO-02_138


HILO-02_139


HILO-02_140


HILO-02_141


HILO-02_142


HILO-02_143

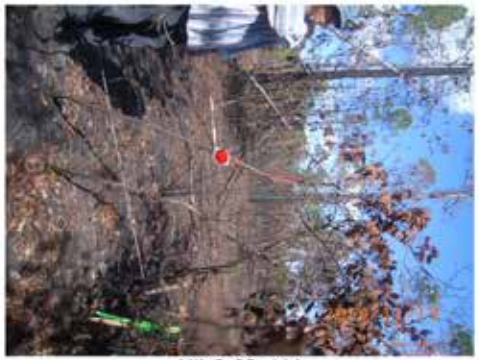
HILO-02_144


HILO-02_145


HILO-02_146

APPENDIX M: FIELD DATA FOR SITE HILO-03

----- General Information ---------
Site ID = HILO-03
Team Leader = MEDEIROS
Participants = DARANPOB, BACOPOULOS, BILSKIE
Date = 11/19/2010
Arrival Time = 1:25 PM
Arrival Weather = WARM, BREEZY, CLEAR
Departure Time = 2:30 PM
Departure Weather = SAME
Datum = WGS84
Coordinate System = UTM17N
Site Photo Looking East = 11B
Site Photo Looking North = 2,3
Site Photo Looking West = 5
Site Photo Looking South = 8,9
Site Photos Looking at the Ground = 12A,12

----- Site Boundary GPS Coordinates ---------

POINT_NAME	EASTING	NORTHING	PHOTO_ID
WEST CENTER	428397.2	3137695.7	11
EAST CENTER	428425.8	3137698.3	6
NORTH WEST	428391.3	3137706.2	10
SOUTH WEST	428397.7	3137690.7	1
NORTH EAST	428424.2	3137706.9	7
SOUTH EAST	428427.7	3137693	4

----- Surface Canopy Estimates ---------

NW	NC	NE	W	C	E	SW	SC	SE
0	0	0	0	0	0	0	0	0
0	0	0	0	0	0	0	0	0
0	0	0	0	0	0	0	0	0
0	0	0	0	0	0	0	0	0

----- Manning's n Component Estimates ---------

n1	n3	n4_PRIME
0.002	0.004	0.01
0.001	0.001	0.01
0.001	0.002	0.023
0.002	0.002	0.02

----- Low Lying Vegetation Measurements ---------

PHOTO_NS	PHOTO_EW	EASTING	NORTHING	DIM_NS	DIM_EW	HEIGHT	DESC
16	17	428412.7	3137699.3	2.2	2.7	1.7	UNIDENTIFIED
	19	428416	3137699.3	0.7	0.7	1.6	UNIDENTIFIED

----- Tree Measurements ---------

PHOTO	EASTING	NORTHING	DBH	HT1	HT2	HT_SB1	HT_SB2	DIM_NS	DIM_EW	DESC
13	428402.9	3137700.3	10.5	6.8	7.7	1	1.2	3.3	3.2	SAND PINE
14	428401.3	3137703	9.9	8	8.5	0.68	0.68	3	3.4	SAND PINE
15	428407.6	3137701.8	7.7	9.2	8.3	1.3	1.3	2.5	2.1	SAND PINE
18	428413.3	3137697.7	11.5	3.27	3.54	0.5	0.5	3.7	4.3	UNIDENTIFIED CLUSTER
23	428420.1	3137697.4	12.5	3.7	3.8	0.5	0.5	3.3	3.5	UNIDENTIFIED CLUSTER

----- Obstacle Measurements ---------

PHOTO	EASTING	NORTHING	DIM_NS	DIM_EW	HEIGHT	DESC

----- Soil Water Content ---------

CONTAINER_ID	MASS_CONTAINER	MASS_CONTAINER_MOISTSAMPLE	MASS_CONTAINER_DRYSAMPLE
A1(1)	50.5	187.9	185.2
A-1(1)	50.3	163.6	161.4
A1(4)	50.2	156.2	154.1

----- Soil Grain Size Distribution ---------

SIEVE_OPENING	MASS_RETAINED
2	1.4
1.18	4.4
0.85	29.5
0.425	384.9
0.25	457.9
0.15	178
0.075	44.3
0	8.7

HILO-03_1

HILO-03_2

HILO-03_3

HILO-03_4

HILO-03_5

HILO-03_6

HILO-03_7

HILO-03_8

HILO-03_9

HILO-03_10

HILO-03_11

HILO-03_11B

HILO-03_12A

HILO-03_12

HILO-03_13

HILO-03_14

HILO-03_15

HILO-03_16

HILO-03_17

HILO-03_18

HILO-03_19

HILO-03_20

HILO-03_21

HILO-03_22

HILO-03_23

APPENDIX N: FIELD DATA FOR SITE LKMO-01

----- General Information ---------
Site ID = LKMO-01
Team Leader = MEDEIROS
Participants = BILSKIE, SMAR, BACOPOULOS
Date = 9/3/2010
Arrival Time = 7:55 AM
Arrival Weather = CLOUDY, 75°
Departure Time = 12:30 PM
Departure Weather = PARTLY CLOUDY, HOT
Datum = WGS 84
Coordinate System = UTM 17N
Site Photo Looking East = 7,9
Site Photo Looking North = 8
Site Photo Looking West = 113
Site Photo Looking South = 114
Site Photos Looking at the Ground = 112

----- Site Boundary GPS Coordinates ---------

POINT_NAME	EASTING	NORTHING	PHOTO_ID
WEST CENTER	480653.9	3190222.7	1
EAST CENTER	480675.8	3190218.3	5
NORTH WEST	480655.8	3190224.8	2
SOUTH WEST	480652.8	3190234.7	3
NORTH EAST	480678.3	3190227.2	6
SOUTH EAST	480682.6	3190212.2	4

----- Surface Canopy Estimates ---------

NW	NC	NE	W	C	E	SW	SC	SE
70	10	90	85	90	80	75	75	95
50	75	99	35	90	70	10	75	90
85	70	99	90	95	95	75	80	100
50	0	65	85	80	80	50	60	85

----- Manning's n Component Estimates ---------

n1	n3	n4_PRIME
0.003	0.002	0.01
0.004	0.008	0.008
0.004	0.004	0.003
0.003	0.005	0.015

----- Low Lying Vegetation Measurements ---------

PHOTO_NS	PHOTO_EW	EASTING	NORTHING	DIM_NS	DIM_EW	HEIGHT	DESC
16	15	480658.2	3190213.1	3.8	4	3.1	SABAL PALM
18	19	480658.7	3190217.7	5.3	4.8	3.5	SABAL PALM
20	21	480654.4	3190220.2	2.35	1.8	1.8	INDIGO
22	23	480659.8	3190214.7	1.5	2.4	2	SABAL PALM
26	25	480666.9	3190212.5	2.05	1.3	1.6	INDIGO
28	27	480660.6	3190217.4	1.1	0.6	0.95	SABAL PALM + WAX MYRTLE
30	29	480670.9	3190209.4	0.95	0.7	0.8	INDIGO
31	32	480668	3190224.8	0.6	0.44	0.85	INDIGO
34	33	480662	3190225.1	0.8	0.8	0.85	INDIGO
37	36	480664.7	3190219.3	5.5	5.9	3.8	SABAL PALM
39	38	480672.5	3190210.9	0.83	0.72	0.82	INDIGO
41	40	480676.1	3190215.9	0.94	0.7	1.05	INDIGO
43	42	480679.3	3190215.2	0.75	0.9	0.85	INDIGO
44	45	480679.3	3190210	1.64	1.7	1.15	SABAL PALM
47	46	480680.4	3190214.6	1.1	0.76	0.76	INDIGO
49	48	480679.9	3190217.7	1.2	1.92	1.8	SABAL PALM
51	50	480675	3190217.1	1.65	1.75	1.2	SABAL CLUSTER
52	53	480654.4	3190220.8	1.7	2.28	1.9	SABAL PALM + SOUTHERN FOX GRAPE
54	55	480658.2	3190222.4	2.75	2.5	1.71	SABAL PALM + SOUTHERN FOX GRAPE
56	57	480656.3	3190221.4	2.15	1.3	2.1	SABAL PALM + SOUTHERN FOX GRAPE
58	59	480653.6	3190228.5	1.7	2.45	1.55	SABAL PALM + SOUTHERN FOX GRAPE
60	61	480657.1	3190229.1	1.75	1.8	1.53	SABAL PALM + SOUTHERN FOX GRAPE
63	64	480647.4	3190218.1	1	1.35	1.4	SABAL PALM
65	66	480657.9	3190231.9	2.6	3.1	1.7	SABAL PALM + INDIGO CLUSTER
69	68	480655.8	3190224.5	2.1	1.5	1.3	INDIGO + SOUTHERN FOX GRAPE
70	71	480659	3190224.5	1.05	1.75	1.25	SABAL PALM + SOUTHERN FOX GRAPE
73	74	480659.5	3190212.2	1.7	1.2	1.53	SABAL PALM
76	75	480664.7	3190221.1	1.2	1.1	1	INDIGO
77	78	480660.6	3190224.5	0.8	1.7	1.2	SABAL PALM
79	80	480660.6	3190222.7	1.9	1.75	1.6	INDIGO

82	81	480658.7	3190222	0.9	0.8	1	RED MAPLE
83	82B	480666.3	3190214.6	2	2	1.7	INDIGO
85	86	480663.6	3190223.6	0.6	0.8	1	INDIGO
87	88	480667.1	3190222	0.8	0.4	1.46	INDIGO
90	91	480675	3190217.1	2.1	1.7	2.85	SABAL PALM
92	93	480669	3190215.6	1.1	0.85	1.3	SABAL PALM
96	97	480675.8	3190218.6	0.3	0.8	1.4	SABAL PALM
99	98	480670.1	3190216.5	1.65	1.8	1.6	SABAL PALM
100	101	480669.3	3190235.9	0.7	0.85	1	SABAL PALM + INDIGO CLUSTER
103	102	480681.5	3190223.2	3.8	4	2.85	SABAL PALM
104	105	480680.7	3190228.2	0.9	1.2	0.85	SABAL PALM
107B	108	480679.9	3190220.2	1.6	2.2	0.9	SABAL PALM + RED MAPLE CLUSTER
110	109	480676.9	3190223.6	1	0.9	1.2	SABAL PALM

----- Tree Measurements ---------

PHOTO	EASTING	NORTHING	DBH	HT1	HT2	HT_SB1	HT_SB2	DIM_NS	DIM_EW	DESC
11	480666.3	3190211.6	44.6	9.4	8.2	5.2	4.8	6	5.2	SABAL PALM
12,13	480650.9	3190216.2	1	1.5	1.5	0.55	0.35	1.3	1.2	COONTIE
14	480674.1	3190171.9	1.5	2.4	2.3	0.9	0.9	2.1	2.6	CHINESE ARBOR VITAE

----- Obstacle Measurements ---------

PHOTO	EASTING	NORTHING	DIM_NS	DIM_EW	HEIGHT	DESC
17	480636.6	3190254.1	6.2	7.2	0.25	LOG
24	480645.2	3190223	1.35	4.3	0.16	LOG
62	480659	3190221.7	4.35	6.55	0.2	LOG
107	480676.6	3190232.2	1.34	0.9	1.3	STUMP

----- Soil Water Content ---------

CONTAINER_ID	MASS_CONTAINER	MASS_CONTAINER_MOISTSAMPLE	MASS_CONTAINER_DRYSAMPLE
A1-1	50.5	166.8	161.9
A2-1	50.3	133.9	130.3
A3-1	50.6	136.9	133.4

----- Soil Grain Size Distribution ---------

SIEVE_OPENING	MASS_RETAINED
2	1.7
1.18	1.6
0.85	2.1
0.425	19.4
0.25	236.7
0.15	655.2
0.075	183.4
0	12

LKMO-01_1

LKMO-01_2

LKMO-01_3

LKMO-01_4

LKMO-01_5

LKMO-01_6

LKMO-01_7

LKMO-01_8

LKMO-01_9


LKMO-01_11


LKMO-01_12


LKMO-01_13


LKMO-01_14


LKMO-01_15


LKMO-01_16


LKMO-01_17


LKMO-01_18


LKMO-01_19

LKMO-01_20

LKMO-01_21

LKMO-01_22

LKMO-01_23

LKMO-01_24

LKMO-01_25

LKMO-01_26

LKMO-01_27

LKMO-01_28


LKMO-01_29


LKMO-01_30


LKMO-01_31


LKMO-01_32


LKMO-01_33


LKMO-01_34


LKMO-01_36


LKMO-01_37


LKMO-01_38

LKMO-01_39

LKMO-01_40

LKMO-01_41

LKMO-01_42

LKMO-01_43

LKMO-01_44

LKMO-01_45

LKMO-01_46

LKMO-01_47


LKMO-01_48


LKMO-01_49


LKMO-01_50


LKMO-01_51


LKMO-01_52


LKMO-01_53


LKMO-01_54


LKMO-01_55


LKMO-01_56


LKMO-01_57


LKMO-01_58


LKMO-01_59


LKMO-01_60


LKMO-01_61


LKMO-01_62


LKMO-01_63


LKMO-01_64


LKMO-01_65

LKMO-01_66

LKMO-01_67

LKMO-01_68

LKMO-01_69

LKMO-01_70

LKMO-01_71

LKMO-01_72

LKMO-01_73

LKMO-01_74

LKMO-01_75

LKMO-01_76

LKMO-01_77

LKMO-01_78

LKMO-01_79

LKMO-01_80

LKMO-01_81

LKMO-01_82

LKMO-01_82B

LKMO-01_83

LKMO-01_84

LKMO-01_85

LKMO-01_86

LKMO-01_87

LKMO-01_88

LKMO-01_89

LKMO-01_90

LKMO-01_91

LKMO-01_92

LKMO-01_93

LKMO-01_94

LKMO-01_95

LKMO-01_96

LKMO-01_97

LKMO-01_98

LKMO-01_99

LKMO-01_100

LKMO-01_101

LKMO-01_102

LKMO-01_103

LKMO-01_104

LKMO-01_105

LKMO-01_106

LKMO-01_107

LKMO-01_107B

LKMO-01_108

LKMO-01_109

LKMO-01_110

LKMO-01_111

LKMO-01_112

LKMO-01_113

LKMO-01_114

LKMO-01_115

APPENDIX O: FIELD DATA FOR SITE LKMO-02

----- General Information ---------
Site ID = LKMO-02
Team Leader = MEDEIROS
Participants = BILSKIE, SMAR, BACOPOULOS
Date = 9/3/2010
Arrival Time = 1:40 PM
Arrival Weather = CLEAR, HOT, 95°
Departure Time = 3:0 PM
Departure Weather = CLEAR, HOT
Datum = WGS 84
Coordinate System = UTM 17N
Site Photo Looking East = 7
Site Photo Looking North = 8
Site Photo Looking West = 9
Site Photo Looking South = 10
Site Photos Looking at the Ground = 12,13,14

----- Site Boundary GPS Coordinates ---------

POINT_NAME	EASTING	NORTHING	PHOTO_ID
WEST CENTER	480742.3	3190436.4	2
EAST CENTER	480771.3	3190436.1	5
NORTH WEST	480746.4	3190441.3	3
SOUTH WEST	480741.7	3190427.8	1
NORTH EAST	480774	3190445.3	6
SOUTH EAST	480773.2	3190430.2	4

----- Surface Canopy Estimates ---------

NW	NC	NE	W	C	E	SW	SC	SE
0	0	90	0	0	60	0	95	0
0	0	95	0	0	99	0	90	0
0	0	90	0	0	35	0	60	0
0	0	80	0	0	70	0	50	0

----- Manning's n Component Estimates ---------

n1	n3	n4_PRIME
0.001	0.002	0.012
0.002	0.001	0.025
0.025	0.01	0.02
0.002	0.002	0.02

----- Low Lying Vegetation Measurements ---------

PHOTO_NS	PHOTO_EW	EASTING	NORTHING	DIM_NS	DIM_EW	HEIGHT	DESC
16	17	480750.1	3190430.5	1.4	1.6	1.2	SABAL PALM + LAUREL OAK
18	19	480747.2	3190429	2	1.5	1.68	LIVE OAK + LAUREL OAK
22	21	480765.9	3190434.5	2.95	3.2	2.63	SABAL PALM
24	25	480769.6	3190430.2	2.8	3	2.6	SABAL PALM
26	27	480773.7	3190437.9	1.6	2.05	1.2	LAUREL OAK CLUSTER
30	29	480769.4	3190441.6	1.5	1.2	1.6	LAUREL OAK CLUSTER
31	32	480767.5	3190441.3	2.5	2.1	1.75	LAUREL OAK CLUSTER
34	33	480766.7	3190441.6	1.2	1.4	1.5	LAUREL OAK CLUSTER
35	36	480764.8	3190442.5	1.2	1.1	1.3	LAUREL OAK CLUSTER
37	38	480766.4	3190440.7	1.7	1.2	1.6	LAUREL OAK CLUSTER
40	39	480762.6	3190438.8	1.5	2	2	LAUREL OAK CLUSTER

----- Tree Measurements ---------

PHOTO	EASTING	NORTHING	DBH	HT1	HT2	HT_SB1	HT_SB2	DIM_NS	DIM_EW	DESC
15	480751.5	3190430.2	16	8.1	7.2	0.6	0.7	5.3	5.6	LONGLEAF PINE
20	480764.5	3190425.9	20.5	8.2	9.1	0.9	0.9	6.9	7	LONGLEAF PINE
23	480766.7	3190434.8	1.5	2.4	2.4	1.74	1.75	0.9	0.5	LAUREL OAK
42	480743.9	3190441	13.5	8.8	8	0.9	0.8	2.9	3.05	LONGLEAF PINE

----- Obstacle Measurements ---------

PHOTO	EASTING	NORTHING	DIM_NS	DIM_EW	HEIGHT	DESC
28	480774	3190435.7	3.1	0.1	0.1	LOG
41	480761.5	3190438.8	0.1	0.1	1.08	STUMP

----- Soil Water Content ---------

CONTAINER_ID	MASS_CONTAINER	MASS_CONTAINER_MOISTSAMPLE	MASS_CONTAINER_DRYSAMPLE
A3-4	50.4	152.1	150.8
A4-T	50.5	192.8	191.2
A4-3	50.4	172.8	171.5

----- Soil Grain Size Distribution ---------

SIEVE_OPENING	MASS_RETAINED
2	0.7
1.18	1.7
0.85	2.1
0.425	27.3
0.25	323.1
0.15	538.1
0.075	93.2
0	4


LKMO-02_1


LKMO-02_2


LKMO-02_3


LKMO-02_4


LKMO-02_5


LKMO-02_6


LKMO-02_7


LKMO-02_8


LKMO-02_9

LKMO-02_10

LKMO-02_11

LKMO-02_12

LKMO-02_13

LKMO-02_14

LKMO-02_15

LKMO-02_16

LKMO-02_17

LKMO-02_18

LKMO-02_19

LKMO-02_20

LKMO-02_21

LKMO-02_22

LKMO-02_23

LKMO-02_24

LKMO-02_25

LKMO-02_26

LKMO-02_27


LKMO-02_28


LKMO-02_29


LKMO-02_30


LKMO-02_31


LKMO-02_32


LKMO-02_33


LKMO-02_34


LKMO-02_35

LKMO-02_36

LKMO-02_37

LKMO-02_38

LKMO-02_39

LKMO-02_40

LKMO-02_41

LKMO-02_42

APPENDIX P: FIELD DATA FOR SITE LKMO-03

----- General Information ---------
Site ID = LKMO-03
Team Leader = MEDEIROS
Participants = BILSKIE, SMAR, PASSERI
Date = 9/17/2010
Arrival Time = 7:45 AM
Arrival Weather = PARTLY CLOUDY, WARM
Departure Time = 2:55 PM
Departure Weather = CLEAR, SUNNY, VERY WARM
Datum = WGS84
Coordinate System = UTM 17N
Site Photo Looking East = 1
Site Photo Looking North = 2
Site Photo Looking West = 3
Site Photo Looking South = 4
Site Photos Looking at the Ground = 5,6,7,8

----- Site Boundary GPS Coordinates ---------

POINT_NAME	EASTING	NORTHING	PHOTO_ID
WEST CENTER	480903	3190302	10
EAST CENTER	480936.9	3190280.7	14
NORTH WEST	480910.9	3190295.2	11
SOUTH WEST	480904.3	3190282.6	15
NORTH EAST	480942	3190283.4	12
SOUTH EAST	480938.5	3190284.4	13

----- Surface Canopy Estimates ---------

NW	NC	NE	W	C	E	SW	SC	SE
70	20	85	100	20	98	0	95	70
35	40	30	95	98	95	0	95	60
20	40	50	95	95	95	0	90	25
95	5	95	100	85	99	0	95	90

----- Manning's n Component Estimates ---------

n1	n3	n4_PRIME
0.01	0.005	0.01
0.004	0.004	0.02
0.009	0.015	0.025
0.015	0.005	0.023

----- Low Lying Vegetation Measurements ---------

PHOTO_NS	PHOTO_EW	EASTING	NORTHING	DIM_NS	DIM_EW	HEIGHT	DESC
55	56	480915.7	3190294.6	1.3	1.3	1.9	SABAL PALM
97	96	480932.8	3190285.3	1.6	1.5	1.5	SABAL PALM

----- Tree Measurements ---------

PHOTO	EASTING	NORTHING	DBH	HT1	HT2	HT_SB1	HT_SB2	DIM_NS	DIM_EW	DESC
16	480905.2	3190269.7	1.5	2.7	2.74	1.04	1.04	0.9	1.5	WAX MYRTLE
17	480915.2	3190279.8	2	2.44	2.44	0.7	0.7	1.3	1.5	WAX MYRTLE
19	480912.5	3190287.8	1.5	3.2	3	1.52	1.35	1.68	1.96	WAX MYRTLE
20	480905.7	3190281.3	2	1.55	1.54	0.84	0.85	2.4	0.57	WAX MYRTLE
21	480909.2	3190286.9	1.5	2.37	2.4	1.09	1.11	0.6	1.03	WAX MYRTLE
22	480906	3190279.8	1.5	2.15	2.26	0.23	0.23	0.68	1.27	WAX MYRTLE
23	480907.1	3190280.4	1.5	2.96	2.98	0.45	0.45	1.62	1.28	WAX MYRTLE
24	480909.2	3190283.2	1.5	1.98	2.16	0.56	0.56	1.07	1.2	WAX MYRTLE
25	480923.3	3190286.2	1	2.18	2.23	0.49	0.9	1.35	1.38	WAX MYRTLE
26	480906.8	3190285.3	11	7.8	8.3	0.6	0.5	6.4	4.1	WAX MYRTLE
27	480906.8	3190284.1	9	7.2	7.8	1.2	1.1	4.92	2.35	WAX MYRTLE
28	480905.7	3190282.3	2	1.53	1.53	0.9	0.9	2.45	2.34	WAX MYRTLE
29	480907.1	3190286	1.5	1.93	2.2	0.7	0.66	2.6	1.48	WAX MYRTLE
30	480907.6	3190272.4	1	1.6	1.17	1.09	1.09	2.3	2.07	WAX MYRTLE
31	480908.4	3190282.3	2	2.24	2.3	0.52	0.5	2.75	1.7	WAX MYRTLE
32	480914.6	3190279.5	1.5	1.88	1.82	0.56	0.56	2.55	1.5	WAX MYRTLE
33	480906.8	3190282.3	1.5	2.4	2.4	0.71	1.06	1.48	1.42	WAX MYRTLE
34	480894.1	3190292.7	1	2.24	2.24	0.47	0.46	1.15	1.3	WAX MYRTLE
35	480904.1	3190286.3	7	8.2	10.3	2.6	2.6	3.6	3	RED MAPLE
36	480906.2	3190278.6	3	5.6	5.2	0.5	0.48	1.45	2.1	RED MAPLE
37	480903.6	3190294	2	3.07	3	0.94	1.32	1.3	1.8	WAX MYRTLE
38	480907.1	3190285.6	10.5	4.4	4.8	1.1	0.4	3	3.9	CLUSTER OF WAX MYRTLE
39	480899.8	3190290.9	3.5	3.16	3.17	0.23	0.23	2	1.01	CLUSTER OF WAX MYRTLE
40	480912.2	3190289.9	16	12.8	7.7	1.7	2.1	6.3	4.8	RED MAPLE
41	480907.1	3190301.6	6	5.9	5.4	1.6	1	2.4	2	RED MAPLE

42	480909.8	3190292.7	14.8	6.5	6.6	1	1	5.7	6.7	CLUSTER OF WAX MYRTLE
43	480904.6	3190291.5	9	9.9	8.1	2.1	3.1	3.2	3.4	RED MAPLE
44	480912	3190295.2	5	4.6	5.6	1.4	1.6	2.7	2.6	RED MAPLE
45	480908.4	3190296.4	9.5	8.3	8.4	2.1	3	2.85	3.3	LONGLEAF PINE
46	480912.5	3190290.6	12.2	7.9	8.4	0.9	1	3.6	2.4	CLUSTER OF WAX MYRTLE
47	480910.9	3190291.8	16	10.3	10.5	2.7	2.4	6.8	4.9	LONGLEAF PINE
48	480911.7	3190296.4	8.3	3.92	4.24	0.66	0.76	2.3	2.6	CLUSTER OF MIXED SPECIES
52	480927.4	3190289.6	4	4.12	4.03	1.4	1.55	1.9	1.7	LONGLEAF PINE
53	480920.1	3190287.8	14	9.8	11	1.9	2	2.8	2.4	LONGLEAF PINE
54	480912	3190296.4	15	10.8	11.3	1.9	2.1	4.17	4.9	LONGLEAF PINE
56A	480887.8	3190295.2	15	9.4	11.5	3.1	3.5	2.7	3	LONGLEAF PINE
58	480917.3	3190276.7	17	12.3	10.7	4.5	5.6	4.9	4.1	LONGLEAF PINE
59,60	480914.9	3190283.2	10	8.6	9.4	2.3	2.9	3.3	2.2	LONGLEAF PINE
61	480908.1	3190286.3	4	5.1	4.7	1.6	0.9	1.9	2.6	RED MAPLE
62	480915.7	3190277.9	3	5.2	4.7	1.1	0.9	1.9	2.1	RED MAPLE
63	480916	3190274.9	4.5	4.8	6.3	1.3	1.2	2.6	2.3	RED MAPLE
64	480918.4	3190282.9	16.5	12.1	10.7	2.7	2.1	4.6	5.7	LONGLEAF PINE
65	480909.5	3190282.6	18	13.1	11.2	4.4	2.5	4.7	3.6	LONGLEAF PINE
66	480931.2	3190280.4	9.5	9.2	8.9	1.9	2	4.7	3.1	RED MAPLE
67	480929.3	3190290.2	7.5	7.6	8.5	2.6	3.5	1.8	2.3	RED MAPLE
68	480919	3190279.8	12	9.8	12.8	2.3	1.5	4.3	2.6	RED MAPLE
69	480919.3	3190284.4	4	7.5	8.4	1.8	2.1	1.58	1.8	RED MAPLE
70	480925.2	3190284.1	14.5	10.5	12	1.7	1.3	4.85	3.9	RED MAPLE
71	480938	3190284.1	13	12.1	12.3	3.9	1.9	3.35	5.11	LONGLEAF PINE
72,73	480927.4	3190283.5	10.5	14.4	11.5	3.7	3	2.85	3.41	LONGLEAF PINE
74	480934.4	3190280.7	10.5	11.6	12	3.3	4.3	1.76	1.94	LONGLEAF PINE
75	480930.6	3190289	22	16.9	18.2	4	1.9	4.33	4.2	LONGLEAF PINE
76	480933.9	3190274.8	14.5	10.5	13.1	4.2	2.4	4.35	3	LONGLEAF PINE
77	480926.3	3190291.2	17	13.9	16.4	0.9	1.2	6.44	5.05	RED MAPLE
78	480927.1	3190297.9	18.5	13.7	14.5	1.8	2.5	4.55	6.26	RED MAPLE
80	480931.4	3190277	15	12.8	11.5	2.9	2.8	4	4.45	LONGLEAF PINE
81	480933.9	3190279.4	13	11.2	12.1	1.5	1.4	4.7	4.91	RED MAPLE
82	480925.7	3190269.3	6	5.7	4.7	1	2.4	2.8	3	RED MAPLE
84	480924.9	3190278.8	15.5	10.7	9.3	1.8	2.6	1.58	2.57	SPLIT LONGLEAF PINE
85	480931.2	3190289.3	14	16.1	15.2	2.4	3.2	4.21	3.6	LONGLEAF PINE
86	480937.7	3190298.2	10.5	14	13.2	2.8	7.1	3.39	2.35	LONGLEAF PINE
87	480920.6	3190288.7	31	17.3	15.7	3.7	2.6	6.75	5.35	LONGLEAF PINE
88	480925.8	3190283.5	11.5	8.3	10.2	1.9	3.9	2.7	2.8	LONGLEAF PINE
89	480915.5	3190279.2	12	13.2	10.3	1.8	2.8	3.26	3.84	SPLIT RED MAPLE

90	480913.6	3190280.1	8	11.5	8.9	1.7	2.9	3	3.3	RED MAPLE
91	480909.7	3190267.2	15	9.6	13.5	1.8	2.6	3.1	3.2	SPLIT RED MAPLE
95	480924.7	3190286.2	16.5	6.7	5.1	1	0.9	6.5	10	CLUSTER OF MIXED SPECIES

----- Obstacle Measurements ---------

PHOTO	EASTING	NORTHING	DIM_NS	DIM_EW	HEIGHT	DESC
49	480919	3190293.3	1.95	1.15	4.72	DEAD TREE
50	480914.4	3190294.9	0.04	0.04	0.86	STUMP
51	480915.2	3190287.2	0.55	0.88	2.88	DEAD TREE
57	480893.5	3190295.2	5.4	2.15	0.58	LOG
79	480928.8	3190296.4	1	4.55	0.8	LOG
83	480930.4	3190285.6	0.25	4.5	0.2	LOG
92	480914.4	3190276.7	4.2	5	4.1	DEAD TREE
93,94	480924.7	3190294.2	1	1.15	3.1	DEAD TREE

----- Soil Water Content ---------

CONTAINER_ID	MASS_CONTAINER	MASS_CONTAINER_MOISTSAMPLE	MASS_CONTAINER_DRYSAMPLE
A3(2)	50.1	137.5	127.3
A-4(4)	50.5	153.9	141.6
A2(3)	50.5	163	149.4

----- Soil Grain Size Distribution ---------

SIEVE_OPENING	MASS_RETAINED
2	12.3
1.18	21.4
0.85	17.1
0.425	52.2
0.25	329.5
0.15	542.4
0.075	59.2
0	9


LKMO-03_1


LKMO-03_2


LKMO-03_3


LKMO-03_4


LKMO-03_5


LKMO-03_6


LKMO-03_7


LKMO-03_8


LKMO-03_9


LKMO-03_10


LKMO-03_11


LKMO-03_12


LKMO-03_13


LKMO-03_14


LKMO-03_15


LKMO-03_16


LKMO-03_17


LKMO-03_18

LKMO-03_19

LKMO-03_20

LKMO-03_21

LKMO-03_22

LKMO-03_23

LKMO-03_24

LKMO-03_25

LKMO-03_26

LKMO-03_27

LKMO-03_28

LKMO-03_29

LKMO-03_30

LKMO-03_31

LKMO-03_32

LKMO-03_33

LKMO-03_34

LKMO-03_35

LKMO-03_36

LKMO-03_37

LKMO-03_38

LKMO-03_39

LKMO-03_40

LKMO-03_41

LKMO-03_42

LKMO-03_43

LKMO-03_44

LKMO-03_45

LKMO-03_46

LKMO-03_47

LKMO-03_48

LKMO-03_49

LKMO-03_50

LKMO-03_51

LKMO-03_52

LKMO-03_53

LKMO-03_54

LKMO-03_55

LKMO-03_56

LKMO-03_56A

LKMO-03_57

LKMO-03_58

LKMO-03_59

LKMO-03_60

LKMO-03_61

LKMO-03_62

LKMO-03_63

LKMO-03_64

LKMO-03_65

LKMO-03_66

LKMO-03_67

LKMO-03_68

LKMO-03_69

LKMO-03_70

LKMO-03_71


LKMO-03_72


LKMO-03_73


LKMO-03_74


LKMO-03_75


LKMO-03_76


LKMO-03_77


LKMO-03_78


LKMO-03_79


LKMO-03_80

LKMO-03_81

LKMO-03_82

LKMO-03_83

LKMO-03_84

LKMO-03_85

LKMO-03_86

LKMO-03_87

LKMO-03_88

LKMO-03_89

LKMO-03_90

LKMO-03_91

LKMO-03_92

LKMO-03_93

LKMO-03_94

LKMO-03_95

LKMO-03_96

LKMO-03_97

APPENDIX Q: FIELD DATA FOR SITE LKMO-04

----- General Information ---------
Site ID = LKMO-04
Team Leader = MEDEIROS
Participants = BILSKIE, SMAR, PASSERI
Date = 7/21/2011
Arrival Time = 8:0 AM
Arrival Weather = HOT, HUMID
Departure Time = 4:0 PM
Departure Weather = STILL HOT AND HUMID
Datum = UTM 17N
Coordinate System = WGS84
Site Photo Looking East = 3
Site Photo Looking North = 11
Site Photo Looking West = 8
Site Photo Looking South = 6
Site Photos Looking at the Ground = 95,96

----- Site Boundary GPS Coordinates ---------

POINT_NAME	EASTING	NORTHING	PHOTO_ID
WEST CENTER	418064.5	3189616.3	2
EAST CENTER	481093.5	3189613.8	9
NORTH WEST	481066.7	3189614.2	4
SOUTH WEST	481065.8	3189599.4	1
NORTH EAST	481096.2	3189617.2	7
SOUTH EAST	481094.3	3189609.8	10

----- Surface Canopy Estimates ---------

NW	NC	NE	W	C	E	SW	SC	SE
0	95	90	0	80	80	0	75	75
0	70	40	0	80	5	0	10	20
0	95	50	0	95	35	0	25	5
75	95	90	0	95	80	0	100	0

----- Manning's n Component Estimates ---------

n1	n3	n4_PRIME
0.005	0.001	0.01
0.005	0.003	0.025
0.0025	0.004	0.02
0.005	0.005	0.015

----- Low Lying Vegetation Measurements ---------

PHOTO_NS	PHOTO_EW	EASTING	NORTHING	DIM_NS	DIM_EW	HEIGHT	DESC
13	12	481085.9	3189619.4	3.8	1.8	2	SABAL PALM
17	18	481081.6	3189614.2	1.75	1.75	2.5	SABAL PALM
20	19	481097.8	3189614.7	0.6	0.5	2.3	DOG FENNEL
22	21	481096.2	3189613.8	0.8	0.6	1.5	SAND LIVE OAK
23	24	481094.6	3189611.7	4.8	4	4	SABAL PALM
25	26	481091.3	3189609.5	1.4	2	1	?
28	29	481090.5	3189618.5	3.5	3.8	1.6	MIXED SOUTHERN FOX GRAPE
33	34	481086.4	3189614.5	1	1.3	1.4	WAX MYRTLE
	35	481087	3189613.2	1.2	0.9	2	SAND LIVE OAK
39B	40B	481091	3189614.8	1.4	1.3	0.6	GRASS
45	44	481085.1	3189623.7	3.3	4.1	1.4	DEAD TREE
47	46	481088.9	3189623.1	1.9	1.1	1.65	SAND LIVE OAK
	62B	481090.2	3189609.2	6.3	3.9	1.9	MIXED
	73B	481074.3	3189639.1	1.69	1.35	1.14	SABAL PALM
	84	481083.5	3189613.5	6.1	5.1	4.6	MIXED
93B	92	481074.8	3189615.4	3.4	2.3	2.7	INDIGO
93,94		WEST END	OF SITE	15	9	1.725	MIXED GRASS

----- Tree Measurements ---------

PHOTO	EASTING	NORTHING	DBH	HT1	HT2	HT_SB1	HT_SB2	DIM_NS	DIM_EW	DESC
14	481091.1	3189622.1	17	11.4	13.1	1.6	2.3	3.6	4.7	SAND PINE
15	481091.1	3189624.3	26.1	16.8	12.5	3.7	2.5	6	5	SAND PINE
16	481088.3	3189613.2	16	10.5	10.1	3.3	3.8	3.7	4	SAND PINE
27	481093.5	3189616.6	3	3.6	3.6	1.2	1.2	2.1	1.75	?
NP	481095.1	3189611.1	1	2.57	2.57	1.1	1.1	0.8	1.1	?
31	481088	3189606.5	1	2	1.94	1.06	1.3	1.4	0.8	SAND PINE
32	481093.2	3189610.1	2	2.65	2.7	1.54	1.6	1.3	1.2	SAND PINE
36	481091.3	3189610.1	2	2.8	2.9	1.2	0.95	1	0.9	SAND LIVE OAK
37	481090.5	3189617.2	1	2.85	2.75	0.75	0.7	0.75	0.8	SAND LIVE OAK
38	481087.5	3189620	2	2.4	2.45	0.8	0.78	0.8	1.4	SAND LIVE OAK

39	481091.3	3189622.1	2.5	3.4	3.43	1.7	0.8	3.2	1.8	SAND LIVE OAK
40	481091.9	3189617.2	2	2.7	2.56	1.9	1.88	2.85	1.85	SAND LIVE OAK
41	481085.9	3189623.1	8.5	7.5	7.8	1.1	1.2	3.3	2.2	WAX MYRTLE
42	481089.7	3189613.5	2.5	1.9	2.07	0.6	0.5	1.9	1.6	WAX MYRTLE
43	481087.3	3189623.1	10	6.3	6	0.8	1	3.4	3.2	WAX MYRTLE
49	481084	3189620.3	11.3	5.6	5.1	0.1	0.1	2.4	3	WAX MYRTLE
50	481088.9	3189621.2	13.1	6.7	6.6	0.4	0.38	3.4	4.3	WAX MYRTLE
52	481081.3	3189624	22.7	10.1	9.4	0.5	0.6	3.7	5.3	WAX MYRTLE
54	481090.5	3189616.6	18.7	7.3	7.7	0.4	0.54	5.5	6.1	WAX MYRTLE
55	481081.6	3189613.5	15.7	7.9	5.3	0.8	0.77	2.7	3.8	WAX MYRTLE
56	481087.3	3189621.8	59.5	6.5	6.8	1.8	1.9	5.3	4.8	SABAL PALM
57	481086.4	3189620.3	9	10.3	8.6	1.8	1.82	2.7	3.1	RED MAPLE
58	481086.4	3189614.5	15.9	7.1	6.3	1.2	0.13	3.4	2.4	WAX MYRTLE
59	481078	3189610.8	17.8	9.3	6.7	0.6	0.8	3.1	3.4	WAX MYRTLE
60	481084	3189618.2	4.5	6.2	6.5	1.4	1.39	2	2.3	SOUTHERN FOX GRAPE
61	481085.6	3189615.7	15.1	8.2	8.2	0.5	0.4	2.7	4.5	WAX MYRTLE
62	481087	3189613.5	22.4	4.9	5.5	0.8	0.77	2.2	6.3	WAX MYRTLE
63	481088	3189600	11.7	7.6	7.5	0.6	0.56	3.5	2.8	WAX MYRTLE
64	481091	3189613.8	11	5.6	5	0.5	0.6	2.9	4.4	WAX MYRTLE
65	481088.6	3189609.2	16.6	6.5	10.8	0.45	0.6	5.3	7.1	WAX MYRTLE
66	481090.5	3189609.8	19.1	8.6	8.2	0.9	1	4.3	6	LIVE OAK
67	481093.7	3189594.8	6.2	4.4	4.5	1.15	1.15	2.1	2.4	LIVE OAK
68	481084	3189617.2	13.5	9.9	8.6	0.8	0.8	5.9	4.6	LIVE OAK
69	481092.1	3189598.8	12	8.7	9	1.2	0.6	4	3.3	LIVE OAK
70	481087	3189606.2	6	6.5	7.6	2.85	2.7	2.3	3.7	LIVE OAK
71	481080.5	3189604.6	13.5	8.7	7.2	1	0.95	3.6	5.4	LIVE OAK
72	481084.8	3189609.2	7.5	5.8	4.7	0.5	0.5	2.5	1.7	LIVE OAK
73	481083.5	3189612.9	12.5	8.9	8	1.3	1.3	2.7	3.2	LIVE OAK
74	481086.4	3189615.7	12.9	6.2	6.5	1.5	1.45	2.7	1	LIVE OAK
75	481079.1	3189618.5	4.5	13.1	7.7	0.9	0.9	2.4	2.4	RED MAPLE
76	481080.5	3189621.9	17.2	9.2	11.9	1.3	1.3	3.7	2.1	SAND LIVE OAK
77	481082.1	3189617.2	31.3	15.9	9.3	1.2	1.3	5.1	5.45	LIVE OAK
78	481078.8	3189613.9	15.5	9.9	9.3	1.1	1.1	4.8	3.7	LIVE OAK
79	481079.7	3189615.7	15.4	8.7	7.5	1.6	1.55	2.2	3.8	LIVE OAK
80	481081.5	3189608.3	26.9	5.8	6.1	1	1.1	3.8	8	LIVE OAK
81	481075.1	3189614.8	21.5	11.2	10.6	0.66	0.65	4.2	3.3	LIVE OAK
82	481072.3	3189613.9	8.5	5.4	6.6	1.9	1.25	2.7	3.7	LIVE OAK
83	481077.2	3189610.8	18.9	4.7	5.1	1.1	1.1	3.8	3.5	LIVE OAK
85	481073.4	3189604.6	25.9	8.4	6.3	1.2	1.15	7.9	6.1	LIVE OAK

NP	481066.7	3189618.2	10	5.3	7.6	0.7	1.4	3.4	4.1	LIVE OAK
87	481082.9	3189609.2	11	8.2	9.9	2.2	2.1	3.1	2.6	RED MAPLE
88	481074	3189614.8	19	9.4	10.5	1	0.8	4.8	5.1	RED MAPLE
89	481071.5	3189612.9	14.5	6.5	6	0.7	0.65	3.4	2.8	RED MAPLE
90	481074.8	3189622.5	33.8	9	9.3	0.9	0.55	6	6.1	LIVE OAK
91	481071.3	3189621.9	24.1	7.5	5.8	1.1	0.6	5.3	5.7	LIVE OAK

----- Obstacle Measurements ---------

PHOTO	EASTING	NORTHING	DIM_NS	DIM_EW	HEIGHT	DESC
48	481084.6	3189625.9	0.5	0.8	2.95	DEAD SAPLING
51	481088.4	3189629.2	0.03	0.03	3.36	DEAD SAPLING
53	481081.6	3189619.4	0.11	2.1	0.11	DEAD TREE

----- Soil Water Content ---------

CONTAINER_ID	MASS_CONTAINER	MASS_CONTAINER_MOISTSAMPLE	MASS_CONTAINER_DRYSAMPLE
19	50.3	102.6	82.6
102	50.2	105.5	85.2
103	50.3	117.8	94.3

----- Soil Grain Size Distribution ---------

SIEVE_OPENING	MASS_RETAINED
2	50.4
1.18	72.9
0.85	52.1
0.425	104.9
0.25	244.9
0.15	153.9
0.075	12.7
0	1.1

LKMO-04_01

LKMO-04_02

LKMO-04_03

LKMO-04_04

LKMO-04_05

LKMO-04_06

LKMO-04_07

LKMO-04_08

LKMO-04_09


LKMO-04_10


LKMO-04_11


LKMO-04_12


LKMO-04_13


LKMO-04_14


LKMO-04_15


LKMO-04_16


LKMO-04_17


LKMO-04_18

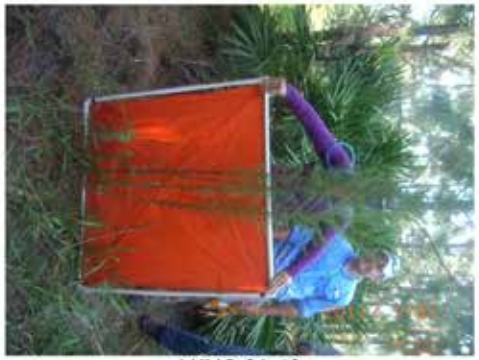

LKMO-04_19

LKMO-04_20

LKMO-04_21

LKMO-04_22

LKMO-04_23

LKMO-04_24

LKMO-04_25

LKMO-04_26

LKMO-04_27

LKMO-04_28

LKMO-04_29

LKMO-04_31

LKMO-04_32

LKMO-04_33

LKMO-04_34

LKMO-04_35

LKMO-04_36

LKMO-04_37

LKMO-04_38

LKMO-04_39B

LKMO-04_40B

LKMO-04_39

LKMO-04_40

LKMO-04_41

LKMO-04_42

LKMO-04_43

LKMO-04_44

LKMO-04_45

LKMO-04_46

LKMO-04_47

LKMO-04_48

LKMO-04_49

LKMO-04_50

LKMO-04_51

LKMO-04_52

LKMO-04_53

LKMO-04_54

LKMO-04_55

LKMO-04_56

LKMO-04_57

LKMO-04_58

LKMO-04_59

LKMO-04_60

LKMO-04_61

LKMO-04_62B

LKMO-04_62

LKMO-04_63

LKMO-04_64

LKMO-04_65

LKMO-04_66

LKMO-04_67

LKMO-04_68

LKMO-04_69

LKMO-04_70

LKMO-04_71

LKMO-04_72

LKMO-04_73B

LKMO-04_73

LKMO-04_74

LKMO-04_75

LKMO-04_76

LKMO-04_77

LKMO-04_78

LKMO-04_79

LKMO-04_80

LKMO-04_81

LKMO-04_82

LKMO-04_83

LKMO-04_84

LKMO-04_85

LKMO-04_87

LKMO-04_88

LKMO-04_89

LKMO-04_90

LKMO-04_91

LKMO-04_92

LKMO-04_93B

LKMO-04_93

LKMO-04_94

LKMO-04_95

LKMO-04_96

APPENDIX R: FIELD DATA FOR SITE SEMF-01

----- General Information ---------
Site ID = SEMF-01
Team Leader = MEDEIROS
Participants = DARANPOB, BACOPOULOS, BILSKIE
Date = 10/5/2010
Arrival Time = 1:45 PM
Arrival Weather = COOL, CLOUDY
Departure Time = 2:30 PM
Departure Weather = COOL, CLOUDY
Datum = WGS84
Coordinate System = UTM17N
Site Photo Looking East = 11
Site Photo Looking North = 4,10
Site Photo Looking West = 9
Site Photo Looking South = 8
Site Photos Looking at the Ground = 12,13,14

----- Site Boundary GPS Coordinates ---------

POINT_NAME	EASTING	NORTHING	PHOTO_ID
WEST CENTER	458156.6	3188061.3	6
EAST CENTER	458182.6	3188063.4	2
NORTH WEST	458155.6	3188071.8	7
SOUTH WEST	458154.2	3188059.8	5
NORTH EAST	458186.2	3188072.3	1
SOUTH EAST	458182.3	3188054.1	3

----- Surface Canopy Estimates ---------

NW	NC	NE	W	C	E	SW	SC	SE
0	0	0	85	0	0	90	0	0
0	0	0	95	0	0	40	0	0
0	0	0	60	0	0	30	0	0
0	0	0	85	0	0	50	0	0

----- Manning's n Component Estimates ---------

n1	n3	n4_PRIME
0.004	0.01	0.003
0.0025	0.01	0.005
0.002	0.02	0.001
0.001	0.03	0.004

----- Low Lying Vegetation Measurements ---------

PHOTO_NS	PHOTO_EW	EASTING	NORTHING	DIM_NS	DIM_EW	HEIGHT	DESC

----- Tree Measurements ---------

PHOTO	EASTING	NORTHING	DBH	HT1	HT2	HT_SB1	HT_SB2	DIM_NS	DIM_EW	DESC
15	458157.4	3188068.4	1.5	1.73	1.7	0.1	0.1	0.4	0.55	LONGLEAF PINE
16	458158	3188061	27	15.4	17.7	5.7	3.2	8.5	2.4	LONGLEAF PINE
17	458159.6	3188056.1	30	15.4	17.4	5	5.2	7.3	6.5	LONGLEAF PINE
18	458159.6	3188063.5	30	13.3	15.7	2	2.7	5.9	6.2	LONGLEAF PINE

----- Obstacle Measurements ---------

PHOTO	EASTING	NORTHING	DIM_NS	DIM_EW	HEIGHT	DESC
19	458164.7	3188067.1	15	3.9	0.97	FENCE W/ 0.18 M OPENING

----- Soil Water Content ---------

CONTAINER_ID	MASS_CONTAINER	MASS_CONTAINER_MOISTSAMPLE	MASS_CONTAINER_DRYSAMPLE
A2(4)	49.7	156	147.8
A3(1)	50.5	163.9	155.9
A4(T)	50.5	176	166.9

----- Soil Grain Size Distribution ---------

SIEVE_OPENING	MASS_RETAINED
2	3.5
1.18	6.6
0.85	8.2
0.425	52.8
0.25	377.9
0.15	426
0.075	88.9
0	4.8

SEMF-01_1

SEMF-01_2

SEMF-01_3

SEMF-01_4

SEMF-01_5

SEMF-01_6

SEMF-01_7

SEMF-01_8

SEMF-01_9

SEMF-01_10

SEMF-01_11

SEMF-01_12

SEMF-01_13

SEMF-01_14

SEMF-01_15

SEMF-01_16

SEMF-01_17

SEMF-01_18

SEMF-01_19

APPENDIX S: FIELD DATA FOR SITE SEMF-02

----- General Information ---------
Site ID = SEMF-02
Team Leader = MEDEIROS
Participants = DARANPOB, BACOPOULOS, BILSKIE
Date = 10/8/2010
Arrival Time = 7:55 AM
Arrival Weather = CLEAR, COOL, FOGGY
Departure Time = 11:45 AM
Departure Weather = WARM
Datum = WGS84
Coordinate System = UTM17N
Site Photo Looking East = 63
Site Photo Looking North = 61
Site Photo Looking West = 59
Site Photo Looking South = 57B
Site Photos Looking at the Ground = 66,67,68

----- Site Boundary GPS Coordinates ---------

POINT_NAME	EASTING	NORTHING	PHOTO_ID
WEST CENTER	459894.4	3189909.7	65
EAST CENTER			
NORTH WEST	457893.1	3189902.9	64
SOUTH WEST	457894.9	3189895.9	62
NORTH EAST	457922.9	3189911.1	58
SOUTH EAST	457924.2	3189894.5	60

----- Surface Canopy Estimates ---------

NW	NC	NE	W	C	E	SW	SC	SE
0	0	0	0	0	0	0	0	0
0	0	0	0	0	0	0	0	0
0	0	0	0	0	0	0	0	0
0	0	0	0	0	0	0	0	0

----- Manning's n Component Estimates ---------

n1	n3	n4_PRIME
0.003	0.001	0.018
0.013	0.03	0.025
0.015	0.009	0.02
0.01	0.025	0.02

----- Low Lying Vegetation Measurements ---------

PHOTO_NS	PHOTO_EW	EASTING	NORTHING	DIM_NS	DIM_EW	HEIGHT	DESC
3	2	457897.4	3189913.4	1.6	1.5	1.05	SAW PALMETTO
8	7	457902.8	3189899.5	3.2	3.4	1.4	SAW PALMETTO CLUSTER
9	10	457907.1	3189897.4	1.1	2	1.2	SAW PALMETTO CLUSTER
11	12	457908.5	3189900.1	2.3	1.8	1.6	SAW PALMETTO CLUSTER
20	21	457913.4	3189898.9	1.1	1.1	0.81	PAW PAW
23	22	457914.2	3189900.1	0.82	0.92	1	PAW PAW
25	26	457917.4	3189900.7	1	1.6	1.3	PAW PAW
27	28	457917.7	3189899.2	1.3	1.6	1.5	PAW PAW
31	30	457913.1	3189902.6	0.5	0.5	0.85	PAW PAW
33	32	457913.7	3189902.9	1.6	2.2	1.2	SAW PALMETTO
35	34	457915	3189897.9	1.1	1.5	1.1	SAW PALMETTO
37	36	457916.1	3189904.4	1.5	1.7	1.1	MIXED SAW PALM AND PAW PAW CLUST
39	38	457917.7	3189904.4	3.1	3	1.6	MIXED CLUSTER
40		457909.9	3189902	9.7	7.7	2.07	LARGE MIXED CLUSTER
57	56	457908.5	3189901.7	0.85	0.85	1	PAW PAW

----- Tree Measurements ---------

PHOTO	EASTING	NORTHING	DBH	HT1	HT2	HT_SB1	HT_SB2	DIM_NS	DIM_EW	DESC
1	457897.7	3189908.5	9.4	7.7	7.3	4.6	5	1.9	2.4	LONGLEAF PINE
6	457898.7	3189898.3	2	2.04	2.04	0.4	0.5	1.2	1.3	LONGLEAF PINE
18	457909.6	3189900.1	4.4	2.87	2.86	0.4	0.4	1.6	2.2	LONGLEAF PINE
49	457917.5	3189907.5	12	8.5	8.2	5.9	5.2	2.4	2	LONGLEAF PINE

----- Obstacle Measurements ---------

PHOTO	EASTING	NORTHING	DIM_NS	DIM_EW	HEIGHT	DESC
4	457899.6	3189904.2	0.45	0.5	0.22	STUMP
5	457900.4	3189903.8	0.75	4.6	0.1	SKINNY LOG
13	457908	3189897.4	0.06	0.06	0.83	SKINNY STUMP
14	457910.4	3189899.8	0.16	0.16	0.26	STUMP
15	457909.3	3189899.8	2.5	2.3	0.16	LOG

16	457906.3	3189899.5	0.23	0.17	0.1	STUMP
17	457896.6	3189911.2	0.04	0.04	1.06	SKINNY STUMP
19	457909.9	3189901.7	0.21	0.21	0.12	STUMP
24	457914.7	3189900.7	0.45	0.7	0.1	LOG
29	457916.9	3189900.1	1.7	1.5	0.08	LOG
42	457917.7	3189906.2	0.05	0.05	2.3	DEAD TREE
43	457918	3189907.8	0.05	0.05	1.07	DEAD TREE
44	457918.6	3189908.4	0.05	0.05	0.47	DEAD TREE
45	457919.1	3189906.5	0.06	0.06	0.41	DEAD TREE
46	457918.3	3189909.9	0.08	0.08	0.32	DEAD TREE
47	457919.1	3189908.7	0.05	0.05	0.67	DEAD TREE
48	457918.3	3189908.1	0.05	0.05	0.32	DEAD TREE
50	457919.1	3189910.2	0.046	0.046	1	DEAD TREE
51	457915.3	3189910.9	0.07	0.07	1.85	DEAD TREE
52	457913.7	3189904.7	2.9	0.13	0.52	LOG
53	457910.4	3189904.7	0.06	0.06	0.56	DEAD TREE
54	457908.3	3189908.4	0.07	0.07	0.67	DEAD TREE
55	457906.4	3189908.1	5.28	5.2	0.2	LARGE LOG

----- Soil Water Content ---------

CONTAINER_ID	MASS_CONTAINER	MASS_CONTAINER_MOISTSAMPLE	MASS_CONTAINER_DRYSAMPLE
A4(2)	41	148.2	137.5
A4(3)	50.3	192.2	180.3
A-4(4)	50.3	169.1	154.9

----- Soil Grain Size Distribution ---------

SIEVE_OPENING	MASS_RETAINED
2	6
1.18	8.4
0.85	10.1
0.425	65.7
0.25	226.3
0.15	448.1
0.075	121.1
0	14.9

SEMF-02_1

SEMF-02_2

SEMF-02_3

SEMF-02_4

SEMF-02_5

SEMF-02_6

SEMF-02_7

SEMF-02_8

SEMF-02_9

SEMF-02_10

SEMF-02_11

SEMF-02_12

SEMF-02_13

SEMF-02_14

SEMF-02_15

SEMF-02_16

SEMF-02_17

SEMF-02_18

SEMF-02_19

SEMF-02_20

SEMF-02_21

SEMF-02_22

SEMF-02_23

SEMF-02_24

SEMF-02_25

SEMF-02_26

SEMF-02_27


SEMF-02_28


SEMF-02_29


SEMF-02_30


SEMF-02_31


SEMF-02_32


SEMF-02_33


SEMF-02_34


SEMF-02_35


SEMF-02_36

SEMF-02_37

SEMF-02_38

SEMF-02_39

SEMF-02_40

SEMF-02_42

SEMF-02_43

SEMF-02_44

SEMF-02_45

SEMF-02_46

SEMF-02_47

SEMF-02_48

SEMF-02_49

SEMF-02_50

SEMF-02_51

SEMF-02_52

SEMF-02_53

SEMF-02_54

SEMF-02_55

SEMF-02_56

SEMF-02_57

SEMF-02_57B

SEMF-02_58

SEMF-02_59

SEMF-02_60

SEMF-02_61

SEMF-02_62

SEMF-02_63

SEMF-02_64

SEMF-02_65

SEMF-02_66

SEMF-02_67

SEMF-02_68

APPENDIX T: FIELD DATA FOR SITE SEMF-03

----- General Information ---------
Site ID = SEMF-03
Team Leader = MEDEIROS
Participants = DARANPOB, BACOPOULOS, BILSKIE
Date = 10/11/2010
Arrival Time = 7:35 AM
Arrival Weather = COOL, PARTLY CLOUDY
Departure Time = 1:15 PM
Departure Weather = HOT, PARTLY CLOUDY
Datum = WGS84
Coordinate System = UTM17N
Site Photo Looking East = 8
Site Photo Looking North = 7
Site Photo Looking West = 10
Site Photo Looking South = 9
Site Photos Looking at the Ground = 11,12,13,14

----- Site Boundary GPS Coordinates ---------

POINT_NAME	EASTING	NORTHING	PHOTO_ID
WEST CENTER	457940.6	3188589	2,3
EAST CENTER	457970.4	3188587.9	15
NORTH WEST	457940.9	3188599.7	4
SOUTH WEST	457938.7	3188582.5	1
NORTH EAST	457969.9	3188594.7	5
SOUTH EAST	457968.8	3188582.4	

----- Surface Canopy Estimates ---------

NW	NC	NE	W	C	E	SW	SC	SE
0	50	95	0	0	0	2	0	0
0	50	90	0	0	0	0	0	0
0	85	95	0	0	0	0	0	0
0	30	100	0	0	0	0	0	0

----- Manning's n Component Estimates ---------

n1	n3	n4_PRIME
0.007	0.004	0.006
0.016	0.025	0.005
0.015	0.02	0.015
0.015	0.012	0.012

----- Low Lying Vegetation Measurements ---------

PHOTO_NS	PHOTO_EW	EASTING	NORTHING	DIM_NS	DIM_EW	HEIGHT	DESC
16	17	457940.3	3188584.4	0.9	2	1.45	SAW PALM CLUSTER
18	19	457941.9	3188583.4	1	1.1	1.32	SAND LIVE OAK
27	28	457943.1	3188597.9	0.6	1.4	1.3	SAND LIVE OAK
29	30	457943.6	3188596.3	0.9	1.7	1.35	CHAPMAN OAK
31	32	457943.9	3188594.2	0.7	0.75	0.9	SAND LIVE OAK
33	34	457943.6	3188592.3	2.3	1.7	1.5	SAND LIVE OAK CLUSTER
36	37	457945.2	3188593.6	0.8	1.4	1.45	SAND LIVE OAK CLUSTER
38	39	457946.3	3188594.2	0.9	1.1	0.5	SAND LIVE OAK CLUSTER
41	42	457947.1	3188598.5	0.4	0.4	1.5	TALL GRASS CLUSTER
44	43	457945.8	3188594.5	1.3	1.1	1.5	TALL GRASS CLUSTER
46	45	457949.8	3188593.2	0.9	1.1	1.4	SAW PALM
48	47	457951.2	3188594.2	0.6	0.4	1.14	SAND LIVE OAK
50	49	457950.9	3188596	0.9	1	1.3	MIXED OAK CLUSTER
53	52	457952.3	3188592.3	2.5	2.7	1.9	SAND LIVE OAK CLUSTER
54	55	457951.7	3188591.4	1.4	1.3	1.5	SAND LIVE OAK
56	57	457950.6	3188591.4	0.9	1.3	1.35	SAND LIVE OAK
74	73	457953.6	3188594.5	2.3	2.7	1.85	SAW PALM
81	80	457957.4	3188595.4	0.9	2.2	2.05	SAW PALM
82B	82	457959.9	3188595.7	1.4	2.3	1.65	SAW PALM
84B	84	457955.3	3188594.1	1.1	1.7	1.25	SAW PALM
86B	86	457958.5	3188592.3	1.05	1.05	1.1	SAW PALM
89	88	457959.6	3188596	1.7	2.7	2.02	SAW PALM CLUSTER
92	91	457964.5	3188591.7	1.1	0.9	0.8	SAW PALM
94	93	457963.4	3188593.8	2	1.9	2.1	SHINY LYNONIA
96	95	457961.5	3188591	2.2	1.4	1.9	SAW PALM
98	97	457964.7	3188590.1	1.8	1.6	1.92	SHINY LYNONIA
100	99	457964.7	3188588	1.1	1.3	1.1	SAW PALM
102	101	457963.9	3188585.8	2	2.3	2	SAND LIVE OAK
104	103	457963.4	3188584.9	1.2	1.2	1.5	SAW PALM
113	112	457959.3	3188583.1	1.1	1.1	1.2	SHINY LYNONIA

115	114	457960.6	3188582.1	1.2	1.4	1.25	SHINY LYNONIA
117	116	457965	3188580.9	1.2	0.5	1.14	SHINY LYNONIA
119	118	457968.5	3188581.2	1.5	1.7	0.9	SAW PALM CLUSTER
121	120	457965	3188582.1	0.8	1	0.8	SHINY LYNONIA
128	127	457966.9	3188595.3	2.4	2.7	2.2	SAW PALM CLUSTER
130	129	457963.9	3188592.3	2.6	1.6	2.1	SAW PALM CLUSTER
149	148	457970.2	3188591.9	1.77	2.22	1.5	SAW PALM

----- Tree Measurements ---------

PHOTO	EASTING	NORTHING	DBH	HT1	HT2	HT_SB1	HT_SB2	DIM_NS	DIM_EW	DESC
58	457948.5	3188588.9	8.5	4.1	3.5	0.2	0.1	2.4	3	RED BAY (2 TRUNKS)
75	457958	3188596.6	8.5	4.6	4.4	0.8	1.9	3.4	3.5	SAND PINE
76	457955.5	3188591.4	12.1	4.2	3.9	0.25	0.1	2.5	2.8	CHAPMAN OAK CLUSTER
77	457961.5	3188593.8	4.5	4.8	4.1	0.6	0.4	1.8	1.7	SAND LIVE OAK
78,79	457956.9	3188598.8	2.5	4.3	4	0.5	0.4	1.5	1.6	SAND LIVE OAK
87	457958.5	3188598.4	2.9	2.63	2.7	1.2	0.7	1.3	2	SAND LIVE OAK
90	457964.7	3188595	11.5	6.2	5.8	0.8	1.5	4.6	3.9	SAND PINE
105	457963.9	3188586.1	4	2.9	3.1	0.34	0.8	2	1.8	SAND PINE
131	457962.6	3188593.2	3	2.4	3.1	0.55	0.6	1.4	2	SAND LIVE OAK
132	457968.3	3188592.3	5.3	4.3	4.4	1.15	1	1.4	2.1	SAND LIVE OAK
134	457965.8	3188592.9	3	3.46	3.5	1.6	0.85	1.2	1	SAND LIVE OAK
135	457968.3	3188594.4	2.6	3.76	3.8	1.1	1.2	0.8	0.7	SAND LIVE OAK
136	457969.1	3188591.3	2.7	3.33	3.2	1.05	1.6	1.5	1.5	SAND LIVE OAK
137	457972.9	3188595.6	7.5	6.1	5.6	0.41	1.3	2.7	2.42	SAND PINE
138	457970.7	3188593.5	5	5	4.7	0.26	0.3	1.9	1.96	SAND LIVE OAK
139	457968	3188591.6	5.1	3.2	4.5	0.55	1.2	1.3	2.55	SAND LIVE OAK
140	457969.1	3188590.7	8.7	3.6	4.1	0.65	0.59	2	2	SAND LIVE OAK CLUSTER
141	457969.1	3188592.6	3.1	3.93	3.5	0.9	0.75	1.3	1.6	SAND LIVE OAK
142	457966.6	3188593.5	4	4.1	3.8	0.27	0.8	1.1	1.9	SAND LIVE OAK
143	457968.2	3188587.3	6.5	4.6	3.7	0.8	0.4	1.8	2.2	SAND LIVE OAK
144	457969.1	3188588.6	9.2	3.3	3.5	0.8	0.75	2.3	1.5	SAND LIVE OAK
145	457966.4	3188591	3.5	2.9	2.83	0.93	0.9	1.7	1.1	SAND LIVE OAK
146	457968.3	3188590.4	7	4.5	4.1	1.1	0.7	2.3	1.8	SAND LIVE OAK
147	457969.9	3188588.9	8.5	4.1	3.8	0.3	0.3	2.2	1.75	SAND LIVE OAK

----- Obstacle Measurements ---------

PHOTO	EASTING	NORTHING	DIM_NS	DIM_EW	HEIGHT	DESC
20	457943.8	3188585.3	1.2	2.25	0.29	DEAD TREE LYING
21	457944.4	3188585.9	2.8	6.8	0.9	DEAD TREE CLUSTER

22	457949.3	3188590.2	2.8	2	0.95	DEAD TREE
23	457943.6	3188589.9	0.35	0.7	0.16	TWISTED LOG
24	457939.8	3188588	1.4	1.1	0.2	DEAD TREE ROOTS
25	457942.8	3188592.7	0.9	0.6	0.15	DEAD PALM
26	457943.1	3188595.7	3.1	2.7	0.8	MIXED FALLEN TREES WITH VEG
35	457944.7	3188596.3	0.5	2.6	0.12	FALEN LOG
40	457948	3188598.5	0.3	1	0.17	LOG
51	457950.9	3188597.9	0.3	0.5	0.2	PALM LOG
59	457950.7	3188595.1	0.95	1.3	0.55	CLUSTER OF DEAD BRANCHES
60	457947.6	3188587.7	0.35	0.4	0.4	TWISTED STUMP
61	457952.6	3188596.9	1.95	2.3	0.77	TWISTED DEAD BRANCHES
62,63	457960.9	3188590.4	2.3	1.5	0.5	TWISTED DEAD BRANCHES
64	457955.2	3188592	2.35	2.1	0.19	TWISTED DEAD BRANCHES
65	457957.4	3188585.2	0.35	1.1	0.25	PALM LOG
66	457953.3	3188586.2	1.1	2.25	0.4	TWISTED BRANCHES
67	457946.8	3188584	1.9	3.2	0.4	TWISTED BRANCHES
68	457947.6	3188585.9	0.7	0.9	0.2	MIXED LOGS
69	457946.8	3188582.2	1.1	0.35	0.15	PALM LOG
70	457950.3	3188583.4	0.9	0.95	0.3	SMALL PALM LOG
71	457952	3188588	0.7	0.4	0.23	PALM LOG
72	457959.3	3188589.2	0.7	0.6	0.3	MIXED PALM LOG
105B	457959.8	3188589.5	1	0.2	0.12	PALM LOG
106	457961.2	3188588	2.4	0.1	0.18	LOG
107	457958.8	3188586.1	0.24	1.1	0.14	PALM LOG
108	457966.3	3188588.9	4.5	2.7	0.3	CLUSTER OF TWISTED BRANCHES
109	457964.5	3188589.8	0.4	0.7	0.1	PALM LOG
110	457965	3188590.1	0.45	1	0.13	PALM LOG
111	457966.6	3188585.8	0.06	1.8	0.25	FALLEN SKINNY TREE
122	457968.8	3188579.9	3	4.2	1.5	FALLEN TREE
123	457969.6	3188581.8	0.5	0.7	0.15	PALM LOG
124	457968.2	3188580.3	0.8	0.44	0.14	PALM LOG
125	457969.3	3188582.4	0.55	0.8	0.16	PALM LOG
126	457966.6	3188588	0.7	0.5	0.15	PALM LOG
133	457968.6	3188599	1.1	0.5	0.15	PALM LOG

----- Soil Water Content ---------

CONTAINER_ID	MASS_CONTAINER	MASS_CONTAINER_MOISTSAMPLE	MASS_CONTAINER_DRYSAMPLE
A-1(2)	50.3	168.6	166.7
A1_4	50.1	166.3	164.4
A1(1)	50.5	181	179

----- Soil Grain Size Distribution ---------

SIEVE_OPENING	MASS_RETAINED
2	4.6
1.18	3.1
0.85	2.3
0.425	21.3
0.25	239.9
0.15	735
0.075	117.3
0	27


SEMF-03_1


SEMF-03_2


SEMF-03_3


SEMF-03_4


SEMF-03_5


SEMF-03_7


SEMF-03_8


SEMF-03_9


SEMF-03_10

SEMF-03_11

SEMF-03_12

SEMF-03_13

SEMF-03_14

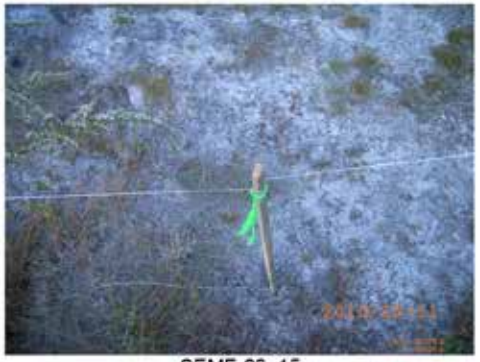

SEMF-03_15

SEMF-03_16

SEMF-03_17

SEMF-03_18

SEMF-03_19


SEMF-03_20


SEMF-03_21


SEMF-03_22


SEMF-03_23


SEMF-03_24


SEMF-03_25


SEMF-03_26


SEMF-03_27


SEMF-03_28

SEMF-03_29

SEMF-03_30

SEMF-03_31

SEMF-03_32

SEMF-03_33

SEMF-03_34

SEMF-03_35

SEMF-03_36

SEMF-03_37

SEMF-03_38

SEMF-03_39

SEMF-03_40

SEMF-03_41

SEMF-03_42

SEMF-03_43

SEMF-03_44

SEMF-03_45

SEMF-03_46


SEMF-03_47


SEMF-03_48


SEMF-03_49


SEMF-03_50


SEMF-03_51


SEMF-03_52


SEMF-03_53


SEMF-03_54


SEMF-03_55

SEMF-03_56

SEMF-03_57

SEMF-03_58

SEMF-03_59

SEMF-03_60

SEMF-03_61

SEMF-03_62

SEMF-03_63

SEMF-03_64

SEMF-03_65

SEMF-03_66

SEMF-03_67

SEMF-03_68

SEMF-03_69

SEMF-03_70

SEMF-03_71

SEMF-03_72

SEMF-03_73

SEMF-03_74

SEMF-03_75

SEMF-03_76

SEMF-03_77

SEMF-03_78

SEMF-03_79

SEMF-03_80

SEMF-03_81

SEMF-03_82


SEMF-03_82B


SEMF-03_84


SEMF-03_84B


SEMF-03_86


SEMF-03_86B


SEMF-03_87


SEMF-03_88


SEMF-03_89


SEMF-03_90

SEMF-03_91

SEMF-03_92

SEMF-03_93

SEMF-03_94

SEMF-03_95

SEMF-03_96

SEMF-03_97

SEMF-03_98

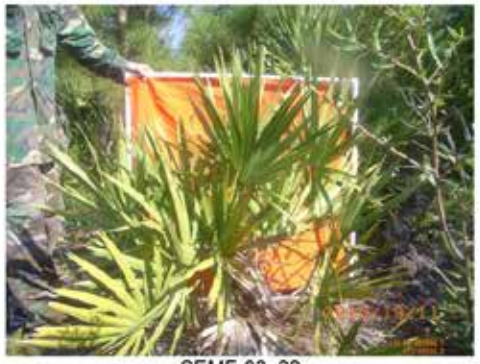

SEMF-03_99

SEMF-03_100

SEMF-03_101

SEMF-03_102

SEMF-03_103

SEMF-03_104

SEMF-03_105

SEMF-03_105B

SEMF-03_106

SEMF-03_107

SEMF-03_108

SEMF-03_109

SEMF-03_110

SEMF-03_111

SEMF-03_112

SEMF-03_113

SEMF-03_114

SEMF-03_115

SEMF-03_116

SEMF-03_117

SEMF-03_118

SEMF-03_119

SEMF-03_120

SEMF-03_121

SEMF-03_122

SEMF-03_123

SEMF-03_124

SEMF-03_125

SEMF-03_126

SEMF-03_127

SEMF-03_128

SEMF-03_129

SEMF-03_130

SEMF-03_131

SEMF-03_132

SEMF-03_133

SEMF-03_134

SEMF-03_135

SEMF-03_136

SEMF-03_137

SEMF-03_138

SEMF-03_139

SEMF-03_140

SEMF-03_141

SEMF-03_142

SEMF-03_143

SEMF-03_144

SEMF-03_145

SEMF-03_146

SEMF-03_147

SEMF-03_148

SEMF-03_149

APPENDIX U: FIELD DATA FOR SITE SEMF-04

----- General Information ---------
Site ID = SEMF-04
Team Leader = MEDEIROS
Participants = DARANPOB, BACOPOULOS, BILSKIE
Date = 10/11/2010
Arrival Time = 2:30 PM
Arrival Weather = HOT, PARTLY CLOUDY
Departure Time = 4:15 PM
Departure Weather = HOT, PARTLY CLOUDY
Datum = WGS84
Coordinate System = UTM17N
Site Photo Looking East = 10
Site Photo Looking North = 3
Site Photo Looking West = 6
Site Photo Looking South = 8
Site Photos Looking at the Ground = 11,12

----- Site Boundary GPS Coordinates ---------

POINT_NAME	EASTING	NORTHING	PHOTO_ID
WEST CENTER	458042.1	3188407.3	1
EAST CENTER	458070.9	3188409.1	5
NORTH WEST	458043.8	3188411.9	9
SOUTH WEST	458041.3	3188400.9	2
NORTH EAST	458070.6	3188415.5	7
SOUTH EAST	458073.8	3188403.8	4

----- Surface Canopy Estimates ---------

NW	NC	NE	W	C	E	SW	SC	SE
4	0	0	30	0	0	6	0	0
0	0	0	0	0	0	0	0	0
0	0	0	0	0	0	5	0	0
0	0	0	0	0	0	15	0	15

----- Manning's n Component Estimates ---------

n1	n3	n4_PRIME
0.01	0.004	0.015
0.005	0.006	0.021
0.013	0.01	0.015
0.003	0.002	0.02

----- Low Lying Vegetation Measurements ---------

PHOTO_NS	PHOTO_EW	EASTING	NORTHING	DIM_NS	DIM_EW	HEIGHT	DESC
20	19	458044.3	3188401.8	1	1.1	1.7	ATLANTIC WHITE CEDAR
42	41	458073.8	3188409.1	0.8	1.1	1.65	SAND PINE

----- Tree Measurements ---------

PHOTO	EASTING	NORTHING	DBH	HT1	HT2	HT_SB1	HT_SB2	DIM_NS	DIM_EW	DESC
15	458048.3	3188397.2	13.5	12.2	12.1	6.4	6.3	3	3.9	SAND PINE
16	458045.6	3188404.6	16.5	13.1	15.2	5.2	6	4.7	4.8	SAND PINE
17	458041.8	3188399.6	11.5	13	15.5	5.9	7.4	1.7	3.5	SAND PINE
18	458048.6	3188402.7	10.5	5.9	8.4	2.6	3.2	1.2	2	SAND PINE
24	458051.3	3188404.5	2	2.22	2.3	0.97	1.4	1	0.8	SAND PINE
27	458056.7	3188403.9	3	2.74	2.8	1.04	1.1	1.45	1.4	SAND PINE
31	458058.4	3188407.3	4.5	3.03	3.45	1	1.05	1.8	1.8	SAND PINE
33	458066	3188411.9	24.6	16.8	17	5.6	7.7	4.9	5.1	SAND PINE
34	458065.7	3188403.6	10	10.1	9.4	3.5	3.8	2.5	2.9	SAND PINE
35	458068.4	3188399.5	5	4.2	3.7	2.34	2.7	0.9	1.2	SAND PINE
36	458067.9	3188403.5	11.3	11.3	12.5	4	4.1	2	2.4	SAND PINE
37	458068.9	3188403.5	17	16.1	15.5	6.4	5.3	3.2	3.8	SAND PINE
38	458067.1	3188407.2	7.3	7.1	7.2	4.2	3.8	1.5	1.3	SAND PINE
43	458064.4	3188412.8	4.7	6	6.3	2.07	3.8	2	1.15	SAND PINE
44	458067.6	3188413.4	15.8	14.6	11.6	3.3	3.2	4.7	3.6	SAND PINE
47	458068.4	3188417.7	8.5	8.5	8.1	1.97	2.1	1.9	2.3	SAND PINE
50	458053.5	3188415.6	9.7	8.7	8.5	3	3.5	1.9	1.5	SAND PINE

----- Obstacle Measurements ---------

PHOTO	EASTING	NORTHING	DIM_NS	DIM_EW	HEIGHT	DESC
13	458044.3	3188402.7	3.7	0.6	0.6	DEAD BENT OVER TREE
14	458044	3188400.6	2.2	1.1	0.12	LOG
21	458049.1	3188401.8	2.4	1.2	0.13	LOG
22	458048.3	3188403	0.35	0.6	0.18	CHUNK OF WOOD
23	458050.5	3188402.1	0.85	1.1	0.1	LOG

25	458051.9	3188406.4	2.2	4.95	0.23	FALLEN DEAD TREE
26	458055.7	3188406.4	5.5	1.9	0.9	FALLEN DEAD TREE
28	458055.7	3188406.4	2.9	2.6	0.07	FALLEN DEAD TREE
29	458057.6	3188406.4	2.2	0.1	0.06	FALLEN DEAD TREE
30	458057.6	3188407.9	0.1	0.1	1.44	DEAD TREE STUMP
32	458064.3	3188406.3	3.3	1.7	0.1	SKINNY LOG
39	458067.3	3188409.1	1.1	1.9	0.74	LOG WITH BRANCHES
40	458067.6	3188408.5	0.5	5.5	0.4	FALLEN TREE
45	458066	3188415.6	1.2	0.7	0.07	LOG
46	458067.6	3188416.8	0.3	0.35	0.24	LOG
48	458059.8	3188413.1	0.13	3.7	0.14	FALLEN LOG
49	458060.8	3188412.5	2.8	0.16	0.17	FALLEN LOG
51	458046.5	3188410.7	0.1	3.4	0.09	FALLEN TREE
52	458043.2	3188410.4	2.5	3.3	0.17	FALLEN TREE

----- Soil Water Content ---------

CONTAINER_ID	MASS_CONTAINER	MASS_CONTAINER_MOISTSAMPLE	MASS_CONTAINER_DRYSAMPLE
A2(2)	50.2	167.7	161.1
B4(5)	50.5	174.6	166.1
A2(1)	50.4	177.2	168.7

----- Soil Grain Size Distribution ---------

SIEVE_OPENING	MASS_RETAINED
2	2.2
1.18	1.5
0.85	2.2
0.425	23.8
0.25	165.7
0.15	692.6
0.075	149.5
0	20.6

SEMF-04_1

SEMF-04_2

SEMF-04_3

SEMF-04_4

SEMF-04_5

SEMF-04_6

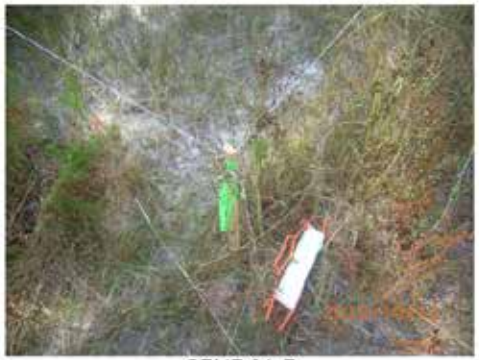

SEMF-04_7

SEMF-04_8

SEMF-04_9


SEMF-04_10


SEMF-04_11


SEMF-04_12


SEMF-04_13


SEMF-04_14


SEMF-04_15


SEMF-04_16


SEMF-04_17


SEMF-04_18

SEMF-04_19

SEMF-04_20

SEMF-04_21

SEMF-04_22

SEMF-04_23

SEMF-04_24

SEMF-04_25

SEMF-04_26

SEMF-04_27


SEMF-04_28


SEMF-04_29


SEMF-04_30


SEMF-04_31


SEMF-04_32

SEMF-04_33


SEMF-04_34


SEMF-04_35


SEMF-04_36

SEMF-04_37

SEMF-04_38

SEMF-04_39

SEMF-04_40

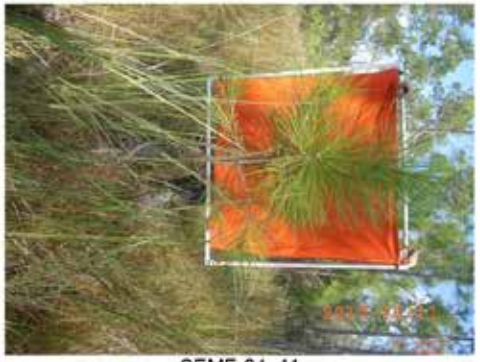

SEMF-04_41

SEMF-04_42

SEMF-04_43

SEMF-04_44

SEMF-04_45

SEMF-04_46

SEMF-04_47

SEMF-04_48

SEMF-04_49

SEMF-04_50

SEMF-04_51

SEMF-04_52

APPENDIX V: FIELD DATA FOR SITE SEMF-05

----- General Information ---------
Site ID = SEMF-05
Team Leader = MEDEIROS
Participants = DARANPOB, BACOPOULOS, SMAR
Date = 10/15/2010
Arrival Time = 8:0 AM
Arrival Weather = COOL, CLEAR, THIN FOG
Departure Time = 10:20 AM
Departure Weather = WARM, BREEZY
Datum = WGS84
Coordinate System = UTM17N
Site Photo Looking East = 8
Site Photo Looking North = 6
Site Photo Looking West = 3
Site Photo Looking South = 11
Site Photos Looking at the Ground = 12,13,14,15

----- Site Boundary GPS Coordinates ---------

POINT_NAME	EASTING	NORTHING	PHOTO_ID
WEST CENTER	457528.8	3189971.7	9
EAST CENTER	457558.4	3189967.9	2
NORTH WEST	457531	3189979.1	
SOUTH WEST	457526.6	3189962.5	7
NORTH EAST	457560.8	3189974.9	1
SOUTH EAST	457556.2	3189960.5	4

----- Surface Canopy Estimates ---------

NW	NC	NE	W	C	E	SW	SC	SE
0	0	0	0	0	0	0	0	0
0	0	0	0	0	0	0	0	0
0	0	0	0	0	0	0	0	0
0	0	0	0	0	0	0	0	0

----- Manning's n Component Estimates ---------

n1	n3	n4_PRIME
0.02	0.002	0.018
0.017	0.015	0.023
0.008	0.006	0.018
0.013	0.003	0.02

----- Low Lying Vegetation Measurements ---------

PHOTO_NS	PHOTO_EW	EASTING	NORTHING	DIM_NS	DIM_EW	HEIGHT	DESC
18	17	457554.6	3189964.8	1.5	1.5	1.32	PAW PAW
20	19	457555.9	3189970	1.1	1.2	1.4	PAW PAW
21	22	457551.1	3189969.7	0.8	0.7	1.3	WAX MYRTLE
23	24	457553.5	3189970	1.6	1.5	1.4	PAW PAW
26	25	457552.1	3189970.7	0.75	0.7	1.2	SAND PINE
29	30	457547.8	3189971	1.1	1.7	1	PAW PAW
33	34	457540.5	3189969.5	1.9	3.7	1.25	CHAPMAN OAK
38	39	457536.4	3189969.5	0.85	0.7	1.15	PAW PAW
40	41	457536.7	3189968.3	0.3	0.5	1.2	PAW PAW
43	42	457536.7	3189968.6	1.25	1.1	1.3	PAW PAW
46	45	457536.4	3189968.9	0.6	0.75	1.6	WAX MYRTLE
47	48	457537.2	3189971.6	2.7	2.7	1.55	PAW PAW CLUSTER
50	49	457538.1	3189971.3	0.3	0.3	0.95	SAND PINE
52	51	457538.1	3189973.2	1.6	1.7	1.75	PAW PAW
54	53	457538.1	3189972.9	1.6	1.3	0.95	DYING BUSH
55	56	457536.4	3189973.5	1.3	1.4	0.8	DYING BUSH GARBERIA
58	57	457535.6	3189976	1	1.4	1.25	GALBERRY
60	59	457534.5	3189972.6	1.9	3.6	1.4	PAW PAW + GALBERRY
61	62	457534	3189976.9	0.65	0.45	1.1	GALBERRY
63	64	457533.7	3189975.4	1.6	1.5	1	DYING GERBERIA
65	66	457531.8	3189974.1	0.5	0.4	1.35	PAW PAW
69	70	457527.8	3189977.2	1.7	1.7	1.5	PAW PAW
71	72	457527	3189975.7	0.62	0.5	1.55	SWEETGUM
74	73	457527.8	3189975.7	1	1.2	1.08	PAW PAW
75	76	457530.2	3189975.7	0.6	0.7	1.4	WAX MYRTLE
77	78	457527.5	3189975.4	0.8	0.43	1.3	WAX MYRTLE
79	80	457527.5	3189974.5	0.55	0.5	1.3	SAND PINE
82	81	457529.4	3189974.1	0.55	0.5	1.4	SAND PINE
84	83	457527.5	3189971.4	1.1	1	1.5	GARBERIA
87	86	457530.7	3189969.2	4.5	1.8	0.96	PAW PAW

88	457556.2	3189964.2	2.9	0	0.9	LARGE MIXED CLUSTER W/ SAW PALM
89	457547.2	3189966.1	4.8	5	2	AND SND LIVE OAK
90	457546.2	3189965.8	5.6	5	2.2	PAW PAW + CHAPMAN OAK
91	457542.1	3189968.5	5.2	5	1.7	PAW PAW + SAW PALM
92	457535.6	3189969.5	7	5	1.46	PAW PAW + SAW PALM
93	457529.1	3189969.2	7.6	5	1.5	SAW PALM + PAW PAW
94	457526.4	3189971.1	7.1	5	1.64	SAW PALM + GARBERIA

----- Tree Measurements ---------

PHOTO	EASTING	NORTHING	DBH	HT1	HT2	HT_SB1	HT_SB2	DIM_NS	DIM_EW	DESC
95	457535.1	3189974.1	10.3	5.4	5.2	2.2	2.2	2.35	2.15	SAND PINE

----- Obstacle Measurements ---------

PHOTO	EASTING	NORTHING	DIM_NS	DIM_EW	HEIGHT	DESC
16	457558.9	3189969.4	0.15	0.15	3.3	DEAD TREE
27	457550.5	3189966.1	0.23	0.2	0.12	STUMP
28	457547.2	3189965.5	0.16	0.16	0.17	STUMP
31	457547	3189966.7	0.31	0.33	0.21	STUMP
32	457543.2	3189969.2	0.37	0.37	0.14	STUMP
35	457540.5	3189969.8	0.26	0.2	0.45	STUMP
36	457539.1	3189968.6	1.3	0.2	0.21	LOG
37	457539.4	3189963.9	5.7	0.5	0.25	LOG
44	457537.5	3189968.9	0.45	0.36	0.42	STUMP
67	457529.1	3189971.4	0.5	2.5	0.32	LOG
68	457529.7	3189976.3	1.9	0.35	0.08	LOG
85	457529.1	3189973.2	3.5	1.9	0.25	LOG

----- Soil Water Content ---------

CONTAINER_ID	MASS_CONTAINER	MASS_CONTAINER_MOISTSAMPLE	MASS_CONTAINER_DRYSAMPLE
A3-3	51	176	174.2
A3(1)	50.6	200.1	197.5
A3(2)	50.2	184.8	182.7

----- Soil Grain Size Distribution ---------

SIEVE_OPENING	MASS_RETAINED
2	2
1.18	2.9
0.85	2.4
0.425	20.5
0.25	299.3
0.15	688.1
0.075	88.4
0	4.4

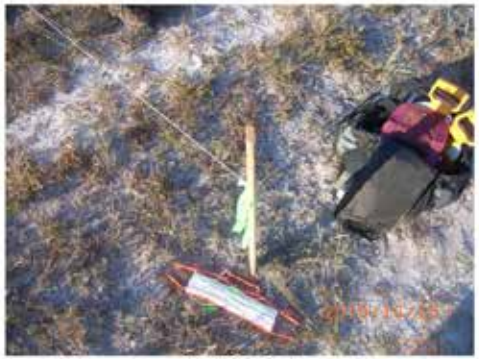

SEMF-05_1

SEMF-05_2

SEMF-05_3

SEMF-05_4

SEMF-05_5

SEMF-05_6

SEMF-05_7

SEMF-05_8

SEMF-05_9

SEMF-05_11

SEMF-05_12

SEMF-05_13

SEMF-05_14

SEMF-05_15

SEMF-05_16

SEMF-05_17

SEMF-05_18

SEMF-05_19

SEMF-05_20

SEMF-05_21

SEMF-05_22

SEMF-05_23

SEMF-05_24

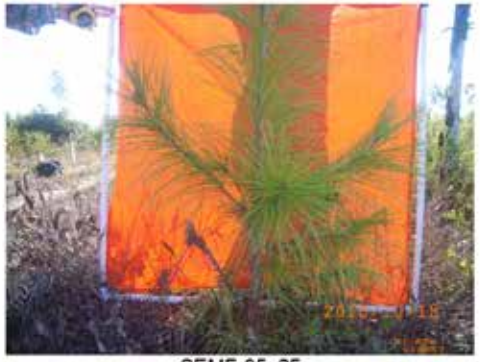

SEMF-05_25

SEMF-05_26

SEMF-05_27

SEMF-05_28

SEMF-05_29

SEMF-05_30

SEMF-05_31

SEMF-05_32

SEMF-05_33

SEMF-05_34

SEMF-05_35

SEMF-05_36

SEMF-05_37

SEMF-05_38

SEMF-05_39

SEMF-05_40

SEMF-05_41

SEMF-05_42

SEMF-05_43

SEMF-05_44

SEMF-05_45

SEMF-05_46

SEMF-05_47

SEMF-05_48

SEMF-05_49

SEMF-05_50

SEMF-05_51

SEMF-05_52

SEMF-05_53

SEMF-05_54

SEMF-05_55

SEMF-05_56

SEMF-05_57

SEMF-05_58

SEMF-05_59

SEMF-05_60

SEMF-05_61

SEMF-05_62

SEMF-05_63

SEMF-05_64

SEMF-05_65

SEMF-05_66

SEMF-05_67

SEMF-05_68

SEMF-05_69

SEMF-05_70

SEMF-05_71

SEMF-05_72

SEMF-05_73

SEMF-05_74

SEMF-05_75

SEMF-05_76

SEMF-05_77

SEMF-05_78

SEMF-05_79

SEMF-05_80

SEMF-05_81

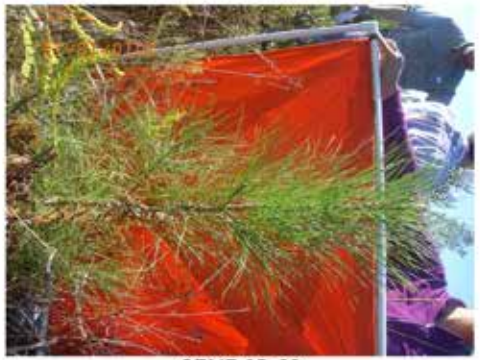

SEMF-05_82

SEMF-05_83

SEMF-05_84

SEMF-05_85

SEMF-05_86

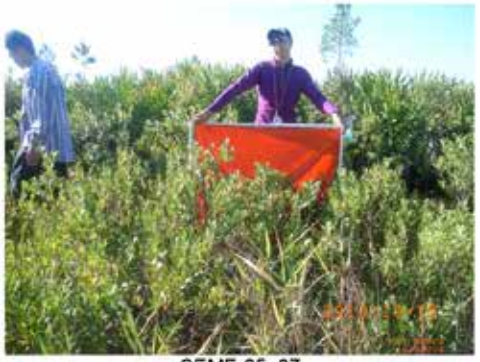

SEMF-05_87

SEMF-05_88

SEMF-05_89

SEMF-05_90

SEMF-05_91

SEMF-05_92

SEMF-05_93

SEMF-05_94

SEMF-05_95

APPENDIX W: FIELD DATA FOR SITE SEMF-06

----- General Information ---------
Site ID = SEMF-06
Team Leader = MEDEIROS
Participants = DARANPOB, BACOPOULOS, SMAR
Date = 10/15/2010
Arrival Time = 11:20 AM
Arrival Weather = WARM BREEZY, CLEAR SKIES
Departure Time = 1:30 PM
Departure Weather = SAME
Datum = WGS84
Coordinate System = UTM17N
Site Photo Looking East = 8
Site Photo Looking North = 9
Site Photo Looking West = 10
Site Photo Looking South = 7
Site Photos Looking at the Ground = 11,12,13

----- Site Boundary GPS Coordinates ---------

POINT_NAME	EASTING	NORTHING	PHOTO_ID
WEST CENTER	458611.5	3188842.3	2
EAST CENTER	458642.6	3188845.6	5
NORTH WEST	458615.8	3188850.3	1
SOUTH WEST	458613.3	3188837.1	3
NORTH EAST	458640.5	3188856	6
SOUTH EAST	458642.3	3188838.2	4

----- Surface Canopy Estimates ---------

NW	NC	NE	W	C	E	SW	SC	SE
40	0	85	0	0	0	15	60	0
5	0	90	0	0	0	15	15	0
5	0	99	0	0	0	100	10	0
5	0	90	0	0	0	50	30	0

----- Manning's n Component Estimates ---------

n1	n3	n4_PRIME
0.002	0	0.001
0.002	0.002	0.003
0.002	0.001	0.001
0.002	0.002	0.001

----- Low Lying Vegetation Measurements ---------

PHOTO_NS	PHOTO_EW	EASTING	NORTHING	DIM_NS	DIM_EW	HEIGHT	DESC
14	15	458617.4	3188838.6	1.2	1.8	1.8	SAW PALMETTO
17	18	458622.6	3188835.5	1.2	1.7	1.95	SAW PALMETTO
20	21	458624.5	3188838.3	2.3	2.1	1.8	DEAD BUSH
25	26	458628.2	3188834.5	1.3	1.2	1.7	DEAD BUSH
31	32	458633.9	3188837.6	2.9	2.1	2	DEAD BUSH
34	33	458635	3188837.3	2.1	2.4	3.55	DEAD CLUSTER OF SAPLINGS (SAND LIVE OAK)
36	35	458634.8	3188837.9	0.6	1.1	1.2	SAW PALMETTO
40	41	458641	3188841.9	2.8	1.3	1	BENT OVER SAND LINE OAK AND SAND PINE

----- Tree Measurements ---------

PHOTO	EASTING	NORTHING	DBH	HT1	HT2	HT_SB1	HT_SB2	DIM_NS	DIM_EW	DESC
16	458614.7	3188836.7	7.3	2.8	3	1.4	1.5	2.5	2.4	BENT OVER DEAD TREE
19	458616.9	3188838.6	21	11	12.5	1.9	4.7	5.1	4.7	SAND PINE
22	458628.5	3188836.4	11.3	5.3	5.5	3.9	3	5.5	4.7	SAND LIVE OAK
23	458627.7	3188839.2	5	4.9	5.6	2.8	1.7	1.4	1.6	SAND LIVE OAK
24	458630.2	3188839.8	17	11.5	8.5	5.3	4.2	5	4.1	SAND LIVE OAK
27	458632.3	3188841.9	17	10.2	9.9	2.3	1.9	5.4	5.3	SAND PINE
28	458629.6	3188838.5	3	3.1	2.95	1.1	1.2	1.4	2.6	DEAD SAND LIVE OAK
29	458633.4	3188842.8	8.1	4.6	4.8	0.9	0.85	2.9	3.1	ALMOST DEAD SAND LIVE OAK
30	458634.8	3188843.8	14	10.5	9.6	2.1	1.8	6.6	4.9	SAND PINE
37	458635	3188843.8	3.5	3.53	3.5	0.2	0.2	1.7	1.6	SAND LIVE OAK
38	458637.2	3188843.7	2	2.95	3	0.4	0.4	0.8	1.4	SAND LIVE OAK
42	458635.6	3188840.1	9	4.4	4.6	0.4	0.35	2.5	2.8	SAND LIVE OAK CLUSTER
44	458641.5	3188841.9	7.5	5.2	5.1	0.7	0.9	3.5	4.1	SAND PINE

----- Obstacle Measurements ---------

PHOTO	EASTING	NORTHING	DIM_NS	DIM_EW	HEIGHT	DESC
39	458638	3188841.9	1.05	1.15	0.16	LOG, LOG
43	458640.5	3188841.3	0.9	0.25	0.15	LOG

----- Soil Water Content ---------

CONTAINER_ID	MASS_CONTAINER	MASS_CONTAINER_MOISTSAMPLE	MASS_CONTAINER_DRYSAMPLE
A-4(4)	50.4	211.4	209
A4(3)	50.4	165.8	164.1
A3(4)	50.4	192	190

----- Soil Grain Size Distribution ---------

SIEVE_OPENING	MASS_RETAINED
2	1
1.18	0.5
0.85	0.8
0.425	24.9
0.25	413.4
0.15	649.3
0.075	100
0	7.7

SEMF-06_1

SEMF-06_2

SEMF-06_3

SEMF-06_4

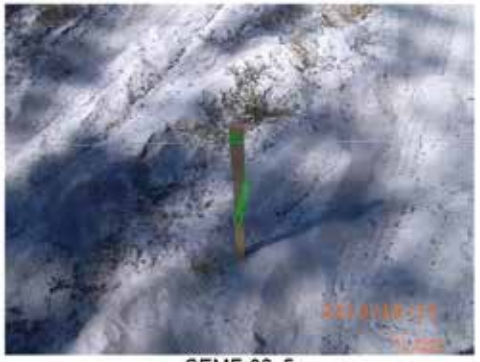

SEMF-06_5

SEMF-06_6

SEMF-06_7

SEMF-06_8

SEMF-06_9

SEMF-06_10

SEMF-06_11

SEMF-06_12

SEMF-06_13

SEMF-06_14

SEMF-06_15

SEMF-06_16

SEMF-06_17

SEMF-06_18

SEMF-06_19

SEMF-06_20

SEMF-06_21

SEMF-06_22

SEMF-06_23

SEMF-06_24

SEMF-06_25

SEMF-06_26

SEMF-06_27

SEMF-06_28

SEMF-06_29

SEMF-06_30

SEMF-06_31

SEMF-06_32

SEMF-06_33

SEMF-06_34

SEMF-06_35

SEMF-06_36

SEMF-06_37

SEMF-06_38

SEMF-06_39

SEMF-06_40

SEMF-06_41

SEMF-06_42

SEMF-06_43

SEMF-06_44

APPENDIX X: FIELD DATA FOR SITE SEMF-07

----- General Information ---------
Site ID = SEMF-07
Team Leader = MEDEIROS
Participants = DARANPOB, BACOPOULOS, SMAR
Date = 11/5/2010
Arrival Time = 7:55 AM
Arrival Weather = COOL (55°), CLEAR SKIES, SUNNY
Departure Time = 1:0 PM
Departure Weather = CLEAR, WINDY
Datum = WGS84
Coordinate System = UTM17N
Site Photo Looking East = 11
Site Photo Looking North = 8
Site Photo Looking West = 5
Site Photo Looking South = 3
Site Photos Looking at the Ground = 12,13,14

----- Site Boundary GPS Coordinates ---------

POINT_NAME	EASTING	NORTHING	PHOTO_ID
WEST CENTER	458660.9	3189337	10
EAST CENTER	458687.5	3189340.3	6
NORTH WEST	458658	3189346.9	1,2
SOUTH WEST	458660.9	3189331.5	9
NORTH EAST	458688.9	3189348.9	4
SOUTH EAST	458691.3	3189333.2	7

----- Surface Canopy Estimates ---------

NW	NC	NE	W	C	E	SW	SC	SE
0	0	0	0	0	0	0	0	0
0	0	0	0	50	0	0	0	0
0	0	0	0	0	0	0	0	0
0	5	0	0	0	0	0	0	0

----- Manning's n Component Estimates ---------

n1	n3	n4_PRIME
0.004	0.005	0.012
0.003	0.003	0.018
0.004	0.02	0.012
0.009	0.025	0.015

----- Low Lying Vegetation Measurements ---------

PHOTO_NS	PHOTO_EW	EASTING	NORTHING	DIM_NS	DIM_EW	HEIGHT	DESC
16	15	458662	3189333.3	1.4	1.8	1.6	SHINY LYNONIA
19	20	458665.2	3189329.6	0.5	0.7	1.5	SHINY LYNONIA
21	22	458665.2	3189330.2	1.4	1.1	1.2	SAW PALM
23	24	458663.6	3189333	3.3	3.2	2.1	SHINY LYNONIA
25	26	458662	3189332.4	1.1	1.4	1.45	NEARLY DEAD SHINT LYNONIA CLUSTER
28	27	458662.3	3189333.3	0.6	0.5	1.3	SAND LIVE OAK
30	29	458661.2	3189331.1	2	0.9	1.4	SAW PALM
32	33	458663.9	3189333.3	1	0.9	1.3	MIXED SAND LIVE OAK + SHINY LYNONIA
35	34	458663.6	3189333.3	0.7	0.9	1.1	NEARLY DEAD SHINY LYNONIA
37	36	458664.4	3189334.8	1	0.9	1.55	NEARLY DEAD SHINY LYNONIA
39	38	458665.3	3189333.3	1.7	2	1.7	NEARLY DEAD SHINY LYNONIA + GRASS
41	40	458663.4	3189334.2	0.75	1.1	1.1	NEARLY DEAD SHINY LYNONIA
42	43	458668.2	3189335.1	1.2	0.8	1.05	NEARLY DEAD SHINY LYNONIA
45	44	458668.2	3189337.3	3.7	2.55	1.6	NEARLY DEAD SHINY LYNONIA
47	46	458663.1	3189336.1	3.8	1.9	1.6	SAW PALM
48	49	458664.5	3189337.3	2.35	2.8	1.6	SAW PALM
51	50	458664.5	3189339.7	2.5	2.6	1.8	SAW PALM
53	52	458664.7	3189339.4	3.3	3.1	1.4	SAW PALM
54	55	458663.4	3189341.3	2.1	2.8	1.65	SAW PALM
57	56,57B	458660.7	3189341.9	2.4	1.6	1.45	SAW PALM
59	58	458661.2	3189341.9	1.4	1.55	0.9	DEAD SHINY LYNONIA
60	61	458661.8	3189342.5	2.1	1.3	1.1	DEAD SHINY LYNONIA
63	62	458662.6	3189343.1	0.6	0.75	1	SAND PINE
64	65	458667.7	3189342.5	2.2	1.65	1.3	SHINY LYNONIA
66	67	458668.2	3189332.4	1.9	1.4	1.1	SHINY LYNONIA
68	69	458665.2	3189331.1	0.8	0.6	0.9	SAW PALM
70	71	458669	3189333	2	1.8	1.35	SAW PALM
72	73	458670.4	3189331.7	0.75	0.8	0.85	MIXED SAND LIVE OAK + DEAD SHINY LYNONIA
75	74	458673.1	3189331.4	0.45	0.45	1.45	GRASS
76	77	458670.7	3189332	0.7	0.5	1.2	GRASS

79	78	458670.1	3189332	0.8	0.9	1.75	GRASS
81	80	458671.2	3189333.6	0.9	1	2	GRASS
83	84	458669.9	3189335.7	0.3	0.3	1.6	GRASS
85	86	458669.9	3189333	1.5	1.4	1	SHINY LYNONIA
87	88	458670.7	3189334.8	0.8	0.9	2.1	GRASS
	89	458669.3	3189337.6	1	0.9	2.2	GRASS
	90	458671.2	3189338.8	0.7	0.7	2.2	GRASS
	91	458669.6	3189337.9	0.3	0.4	1.5	GRASS
	92	458671	3189337.3	0.4	0.4	2	GRASS
	93	458671	3189337.6	1.2	0.7	2.3	GRASS
	94	458671	3189338.8	0.3	0.3	1.9	GRASS
	95	458669.9	3189341.3	0.5	0.4	1.7	GRASS
	106	458668.3	3189342.5	1.1	1.4	2	GRASS
	107	458668.3	3189342.5	0.3	0.3	2.2	GRASS
	108	458669.9	3189343.4	0.2	0.2	1.6	GRASS
	109	458669.9	3189345	0.5	0.5	2	GRASS
	110	458672.3	3189344.3	0.6	0.6	1.8	GRASS
	111	458671.5	3189343.4	0.8	0.8	1.7	GRASS
	112	458672.9	3189341.6	0.5	0.5	2.2	GRASS
	113	458674.5	3189341.3	0.5	0.6	2.1	GRASS
114B	114	458673.4	3189340	0.4	0.5	0.8	SHINY LYNONIA
	115	458673.1	3189340.3	0.6	0.5	2.1	GRASS
	116	458673.9	3189337.9	0.5	0.5	2.3	GRASS
	117	458673.1	3189338.8	0.4	0.4	2	GRASS
	118	458671.8	3189337.3	1	0.6	2.2	GRASS
	119	458675.3	3189338.2	0.9	1	2.1	GRASS
	120	458673.9	3189332.6	0.7	0.7	2	GRASS
	121	458672.3	3189335.1	0.8	0.7	1.7	GRASS
	122	458669.9	3189333	0.7	0.6	1.8	GRASS
	123	458672.6	3189332	0.7	0.7	2	GRASS
	124	458671.8	3189333	0.3	0.4	1.8	GRASS
127	128	458673.9	3189331.1	0.3	1.8	1.1	SHINY LYNONIA
	129	458676.1	3189333.2	0.6	0.5	1.4	GRASS
	130	458675.3	3189331.7	0.7	0.5	1.4	GRASS
	131	458675	3189338.8	0.7	0.7	2	GRASS
	132	458675	3189337.6	0.4	0.4	2	GRASS
	133	458675.8	3189337.2	0.25	0.25	1.5	GRASS
	134	458675	3189337.9	0.4	0.3	2.1	GRASS
	135	458677.2	3189337.6	0.4	0.5	1.9	GRASS

	136	458677.5	3189336.9	0.8	0.8	2.2	GRASS
	137	458676.6	3189337.2	0.4	0.4	1.8	GRASS
	141	458675.8	3189340.3	0.4	0.3	1.4	GRASS
	142	458675	3189340.9	0.4	0.4	1.9	GRASS
	143	458675.3	3189338.8	0.6	0.3	1.7	GRASS
	144	458676.4	3189340.6	0.4	0.4	1.6	GRASS
	146	458681	3189343.7	0.9	0.8	2	GRASS
	147	458678.3	3189344	0.6	0.6	2.3	GRASS
	148	458675.9	3189344	1.1	0.8	1.7	GRASS
	149	458675.3	3189343.7	0.2	0.3	2.1	GRASS
150	151	458680.2	3189347.1	4.1	7	2.2	LARGE CONTIGUOUS GRASS AREA
	152	458679.6	3189342.8	0.8	0.8	2.1	GRASS
	153	458679.6	3189341.2	0.4	0.4	1.9	GRASS
	154	458679.1	3189342.5	0.25	0.25	1.8	GRASS
	155	458678.3	3189339.7	0.7	0.4	2.1	GRASS
	156	458679.1	3189338.8	0.7	0.5	2.1	GRASS
	157	458676.9	3189339.1	1	1.2	2	GRASS
	158	458678.3	3189337.5	0.2	0.2	1.5	GRASS
	159	458679.1	3189337.2	1.3	0.8	1.9	GRASS
	160	458680.7	3189335.1	2.2	2.5	2.2	GRASS
	161	458674.7	3189329.6	0.4	0.4	1	GRASS
	162	458676.9	3189331.1	1.3	1.5	1.7	GRASS
	163	458679.3	3189332	0.6	0.6	1.4	GRASS
	164	458681	3189331.4	1.5	0.9	1.2	GRASS
	165	458679.6	3189331.1	0.9	0.8	1.1	GRASS
	166	458680.2	3189333.2	1.2	2.2	1.4	GRASS
	167	458680.7	3189335.1	1.1	1.3	1.8	GRASS
	168	458684.2	3189333.8	0.7	0.6	1.6	GRASS
	169	458682.3	3189337.5	2.1	1.8	2.1	GRASS
	170	458682.9	3189340.3	0.8	0.9	1.9	GRASS
	171	458680.7	3189339.7	1.9	3	2.4	GRASS
	179	458688.3	3189343.4	4	5.3	2.3	GRASS
	180	458690	3189346.7	0.6	0.8	2	GRASS
	181	458690.2	3189343.4	1.5	1.4	1.5	GRASS
	182	458691.6	3189342.7	1	1	1.4	GRASS
	183	458691.8	3189339.7	1.8	2	1.8	GRASS
	184	458690.2	3189341.5	0.6	0.5	1.1	GRASS
	185	458689.9	3189340.6	2.9	5	2.1	GRASS
	186	458687.5	3189337.5	1.6	3.1	1.9	GRASS

187	458684.8	3189338.8	0.5	0.6	2.2	GRASS
188	458682.1	3189338.5	1	1.2	1.2	GRASS
189	458686.1	3189335.7	4.2	5.2	2.3	GRASS
190	458691.8	3189335	1.8	1.5	1.7	GRASS
191	458689.6	3189332.3	1.4	2	1.1	GRASS
192	458688.6	3189332.3	1.8	1.9	1.3	GRASS

----- Tree Measurements ---------

PHOTO	EASTING	NORTHING	DBH	HT1	HT2	HT_SB1	HT_SB2	DIM_NS	DIM_EW	DESC
17	458660.6	3189332.4	1.9	1.9	1.95	0.6	0.61	0.8	0.6	SAND LIVE OAK
18	458663.6	3189330.5	0.9	1.8	1.85	0.6	0.7	0.5	0.55	SAND LIVE OAK
105	458669.9	3189340.7	69.2	9.4	9.6	2.2	2.4	8.9	10.4	SAND LIVE OAK W/OLDMANS BEARD
125	458673.7	3189332.6	12	6.1	6.1	1.2	1.2	3.1	3	SAND PINE
138	458678.3	3189336.6	15.1	5.8	6.3	2.2	2.1	3	2.8	SAND PINE

----- Obstacle Measurements ---------

PHOTO	EASTING	NORTHING	DIM_NS	DIM_EW	HEIGHT	DESC
31	458660.9	3189332.1	2.3	0.4	2.35	DEAD TREE PARTIALLY FALLEN
82	458669.9	3189334.5	1.6	4.6	0.9	LOG W/ BRANCHES
96	458671.8	3189335.7	1.1	1.2	1.8	DEAD TREE W/ BRANCHES
97	458669.9	3189339.1	1.2	1.7	1.9	DEAD TREE W/ BRANCHES
98	458668.3	3189339.7	0.6	0.5	1.2	DEAD TREE W/ BRANCHES
99	458668.2	3189337.9	0.9	0.9	2.1	DEAD TREE W/ BRANCHES
100	458667.7	3189340.7	0.5	3	0.2	LOG
101	458665.8	3189340.7	0.4	2.2	0.15	LOG
102	458668.8	3189343.1	3.6	1.1	0.4	PILE OF LOGS
103	458671.8	3189342.2	3.3	2.6	0.1	LOG
104	458673.9	3189339.1	0.13	0.13	0.8	STUMP
126	458673.9	3189335.1	0.3	0.4	1.3	BURNT STUMP
139	458676.9	3189339.7	0.4	1.9	0.6	LOG WITH BRANCHES
140	458678.3	3189335.4	3.4	1.1	0.4	LOG WITH BRANCHES
172	458679.7	3189345.2	0.17	0.17	5.3	DEAD TREE
173	458685.6	3189340.3	1.4	3.5	0.3	LOG
174	458684.5	3189342.4	4.1	2.4	0.45	LOG
175	458682.4	3189341.8	1.2	3.6	0.18	LOG
176	458682.1	3189342.1	1.8	1.8	0.13	LOG
177	458691.8	3189334.1	2.2	1.8	7.6	DEAD TREE
177	458691.8	3189334.1	2.4	2.4	10.8	DEAD TREE
178	458688.8	3189336.6	1.1	2.1	0.9	LOG WITH BRANCHES

----- Soil Water Content ---------

CONTAINER_ID	MASS_CONTAINER	MASS_CONTAINER_MOISTSAMPLE	MASS_CONTAINER_DRYSAMPLE
A2(1)	50.4	160	145.7
A2(2)	50.2	165.3	151.1
A3(3)	51	159.6	145.6

----- Soil Grain Size Distribution ---------

SIEVE_OPENING	MASS_RETAINED
2	5.3
1.18	5.3
0.85	4.5
0.425	38.9
0.25	457.8
0.15	419
0.075	19.1
0	1.5

SEMF-07_1

SEMF-07_2

SEMF-07_3

SEMF-07_4

SEMF-07_5

SEMF-07_6

SEMF-07_7

SEMF-07_8

SEMF-07_9

SEMF-07_10

SEMF-07_11

SEMF-07_12

SEMF-07_13

SEMF-07_14

SEMF-07_15

SEMF-07_16

SEMF-07_17

SEMF-07_18

SEMF-07_19

SEMF-07_20

SEMF-07_21

SEMF-07_22

SEMF-07_23

SEMF-07_24

SEMF-07_25

SEMF-07_26

SEMF-07_27

. . .


SEMF-07_28


SEMF-07_29


SEMF-07_30


SEMF-07_31


SEMF-07_32


SEMF-07_33


SEMF-07_34


SEMF-07_35


SEMF-07_36


SEMF-07_37


SEMF-07_38


SEMF-07_39


SEMF-07_40


SEMF-07_41


SEMF-07_42


SEMF-07_43


SEMF-07_44


SEMF-07_45


SEMF-07_46


SEMF-07_47


SEMF-07_48


SEMF-07_49


SEMF-07_50


SEMF-07_51


SEMF-07_52


SEMF-07_53


SEMF-07_54

SEMF-07_55


SEMF-07_56


SEMF-07_57


SEMF-07_57B

SEMF-07_58


SEMF-07_59


SEMF-07_60

SEMF-07_61


SEMF-07_62

SEMF-07_63

SEMF-07_64

SEMF-07_65

SEMF-07_66

SEMF-07_67

SEMF-07_68

SEMF-07_69

SEMF-07_70

SEMF-07_71

SEMF-07_72

SEMF-07_73

SEMF-07_74

SEMF-07_75

SEMF-07_76

SEMF-07_77

SEMF-07_78

SEMF-07_79

SEMF-07_80

SEMF-07_81

SEMF-07_82

SEMF-07_83

SEMF-07_84

SEMF-07_85

SEMF-07_86

SEMF-07_87

SEMF-07_88

SEMF-07_89

SEMF-07_90

SEMF-07_91

SEMF-07_92

SEMF-07_93

SEMF-07_94

SEMF-07_95

SEMF-07_96

SEMF-07_97

SEMF-07_98

SEMF-07_99

SEMF-07_100

SEMF-07_101

SEMF-07_102

SEMF-07_103

SEMF-07_104

SEMF-07_105

SEMF-07_106

SEMF-07_107

SEMF-07_108

SEMF-07_109

SEMF-07_110

SEMF-07_111

SEMF-07_112

SEMF-07_113

SEMF-07_114

SEMF-07_114B

SEMF-07_115


SEMF-07_116


SEMF-07_117


SEMF-07_118


SEMF-07_119


SEMF-07_120


SEMF-07_121


SEMF-07_122


SEMF-07_123


SEMF-07_124

SEMF-07_125

SEMF-07_126

SEMF-07_127

SEMF-07_128

SEMF-07_129

SEMF-07_130

SEMF-07_131

SEMF-07_132

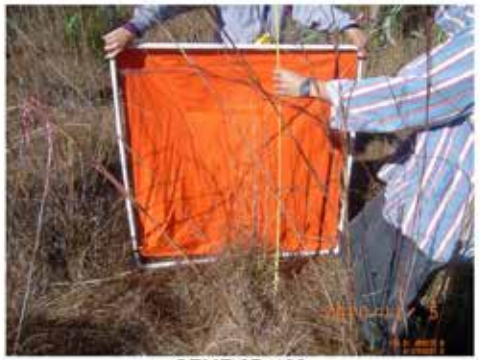

SEMF-07_133

SEMF-07_134

SEMF-07_135

SEMF-07_136

SEMF-07_137

SEMF-07_138

SEMF-07_139

SEMF-07_140

SEMF-07_141

SEMF-07_142


SEMF-07_143


SEMF-07_144


SEMF-07_146


SEMF-07_147


SEMF-07_148


SEMF-07_149


SEMF-07_150


SEMF-07_151


SEMF-07_152

SEMF-07_153

SEMF-07_154

SEMF-07_155

SEMF-07_156

SEMF-07_157

SEMF-07_158

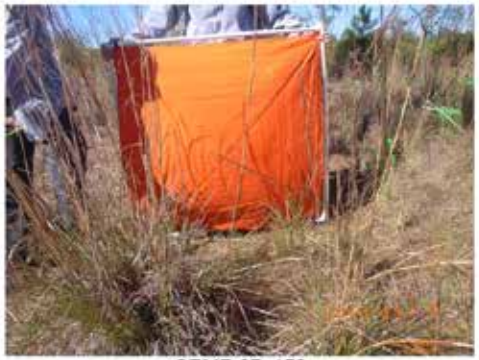

SEMF-07_159

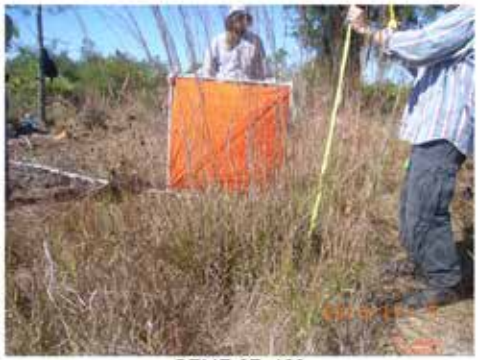

SEMF-07_160

SEMF-07_161

SEMF-07_162

SEMF-07_163

SEMF-07_164

SEMF-07_165

SEMF-07_166

SEMF-07_167

SEMF-07_168

SEMF-07_169

SEMF-07_170

SEMF-07_171

SEMF-07_172

SEMF-07_173

SEMF-07_174

SEMF-07_175

SEMF-07_176

SEMF-07_177

SEMF-07_178

SEMF-07_179

SEMF-07_180

SEMF-07_181

SEMF-07_182

SEMF-07_183

SEMF-07_184

SEMF-07_185

SEMF-07_186

SEMF-07_187

SEMF-07_188

SEMF-07_189

SEMF-07_190

SEMF-07_191

SEMF-07_192

APPENDIX Y: FIELD MEASUREMENTS METADATA

Introduction

This appendix serves as a guide to the field measurements data presented in the previous appendices. All non-obvious information such as abbreviations and measurement units are defined.

Photograph Numbering

The photographs for each site are numbered sequentially beginning with 1. Due to data recording errors in the field, there are instances of duplicate numbers being used. In these cases, the suffix A, B, etc is used. Also, in certain instances a number required deletion to maintain consistent referencing between the photograph and the subject.

Only the photo identification numbers are listed in the field measurements text; the actual photograph name contains a prefix corresponding to the site name. For example, the tenth photo on site ANER-01 has the filename ANER-01_10.

Section: General Information

No clarification or additional information required.

Section: Site Boundary GPS Coordinates

This section describes the location of the boundary points (POINT_NAME) along with their EASTING, NORTHING and PHOTO_ID. The easting and northing are relative to the datum and projection listed in the General Information section.

Section: Surface Canopy Estimates

The numbers represent the surface canopy coverage estimate as a percentage. For example, if 50% of the sky at a specific location is obscured by tree canopy, a value of 50 is listed. Each row of numbers represents the estimations of a single participant; since there were four participants on each site there are four rows of independently estimated data. The header row indicates the location of the estimate:

- NW = northwest corner;
- NC = center of northern edge;
- NE = northeast corner;
- W = center of western edge;
- C = center of site;
- E = center of eastern edge;
- SW = southwest corner;
- SC = center of southern edge; and
- SE = southeast corner.

Section: Manning's *n* Component Estimates

The participants each independently estimated the Manning's *n* values associated with microtopography, obstacles and low lying vegetation, respectively, as explained in CHAPTER 4. Each row of numbers represents the estimations of a single participant; since there were four participants on each site there are four rows of independently estimated data. The header row indicates the component of Manning's *n* being estimated:

- n1 = n_1, microtopography or surface irregularities;
- n3 = n_3, obstacles in the floodplain;
- n4_PRIME = n_4, low lying vegetation;

Please note that the 'prime' designation of n_4 indicates that this value does not include trees.

Section: Low Lying Vegetation Measurements

This section presents the measurements of low lying vegetation. The following is a description of the measurement headers along with the measurement units, if applicable:

- PHOTO_NS = Photograph number, taken facing either north or south;
- PHOTO_EW = Photograph number, taken facing either east or west;
- EASTING = X coordinate at the approximate center of the subject, referenced to the datum and projection listed in the General Information section;
- NORTHING = Y coordinate at the approximate center of the subject, referenced to the datum and projection listed in the General Information section;
- DIM_NS = Total width of the subject in meters, measured in the north-south direction;
- DIM_EW = Total width of the subject in meters, measured in the east-west direction;
- HEIGHT = Total height of the subject in meters, measured from the local ground; and
- DESC = Description of the subject, including the species if applicable.

Please note that where only one photo is listed, the participants determined in the field that the subject was symmetrical and required only one photograph to adequately document it.

Section: Tree Measurements

This section presents the measurements of trees. The following is a description of the measurement headers along with the measurement units, if applicable:

- PHOTO = Photograph number;
- EASTING = X coordinate at the approximate center of the subject, referenced to the datum and projection listed in the General Information section;
- NORTHING = Y coordinate at the approximate center of the subject, referenced to the datum and projection listed in the General Information section;
- DBH = Diameter at breast height in centimeters;
- HT1 = First total height measurement in meters;
- HT2 = Second total height measurement in meters, taken independently by a different participant;
- HT_SB1 = First height measurement of the tree's lowest significant branch in meters;
- HT_SB2 = Second height measurement of the tree's lowest significant branch in meters, taken independently by a different participant;
- DIM_NS = Total width of the subject tree canopy in meters, measured in the north-south direction;
- DIM_EW = Total width of the subject tree canopy in meters, measured in the east-west direction; and
- DESC = Description of the subject, including the species if applicable.

Section: Obstacle Measurements

This section presents the measurements of obstacles. The following is a description of the measurement headers along with the measurement units, if applicable:

- PHOTO = Photograph number;
- EASTING = X coordinate at the approximate center of the subject, referenced to the datum and projection listed in the General Information section;
- NORTHING = Y coordinate at the approximate center of the subject, referenced to the datum and projection listed in the General Information section;
- DIM_NS = Total width of the subject in meters, measured in the north-south direction;
- DIM_EW = Total width of the subject in meters, measured in the east-west direction;
- HEIGHT = Total height of the subject in meters, measured from the local ground; and
- DESC = Description of the subject, including the species if applicable.

Section: Soil Water Content

This section presents the measurements of soil water content conducted at the University of Central Florida. Three sub-samples from each site soil sample were tested for water (moisture) content. The following is a description of the measurement headers along with the measurement units, if applicable:

- CONTAINER_ID = Alphanumeric identification marking on the moisture can;
- MASS_CONTAINER = Mass of the empty moisture can in grams;
- MASS_CONTAINER_MOISTSAMPLE = Mass of the moisture can containing moist (raw) soil sample in grams; and
- MASS_CONTAINER_DRYSAMPLE = Mass of the moisture can containing the oven dried soil sample in grams.

Section: Soil Grain Size Distribution

This section presents the measurements of soil grain size distribution determined by sieve analyses conducted at the University of Central Florida. The following is a description of the measurement headers along with the measurement units, if applicable:

- SIEVE_OPENING = Sieve mesh opening size in millimaters; and
- MASS_RETAINED = Mass oven dried soil retained on each sieve in grams.